Lignin Separation from Ethanol Water Pulping Liquors

Dissertation

zur Erlangung des akademischen Grades

Doktoringenieur

(Dr.-Ing.)

von   Dipl.-Ing. Peter Schulze

geb. am   28.02.1986   in Schönebeck/Elbe

genehmigt durch die Fakultät für Verfahrens-und Systemtechnik

der Otto-von-Guericke Universität Magdeburg

Promotionskommission: Prof. Dr.-Ing. Andreas Seidel-Morgenstern (Vorsitz)

Prof. Dr. rer. nat. Herbert Sixta (Gutachter)

Prof. Dr.-Ing. Ulrich Teipel (Gutachter)

apl. Prof. Dr. rer. nat. Heike Lorenz (Mitglied)

eingereicht am: 07.02.2018

Promotionskolloquium am: 06.07.2018

Danksagung

Zuallererst hatte ich großes Glück in einem hochentwickelten Land wie Deutschland geboren zu werden und immer satt, gesund, in einer intakten Familie und mit ausgereiften Infrastrukturen aufzuwachsen.

Obendrein hatte und habe ich viele tolle Verwandte, Freunde, Kollegen und Mentoren, die mich Vieles lehrten und mich unterstützten.

Diese glücklichen Umstände und eine angeborene Affinität zu Technik und Naturwissenschaften ermöglichten mir schlussendlich diese Doktorarbeit zu schreiben.

Im Einzelnen bedanke ich mich bei:

- meinen „Doktoreltern" Prof. Heike Lorenz und Prof. Andreas Seidel-Morgenstern für die tolle Möglichkeit am MPI unter exzellenten Bedingungen zu promovieren und die gemeinsame lehrreiche Zeit;
- meinen engsten Kollegen Hannes Buchholz, Elena Horosanskaia, Anne-Kathleen Morgner, geb. Kort und allen anderen Doktoranden, die Freud und Leid mit mir teilten und stets für fruchtbare Diskussionen bereit standen;
- allen Kollegen vom technischen Stammpersonal des MPI und der OvGU, insbesondere Stefanie Leuchtenberg, Jacqueline Kaufmann, Detlef Franz, Steve Haltenhof, Stefan Hildebrandt, Markus Ikert, Liane Hilfert und Sabine Busse, die mir stets mit Rat und Tat zur Seite standen;
- meinen lieben Kollegen vom Fraunhofer CBP Moritz Leschinsky, Marlen Verges und Christine Roßberg für die tolle Zusammenarbeit an der Pilotanlage und auf Konferenzen;
- meinen fleißigen Studenten Ann-Karolin Schuldt, Katja Schelm, Anja Kusian, Johannes Keitel, Shahin Mohseni und Jan-Niklas Veldhuizen Dijkstra, die mir viel Arbeit abnahmen;
- meinen alten und neuen Freunden aus Pömmelte und Umgebung, die mich ermuntert und zerstreut haben, wenn ich es nötig hatte;
- meiner gesamten Familie, aber insbesondere meinen Großeltern Georg und Erika Pohler, sowie Walter und Elfriede Schulze, meinem Bruder Christian Schulze mit Familie und natürlich meinen Eltern Doris und Wilfried Schulze, die mir allesamt unmessbar viel beigebracht und meine Persönlichkeit mit geformt haben;
- meiner Liebsten Marie-Kristin Kohlen mit unserer Hündin Jolla, die mich durch meine Promotion begleitet und mir stets ein liebevolles Zuhause zum Erholen bereitet hat.

Kurzfassung

Lignin ist die größte Quelle von nachwachsenden aromatischen Kohlenwasserstoffen in der Natur und könnte fossile Rohstoffe teilweise ersetzen. Gegenwärtig ist Lignin jedoch immer noch weitestgehend ungenutzt. Lignozellulose-Bioraffinerien, die nachhaltig Zellulose, Lignin und Hemizellulose aus verholzter Biomasse durch einen OrganoSolv-Aufschlussprozess (fraktionierte Auflösung von Biomasse in organischem Lösungsmittel) liefern können, befinden sich derzeit in der Entwicklung (z.B. am Fraunhofer Zentrum für Chemisch-Biotechnologische Prozesse (CBP)). Die Abtrennung von gelöstem Lignin aus OrganoSolv-Aufschlusslösungen ist jedoch noch nicht vollständig verstanden und daher auch noch nicht optimiert worden.

In dieser Arbeit wurden das Löslichkeits- und Erweichungsverhalten von Lignin in verschiedenen Ethanol/Wasser-Lösungsmittelgemischen in einem geeigneten Temperaturbereich untersucht. Die Prozessbedingungen für einen optimierten Lignin-Abtrennungsprozess wurden vom ermittelten Phasenverhalten des Lignins abgeleitet, um die Abscheidung von verflüssigtem und klebrigem Lignin, das Verkrustungen bildet, zu vermeiden.

Der hier untersuchte Lignin-Abtrennprozess wurde schrittweise, ausgehend von semi-kontinuierlich arbeitenden Labor- und Pilotanlagen, hin zu kontinuierlich betriebenen Labor- und Pilotanlagen mit Fallfilmverdampfer und Inline-Prozessanalytik zur Verfolgung der Lignin-Partikelgrößenverteilung und des Ethanolgehaltes in der Dispersion, entwickelt und schließlich patentiert. Der „hybridartige" Prozess kombiniert die Vorteile der bekannten Verdünnungs- und Verdampfungsfällungs-Prozesse ohne ihre Nachteile aufzuweisen. Kontrollierte Lignin-Partikelagglomeration wird durch die Temperatur und den Ethanolgehalt der Dispersion gesteuert und mittels der Inline-Partikelanalytik überwacht, was in einer guten Filtrierbarkeit der Lignindispersionen mit mittleren Filterkuchenwiderständen zwischen 10^{11} und 10^{13} m^{-2} resultiert. Ethanol-Organosolv Kochlaugen aus Buchen-, Fichten- und Eukalyptusholz wurden in der Lignocellulose-Bioraffinerie-Pilotanlage am Fraunhofer CBP produziert und in Labor- und Pilotanlagen bei den folgenden typischen Bedingungen fraktioniert: 80-120 mbar (absolut) Druck, 6 - 9 Ma.% Ethanol in der Flüssigphase der Lignindispersion und einer resultierenden Siedetemperatur von 38 - 44 °C. Verkrustungen konnten komplett vermieden und somit Ligninausbeuten nahe 100 Ma. % erzielt werden.

Der Energiebedarf des vorgestellten Prozesses ist noch nicht optimiert. Daher werden Konzepte zur Verringerung des spezifischen Energiebedarfes, wie Kochlaugen-Voreindickung und Lignin-Kühlungsfällung, als Gegenstand für zukünftige Untersuchungen vorgeschlagen.

Abstract

Lignin is the largest renewable resource of aromatics in nature and could partially substitute fossil sources. Currently it is still widely unexploited. Lignocellulose biorefineries that could sustainably provide cellulose, lignin and hemicellulose from woody feedstocks by organosolv fractionation are currently in the development phase (e.g. at Fraunhofer Center for Chemical-Biotechnological Processes CBP). The separation of dissolved lignin from organosolv pulping liquor is still not deeply understood and therefore also not optimized.

In this work the solubility and softening behavior of lignin in various ethanol/water solvent mixtures have been determined in a reasonable temperature range. The operation conditions for an optimized lignin separation process have been derived from the determined lignin phase behavior in order to prevent the formation of soft and sticky lignin that causes incrustations.

The finally patented lignin separation process has been developed stepwise from semi-continuous lab and pilot scale plants to continuous lab and pilot scale plants with a falling film evaporator setup and inline process analytics for particle size and ethanol content. The "hybrid-like" process combines the advantages of prominent dilution- and evaporation-precipitation processes without adopting their drawbacks. Controlled particle agglomeration is tuned by temperature and ethanol content of the lignin dispersion and is monitored via inline particle size analysis, resulting in a good filterability of the lignin dispersion with average filter cake resistances of 10^{11} to $10^{13}\,\mathrm{m^{-2}}$.

Beech, spruce and eucalyptus ethanol organosolv pulping liquors provided by the Lignocellulose Biorefinery pilot plant at the Fraunhofer CBP have been processed in lab and pilot scale plants at the following typical process conditons: pressure 80-120 mbar abs., 6 – 9 wt. % ethanol in the aqueous phase of lignin dispersion and resulting boiling temperatures of 38-44 °C. Incrustations could be completely avoided and therefore lignin yields near 100 % have been achieved.

However, the energy consumption of the presented process is not fully optimized yet. Therefore, process concepts to decrease the specific energy consumption of lignin separation, like pulping liquor pre-concentration and lignin cooling-precipitation, are proposed for future investigations.

Contents

1. Introduction

The industrialized world still relies predominantly on fossil-based resources for materials, chemicals and energy supply. The exploitation of fossil carbon resources comes along with some disadvantages, like carbon dioxide enrichment in the atmosphere and approaching shortage of finite resources. For those reasons, improved methods for the efficient and sustainable utilization of renewable carbon resources, like lignocellulosic biomass, have been a long time focus of research.

Since the end of the 19th century most conservative pulping mills use the Sulfite-Pulping and Sulfate-Pulping (Kraft) processes and exploit wood as a renewable resource to mainly produce cellulose (Dahl 1884). The other two main constituents of wood-based biomass, namely lignin and hemicellulose, are separated from cellulose during the wood-cooking process in aqueous solutions of alkaline and sulfate salts. Usually, the lignin and hemicellulose solution, called black liquor, is combusted in recovery boilers in order to recycle the pulping chemicals and to provide energy for the process. There are currently around 300 million tons of lignin that are combusted every year in the worldwide pulping industry, instead of being used as source for renewable aromatic materials and chemicals. Only about 5 % of the lignin currently processed worldwide is separated as a product with different application areas (Cazacu et al. 2013). Various processes for separation of lignin from Kraft black liquors have been developed (Loutfi et al. 1991, Öhman 2006, Niemi et al. 2011), but the obtained lignin quality is inferior compared to lignins produced by an organosolv (organic solvent) pulping process (Menon and Rao 2012).

The original organosolv pulping process using an ethanol/water mixture as solvent for lignin and hemicellulose (Kleinert and Tayenthal 1931) is considered to be advantageous with regard to the production of high-purity cellulose, lignin and hemicellulose with high yields from lignocellulose. Another benefit is the relatively simple organic solvent recycling by distillation. Woody biomass could be almost completely fractionated in a lignocellulose biorefinery, as described in numerous publications (Kamm et al. 2005, Michels and Wagemann 2010, Sannigrahi et al. 2010). An organosolv lignocellulose biorefinery demonstration plant, processing hardwood in a patented ethanol/water pulping process variant for the production of cellulosic ethanol, high-purity lignin and furfural (Berlin et al. 2013), was announced by the US government to start-up in 2017 (Lignol 2011, DOE 2017). Other demonstration and commercial plants (e.g. Alcell in Canada and Organocell in Germany) already have been running in the 1990th but were shut down again (Pye and Lora 1991).

Efficient separation processes are essential for the economic viability of a lignocellulose biorefinery. Especially, the organic solvent recycling and the accompanying lignin separation processes that have a great impact on the energy consumption of the refinery are of great importance (Vishtal and Kraslawski 2011, Viell et al. 2013). Processes for the separation of lignin from organosolv pulping liquors have already been developed in the past (Tayenthal and Kleinert 1932, Kleinert 1971, Thring et al. 1990, Botello et al. 1999, Hallberg et al. 2013). Besides the development of membrane separation techniques (Alriols et al. 2010, Weinwurm et al. 2014), two general methods for lignin precipitation are usually described in the literature: a) dilution of pulping liquor with water or another aqueous process stream and b) direct

evaporation of ethanol from the pulping liquor. The first and most commonly used method mostly leads to lignin dispersions with poor filtration properties due to small particle sizes and to an increase in process streams of filtrate after lignin filtration. The second method leads to lignin-fouling in the apparatus due to the precipitation of a soft and adhesive lignin phase.

Plants with increased process streams require larger plant equipment with a higher energy demand in downstream processes, like filtration and distillation. Poor filtration properties require larger specialized filtration apparatuses with increased energy demands. Fouled plant parts need to be regularly cleaned and the lignin yield may be therefore decreased. All these disadvantages of the state-of-the-art lignin separation processes result in increased operation and investment costs, lowering economic viability of the whole biorefinery.

This work, performed in cooperation with the Fraunhofer Center for Chemical-Biotechnological Processes (CBP), had the goal to develop an improved lignin separation process on the basis of a fundamental understanding of the lignin phase behavior. The Fraunhofer CBP, co-funded by the German government, was inaugurated in 2012 in Leuna, Germany. Besides other experimental plants at the Fraunhofer CBP, an organosolv pilot plant has been constructed in order to develop an advanced lignocellulose biorefinery concept that could be up-scaled to industrial standards and would produce high-value products from the lignocellulose fractions. The Max Planck Institute for Dynamics of Complex Technical Systems (MPI) in Magdeburg was incorporated as an associated partner of the Fraunhofer CBP within research projects funded by the German government between 2013 and 2017.

Goal of this work was to develop a superior process for the precipitation and controlled agglomeration of lignin from organosolv pulping liquors on the basis of phase behavior and softening properties of lignin. The continuous process presented below yields an improved filterable lignin dispersion while avoids at the same time lignin incrustations both in lab and pilot scale plants.

1.1.   Objectives and structure of the thesis

The overall objective was the development of a process for continuous lignin precipitation from ethanol organosolv pulping liquors on the basis of solvent evaporation that should meet also the following requirements:

- no incrustations of precipitated lignin in the apparatuses used
- high lignin yield
- good filterability of resulting lignin dispersion
- no addition of aqueous streams for dilution
- up-scalable process concept (to industrial scale)
- feasible for pilot plant implementation at Fraunhofer CBP
- low energy consumption

The work is structured as follows:

In **Chapter 2** theoretical foundations regarding lignocellulose, lignin and organosolv pulping are introduced in the context of the lignocellulose biorefinery concept. Further,

the state the art in lignin separation from organosolv pulping liquors, the solubility of lignins in various solvents and the glass transition temperatures of pure and solvated lignins and polymers in general are reviewed. Finally the mechanisms of phase separations in polymer-solvent-antisolvent systems and the interactions between the resulting polymer particles are theoretical explained.

Chapter 3 introduces the different pulping conditions that have been used in the Fraunhofer CBP pilot plant to produce the pulping liquors and lignins that have been investigated in this work. Further, the analytical methods and procedures for the characterization of the occurring process streams and materials are explained. The experimental setups and procedures for the lignin phase behavior characterization and various precipitation processes are finally also introduced.

A simplified mathematical model of the continuous lignin precipitation process is presented in **Chapter 4**. The model comprises mass and energy balances of the major apparatuses of the real plant and combines them. A sub-model of the solid-liquid-equilibria of lignin in ethanol/water mixtures in a reasonable temperature range is applied to describe the lignin precipitation process and another sub-model of the vapor-liquid equilibria of ethanol and water is used to describe the evaporation of ethanol and water from the lignin dispersion. The model is applied for process illustrations and the prediction of suitable process parameters in the pilot plant.

Chapter 5 comprises the experimental results and discussion. The physical and chemical properties of pulping liquors and lignins investigated are presented at first. The thermal properties and phase behavior of selected lignins in ethanol/water mixtures over a process relevant temperature range are presented and describe the basis of the performed lignin separation processes. The results of the numerous batch, semi- and continuous lignin precipitation and agglomeration experiments in lab and pilot plants are presented and discussed.

Finally, summarizing illustrations of the batch and (semi-) continuous processes in the triangular phase diagrams of lignin, ethanol and water are given.

In **Chapter 6** the findings of the work are summarized and conclusions are complemented by outlooks for promising future investigation.

Supplementary information is provided in **Chapter 7** that comprises the complete Matlab™ code of the mathematical model described in Chapter 4. Additionally, diagrams of various physical and chemical data of different lignins that have been determined within this thesis are presented and may be further used by others. A table of all the lignin precipitation experiments performed is presented as well.

2. Fundamentals

Below is given a brief overview of the theoretical foundations of lignin separation and state-of-the art processes in the field of lignin processing in lignocellulose biorefineries (LC BR).

2.1. Lignocellulose and lignin

The structures of lignocellulosic materials and different native lignins before and after pulping processes are explained in this section. Some relevant possibilities to utilize lignin, as reported in the literature, are introduced as well.

2.1.1. Native lignin in lignocellulose

Lignin follows cellulose as the second most abundant renewable feedstock on earth. The lignin biosynthesis via the phenylpropanoid pathway has been extensively investigated and the latest state of knowledge was summarized recently by Rinaldi et al. in 2016 (Rinaldi et al. 2016). Lignin is formed during the lignification of a plant and enables the plant to grow high by giving stiffness to the plant. Lignin is mainly incorporated within the secondary plant cell walls of lignocellulosic plant material. The secondary plant cell wall consists mainly of crystalline cellulose fiber bundles (fibrils) that are covered by hemicellulose and glued by the aromatic mesh of lignin. Lignin is mainly situated between the cellulose microfibrils as "incrusting material" and a schematic structure of lignocellulose was illustrated by Streffer in 2014 (Streffer 2014) in Figure 1.
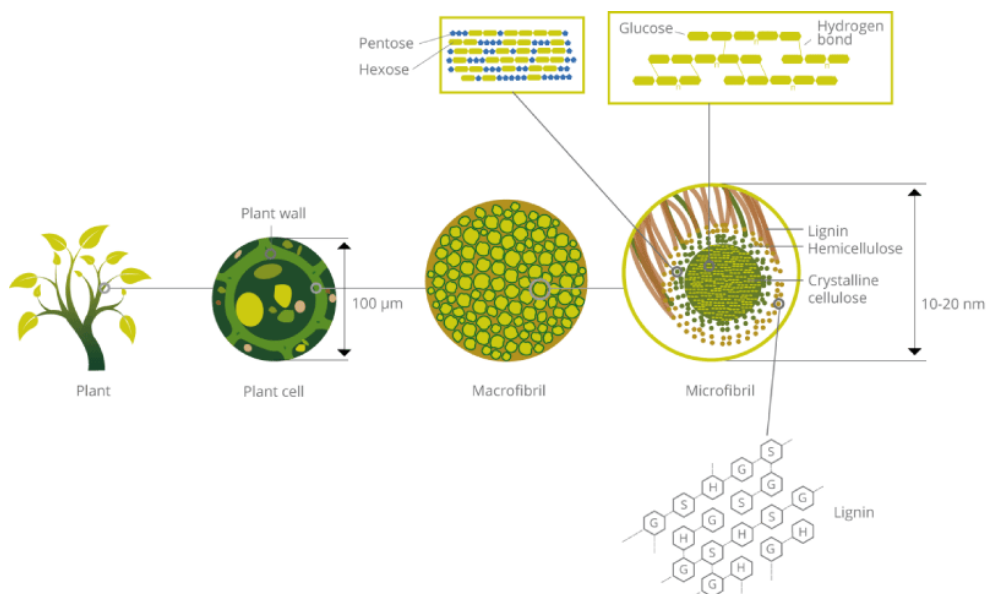

Figure 1: Schematic structure of lignocellulose. The hexagons denote the lignin subunits p-coumaryl alcohol (H), coniferyl alcohol (G) and sinapyl alcohol (S) (Streffer 2014).

Lignocellulose composition

The relative ratios of cellulose, hemicellulose and lignin depend on the plant species. Therefore, lignin contents between zero (cotton) and 40 wt. % (nut shells) are possible in different lignocellulosic materials. Table 1 illustrates compositions of different feedstocks (Menon and Rao 2012).

Table 1: Composition of representative lignocellulosic feedstocks, modified from Menon and Rao (Menon and Rao 2012).

Feedstocks	Carbohydrate composition (% dry wt)		
	Cellulose	Hemicellulose	Lignin
Barley hull	34	36	19
Barley straw	36–43	24–33	6.3–9.8
Bamboo	49–50	18–20	23
Banana waste	13	15	14
Corn cob	32.3–45.6	39.8	6.7–13.9
Corn stover	35.1–39.5	20.7–24.6	11.0–19.1
Cotton	85–95	5–15	0
Cotton stalk	31	11	30
Coffee pulp	33.7–36.9	44.2–47.5	15.6–19.1
Douglas fir	35–48	20–22	15–21
Eucalyptus	45–51	11–18	29
Hardwood stems	40–55	24–40	18–25
Rice straw	29.2–34.7	23–25.9	17–19
Rice husk	28.7–35.6	11.96–29.3	15.4–20
Wheat straw	35–39	22–30	12–16
Wheat bran	10.5–14.8	35.5–39.2	8.3–12.5
Grasses	25–40	25–50	10–30
Newspaper	40–55	24–39	18–30
Sugarcane bagasse	25–45	28–32	15–25
Sugarcane tops	35	32	14
Pine	42–49	13–25	23–29
Poplar wood	45–51	25–28	10–21
Olive tree biomass	25.2	15.8	19.1
Jute fibres	45–53	18–21	21–26
Switchgrass	35–40	25–30	15–20
Grasses	25–40	25–50	10–30
Winter rye	29–30	22–26	16.1
Oilseed rape	27.3	20.5	14.2
Softwood stem	45–50	24–40	18–25
Oat straw	31–35	20–26	10–15
Nut shells	25–30	22–28	30–40
Sorghum straw	32–35	24–27	15–21
Tamarind kernel powder	10–15	55–65	–
Water hyacinth	18.2–22.1	48.7–50.1	3.5–5.4

Lignin composition

The monomeric composition of lignin itself depends on the type of lignocellulosic feedstock. The monomers and their abbreviations are introduced in Figure 2. Lignin in softwood from gymnosperm plants consists mainly of G monomers. Hardwood from angiosperm plants contains lignin that consists of a mixture of S and G monomers. A mixture of H, G and S monomers is the basis of lignin in herbaceous plants.

Broad overviews of analytical methods for the determination of lignin structures are given in literature (Lin and Dence 1992, Hatakeyama and Hatakeyama 2009, Morreel et al. 2010, Lupoi et al. 2015, Constant et al. 2016).
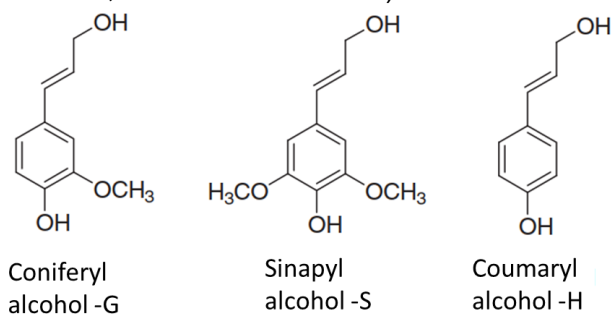
Figure 2: Phenyl propanoid units employed in the biosynthesis of lignin with abbreviations G, S and H (Sannigrahi et al. 2010).

The lignin monomers are linked by different inter-monomer chemical bonds. The most prominent bonds are shown in Figure 3. The proportions of bonds to each other again depend on the type of lignocellulose, however the β-O-4, β-β and β-5 linkages are the most prominent ones (Sannigrahi et al. 2010, Lupoi et al. 2015)
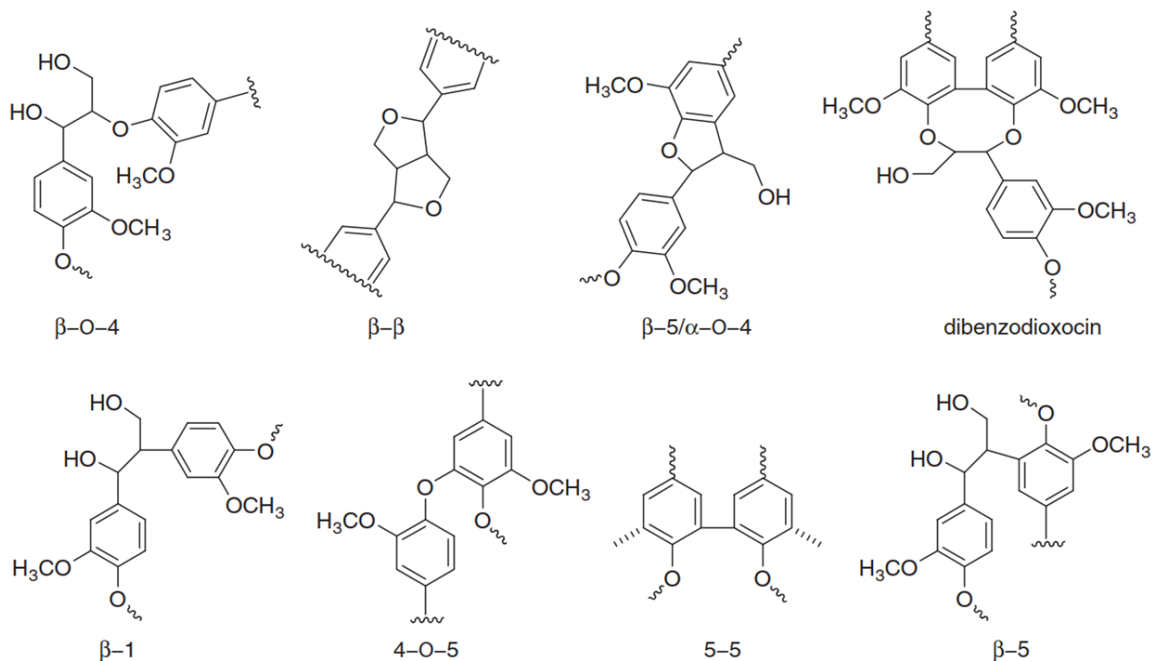
Figure 3: Primary inter-unit linkages in softwood lignin (Sannigrahi et al. 2010).

The molecular mass of native lignin, like it is present in living trees, cannot be determined because the lignin sample has to be prepared and mostly dissolved before applying the typical analytical methods (HPSEC, MS). Native lignin is not soluble (without degradation) and therefore also not measurable with these methods. It is imaginable that the whole plant could contain one big interwoven lignin molecule which would have a mass from grams to tons, depending on the plant. Mostly "milled wood lignin" (MWL) is considered to be the nearest type of prepared (pulped) lignin to native lignin. However, even MWL is far from its native state because it is prepared by ball milling of the wood for many hours until it became a fine powder and then the lignin is extracted with dioxane (kind of organosolv extraction).

2.1.2.   Technical lignins (after pulping process)

Technical lignins are normally categorized according to the isolation procedure and the original plant material (e.g. Norwegian spruce kraft lignin or beech wood ethanol organosolv lignin). To be more specific, even the pulping conditions, like temperature, duration, solvent composition and liquid/wood ratio, should be considered.
This categorization of technical lignins is necessary because each isolation or pulping method affects lignin properties, like molar mass distribution, functional groups, remaining chemical linkages and purity (Hatakeyama and Hatakeyama 2009, Menon and Rao 2012). Lignins from organosolv pulping (OSL) are usually purer, have less ash, sulfur and sugar content and have a higher content of functional groups than Kraft lignin and Lignosulfonates (see Table 2).

The molar mass distribution (MMD) of lignin is an important characteristic property as generally for polymers. The MMD can be measured by Size Exclusion Chromatography (SEC), as described in section 3.2.3.2. A MMD can be condensed into averaged values, as the number-average molar mass (M_n) or weight-average molar mass (M_w).

$$M_n = \frac{\sum M_i \cdot N_i}{N_i} \tag{1}$$

$$M_w = \frac{\sum M_i^2 \cdot N_i}{N_i} \tag{2}$$

Whereby N_i is the number of moles of each polymer species i and M_i is the molar mass of that species i.

According to the literature (Baumberger et al. 2007, Hatakeyama and Hatakeyama 2009) the weight average molar mass (M_w) of technical lignins is in the range of 10^3–10^5 g/mole depending on plant species, processing method, and also measuring method. Molecular mass distribution depends on plant species, isolation methods, and measuring conditions. Lignin molecules in solution are approximately spherical particles. They are slightly solvated with solvent.
Constant et al. performed in 2016 a comparative study of different technical lignins and the results are summarized in Table 2 (Constant et al. 2016). The first row of the table indicates the pulping methods (Induline Kraft: alkaline sulfide (Kraft) pulping, Soda P1000: alkaline pulping, Alcell: auto-catalyzed ethanol-water pulping, OS: acidified ethanol-water pulping) and the second row the type of lignocellulose.

Table 2: Summary of compositional and structural characteristics of six technical lignins taken from Constant et al. (Constant et al. 2016). (Pyro-GC-MS: gas chromatography and mass spectrometry of pyrolysis gas, HSQC and P NMR: heteronuclear single quantum coherence and phosphor nuclear magnetic resonance spectrometry, SEC: size exclusion chromatography, Mw: weight average molar mass, PD: polydispersity)

		Indulin Kraft	Soda P1000	Alcell	OS-W	OS-P	OS-S
		Softwood	Straw/grass	Mixed hardwood	Wheat straw	Poplar	Spruce
Composition/ elemental analysis	Ash content (wt%)	2.6	2.5	None/very low	None/very low	None/very low	None/very low
	Sulphur content (wt%)	1.7	1.0	None	0.1	None	None
	Other main minerals	Na, K	Na, K	Ca	—	—	—
	Carbohydrate content	Intermediate	High	Low	Low	Low	Intermediate
Pyro-GC-MS			High fatty acid content		High fatty acid contents		
HSQC NMR	General structure	All technical lignins are highly condensed, few ether linkages remaining					
	Total ether linkages (per 100 Ar units)	7.4	4.1	8.9	8.9	3.0	3.5
				β-O-4 > β–β	β-O-4 ≈ β-5	β-5 > β–β	Almost exclusively β-5
		Mainly β-O-4	Mainly β-O-4	Very low in β-5	Very low in β–β	Very low in β-O-4	Very low in β-O-4 and β–β
	Aromatic composition	Exclusively G	S and G	S and G	S and G	S and G	Exclusively G
	S/G/H ratio	0.00/0.97/0.03	0.50/0.39/0.11	0.63/0.37/0.00	0.39/0.59/0.03	0.53/0.47/0.00	0.00/1.00/0.00
	Other components		Ferulates p-Coumarates		Ferulates Tricin p-Coumarates	p-Hydroxy benzoates	
	Stilbenes	✓	×	✓	✓	×	✓
	Furfural units	×	×	✓	✓	✓	✓
^{31}P NMR	General structure	5-Substituted OH signals suggest a high degree of condensation					
		High ratios of phenolic OH/aliphatic OH supports extensive phenol ether cleavage during pulping					
	Specific OH	Highest ratio of aliphatic to phenolic OH groups	High in carboxylic acids		Tricin units detected		
SEC (method D)	M_w (g mol^{-1})	4290	3270	2580	1960	2180	2030
	PD	8.1	5.2	4.3	4.4	3.8	4.9

2.1.3. Lignin utilization possibilities

The development of processes for the utilization of lignin as renewable resource in various products is of great importance for the successful implementation of a lignocellulose biorefinery. In the following section, some important developments in the research field of lignin utilization are introduced that draw an optimistic picture for future lignin products.

In several review articles (Holladay et al. 2007, Ayyachamy et al. 2013), it was concluded that lignins have been proven to elicit a number of health benefits, e.g. anti-inflammatory, anti-carcinogenic, antimicrobial, prebiotic and antioxidant. In addition, lignins have been widely utilized in polymeric materials, carbon fibers, fuels, construction and agriculture. The review of Beisl et al. (Beisl et al. 2017) gives a broad overview of production and utilization possibilities of lignin nanoparticles.

Hu's publication (Hu 2002) covers developments in chemical modification and utilization of lignin. Opportunities and new findings on the use of lignin as a component of polymeric materials such as starch films, conducting polymers, polyurethanes and

thermoplastics, and as a key building block to make carbon fibers, soil conditioners, nitrogenous fertilizers, and pulping catalysts are discussed.

The group of Sixta at the Aalto University in Finland (Ma et al. 2015) produced composite fibers from ionic liquid solutions by dry-jet wet spinning that contained cellulose and up to 50 wt.% lignin. Eucalyptus dissolving pulp and organosolv lignin blends in different ratios were dissolved in the ionic liquid 1,5-diazabicyclo[4.3.0]non-5-enium acetate [DBNH][OAc] to prepare a spinning dope from which composite fibers were spun successfully. Finally, the composite fiber was found to be a potential raw material for textile manufacturing and as a precursor for carbon fiber production.

According to the review of Liu et al. (Liu et al. 2015), thermochemical conversion, including pyrolysis and hydrothermal carbonization, is a well-recognized process for the valorization of lignin to chemicals and functional materials. The review clearly shows that a rational design of the functionalized lignin-based materials could lead to numerous hybrid functional carbon materials with various applications toward a green and sustainable future.

The production of carbon fibers from lignin was and will be of large interest in order to reduce the costs for the light-weight and high-strength material (Mainka et al. 2015). Physical and chemical phenomena during the carbon fiber production from lignin have been investigated in order to find ways for further improvement of the fiber quality (Mainka et al. 2015).

Carbon micro-particles have been produced from organosolv lignin at 2000 °C under an argon atmosphere following oxidative thermos-stabilization at 250 °C by Köhnke et al. in 2016 (Köhnke et al. 2016). Poly-lactic acid filled with various amounts of lignin-derived carbon micro-particles showed higher tensile stiffness increasing with particle load, whereas strength and extensibility decreased. Electric conductivity was measured at filler loads equal to and greater than 25% w/w.

According to Nandanwar et al. (Nandanwar R.A. 2012), lignin has a greater potential to be a major source of polymer based products for different industries which includes fillers, adhesives, binders and coatings. Progress has already been made in few fields such as lignin graft copolymers, lignin thermosetting polymers (Figure 4) and lignin-elastomer- blends and continued research in these areas will no doubt yield an increased demand for lignin and lignin products in the future.

Figure 4: Bottle opener consisting of an experimental lignin-cellulose composite manufactured by injection molding in a joint project of Fraunhofer CBP, Tecnaro GmbH, FWS GmbH and MPI Magdeburg.

Kühnel et al. firstly synthesized lignin-based polyether polyols by oxyalkylation with cyclic organic carbonates using five lignins from three different sources (softwood, hardwood and annual plants) and three different pulping processes (Kraft, Soda and Organosolv) (Kühnel et al. 2017). This oxyalkylation procedure seems to be a universal method contributing to enhanced applicability of various lignins as polyols for the synthesis of polyurethanes and polyesters.

The review of Zakzeski et al. gives a broad overview of catalytic systems that have been already tested in order to synthesize valuable chemicals from numerous lignins and points out some parallels between the development of petrochemical refinery in the beginning of 20th century and biorefinery in the 21st century (Zakzeski et al. 2010). It is concluded that by the development of bio-specialized catalysts and the integration of material and energy streams, according to the example of a petrochemical refinery, the development of an economic viable and sustainable biorefinery will be successful.

Zhang et al. reviewed thermochemical, chemical pulping, and bleaching methods for production of polymeric and monomeric chemicals from lignin products (Zhang et al. 2011). It was concluded that peroxyacid chemistry for phenol and ring-opened products looks most promising.

2.2. Lignocellulose biorefinery concept

Lignocellulosic biorefineries are supposed to supply a bunch of renewable platform chemicals and materials like cellulose, hemicellulose, lignin and extractives in the future (Kamm et al. 2005). Figure 5 illustrates possible production chains from lignocellulose to exemplary products.
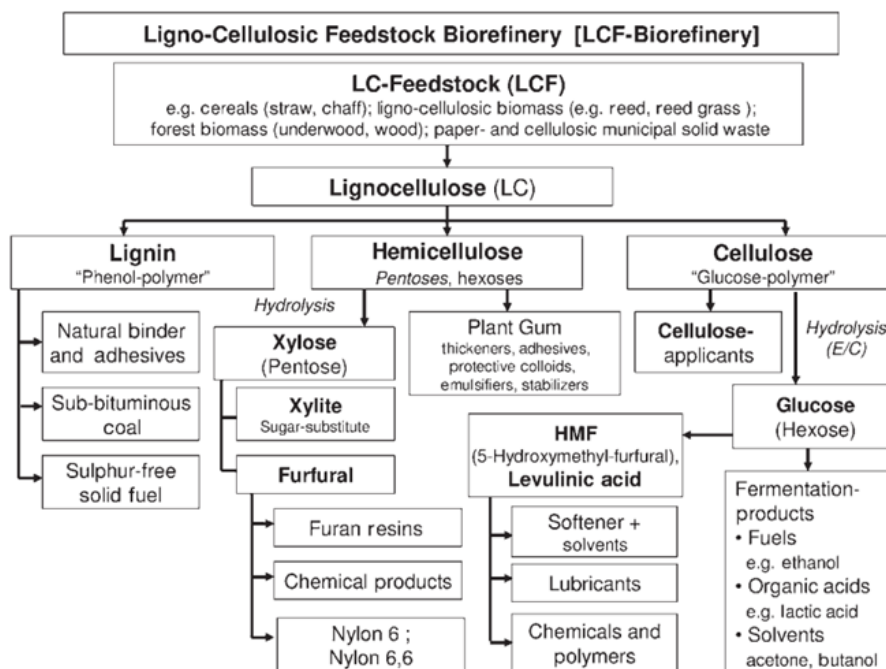

Figure 5: Examples of products of a lignocellulose biorefinery (Kamm et al. 2005).

Several research programs have been started in Germany and other countries to develop a lignocellulose-based value chain (FNR 2009, Bundesregierung 2010, FNR 2012). As part of these actions a pilot plant for the fractionation of lignocellulose was constructed at the Fraunhofer Center for Chemical-Biotechnological Processes (Fh CBP) to prepare the process for the next scale-up (demonstration plant) (Michels and Wagemann 2010). The setup of this pilot plant for lignocellulose organosolv fractionation is illustrated in Figure 6. The plant mainly consists of different modules for pulping, lignin separation and solvent recycling; fiber washing and dewatering; and xylose solution preparation.
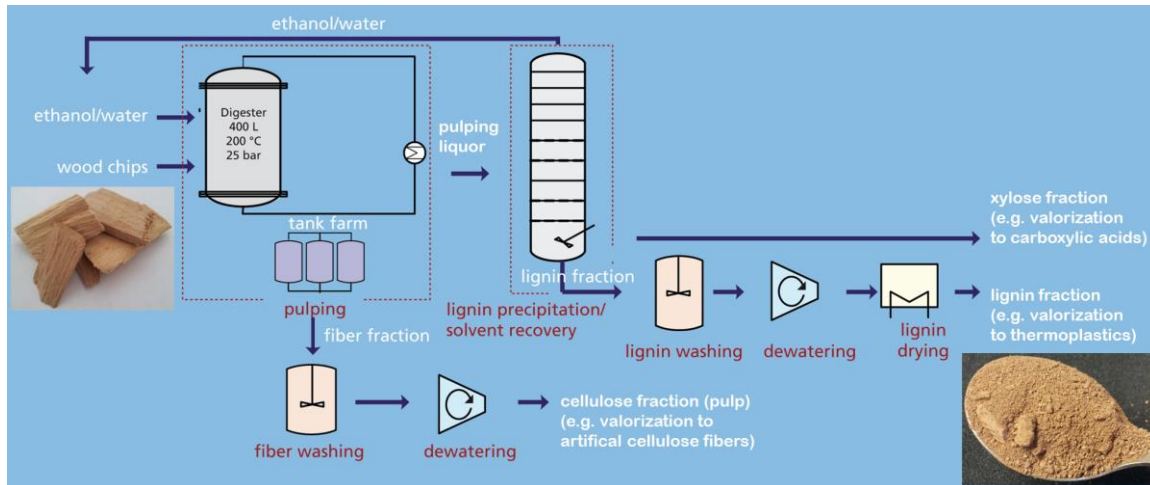

Figure 6: Process flow sheet of the lignocellulosic biorefinery pilot plant at the Fraunhofer CBP (modified from Fraunhofer CBP webpage https://www.cbp.fraunhofer.de/).

Lignocellulosic biomass has to be fractionated to the greatest possible extent into its constituents without uncontrolled degradation or formation of valueless residuals. The fractionation process has to be efficient in terms of energy and chemical consumption, as well as simple as possible, in terms of the required processing techniques, in order to keep the investment and operational costs on a level where the products can be sold below the prices of conventional fossil-based resources (Laure et al. 2014). This is a demanding task because the spectrum of lignocellulose is very heterogeneous in its composition and structure. The main constituents of lignocellulose cellulose, hemicellulose and lignin grow to a complex interwoven structure that has different properties depending on the species and growing-environment (Mansfield et al. 2012). Furthermore, the lignin composition depends on the plant family (e.g. hardwood, softwood or annual weeds), and even the species (e.g. beech, poplar or eucalyptus) and is described in more detail in section 2.1.1. The fractionation process should be flexible enough to perform efficient pulping even when the biomass input is diverse and demands custom operation conditions.

As mentioned above an array of pulping processes has been developed in the last century for this purpose (Menon and Rao 2012). Pulping technologies can be divided into mechanical, physico-chemical, chemical and biological treatments. Promising chemical pulping processes, such as Organosolv, use organic solvents like ethanol in a mixture with acidified water to break down the biomass structure and recover relatively pure fractions of cellulose, lignin and hemicellulose (Zhang et al. 2016). A broad overview about organic solvent pulping is given in Muurinen`s doctoral thesis (Muurinen 2000). Besides short–chain aliphatic alcohols such as ethanol, ketones

(acetone), organic acids (acetic acid) and esters (ethyl acetate) are also suitable for Organosolv pulping. The organic solvents can be recycled and reused in the pulping process.

A more detailed description of the pulping process performed in the context of this work is given in the next section.

2.2.1.   Ethanol Organosolv pulping

The ethanol organosolv (EOS) fractionation of lignocellulosic material has been known since the late 19th century (Klason 1893) and was first patented in the early 20th century (Tayenthal and Kleinert 1932). Meanwhile, a lot of patents for EOS pulping and downstream technologies have been applied (Kleinert 1971, Diebold et al. 1978, Pye 2002, Fackler et al. 2012, Berlin et al. 2013, Hallberg et al. 2013).

Generally, different types of lignocellulose (LC), like hardwood, softwood, straw and grasses can be fractionated by EOS pulping and the pulping conditions have to be adjusted for each type in order to produce fractions of the desired quality. The LC material, normally sized in the range of some centimeters, is mixed with the solvent mixture in a weight ratio between 1:3 and 1:10 (dry LC: solvent). The pulping solvent consists of ethanol, water and an acid. The ethanol mass percentage ranges typically between 40 and 80 %. The acid content ranges normally from 0 to 10 wt. % on dry wood mass, depending on the acid. Sulfuric acid is most commonly used but also organic and other inorganic acids can be used. The mixture is then usually heated to about 170 ± 30 °C in a pressure reactor at pressures around 20 bars for 90 ± 30 minutes. The heating-up and constant temperature phases can be summarized to an H-factor, which is used in pulping industry as a measure for the cooking intensity (Vroom 1957). An H-factor between 1000 and 1500 is typical. During the pulping process, the liquor may be circulated through the LC material bed (lower liquid content) or the LC material is dispersed by a stirrer (higher liquid content).

Ethanol Organosolv pulping conditions in combination with various techniques have been widely investigated (Tjeerdsma et al. 1994, Papatheofanous et al. 1995, Pan et al. 2005, Berlin et al. 2007, Iakovlev et al. 2011, Garcia et al. 2012, Hideno et al. 2012, Wildschut et al. 2013, Schwiderski and Kruse 2015).

During pulping, mainly α-ether and β-ether linkages of the native lignin molecule are cleaved (Mcdonough 1992) and smaller lignin molecules emerge. Additionally, chemical bonds between lignin, hemicellulose and cellulose are also cleaved by hydrolysis reactions under acidic conditions. The lignin molecule fragments are soluble in the ethanol/water solvent. The weight average molecular mass (MM_w) of lignin fragments is between 1000 and 5000 g/mole (Baumberger et al. 2007). The MM_w, functional groups content and degree of condensation depend on the native lignin structure and the pulping conditions (e.g. temperature, duration, acidic catalyst concentration and solvent composition). The more intense the pulping conditions (e.g. temperature and duration), the less functional groups remain, the more condensed the lignin is and the smaller the obtained lignin molecules are. However, larger lignin molecules can be formed by condensation reactions under extreme pulping conditions (Xu et al. 2007).

Depending on the process design, after pulping the spent liquor is replaced by hot washing liquor with the same ethanol/water composition. Subsequently, the fibers and liquor are simply separated by filtration, or filtration is done without prior washing.

However it should be noted that washing leads to better removal of lignin from pulp fibers (Ni and Van Heiningen 1994).

Consequently, the cellulose fraction remains as a fibrous compound, while lignin and hemicellulose remain dissolved in the pulping liquor (spent + washing liquor). The ethanol has to be recycled to the cooking process. Lignin and hemicellulose sugars have to be separated for further processing. The separation of these three constituents can be performed in the lignin precipitation process, whereby the ethanol is removed by distillation, lignin separates in the solid phase and the sugars remain in aqueous solution. However, the process had to be optimized within this work for reasons that will be described in the following section.

To summarize, the organic solvent pretreatment is a promising method for the fractionation of lignocellulosic biomass because of its inherent advantages, like high purity lignin production and solvent recycling (Zhang et al., 2015). Additionally, EOS pulping is a proven alternative process to produce pulp, lignin and furfural in a good quality that can be used in various applications, as has been shown during an 18 month period of operation of an Alcell™ process demonstration plant in Canada (Pye and Lora 1991). The main reasons for the shut-down of the Alcell™ demonstration plant were ethanol losses within the process and external economic factors (Acton 2013).

2.2.2.   Separation of lignin and solvent from Organosolv pulping liquors

All lignin separation methods have in common that the solvent composition is changed to compositions of lower lignin solubility or the lignin concentration is increased by selective solvent removal (membrane processes). In the following section the lignin separation techniques reported in literature are introduced.

Evaporation-precipitation

OS lignin is practically insoluble in water and therefore decreasing the organic solvent content is a good way to separate a lignin-rich phase from the pulping liquor. If OS pulping is performed with a low-boiling organic solvent (e.g. ethanol or acetone) and water, the most obvious method to reduce the organic solvent content is evaporation or rectification, whereby most of the organic solvent can be recycled simultaneously. The first patents regarding OS fractionation of lignocellulose claimed this kind of lignin separation method (Tayenthal and Kleinert 1932, Kleinert 1971, Diebold et al. 1978). Unfortunately, the separating lignin phase tends to be sticky and forms undesired incrustations in the apparatus (Michels et al. 2014).

Within the German "Lignocellulose-Bioraffinerie" project evaporation-precipitation of lignin from ethanol organosolv pulping liquors has been performed in lab and mini-plant setups (Michels et al. 2014). The lab plant setup consisted of a rotary evaporator equipped with a tube to feed pulping liquor during the evaporation process (fed-batch). Evaporation-precipitation experiments have been carried out at pressures (temperatures) of 250 mbar (64-66 °C) and 90 mbar (44-46 °C). The ethanol content in the dispersion during the fed-batch process was not reported but according to the pressure and corresponding temperature reported, the ethanol content must have been close to zero. It was found that a pH value ≤ 2 of the pulping liquor helps to prevent the formation of lignin incrustations and supports the flocculation of lignin particles in the resulting dispersion. The lignin particles could be separated from the dispersion by

centrifugation at 3000 g for 15 to 120 seconds. A continuous operating mini-plant including evaporation and was not described in detail.

Dilution-precipitation

In order to prevent these lignin incrustations, the pulping liquor can be diluted with an antisolvent to lower the organic solvent concentration. The antisolvent is mostly water which can be acidified, cold and/or warm (Thring et al. 1990). This kind of lignin separation method is the most reported in literature because it is easy to conduct. However, the pulping liquor mass is at least tripled by the addition of water or another aqueous stream and therefore substantial larger amounts of lignin dispersion and liquor have to be processed downstream. The amount of lignin dispersion after dilution-precipitation can be distinctly decreased (by ca. 50 wt. %) by prior pre-concentration of the pulping liquor by flashing before mixing with the dilutant (Botello et al. 1999, Fernando et al. 2010).

Another challenge of dilution-precipitation is the bad filterability of the large amounts of lignin dispersion because the primary lignin particles usually have diameters between 0.5 and 2 µm. However, the filterability of diluted lignin dispersion can be improved by optimized dilution profiles and low pH values (Michels et al. 2014) that allow lignin particle agglomeration but also increase the risk of incrustations (Thring et al. 1990).

Average filter cake resistances around 10^{13} m^{-1} (moderate filterability) could be achieved with the optimization of water to liquor ratio, temperature, mixing, pH value and timing within the German "Lignocellulose-Bioraffinerie" project (Michels et al. 2014). A combination of water dilution with flotation by spraying the pulping liquor in cold acidified water in order to decrease the filtration efforts was reported by some authors (Macfarlane et al. 2009, Huijgen et al. 2010).

Process patents that claim lignin separation by dilution mostly describe the usage of internal recycled aqueous streams to dilute the pulping liquor, which has been flashed upstream (Pye 2002, Berlin et al. 2013, Hallberg et al. 2013).

A recent patent claims a lignin separation process by dilution or solvent evaporation that applies a solid additive (e.g. gypsum) that combines with the lignin which promotes separation (Retsina et al. 2014).

In an early work, Schuerch used ligroin (light petrol) as an antisolvent instead of water to precipitate lignin from chloroform-ethanol OS pulping liquor (Schuerch 1952).

Membrane separation

Ultrafiltration of OS pulping liquor in order to fractionate the lignin molecules in groups of different molar mass has been investigated by Alriols et al. in 2010 (Alriols et al. 2010). The different fractions were diluted with acidified water to precipitate the lignin as solid fractions. The solid lignin produced had different molar masses and slightly different group functionalities.

Weinwurm et al. (Weinwurm et al. 2014, Weinwurm et al. 2016) investigated recently the influence of pre-concentration of ethanol OS pulping liquor by nanofiltration and evaporation prior to dilution-precipitation on the process economics and concluded that pre-concentration by nanofiltration reduces the energy and chemical demand more than pre-concentration by evaporation.

A recent patent claims a membrane separation process to yield lignin, sugar and solvent fractions using acetone OS pulping liquor (van Tuel et al. 2016). The lignin from

the resulting pre-concentrated lignin solution is said to be precipitated by any capable technique.

Table 3 gives an overview of the methods for lignin separation from organosolv pulping liquors (OS PL) that have been mentioned before.

Table 3: Methods for lignin separation from organosolv pulping liquors (OS PL) reported in literature (the order of the list is no ranking and also not intended to be systematic).

OS lignin separation method	pulping liquor (PL) and specific conditions	References
flashing + (multieffect) solvent evaporation at reduced pressure	general and preferred ethanol OS PL	Tayenthal and Kleinert 1932, Kleinert 1971, Diebold et al. 1978
flashing + dilution with aqueous process stream	general OS PL	Hallberg et al. 2013, Pye 2002, Berlin et al. 2013
fed-batch vacuum distillation	acidic ethanol-water PL, pH 2	Michels et al. 2014
dilution + flotation in fresh water (cold)	acetone-water PL	Huijgen, Reith and den Uil 2010, Macfarlane et al. 2009
dilution with fresh water	acidic ethanol-water PL, pH 2, 3:1 water:liquor	Michels et al. 2014
flashing + dilution with fresh water (acidified)	autocatalyzed methanol and ethanol OS PL	Botello et al. 1999, Fernando, Vallejos and Area 2010
dilution with fresh water (acidified and warm 50-60 °C)	ethylen glycol OS PL , hot filtration (100 °C)	Thring et al. 1990
dilution with ligroin (petroleum C7-C8 fraction)	HCl catalyzed chloroform-ethanol OS PL	Schuerch 1952
dilution or evaporation of PL and solid additive that combines with lignin	SO_2 catalyzed OS PL	Retsina et al. 2014
ultrafiltration size fractionation + dilution with aqueous process stream	autocatalyzed ethanol OS PL	Alriols et al. 2010
pre-concentration by evaporation or nanofiltration + dilution with acid water	autocatalyzed ethanol OS PL	Weinwurm et al. 2014, Weinwurm et al. 2016

All methods have their advantages and drawbacks; however, the concept of pre-concentration by membrane filtration and subsequent dilution seems to be the most promising lignin separation method yet because the amount of dilutant needed is

distinctly less, incrustations have not been reported and the filterability of the resulting dispersion can be optimized by a suitable dilution profile. Nevertheless, the membrane performance stability seems to be a critical point.

2.3. Thermodynamic properties of lignin

In this section important thermodynamic properties of lignin that are relevant for this work are introduced and previous works in this field reported in literature are discussed. These properties are the basis for the design of the solid-liquid phase separation process investigated in this work.

2.3.1. Solubility behavior of lignins

The semi-quantitative solubility of lignins in different solvents has been already investigated since many years. In the following part some previous works are listed.

Junker determined the solubility of spruce dioxane lignin in sodium hydroxide solutions with different pH values at room temperature (Junker 1941). Lignin dispersion with 0.1224 g lignin/ml was mixed with NaOH solution and sporadically shaked for 1 to 20 hours, filtered and the lignin content in the solvent was measured by light absorption.

Schuerch investigated the properties of various solvents and their relation to the solubility, swelling (solvation), isolation and fractionation of lignin (Schuerch 1952). The ability of solvents to dissolve or swell a variety of isolated lignins increases as the hydrogen-bonding capacities of the solvents increase and as their solubility parameters (according to Hildebrand) approach a value of around eleven.

Ni and Hu measured the solubility of Alcell™ lignin in ethanol/water mixtures at room temperature (20g and 40g lignin/l solvent mixed for 3 hours in an ultrasonic bath, filtered and measured by light absorption at 280 nm) and found the maximum solubility of 18.6 and 36 g/l, depending on the original mass of lignin dispersed in the solvent, in a mixture of about 80 wt. % ethanol/water (Ni and Hu 1995). Fractionated dissolution of small lignin molecules from the assortment of different sized lignin molecules is assumed because similar mass fractions of lignin were dissolved at different original dispersed mass fractions of lignin in the solvent. Eventually, only the better soluble small molecule fraction was dissolved from the bimodal molecular mass distribution and the less soluble larger molecule fraction remained as solid residue.

Thring et al. qualitatively determined the solubility of Alcell™ lignin in numerous organic solvents (0.01g lignin/ml solvent shaked and dissolution visually estimated) and conducted a fractionation of Alcell™ lignin into fractions with particularly different group functionalities by sequential solvent extraction (Thring et al. 1996). The results demonstrated the heterogeneity of the lignin.

Pu et al. investigated the solubility of softwood kraft lignin in some ionic liquids (Pu et al. 2007). Samples of the ionic liquid (0.50 g) were mixed with weighed lignin samples and

if needed, were heated in an oven for accelerated dissolution. They found the highest solubility of 344 g/l in 1,3-dimethylimidazolium methyl sulfate ([mmim][MeSO$_4$]) at 50°C.

Cybulska et al. measured isothermal solubilities of lignin isolated from three herbaceous plants in different organic solvents and found very low solubilities (e.g. prairie cord grass lignin in ethanol at 40 °C, 0.035 wt. %) (Cybulska et al. 2012). In fact, all solubility values are lower than 0.5 g/l, which seems to be very low and therefore they are not listed in the table below. Solutions were prepared in 100 mL volumetric flasks, using 0.05 g of each lignin type. The solutions were kept at 40 °C with constant agitation for 48 h. Subsequently, the solutions were filtered through paper filter (Whatman No. 1), and the solid residue was air dried and weighed. The percent solubility of the lignin sample in a particular solvent was based on the comparison between the initial sample weight and remaining solid residue after the analysis.

The Hansen solubility parameters of polyether sulfone, lignin, and bitumen have been calculated by an alternative optimization procedure in order to predict solubilities in different solvents (Vebber et al. 2014).

Weinwurm et al. measured a solubility of ca. 2.8 wt. % of ethanol OS lignin in a 60 wt. % ethanol/water mixture by dispersing the lignin in solvent for 40 minutes in an ultrasound bath but mentioned that the duration in bath was probably too short (Weinwurm et al. 2014).

Le et al. investigated the pseudo-ternary phase diagram of lignin, γ-valerolactone and water and therefore was the first author that presented a ternary phase diagram of lignin, solvent and antisolvent (Le et al. 2016). The heterogeneous mixture of polymer fragments of beech wood ethanol OS lignin is treated as one pseudo-compound. Additionally, the Hildebrand solubility parameter of lignin was calculated. The determined phase diagram is predominantly of qualitative character as the complex phase behavior of the system could not completely be elucidated by the applied microscopic analysis method. However, the results show a similar phase behavior and a miscibility gap in the liquid state like the lignin-ethanol-water system investigated in this work, as will be presented in section 5.2.

To give an overview of solubilities of various lignins in a range of solvents, some data reported in literature have been summarized in Table 4.The table is surely not complete but the aim here is to give a brief overview of work that has been already done in this field. It is noteworthy at this point that a part of the announced solubility values are probably only qualitative and have not been measured at the thermodynamic equilibrium because samples have not been sufficiently mixed, lignin dissolved completely or the equilibration time was too short.

Table 4: Solubility of various lignins in different solvents or solvent mixtures found in literature. Values without unit are qualitative ones. Solubility quality levels: 0=insoluble (solvent not colored+solid residue), 1=slightly soluble (solvent slightly colored+solid residue), 2=moderately soluble (solvent deep colored+solid residue), 3=soluble (no solid residue).

Lignin and Reference / Solvent	Dioxane OS lignin from spruce @ 23 °C, (Junker 1941)	EtOH OS lignin from maple @ 23 °C, (Schuerch 1952)	Alcell (EtOH OS) lignin @ 23 °C, (Ni and Hu 1995)	Alcell (EtOH OS) lignin from birch (15%), maple (50%) and poplar (35%) @ 23 °C, (Thring et al. 1996)	Kraft lignin from softwood, (Pu et al. 2007)	Ethanol OS lignin from beech, (Le et al. 2016)
Hexane		0		0		
Carbon tetrachloride		0		0		
Carbon disulfide		0				
Water		0		0		
Benzene		1		1		
Ethylether		1		1		
Toluene				1		
n-propanol				1		
2-Octanol				1		
Nonanol				1		
Hexanol				1.5		
Acetone		3		2		
Ethylene glycol		3		2		
Ethylacetate				2		
Iso-propylalcohol				2		
Methanol				2		
Methylene chloride				2		
1-Butanol				2		
Chloroform		2		3		
Dioxane		2		3		
Tetrahydrofuran				3		
Pyridine		3				
2-Methoxyethanol		3				
100 % Ethanol		2		2		
9.5 wt. % ethanol/water			1.14 g/l			
28.5 wt. % ethanol/water			4.58 g/l			
38 wt. % ethanol/water			8.95 g/l			
47.5 wt. % ethanol/water			13.82 g/l			
57 wt. % ethanol/water			16.79 g/l			
68.5 wt. % ethanol/water			18.02 g/l			
71.3 wt. % ethanol/water			18.67 g/l			
85 wt. % ethanol/water			17.78 g/l			
95 wt. % ethanol/water			16.65 g/l			
NaOH in water pH 11-12	ca. 0.94 g/l					
[mmim][MeSO$_4$] 25/50 °C					74.2 / 344 g/l	
[hmim][CF$_3$SO$_3$] 50/70 °C					<10 / 275 g/l	
[bmim][MeSO$_4$] 25/50 °C					61.8 / 312 g/l	
[bmim]Cl 75 °C					13.9 g/l	
[bmim]Br 75 °C					17.5 g/l	
[bmim][PF$_6$] 70–120 °C					0	
[bm 2 im][BF$_4$] 70–100 °C					14.5 g/l	
[bmpy][PF$_6$] 70–120 °C					0	
γ-valerolactone 21 °C						ca. 500 g/l

2.3.2.   Glass transition, softening and solvation

According to one of the most recent thermodynamic theory models (locally correlated lattice LCL model) for glass transitions introduced by White and Lipson in 2016 (White and Lipson 2016), the transition of a solid amorphous glass to a liquid happens when the free volume (gray + white areas in the sub-figure in the lower-right corner of Figure 7) between the hard core polymer chain segments (black areas in the sub-figure in the lower-right corner of Figure 7) exceeds a specific fraction while heated. This specific free volume fraction border is a linear function of the temperature (black line in Figure 7) and indicates the minimal free volume in any liquid polymer matrix that is necessary to allow the molecules to move relative to each other (to stay liquid) at a given temperature. The free volume fraction of a specific polymer is also a function of temperature (thermal expansion coefficient). The free volume-temperature function of the polymer (red line in Figure 7) crosses the "universal" border (black line) at the glass transition temperature of a polymer (shown for the example of Polystyrene PS).
This theory (White and Lipson 2016) was evaluated for 51 polymers (black dots around black line in Figure 7).
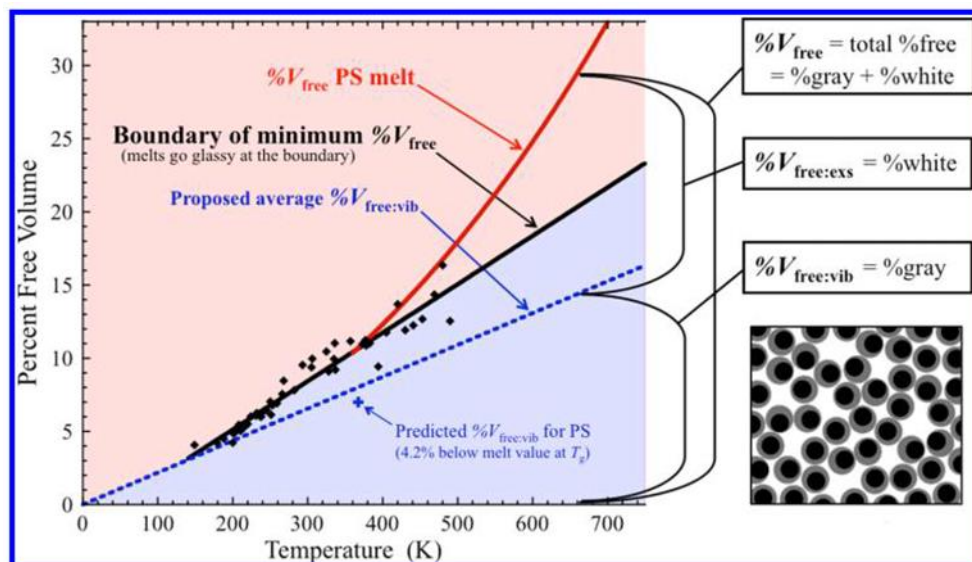

Figure 7: Plot of the percent free volume (%V_{free}) of a polymer against temperature adapted from White and Lipson (White and Lipson 2016). Boundary of minimum total %V_{free} (black line) depicted together with a proposed location for %$V_{free:vib}$ (dashed blue line) and a corresponding quantification of excess free volume, %$V_{free:exs}$. The points mark total %V_{free} at the experimental T_g for each of the 51 polymers in the sample set. The red curve shows an example of a melt curve, %$V_{free}(T)$, the total percent free volume as a function of T for the case of the Polystyrene (PS) melt; the point where the %V_{free} (T) curve intersects the boundary is a prediction for (and is close to) where PS becomes glassy.

Consequently, the swelling (solvation) of a polymer by small molecular solvents (e.g. water, ethanol) decreases the glass transition temperature because the free volume between the polymers is increased by the solvents or plasticizers (Williams et al. 1955). Goring already observed and measured the softening temperatures of different lignin and wood samples (Goring 1962). Additionally, the decrease in lignin softening temperature by the sorption (= solvation, plasticizing or swelling) with water has been determined. It was also found that the softening temperature difference between water plasticized and dry lignin samples can be approximately calculated by a model postulated in literature (Williams et al. 1955, Kishimoto and Fujita 1958). Blechschmidt

et al. found the glass transition temperatures of different dry and wet woods to be 145 and 115 °C, respectively, independent from the type of wood (spruce, pine, aspen) (Blechschmidt et al. 1986). It is assumed that the measured temperatures correspond to the glass transition of the native lignin.

Hatakeyama measured glass transition temperatures (T_g) of different kinds of lignin (Hatakeyama and Hatakeyama 2005). They found an increase of T_g from 380 to 395 K at an increase of M_w from 2000 to 7500 g/mole for dioxane extracted lignin. It was also reported that T_g of lignin significantly decreases from 425 to 300 K at an increase of methoxyl groups from 15 to 19 %. An increase in acetyl groups in the lignin also lowered the T_g by around 50 K.

The glass transition can be detected as a stepwise change or a kink in heat capacity (DSC), viscosity (TMA), density (TMA) or avg. polymer chain distance (XRD) when measured at different temperatures or during a heating/cooling profile.

It should be pointed out, that amorphous thermoplastics, like lignin, undergo a second order phase transition between their brittle solid (glass) and liquid phases at its glass transition but not "thermodynamically melt" because the glass state characterizes a solidified subcooled liquid. In contrast, crystalline polymers undergo melting as a first order phase transition between crystal and liquid phase by absorbing the lattice energy of the crystal (Gruber 1980).

A thermoplastic gets visibly flowable (deliquesces or phenomenological "melts") above its glass transition temperature. The temperature difference between glass transition and deliquescence, where the polymer is more or less plastic deformable, depends on how wide-meshed and crosslinked the polymer chains are. Wide-meshed and crosslinked polymers, like elastic thermoplastics, have a wider temperature range between glass transition and deliquescence. A polymer matrix of less crosslinked single polymer bundles, like lignin, becomes deliquescent shortly above the glass transition temperature (Hatakeyama and Hatakeyama 2009).

2.4. Formation of particles from polymer-solutions and soft particle interactions

This section introduces the fundamentals of phase separation in a (pseudo-) ternary system with miscibility gap in the liquid phase and (soft) particle interactions (agglomeration) of the evolved dispersed phase. It is anticipated that the lignin-ethanol-water system exhibits a miscibility gap, as presented later in this work (see 5.2.2) and was reported for the lignin/γ-valerolactone/water system (Le et al. 2016).

Phase separations in polymer-solvent-antisolvent systems with a miscibility gap
The separation of a disperse lignin phase from organosolv pulping liquors can be illustrated and simplified in a pseudo-ternary phase diagram (simplified because the pulping liquor actually contains more than three substances). Therefore, the heterogeneous mixture of lignin molecules is simply described as the polymeric pseudo-substance. Water and water-soluble substances (e.g. sugars, sulfuric acid) are described as the aqueous antisolvent (or non-solvent) phase and ethanol represents the solvent phase.

In 2002 Laity et al. (Laity et al. 2002) investigated the phase behavior of cellulose-solvent-antisolvent systems and gave a good overview of possible process routes for polymer coagulation from solutions in isothermal processes, like other authors did before (van de Witte et al. 1996, Wienk et al. 1996).

Figure 8 and the subsequent paragraph that describes the different routes of polymer coagulation have been taken from Laity et al. (Laity et al. 2002).
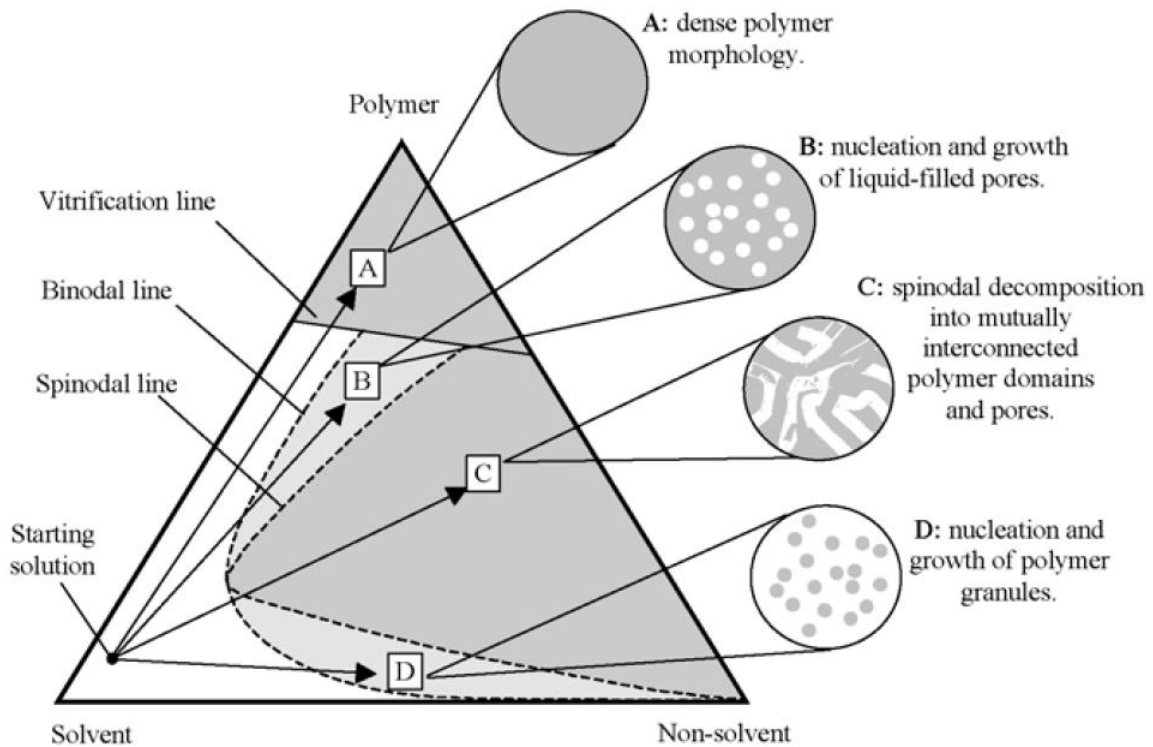

Figure 8: Isothermal phase diagram of a hypothetical polymer, solvent and non-solvent system showing four coagulation routes and representations of the resulting morphologies, taken from Laity et al. (Laity et al. 2002).

"Route A represents vitrification. As the polymer concentration increases, the solution becomes progressively more viscous; chain motion and diffusion slow down and the polymer plus any residual solvent effectively reverts to a glass. This results in a dense morphology with little or no porosity. Vitrification is frequently encountered during 'dry-casting', where a volatile solvent is removed by evaporation. However, it may also occur in non-solvent induced coagulation if the 'outward' diffusion of a solvent is significantly faster than the 'inward' diffusion of a non-solvent.

In example B, phase separation occurs in the metastable region between the binodal and spinodal lines, at higher polymer concentrations than the critical point. Nucleation and growth of non-solvent droplets occurs, which results in the formation of liquid-filled pores in a continuous polymer matrix. This route is common for the immersion-coagulation of many polymer/solvent/non-solvent systems, but can also occur during dry-casting, where a small amount of less volatile non-solvent is included in the polymer solution, along with the more volatile solvent.

In example C, phase separation occurs in the unstable region of the phase diagram, bounded by the spinodal line. Here, polymer-rich and polymer-depleted phases separate initially by the progressive growth of 'concentration waves' of constant

wavelength but increasing amplitude, in a process known as 'spinodal decomposition'. This results in a mutually continuous, interwoven network of polymer domains and pores.

Route D enters the metastable region at a polymer concentration below the critical point. In this case, the nucleation and growth of polymer particles produces a granular morphology.

While the above examples have been presented in terms of isothermal composition changes, which may occur during dry- or wet-casting, similar processes can also be described for thermally induced phase separation. Parallels between vitrification as a result of composition change and melt processing are obvious. However, phase separations in other regions of the phase diagram can also be initiated by temperature changes, i.e., if a composition is miscible at one temperature but immiscible at another. Examples of this include the upper- or lower critical solution behavior of some polymer solutions." (Laity et al. 2002)

The separation of lignin from most organosolv pulping liquors can be described by the latter route D in Figure 8. The solvent concentration is decreased by dilution with the antisolvent or by solvent removal (evaporation). Lignin nucleates as a fine particulate precipitate when the solvent composition enters the metastable region of the phase diagram. Different particle sizes can be obtained by changing the dilution profile (Beisl et al. 2017).

Additionally, the particles interact with each other and agglomeration of the particles can be specifically triggered as will be described in the next paragraph.

Soft particle interaction
A dispersed particle normally exhibits a charged surface. The surface charge is mostly negative and consequently the molecules of the continuous phase arrange according to their surface charge. The molecules will arrange in several layers (electrochemical double layer) around the particle as illustrated in Figure 9. The Nernst potential is the original surface charge of the particle and cannot be directly measured. The Stern potential is the combined potential of the particle surface and a fixed layer (of a thickness of one molecule) on the particle. The Zeta potential is the measurable charge, which results from the combined particle potential, Stern potential and the potential of a molecular layer which sticks to the particle, even when the particle is moving through the continuous phase of the dispersion due to an electric field. Therefore, the Zeta potential can be determined by exposing the particle dispersion to an electric field of known tension in an electrophoresis setup and measuring the velocity of the particles that migrate to one of the electrodes.

Tomas summarizes these fundamentals of particle interaction in his university lecture script (Tomas 2017).
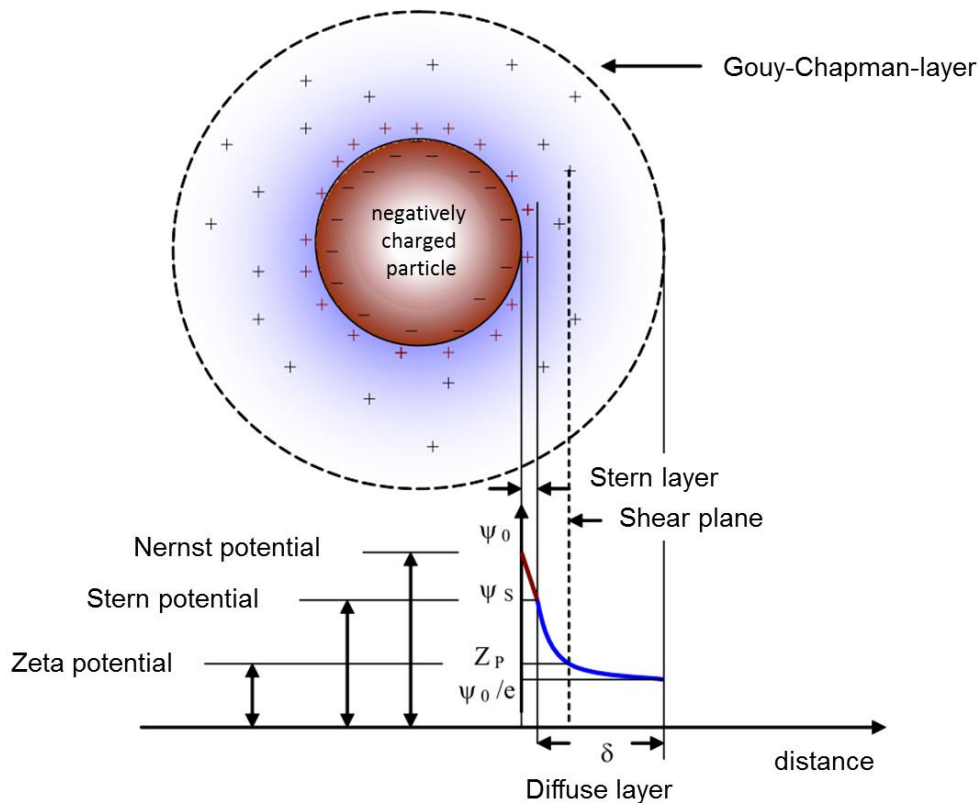
Figure 9: Model of the electrochemical double layer (Tomas 2017).

The Zeta potential is often used as a measure for the stability of dispersions. Thereby, a Zeta potential larger or smaller than ± 30 mV normally means that the dispersed phase will not sediment even after a longer period of time (month) when the particles are small enough (colloidal) because the particles electrostatically repel each other and stay dispersed by Brownian molecular movement. The more the Zeta potential of a dispersion approximates to 0 mV, the more unstable the dispersion becomes because the particles tend to agglomerate. The agglomerated particles then will sediment or float without mixing and the dispersion will break.

The stability of those colloidal dispersed systems is described by the DLVO theory model (Russel et al. 1989).

The electrochemical double layer around a dispersed particle can be affected by metal ions, pH value and polyelectrolytes. Especially positively charged metal ions can compress the electrochemical double layer and approximate the Zeta potential nearer to zero. Thus, the stability of a colloidal dispersion can be tuned by changing the metal ion strength or pH value. Junker investigated the colloid chemical properties of lignin as one of the first and found a Zeta potential of -54 mV for lignin particles (0.1 to 1µm) dispersed in acidified water with a pH of 4.2 (Junker 1941). The lignin particles could be coagulated by addition of alkali and aluminum salts.

Wang and Chen measured the Zeta-potential of lignin dispersions after acid precipitation of alkaline pulping liquor and revealed that higher Zeta potentials and larger particle sizes, that were formed by high molecular weight lignin, accelerated the precipitation (Wang and Chen 2013).

In the case of lignin, a certain degree of agglomeration is desired because the agglomerates expose a better filterability than the very small primary lignin particles

right after precipitation. Thring et al. already described the agglomeration of lignin particles in a dispersion that was prepared by mixing one part of ethylene glycol OS pulping liquor with three parts of 0.05 wt. % HCl in water at 50-60 °C (Thring et al. 1990). The filterability was significantly improved by the agglomeration.

To be more precise, the general term 'agglomeration' is used in this work as a synonym for the sintering of at least superficially softened lignin particles that can also coalesce to a completely new monolithic sphere (drop) if they are soft enough.

Figure 10 illustrates the stages of agglomeration and detachment of two soft particles (Tomas 2006).
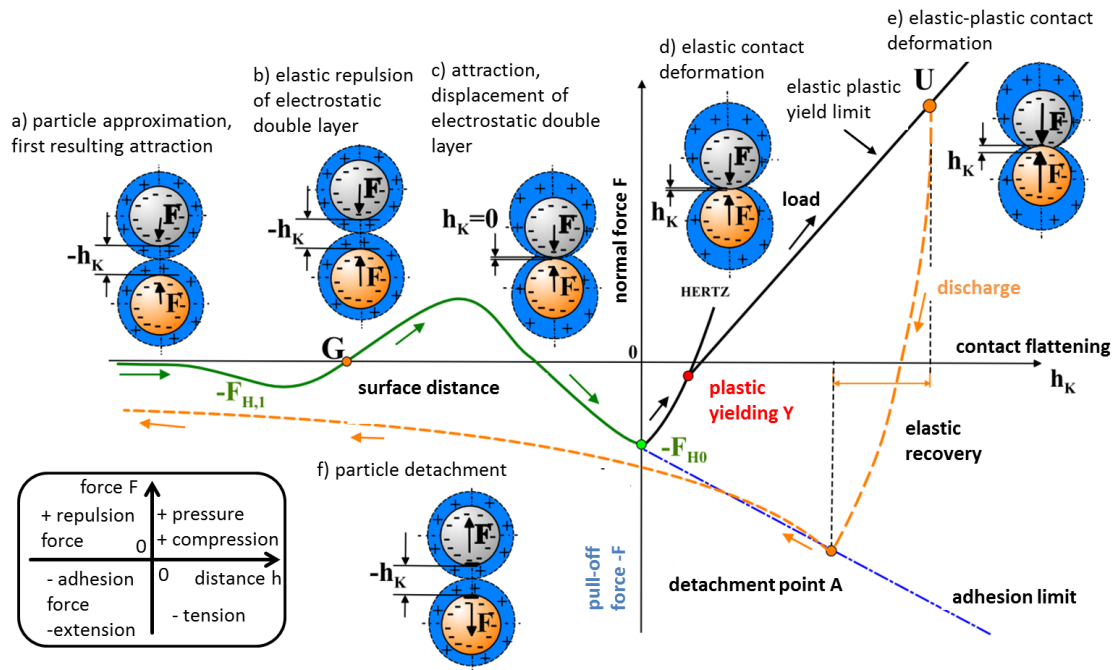
Figure 10: Force-distance diagram of approximation, double layer displacement and contact deformation of soft particles. Translated and redrawn from (Tomas 2006, Tomas 2017).

According to Figure 10, the electrochemical double layer has to be displaced before the particle surfaces touch each other and unite (a-c). Consequently, a thinner or compressed electrochemical layer (Zeta potential near zero) promotes agglomeration. For successful agglomeration the impulse of both particles has to be big enough to displace the electrochemical layer and the contact time has to be sufficient to drain the continuous phase from the space between the flattened contact areas. Additionally the particles have to be soft enough to float fast enough into each other and form a stable bridge between each other (d-e). Zdravkov investigated the interfacial phenomena during drop coalescence in polymeric systems in detail (Zdravkov 2004). If the bridge between the particles is not strong enough or the pull-off forces are too strong, the particles can be detached again from each other (f). Zlokarnik describes how stirring and properties of continuous and dispersed phases influence the degree of dispersion and particle (droplet) size distribution of the dispersed phase (Zlokarnik 1999). The influence of the droplet size on the rheological behavior of emulsions has been investigated by Teipel (Teipel 2002). Beisl et al. gives a review of lignin particle formation and design and shows that a wide range of different sized and shaped lignin particles can be produced at specific process conditions (Beisl et al. 2017).

3. Materials, Methods, Experimental setups and Procedures

In this paragraph the preparation of investigated pulping liquors and lignins is described and the most important analytical methods and experimental procedures are introduced. Further, the experimental setups of the various lab and pilot plants for lignin precipitations are presented.

3.1. Materials

The investigated pulping liquors and lignins from these pulping liquors were produced in the lignocellulose biorefinery pilot plant at Fraunhofer CBP in Leuna (see 2.2). Table 5 gives an overview of the pulping conditions at which the investigated pulping liquors were produced.

Table 5: Overview of the applied pulping conditions to produce the investigated pulping liquors and lignins.

Pulping batch No.	Ligno-cellulose type	Pulping temp. (°C)	Sulfuric acid (wt. % of dry wood)	Ethanol in pulping solvent (wt. %)	Time at pulping temperature (minutes)
K1	beech	170	0.5	50	90
K6	beech	170	0.5	50	90
K8	beech	170	0.5	50	90
K9	beech	170	0.5	50	90
K29	beech	170	0.5	50	90
K37	beech	190	0.5	50	180
K39	beech	180	1	50	180
K40	beech	170	1	50	180
K41	beech	190	1	50	180
K42	beech	180	0	50	180
K43	beech	170	0.5	50	180
K44	beech	190	0	50	180
K45	beech	170	0	50	200
F02	spruce	170	1.1	65	90
K103	beech	170	1	50	90
K128	eucalyptus	170	1	50	90
K138	beech	170	0.8	50	145
K139	beech	170	0.8	50	145

Pulping liquors were produced by fractionation of wood chips by ethanol-water-pulping using a batch process. In each batch, 70 kg (oven dry weight) of air-moist wood chips were pulped in a 540 liter batch digester with forced circulation at 170-190 °C for 100-

180 minutes using a mixture of 50-65 wt. % ethanol and water, respectively, and addition of 0-1.1 wt. % of sulfuric acid (based on oven dry wood (o.d.w.)) as a catalyst. A liquor-to-wood ratio of 3.2:1 (w/w) was applied and the pressure was maintained at around 20 bar using nitrogen gas during pulping and washing. After reaching the desired pulping time, the hot spent liquor was displaced with 380 kg of fresh ethanol-water at a temperature of 80-100 °C using two additional temperature controlled pressure vessels. The fresh ethanol-water mixture was circulated through the pulped wood chips by forced circulation for about 20 min as a washing procedure and subsequently was displaced by 450 kg of cold water using a diaphragm metering pump. The displaced spent liquors from pulping and washing were immediately cooled to 40 °C and mixed to become the pulping liquor.

3.2. Analytical methods

3.2.1. Gravimetrical analysis

For the robust and simple quantitative analysis of the dissolved solids mass fraction (e.g. lignin and sugars) in solution, the solution was dried and the masses of the initial solution and of the dry substance were determined. Drying was carried out usually in a vacuum oven at around 60 °C and down to 10 mbara until the pressure remained constant after turning off the pump, meaning that no further liquid evaporated into the gas phase. The mass fraction of the dry solids was calculated as follows:

$$w_{dry\ solids} = \frac{m_{dry\ solids}}{m_{solution}} \tag{3}$$

The lignin and sugar mass fraction in pulping liquor was determined gravimetrically. The pulping liquor was first dried as described above. The dry solids of the pulping liquor were assumed to be a mixture of water soluble sugars and water insoluble lignin. The dry solids were suspended in water in order to dissolve the water-soluble sugar fraction. The water insoluble solid lignin fraction was dried after filtration as described above. Then the mass fractions of lignin and sugars in the pulping liquors were calculated as follows.

Lignin (or water insolubles) mass fraction:

$$w_L = \frac{m_{lignin}}{m_{solution}} \tag{4}$$

Sugars (or water solubles) mass fraction:

$$w_S = w_{dry\ solids} - w_L \tag{5}$$

3.2.2. Inline process analytics

Besides well-known inline temperature measurement by means of a PT100 electrical resistance probe also analytical probes have been applied for in-process analysis of lignin particle size and shape and composition determination of process streams.

3.2.2.1.   Focused Beam Reflectance Measurement

The Particle Track G400 probe with **F**ocused**B**eam**R**eflectance**M**easurement-Technology (FBRM®) from Mettler Toledo was utilized to monitor the changes of the chord length distribution of lignin particles, agglomerates and droplets during several experiments. The technology is based on the backscattering of a rotating laser beam from particles flowing in front of the probe window (Figure 10). As particles can be scanned at smaller or larger parts than their average size, the detected value is called "chord length" instead of "particle size". The chord length of the scanned particle is calculated from the laser speed and the backscatter time. Usually, several thousand particles are scanned per second, providing robust statistics of the particle chord length distribution (PCLD) and its changes. The obtained PCLD is not identical with the particle size distribution (PSD) derived from a sieve analysis but in this stage of process development it is more important to detect changes in the PCLD to understand the system behavior in the process, than to know the exact particle size.
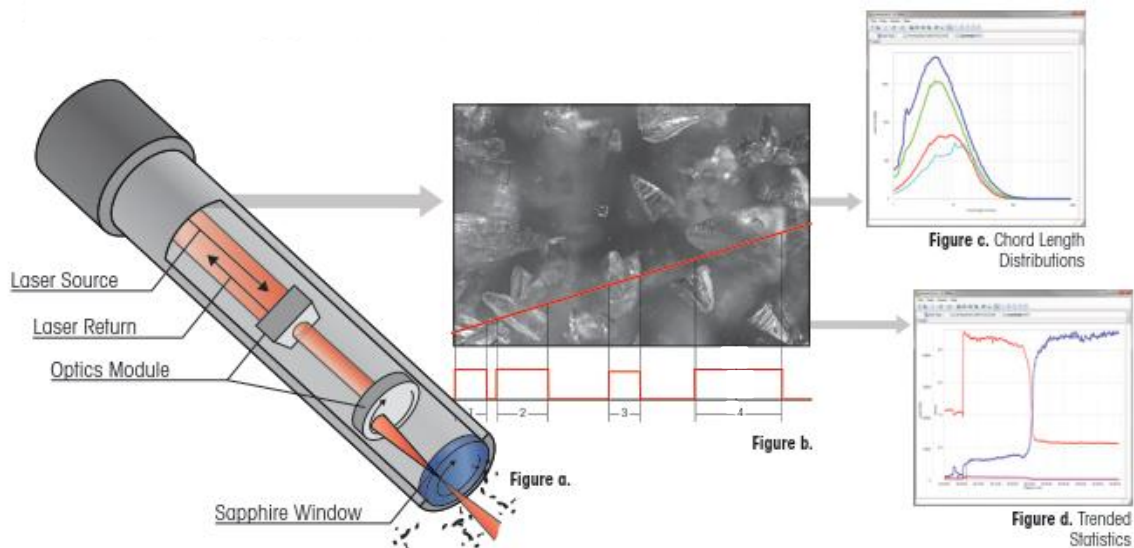
Figure 11: FBRM® technology: Figure a) shows the principle setup of the probe and the path of the laser beam. Figure b) illustrates the laser beam scanning some crystals and the resulting backscattering signals. Graph c) shows the PCLD derived from the signals in b). Figure d) presents the trends of different chord length bands over process time. The figures are extracted from a Mettler-Toledo review (Smith 2013).

The measurement technique is described in more detail on the Mettler Toledo website (www.mt.com).

3.2.2.2.   Video microscopy

The V19 video microscope with PVM (Particle Vision and Measurement) technique from Mettler Toledo was applied additionally to the FBRM® probe in order to better understand the mechanisms between the particles causing changes of the PCLD (e.g. agglomeration and coalescence). The probe provided pictures with about 2 µm optical resolution. The smallest lignin particles of around 1 µm diameter could not be resolved with the microscope but the aggregates of primary lignin particles and the formation of aggregates could be imaged. Focus, illumination and picture enhancement had to be adjusted manually to derive satisfactory image quality. The associated icPVM software

provided an image derived relative backscatter index (RBI) that indicated changes of particle properties. More detailed information is provided on the Mettler Toledo website (www.mt.com).

3.2.2.3.   Infrared spectroscopy

Attenuated total reflection Fourier transform mid-infrared (ATR-FT-MIR) spectroscopy has been used to measure spectra of mixtures of lignin, water and ethanol. Multivariate chemometric models for the calculation of concentrations of lignin, water and ethanol from infrared spectra have been calibrated. The calibration models have been used to measure the ethanol concentration in the aqueous phase of lignin dispersion during lignin precipitation processes (see 3.6). Further, a calibration model was applied to investigate liquid-liquid-equilibria (LLE) in the lignin-water-ethanol system (see 3.3).

The ReactIR 45m (Mettler Toledo) spectroscope with fiber optical probe was utilized to collect spectra inside of the reaction vessels and vials. The silver-halide optical fiber and the diamond optical window allow collecting spectra in the wavenumber range of 1900 to 650 cm^{-1}. The figure below shows the spectroscope module with optical fiber and probe.

Figure 12: ReactIR 45m spectroscope with optical probe (diamond window) connected by a silver-halide optical fiber from manufacturer Mettler Toledo (picture adapted from www.mt.com).

Irradiation source, interferometer and the MCT detector are placed inside the spectrometer module. The optical fiber transports the radiation from the interferometer to the diamond window at the tip of the probe. The radiation is then attenuated and totally reflected at the diamond window (Figure 12). The radiation is attenuated because of the interaction with the phase covering the diamond window. The radiation emigrates several times about half of its wavelength into this phase and back into the window again. Some characteristic wavelengths of the radiation are absorbed by distinct chemical groups. The attenuated radiation is then transported through the optical fiber back to the MCT detector. The detector measures an interferogram and a computer calculates the absorption spectrum by Fourier transformation of the interferogram. More detailed descriptions of this spectrometric technique can be found in the literature (Griffith and de Haseth 2007).
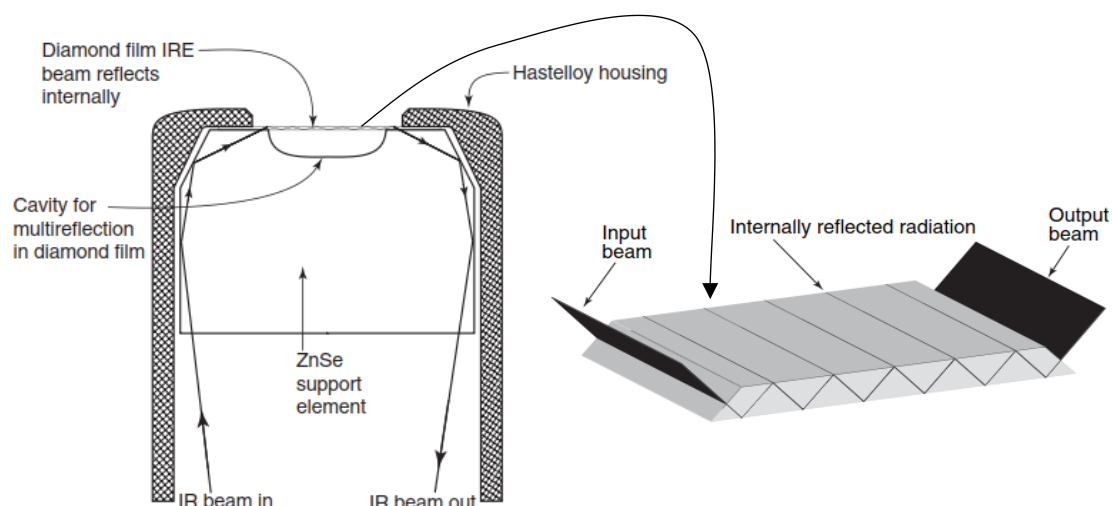
Figure 13: Left side: DiComp diamond film internal reflection element (IRE) sensor. The radiation passes through the ZnSe support into the diamond film for internal reflection. The sensor housing acts as a waveguide to direct the radiation to and from the diamond IRE. Right side: Diamond film with a six times internally reflected beam of infrared radiation (Griffith and de Haseth 2007).

3.2.3.   Chromatography

Liquid (LC) and gas chromatography (GC) were applied to quantify constituents of the pulping liquors (e.g. ethanol) and to measure the molecular mass distribution (MMD) of the lignin samples.

It is out of the scope of this section to explain the fundamentals of chromatography in detail. A brief description will be given in the following lines. A mobile phase (gaseous or liquid) flows through a stationary phase (packed in a column) and interacts with its surface and pores. The analyte is injected into the mobile phase flow and gets dissolved. The constituents of the analyte interact in different ways with the surface of the stationary phase and are retarded. Constituents with less affinity to the stationary phase exit the column earlier than the ones with higher affinity. So, the substances in the analyte are fractionated by their different retention times and are detected by a suitable detector at the end of the column. The concentration of the constituents can be determined by calibration (detector response vs. calibrations sample concentration). Detailed explanations are given in literature (Engelhardt 1979).

3.2.3.1.   High performance liquid chromatography (HPLC)

An HPLC method for analyzing the composition of pulping liquor (without lignin), mother liquor (filtrate after lignin precipitation) and other liquors containing sugars, acetic acid, ethanol and furfural was used according to a standard procedure of the NREL (Sluiter et al. 2008). Prior to injection, pulping liquor was diluted with water and the lignin precipitate was removed via 0.45 µm syringe filter to prevent lignin precipitation in the HPLC system. The following Table 6 shows the method parameters.

Table 6: HPLC method for quantitative analysis of sugars, ethanol, acetic acid and furfural in aqueous solutions.

Parameter	Value
Column (+ precolumn)	Biorad Aminex HPX-87H
Column temperature	60 °C
Detector	Refractive index
Detector temperature	40 °C
Eluent	0.005 M H_2SO_4
Flux	0.6 ml/min
Injection volume	20 µl

Calibration solutions were prepared as dilution series of single analytes and mixtures of analytes with mass fractions between 0.1 and 1 %.

However, pulping liquor test samples contained many more components than calibrated – and base line resolution was not achieved any more. Reliable peak integration was not possible with the real samples, so the method was rejected as an analysis method. Nevertheless, the method is mentioned in this work to point out its unsuitability for real pulping liquors.

3.2.3.2.   Size exclusion chromatography (SEC)

Size exclusion (or gel permeation) chromatography (Aekta, GE Healthcare) was performed in order to investigate the molecular mass distributions of lignin from different batches. Most known SEC methods provide different MMD´s for the same lignin sample (Baumberger et al. 2007). These differences mainly originate from the various aggregation of lignin molecules in the eluent according to the solubility (affinity between lignin and eluent/solvent), from (non-size exclusion) interactions with the surface and pores of varying stationary phases and from the applied detection technique, which can have different sensitivities for various molecular masses (Gidh et al. 2006).

Taking these uncertainties into account, a robust method with 0.1 M NaOH, used as a good lignin solvent to prevent molecule aggregation, a Superdex stationary phase (GE healthcare) and a UV detector were selected (Table 7).

A calibration (molecular mass vs. elution time) was not performed because lignin standards with distinct MMD´s were not available on the market and the comparability of lignin with polystyrene standards was questionable.

A second High Performance Size Exclusion Chromatography (HPSEC) method was performed at the Fraunhofer CBP in Leuna. This method was calibrated with dextran standards with M_w between 180 and 11260 g/mol. All molecular mass values in this work were determined with this method. The samples were dissolved in the eluent and were filtered through a 0.1 µm filter prior to injection. The software Parsec was used for interpretation of the lignin elution profile.

Parameters from both methods are displayed in Table 7.

Table 7: SEC and HPSEC methods for the determination of MMD´s of lignin.

Parameter	Value (MPI method)	Value (CBP method)
Principle	SEC (max. 18 bar)	HPSEC
Column	Superdex 75 10/300 GL	AppliChrom ABOA DMSO-Phil-P-350 and DMSO-Phil-P-250
Column temperature	23 ˚C	80 ˚C
Detector	UV 280 nm	Refractive index
Detector temperature	23 ˚C	40 ˚C
Eluent	0.1 M NaOH	DMSO + 0.075 mol/l $NaNO_3$
Flux	0.8 ml/min	0.5 ml/min
Injection volume	50 µl	100 µl
Sample concentration	≈1 wt. %	≈0.4 wt. %

3.2.3.3. Headspace gas chromatography (GC-headspace)

GC-headspace (GC device Agilent 6890N and headspace device Agilent 7697A) has been utilized to measure the ethanol mass fraction in aqueous mixtures containing also lignin, sugars and other pulping liquor constituents. Samples were prepared with 1 wt. % of acetonitrile as internal standard and were diluted with deionized water to ethanol contents below 10 wt. % to measure inside the calibration range. The most important parameters of the GC-headspace method are displayed in Table 8.

Table 8: GC- headspace method parameters for ethanol content measurement.

Parameter	Value
Column	Agilent J&W VF-624ms (30 m, 0.25 mm, 1.40 µm)
Column temperature	40-150 ˚C @ 10 ˚C/min.
Detector	Flame Ionization Detector FID (hydrogen+air flame)
Detector temperature	250 ˚C
Eluent	Helium
Flux	75 ml/min (split 50:1)
Vial volume	20 ml
Vial equilibration	20 min. @85 ˚C + shaking
Injection loop size	1 ml
Injection duration	0.5 min.
Extraction mode	single extraction
Internal Standard	Acetonitrile 1 wt.%

The calibration for ethanol has been conducted with gravimetrically prepared samples of ethanol, water and internal standard. The charts in Figure 14 show, left, the ethanol content versus peak height plot with the linear least squares regression formula and right, the actual versus predicted plot of the calibration model for calculating the ethanol mass percent in a sample from the peak area of GC measurement with a RMSEC (root mean square error) of 0.16 wt. %.
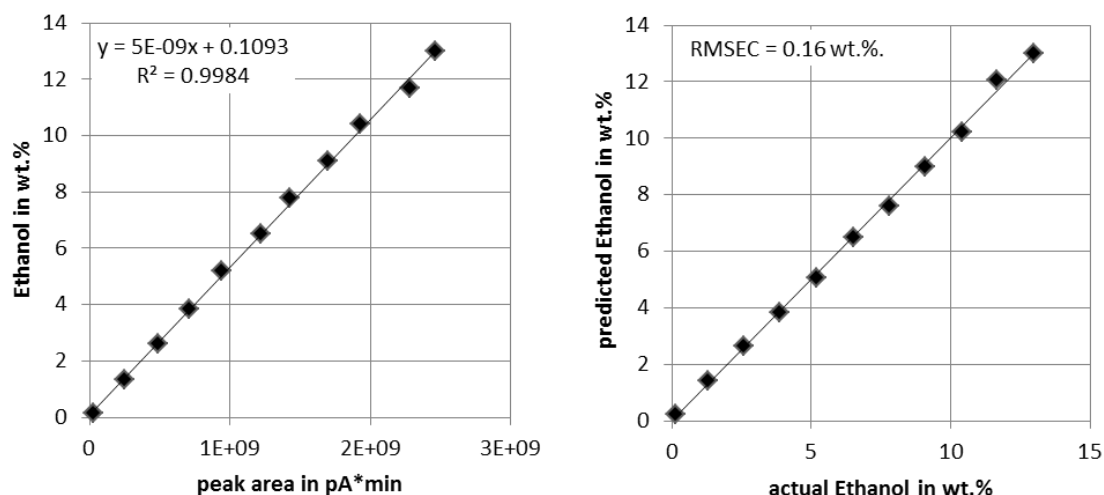
Figure 14: Left: Ethanol percentage in the calibration solutions versus peak area of the ethanol peak at around 10 minutes retention time. Right: actual versus predicted plot of the GC-headspace calibration model for ethanol mass percent in solution.

3.2.4.   Nuclear magnetic resonance spectroscopy (NMR)

NMR measurements have been carried out at the Otto-von-Guericke University in Magdeburg, Faculty of Process and Systems Engineering, Institute of Chemistry by Dr. L. Hilfert. The applied method has already been used before to characterize hardwood lignin (Mainka et al. 2015).

The 2D HSQC (Heteronuclear Single Quantum Coherence) NMR spectra were acquired on a Bruker AVANCE 600 NMR spectrometer equipped with a 5 mm TBI-1H-13C/15N/2H probe head with z-gradients at 295 K (±0.1 K) using the "hsqcedetgpsp.3" pulse program. The samples were dissolved in DMSO-d6. The ^{1}H and ^{13}C chemical shifts were determined relative to internal DMSO-d6 and were given in parts per million downfield to TMS. The operating frequency was 600.13 MHz for ^{1}H and 150.9 MHz for ^{13}C.

A semi-quantitative analysis of the HSQC spectra was performed by integration of correlating peaks in the different regions of the spectra and using the aromatic regions as internal standard. The relative quantity of side chains involved in the inter-unit and terminal substructures was calculated as a number per 100 aromatic units, according to the procedure described in literature (Constant et al. 2016).

3.2.5.   Elemental analysis

Elemental analysis and water content determination of selected lignin samples have been conducted with LECO CHN628, LECO CS230 and Satorius MA45. The measurements have been conducted in the labs of Dr. Sabine Busse at the Otto-von-Guericke University.

3.3.   Lignin phase behavior studies

3.3.1.   Isothermal solubility measurements

The measurements were performed in two different setups. In the first setup, the lignin mass fraction in the solvent phase was solely gravimetrically determined. In the second setup, the mass fractions of all three constituents were determined via infrared spectrometry in the solvent and lignin phase.

3.3.1.1.   Gravimetrical measurement of lignin mass fraction in the solvent phase

From a thermodynamic point of view, dry lignin at room temperature can be characterized as a glass or as solidified subcooled liquid phase. It is completely amorphous and has no measureable enthalpy of fusion. Lignin in its glassy state appears mechanically solid and above its glass transition temperature it appears more or less like a soft material or liquid. Additionally, not only does lignin dissolve in ethanol/water mixtures, but ethanol and water dissolve in lignin as well, causing a swelling (solvation) of the lignin phase. The glass temperature of lignin decreases with increasing solvation, resulting in a viscous liquid lignin phase at room temperature from a certain degree of solvation onwards. Because of these specific properties of lignin, the solid and soft phase will be just called the "lignin phase".

In isothermal solubility measurements, a sample mixture of lignin, water and ethanol was stirred at a constant temperature until the thermodynamic equilibrium between the lignin and solvent phase was reached. If the lignin-rich phase was dissolved by the solvent phase, more lignin was added to ensure equilibrium between both phases. Time to equilibrium was determined in a pre-experiment by intervallic sampling of the solvent phase. The equilibrium was reached as the lignin mass fraction in the solvent phase became constant in three consecutive samples (after 48 hours).

The details of the procedure have been published in conference proceedings (Schulze et al. 2014).

Sample mixtures were put in 30 ml roll edge glasses and sealed by gas-tight crimping caps with a septum. Every glass was filled with a different ethanol/water mixture and about 15 % w/w of oven dry lignin. The glasses were put in a thermostatic shaking water bath (GFL Schüttelwasserbad 1092) for isothermal conditions and thorough mixing of the adhesive samples. After changing the temperature, the samples were equilibrated for a minimum of 48 hours before sampling. For taking liquid samples, a cannula was inserted through the septum and the liquid phase was sucked through a 0.45 µm syringe filter into the syringe. Two samples were taken for comparison purposes. The liquid samples were filled in an open glass and weighed. The weighed samples were dried at 80 °C and about 50 mbar until constant weight. The mass fraction of lignin in the liquid sample was calculated. Liquid samples were taken from 70 to 10 °C, beginning with 70°C. The ethanol mass fraction of the solvent was 0 to 100 % w/w in 10 % steps. Solutions with ethanol contents above 40% could not be quantitatively evaluated due to problems in separating the viscous liquid lignin phase.

3.3.1.2.   Spectrometric determination of the lignin-water-ethanol phase diagram

The determination of LLE in the LWE (lignin-water-ethanol) system was rather complicated. The lignin-phase was a sticky and viscous black mass in large areas of the ternary phase diagram. The solvent phase became harder to divide from the lignin-phase the more soluble lignin became. So fractionation and subsequent analysis of the two phases was dismissed because of the uncertainties in sampling and fractionation of the phases. Further, the gravimetrical analysis after drying of the single phases would have resulted in the lignin mass fraction only and the solvent composition would have been unclear. Other suitable analytical methods for the single phase had not been developed and showed uncertainties because of the sample preparation.

Therefore, a method with poly- and isothermal sections for the spectrometric determination of LLE in the LWE system has been developed. Known masses of lignin (batch K8) and ethanol were mixed in a stirred double wall reactor (around 100 ml in size) displayed in Figure 15. The reactor was brought to the desired temperatures by a Lauda RP845 thermostat. The stirrer was coupled to the motor by a gas tight magnetic coupling and all other openings in the reactor were also sealed gas-tight in order to prevent solvent losses through evaporation. An infrared probe (see 3.2.2.3) and a FBRM® probe (see 3.2.2.1) were immersed in the mixture. Water has been added stepwise to the mixture. After each water addition the mixture was heated at 0.1 K/min above the mixing temperature where only one phase (no particles or droplets) was detected by the FBRM® probe and by the infrared probe. This temperature was recorded as mixing temperature. The infrared probe was always covered with the lignin-phase when two phases occurred, as the lignin-phase was stickier than the solvent phase. While heating the two phase mixture the measured lignin IR-band intensities decreased and stabilized after reaching complete miscibility. If miscibility was not reached before boiling temperature, heating was stopped and no mixing temperature was recorded. The IR probe was pulled out of the mixture and placed in the gas phase above to get cleaned by the condensing solvent. Afterwards, the mixture was cooled to ambient temperature (23 °C at 0.1 K/min) to measure the demixing temperature. Afterwards, the stirrer was switched off to allow phase separation by sedimentation of the lignin phase. During cooling, the demixing temperature was recorded by the FBRM® probe, which detected the first particles or droplets. The isothermal phase equilibrium has been determined after a sedimentation time of a minimum of two hours and a, if necessary, more intense IR probe cleaning. The infrared probe was pushed first into the upper few millimeters of the solvent-rich phase to measure the IR absorption spectrum. Subsequently, the IR probe was pushed further down into the lignin-rich phase at the bottom of the reactor to also measure the spectrum. After collecting the spectra at isothermal conditions, the next amount of water was added and the procedure was repeated. The path of mixture compositions with increasing water contents is shown in the pseudo-ternary phase diagram plot below (Figure 15, right). As lignin is not one distinct molecule but a mixture of chemically similar molecules with a size distribution, it is treated in this work as a pseudo-compound.
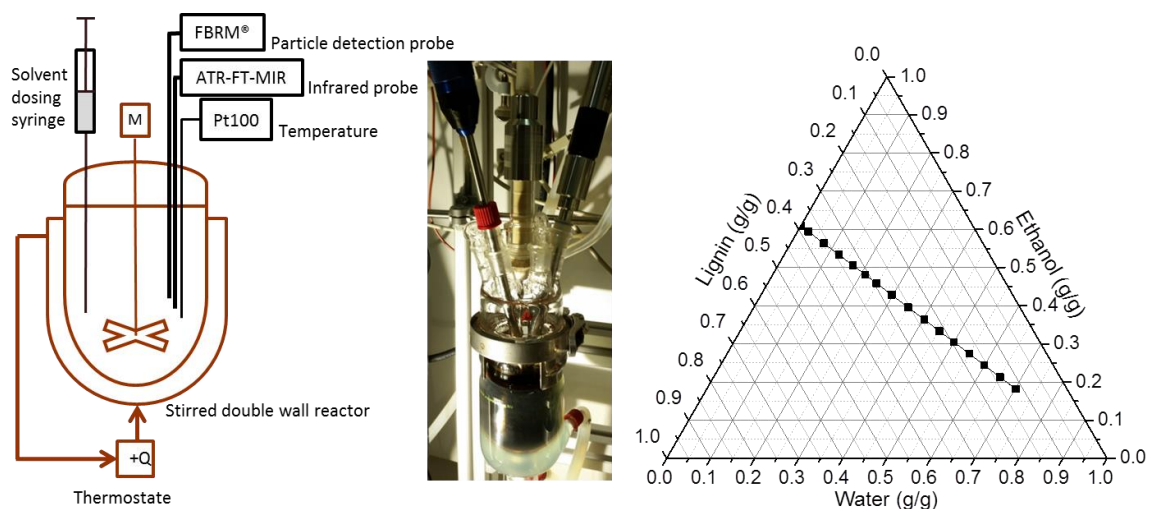
Figure 15: Left and middle: Process sketch and photograph of the experimental setup for the spectrometric determination of liquid-liquid phase equilibria the lignin-water-ethanol system. Right: Path of mixtures in the pseudo-ternary phase diagram of lignin, water and ethanol prepared by water dilution of a lignin-ethanol mixture for LLE measurement.

A model has been calibrated within the "iCQuant" Software from Mettler Toledo to predict the mass fractions of lignin, water and ethanol from the infrared spectra collected during the experiments described above. For this purpose, the infrared spectra of 48 mixtures of lignin, water and ethanol with known compositions have been measured at 23 °C except two samples without and below 5 wt.% water, that have been measured at above 23 °C to ensure complete miscibility. All other samples were completely miscible at room temperature. Thereby, it was ensured to measure one phase with known composition. The mixtures were partly prepared in the experimental setup shown in Figure 15. Some additional samples have been prepared in 8 ml glass vials. The compositions of the 24 calibration samples and 10 test samples are shown in Figure 16 (14 samples dismissed).
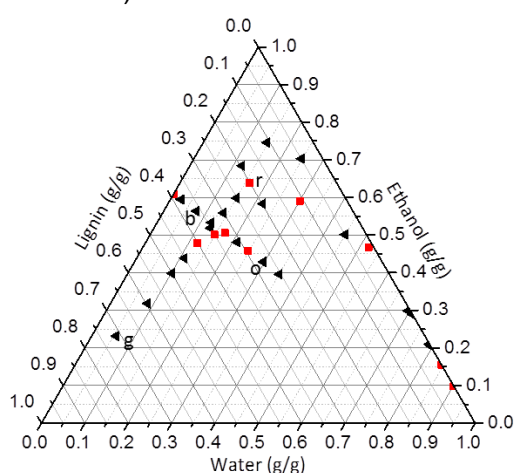
Figure 16: Compositions of the samples used for the calibration (black triangles) and testing (red squares) of the multivariate PLS model for the prediction of lignin, water and ethanol mass fractions from infrared spectra of samples with unknown composition at 23 °C. The samples marked with the letters g (green), b (blue), o (orange) and r (red) correspond to the spectra colors in Figure 17.

Figure 17 shows some exemplary spectra of calibration and test samples measured as described above. The sample compositions are visualized in the ternary plot above (Figure 16) by the first letters of the spectra-colors. The specific lignin bands between 1600 and 1100 cm^{-1} got more intense as the lignin mass fraction increased. The water band around 1650 cm^{-1} and the ethanol bands at around 1120, 1045 and 880 cm^{-1} respond to changes in the mass fractions of water and ethanol, respectively.
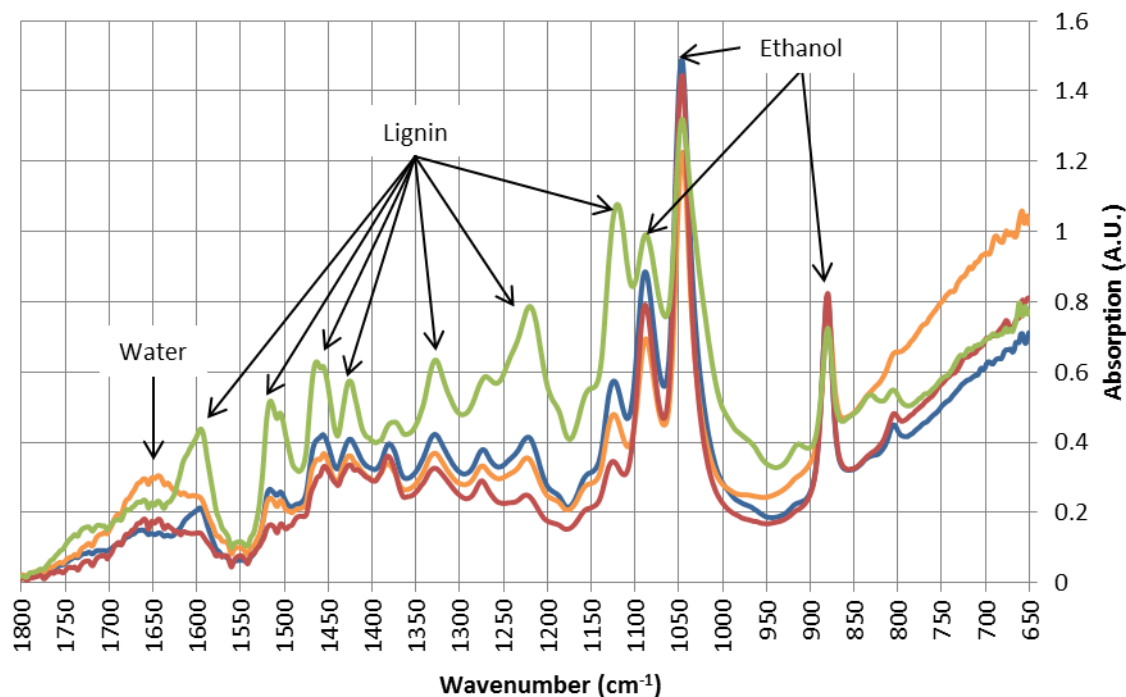
Figure 17: Infrared spectra of some exemplary calibration and test samples. The composition of the samples is shown in Figure 16. Some characteristic peaks of the three components are labeled with black arrows.

The spectra have been analyzed between 1800 and 750 cm^{-1}. Prior to the partial least squares (PLS) regression the spectra have also been mean centered and variance scaled by the iCQuant software (Mettler Toledo). Mean centering subtracts the mean absorption value of a spectrum from all values of the spectrum (of every wavenumber) and shifts the intercepts of all regression functions to zero. Variance scaling subtracts the mean value of all training sample spectra at one certain wavelength from every single spectrum at this certain wavelength. This is done for every wavelength. Several models had to be calibrated and tested before the most accurate model was found. 14 samples were dismissed as outliers because of their bad influence on the model performance. The number of factors for the PLS regression were selected automatically by the iCQuant software. Since it is not goal of this work to explain PLS in detail, more information can be found in literature (Griffith and de Haseth 2007).

The model performance plots of lignin, water and ethanol are displayed in Figure 18 with the PLS-factor number, root mean square errors of calibration (RMSEC), cross-validation (RMSECV) (leaving out 5 training samples) and prediction (RMSEP) in each components plot.
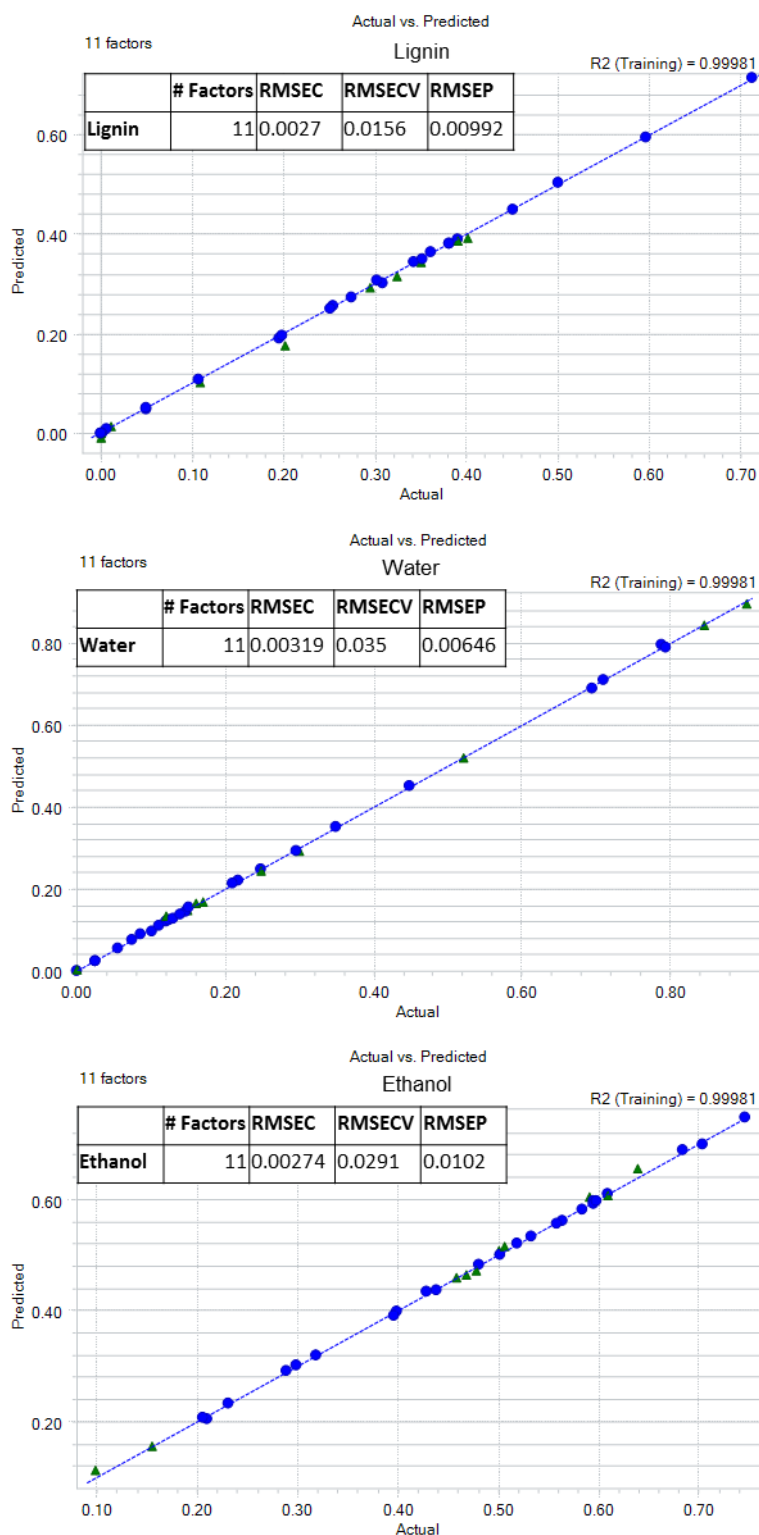
Figure 18: Actual vs. predicted plots (values are mass fractions) of the model calibrated by the iCQuant software using PLS regression. The model has been calibrated to predict mass fractions of lignin, ethanol and water from infrared spectra of mixed samples. Each plot shows the model performance for lignin, water and ethanol (from top to bottom). Blue dots and green triangles represent training and test samples, respectively.

3.3.2. Polythermal solubility measurements

Polythermal solubility measurements have been performed in the "Crystal16" reactor system from Technobis (formerly Avantium). Dry substance of pulping liquor (dried at 60 °C and 10 mbara) and pulping liquor were mixed in different proportions to prepare mixtures with dry substance concentrations above the original pulping liquor concentration. Mixtures of pulping liquor and pulping liquor distillate were prepared to provide dry substance concentrations below the original pulping liquor concentration. All mixtures, prepared from batch K103 pulping liquor, were first heated until complete miscibility was achieved and then cooled down at 0.1 or 0.02 K/minute while stirred by a magnetic stirrer. The demixing was detected by turbidity measurement. Turbidity was measured by a red laser beam radiating through the 1.2 ml glass vial with the sample inside and detecting the laser intensity on the opposite side of the vial. The demixing temperature was recorded when the detected laser intensity decreased 1 % below the intensity value at complete miscibility. Mixing temperatures have not been measured because the precipitated lignin stuck on the stirrer and was not dispersed in the solvent and could therefore not be detected by the turbidity measurement.

3.3.3. Liquid-Liquid-Equilibrium calculations (COSMO-RS)

The phase equilibria calculations have been conducted by Hannes Buchholz (college in the PCF group at MPI Magdeburg). The liquid-liquid-equilibria (LLE) between the two phases I and II in equilibrium of the ternary system have been calculated according to equation 4 where x is the molar fraction, γ the activity coefficient and i represents the components lignin, water and ethanol.

$$x_i^I \gamma_i^I = x_i^{II} \gamma_i^{II} \tag{6}$$

The activity coefficients γ have been determined using the COSMO-RS model (Klamt 1995) within the COSMOthermX program (version C30_1301) from COSMOlogic GmbH & Co KG. COSMO-RS has already been applied in former works for the prediction of multicomponent liquid−liquid equilibria of aromatic extraction systems (Banerjee et al. 2007).

The lignin model molecules have been defined by the author on the basis of analytical results and published molecular structures of organosolv lignin, that are described later in this section.
Lignin model molecules with molecular masses of approximately 600, 1500 and 3000 g/mole have been selected to investigate the influence of chemical properties and molecular mass on the LLE. The molecules have been partly defined on the basis of chemical and structural analysis of lignin from the K8 batch (see 5.1.2). K8 lignin was also used in experimental LLE investigations, described in section 5.2.2.
The model molecule with approx. 1500 g/mole was derived from the "PubChem Open Chemistry Database" under the PubChem CID: 73555271. The 2D dataset was converted and slightly adapted to the molecular structure displayed in Figure 19. The ≈ 600 g/mole model molecule was designed by removing parts of the ≈ 1500 g/mole molecule.

Results of the NMR spectroscopy have been used to elucidate and semi-quantify the monomer composition and the chemical bonds between the monomers of K8 lignin to design the ≈ 3000 g/mole model molecule on the basis of these findings (see 5.1.2). Due to the relative small number of monomers in the designed molecules (14 monomers for 3000 g/mole molecule), only the most prominent monomers and chemical bonds could be built into the model molecules. Semi-quantification of the NMR spectra gave only 9 bonds for 14 monomers, which need at least 13 bonds to form a polymer molecule (minimum 1 bond per molecule, except the end of chain). Therefore, two β-O-4, one β-5 and one 5-5 bond were added to be able to form a molecule with two branches and the desired S/G-monomer ratio.

The lignin model molecules and their properties are listed in Table 9.

Table 9: Properties of the lignin model molecules for quantum mechanical calculations of the liquid-liquid equilibria of the lignin-water-ethanol system with the COSMO-RS software.

Molecular mass (g/mole)	587 (600)	1517 (1500)	2977 (3000)
Number of monomers	3	8	14
Monomer composition (S/G/H)	1/2/0	1/7/0	10/4/0
Number of bonds	2	7	13
α-O-4	1	2	0
β-O-4	1	3	8
β-5	0	1	2
β-β	0	1	2
5-5	0	0	1
Number of branches	1	2	2
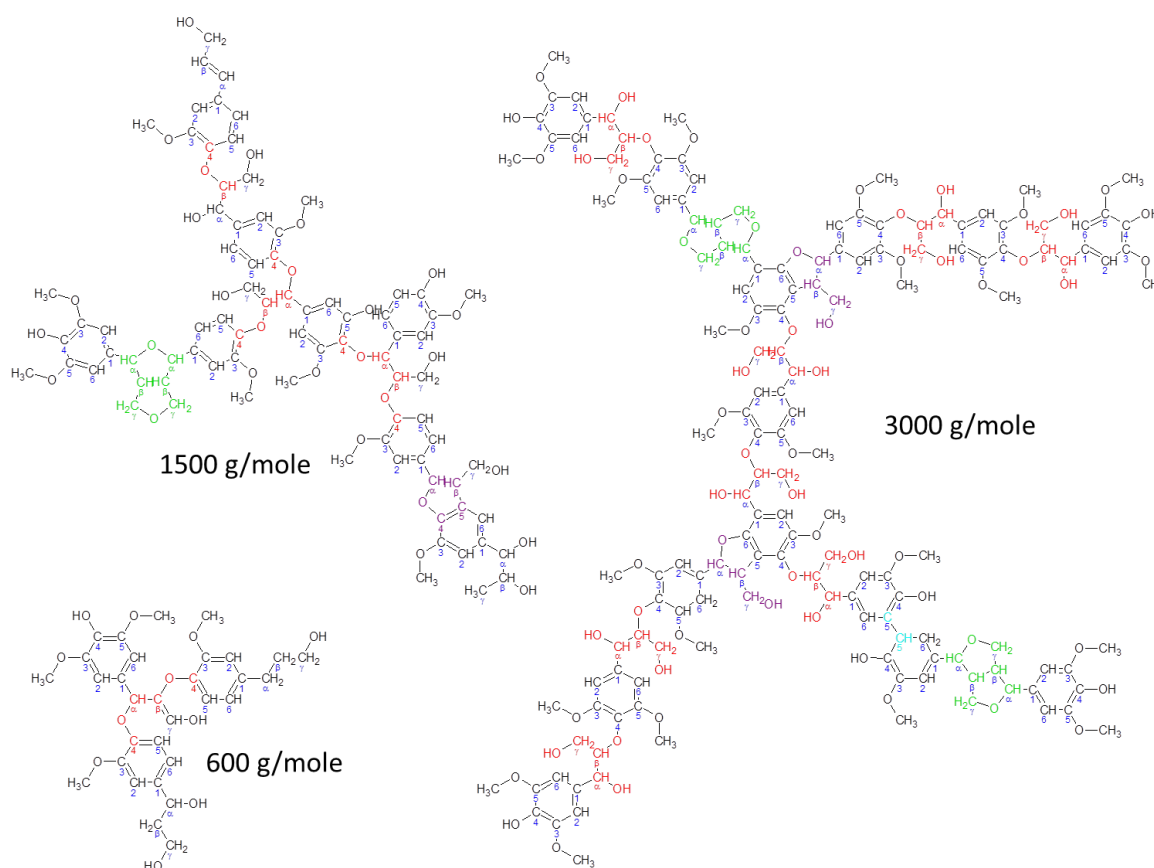
Figure 19: Lignin model molecules for the quantum mechanical calculations of the liquid-liquid-equilibria in the lignin-water-ethanol system with the COSMO-RS software.

The atomic coordinates of the 2D model molecules have been used for geometry optimizations using TURBOMOLE (V6.5). Due to convergence issues using the B-P86 (Perdew 1986, Becke 1988) density functional and a small Gaussian type split valence basis set, the molecular structures where first geometry optimized using the Hartree-Fock method (HF) and the def2-SVP basis set. The optimized structures where then re-optimized within COSMOthermX using the BP_TZVP_C30_1701 parameterization as suggested within the COSMO-RS model.

The COSMO-RS theory uses additional calculations of the polarization charge density which are obtained from the polarizable continuum solvation model COSMO (Klamt and Schüürmann 1993). Hereby, a solute molecular surface is calculated and divided into segments. For each segment a specific electric (surface) charge is calculated assuming that the molecule is surrounded by an ideal conductor with a dielectric constant of infinity, $\varepsilon = \inf$. The binary interactions between all segments in the mixture give the excess chemical potential in solution and thus the activity coefficients of each constituent. The distributions of the electric charges on the surface of the molecules, the so-called sigma surface, are shown in Figure 20. For the solvents, ethanol and water, molecular structures and screening charge densities have been used from the molecular database of COSMOthermX.

1500 g/mole

3000 g/mole

600 g/mole
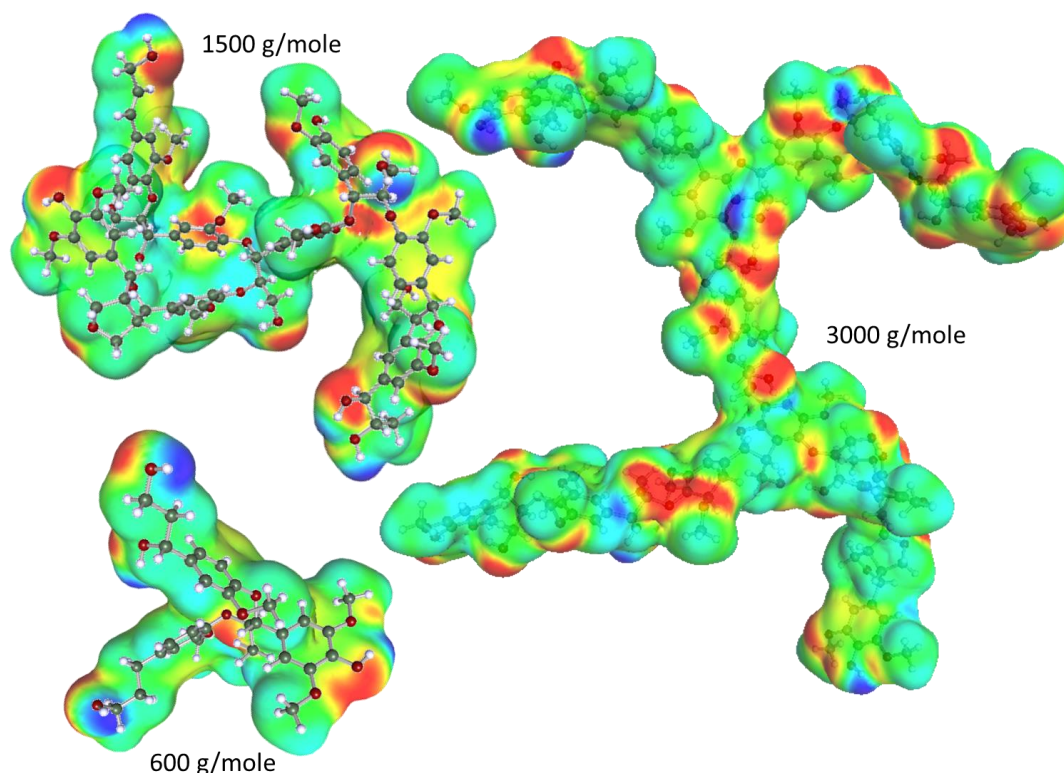
Figure 20: Structure optimized lignin model molecules with sigma surface calculated by the COSMOthermX software.

3.3.4.   Softening and agglomeration properties measurements

Softening temperatures of lignin particles in relation to the ethanol mass fraction in aqueous dispersions were measured indirectly by observing agglomeration of lignin particles. It was assumed that the lignin particles first had to become soft before forming agglomerates with solid bridges between the primary particles. The first measurements have been conducted in 200 ml scale and lignin solid contents of about 5 wt. %. This procedure has been already described in a journal article (Schulze et al. 2016).

Prior to the experimental procedure, lignin dispersion was prepared as described in the following text. Pulping liquor was diluted with ultrapure water (Milli-Q®) to an ethanol content of about 10 % wt. by pouring the spent liquor into an adequate amount of water. This diluted dispersion was concentrated in a rotary evaporator at a pressure below 100 mbar and a bath temperature below 50 °C until the mass reached about 50 % wt. of the original pulping liquor mass. It was assumed, that the ethanol was completely evaporated from the dispersion and no premature agglomeration occurred. Different ethanol contents of the dispersion were adjusted afterwards by addition of pulping liquor.

The experiments were performed in a sealed double jacketed glass beaker with a volume of 1000 ml (see Figure 21). Lignin particle pictures were recorded in the

dispersion by means of a Lasentec PVM inline video microscope probe to register the formation of agglomerates and droplets. An FBRM® probe (Mettler Toledo D600L) was utilized to quantify the change of mean lignin particle sizes during agglomeration and coalescence. The thermostat regulated the temperature of the dispersion, measured by a PT100 temperature probe.

About 200 g lignin dispersion was heated at 0.5 K/min to a temperature between 60 and 95 °C (depending on the droplet formation temperature) under constant stirring at 200 rpm. The temperature, at which the first loose aggregates of lignin particles formed agglomerates and droplets, was defined as agglomeration temperature. The subsequent coalescence of the agglomerates and droplets proceeded with temperature and was followed by both PVM and FBRM® probes.
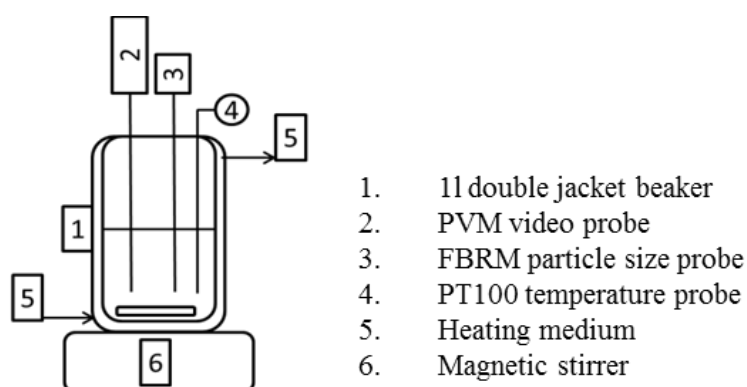
Figure 21: Sketch of the experimental setup for lignin agglomeration temperature measurement.

1.   1 l double jacket beaker
2.   PVM video probe
3.   FBRM particle size probe
4.   PT100 temperature probe
5.   Heating medium
6.   Magnetic stirrer

Later, a second and simplified method for the agglomeration temperature measurement was conducted by utilization of the "Crystalline" reactor system of the company Technobis (former Avantium).

Pulping liquor was diluted with ultrapure water to form lignin dispersion with different ethanol mass fractions. The dispersions were mixed in 8 ml glass vials by magnetic stirring in the Crystalline reactor. The samples were heated from room temperature to a maximum of 95 °C at 0.5 K/min. Turbidity was measured by a red laser beam that radiated through the sample and was detected on the opposite side of the vial. At the same time, micrographs of the particles were recorded once a minute by a built-in microscope camera.

During the heating process, particles started to agglomerate at certain temperatures. Agglomeration was detected by turbidity measurement and the agglomeration temperature was defined at the temperature, at which the turbidity started to decrease or the transmissivity started to increase, respectively. Particle micrographs were additionally considered to ensure agglomeration really occurred.

3.3.5.   Glass transition measurement

The glass transition temperatures of lignins have been measured by temperature-modulated differential scanning calorimetry (Mettler Toledo, DSC3 with FRS 5+ sensor, 30 ml/min nitrogen flow, stochastic temperature-modulation (TOPEM), 1K amplitude, 60-90 seconds period range). Conventional DSC measurement was not able to measure the glass transition because of the overlaid water evaporation in the same

temperature region. Temperature-modulated DSC was able to distinguish between irreversible heat flow (water evaporation) and reversible heat flow (glass transition). The lignin samples were measured in perforated aluminum crucibles to allow sample drying and in gas-tight mid-pressure stainless steel crucibles to keep moisture or solvent inside the sample. Lignin samples have been measured dry and in various water/ethanol mixtures to determine the decrease of glass transition temperatures by solvent swelling.

3.3.6.   Deliquescence temperature determination

The deliquescence temperature range of dry lignin has been measured by **hot stage microscopy**. Dry lignin powder was placed on a glass crucible of the hot stage (FP84HT, Mettler Toledo) and was first pre-heated from 35 to 120 °C at 10 K/min. Slow heating from 120 to 150 °C was performed at 1 K/min before cooling down to 35 °C at 5 K/min again. During the temperature program, micrographs of the lignin particles were recorded with a stereo microscope and camera (Zeiss Axioskop 2). The melting temperature range was determined optically by interpretation of the micrographs.

A **second method** was conducted by heating a lignin sample in an open crucible that was protected from its environment by a glass dome in a DSC3 from Mettler Toledo. A microscope camera recorded images of the lignin sample during heating in order to track melting or other changes.

3.4.   Batch lignin precipitation

Parts of the following section have already been published in conference proceedings and have been slightly changed (Schulze et al. 2014).

Earlier experiments on separation of lignin from organosolv pulping liquor by ethanol evaporation without any previous water dilution showed that a significant part of the separated lignin behaves like a semi-liquid sticky phase, which is difficult to handle in downstream processing and causes incrustations.
The purpose of these first lignin separation experiments was to find suitable evaporation conditions for improving the filtration properties of lignin dispersions and to prevent incrustations of lignin in the reactor. An overview of the experiments that have been performed is given in the appendix A.2.

The experiments were carried out in a reactor system shown in Figure 22 (HEL low-pressure Automate plus reactor system) consisting of a 300 ml glass reaction vessel, a heating and cooling steel jacket, an overhead propeller stirrer with vacuum tight magnetic coupling, a distillation bridge with a reflux valve, a distillate balance and a vacuum pump. The temperatures of the dispersion, the distillate vapor and the heating/cooling jacket were tracked online. The heating and cooling rates, the mass of distillate, the pressure, the stirring speed and the heating power were monitored and partially controlled via the HEL software. The particle size distribution in the dispersion was measured inline by a FBRM® probe (Mettler Toledo FBRM® probe S400A). The density of the distillate samples were measured offline (manually) by means of a

density meter (Mettler Toledo DM40) for calculating the ethanol content in the distillate. Assuming the distillate only consists of water and ethanol, the ethanol content in the stillage was calculated, neglecting losses through the vacuum pump. Cooling power had to be supplied by a thermostat (Lauda Proline RP845) for achieving low temperatures for ethanol condensation at low pressures.

Before starting the experiments, a defined mass of pulping liquor (around 300 g) was filled into the reactor. The reactor was then sealed gas-tight and the pressure was adjusted.

Batch precipitation experiments were carried out at different pressures (1000, 400, 200, 100, 50 mbara), without distillate reflux and a heating jacket temperature of 50 K above the lignin dispersion or pulping liquor temperature. The boiling temperature was adjusted by the pressure over the pulping liquor. During ethanol/water evaporation, lignin precipitated from the liquor when the lignin mass fraction exceeded the solubility at a certain ethanol/water composition and temperature. The occurrence and changes of the chord length distribution of lignin particles in the formed dispersion was measured by the FBRM® probe. The experiment was stopped, when the dispersion temperature reached the boiling temperature of water at its respective pressure. The lignin dispersion was cooled down to room temperature and filtered by means of vacuum filtration. The mass of the filtrate and the mass fraction of the dissolved solids were then determined. The filter cake was dried and weighed. Incrustations were dissolved with clean ethanol and dried in a rotary evaporator to determine the mass of lignin incrustations.
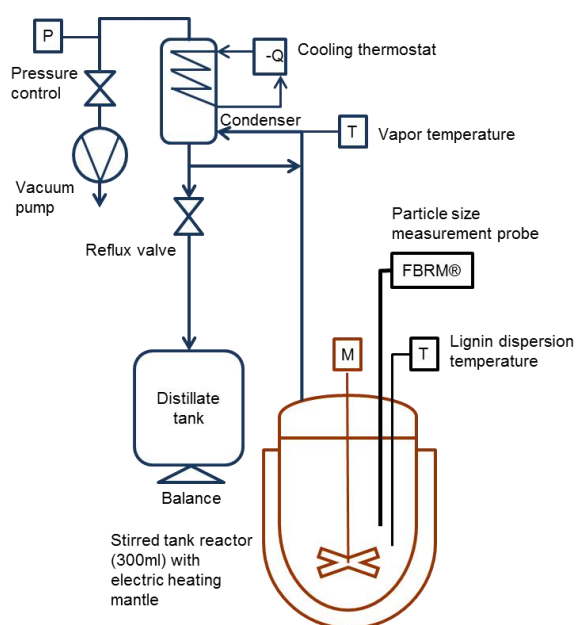
Figure 22: Left: Process flow chart of the experimental setup for lignin precipitation in a batch reactor. Right: Photograph of the experimental setup for lignin precipitation in the batch reactor (300 ml).

3.5.   Semi-continuous lignin precipitation

Parts of these section have already been published in a journal article (Schulze et al. 2016) and have been only slightly changed.

The semi-continuous lignin precipitation experiments have been developed basing on the results of the batch precipitation experiments and represent an advancement of the batch setup. The semi-continuous experiments were first performed at lab-scale at MPI Magdeburg and then in pilot scale at the Fraunhofer CBP Leuna. An overview of the experiments that have been performed is given in the appendix A.2.

3.5.1.   Lab scale experiments at MPI Magdeburg

The fed-batch or semi-continuous precipitation experiments were carried out in a 300 ml reactor system shown in Figure 23 (HEL low-pressure Automate plus reactor system). At the beginning, the empty reactor was sealed gas-tight and the pressure was regulated to the desired amount by a vacuum pump and control valve. About 140 g of a mixture of ultrapure water (Milli-Q®) and pulping liquor (from batch K001) with 10 % wt. ethanol was prepared as start-up dispersion in the reactor vessel by sucking in first water and then liquor. Afterwards, constant heat was supplied via the heating-cooling jacket by regulating its temperature 50 K above the lignin dispersion temperature. The stirred start-up dispersion was heated to boiling temperature and the distillation column was equilibrated while the reflux valve was completely closed. Column equilibration was achieved when both steam and dispersion temperatures were constant. The spent liquor feed pump was started with around 1 ml/min (later 1.3 ml/min). At nearly the same time the reflux valve was opened. The lignin precipitated continuously in the area of the feed pipe inlet because of the ethanol mass fraction drop while mixing with the (start-up) dispersion in the reactor. During the fed-batch process the reflux valve was adjusted such that the temperatures of steam and dispersion remained close to the amounts during the column equilibration phase. In this way, an ethanol concentration close to the start-up concentration in dispersion was ensured and distillate with azeotrope composition was removed, while water remained in the dispersion to regulate solid concentrations. The chord length distribution of lignin particles in the dispersion was monitored by a FBRM® probe (Mettler Toledo, S400A). Distillate mass was recorded using a balance, while distillate density was determined by means of a density meter (Mettler Toledo DM40) for calculating the ethanol content in the distillate. Cooling power had to be supplied by a thermostat (Lauda Proline RP845) for achieving low temperatures for ethanol condensation at low pressures. The spent liquor feed pump was stopped when the reactor vessel reached its maximum level or the boiling-foam reached the column. Evaporation was carried on until the dispersion temperature passed the boiling temperature of water at its respective pressure, assuming the ethanol evaporated completely from the dispersion. The dispersion was cooled down to room temperature and filtered or heated up at environmental pressure to increase the lignin particle size by agglomeration and/or droplet coalescence.
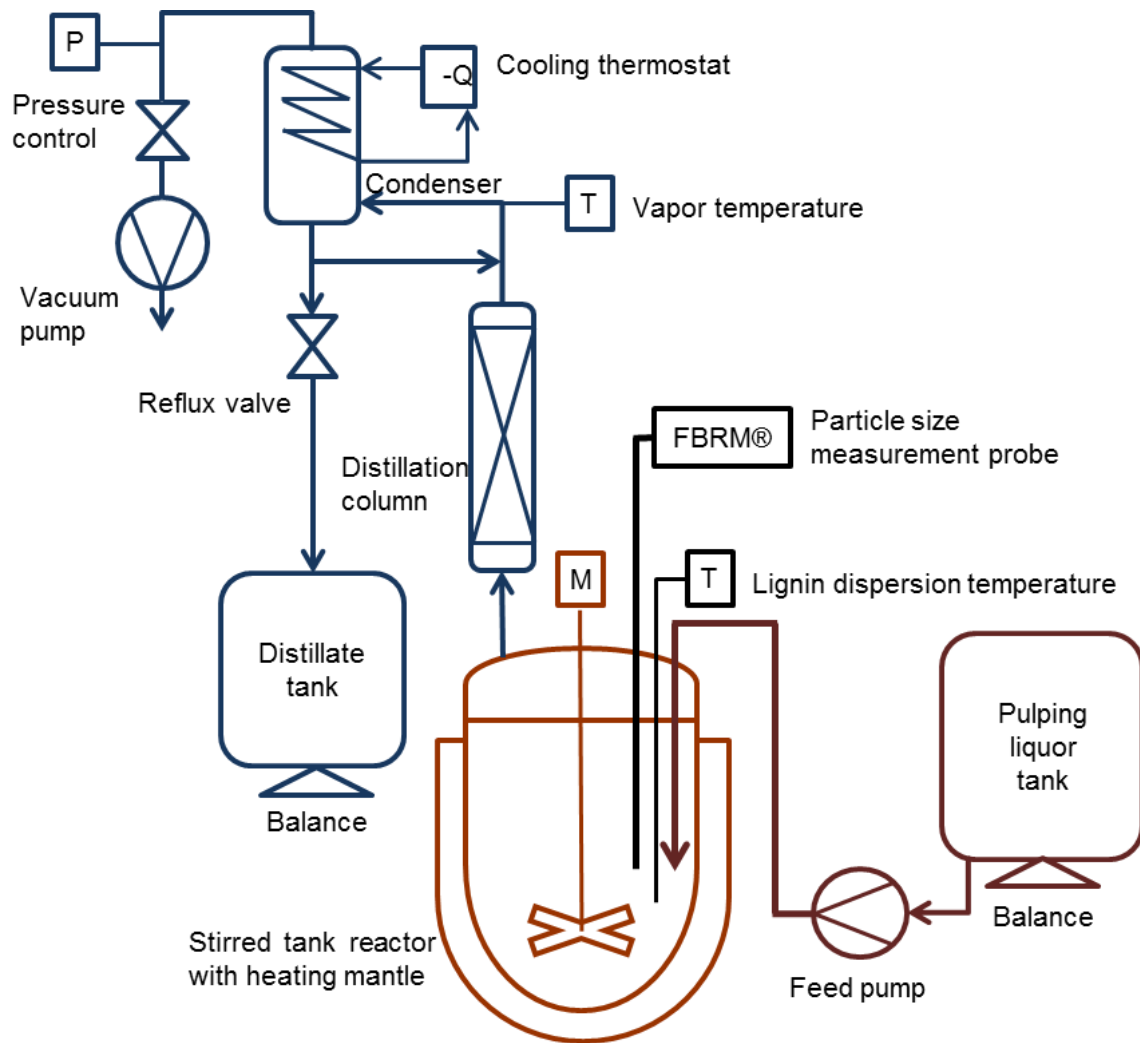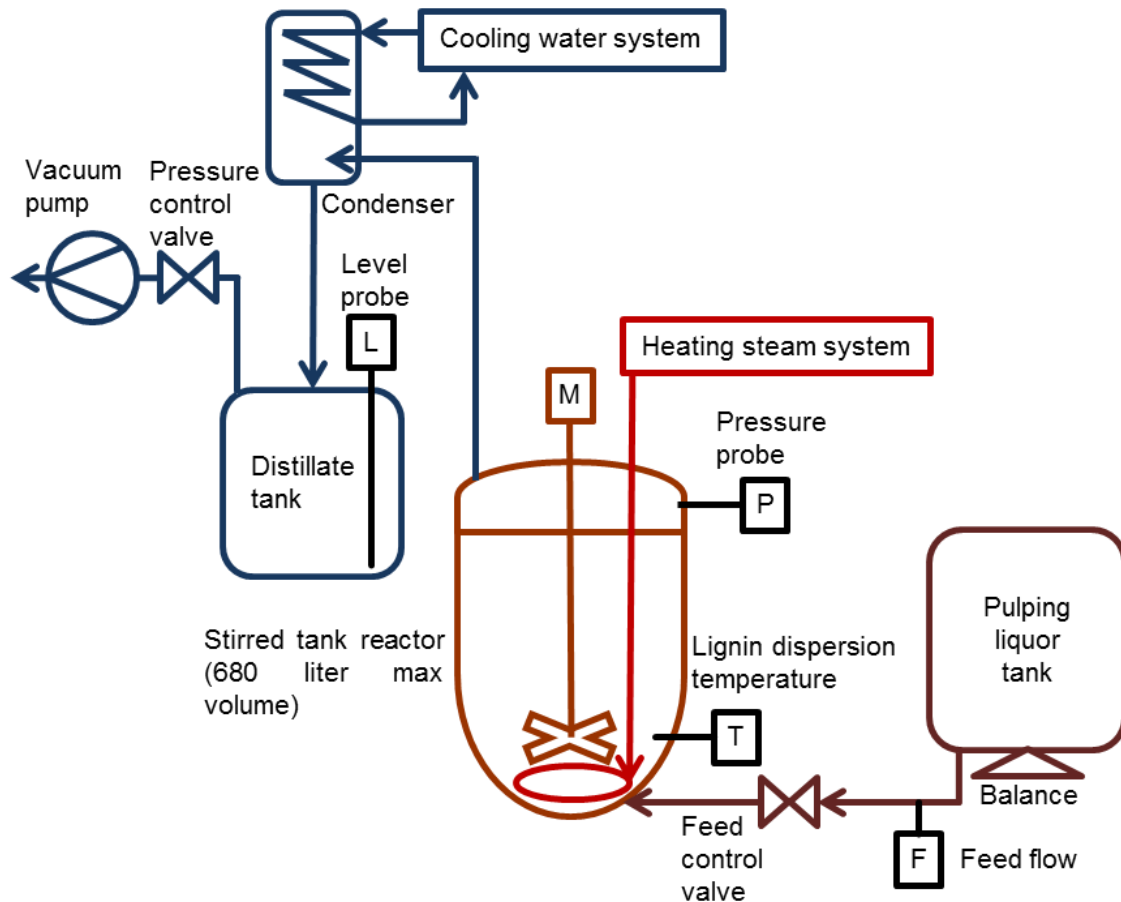
Figure 23: Process flow chart of the experimental setup for semi-continuous lignin precipitation in a lab scale reactor (300 ml) at MPI Magdeburg.

3.5.2.   Pilot scale experiments at Fraunhofer CBP Leuna

The experimental setup at pilot scale (Figure 24) differed mainly in the equipment size (≈ 680 l reactor) and the missing distillation column from the lab scale setup. At the beginning, about 150 kg of a mixture of deionized water and spent liquor (from pulping batch K029) with 10 % wt. ethanol was prepared as start-up dispersion in the stirred tank reactor. The desired pressure of 100 mbara was adjusted by means of a pressure control unit. Heating power was supplied by direct input of steam into the dispersion. The dispersion was heated up to boiling temperature and at nearly the same time the spent liquor feed was started at a rate of circa 50 kg/h. During the fed-batch process the spent liquor flow was adjusted (up to 60 kg/h) such that the dispersion temperature remained close to the amount at the beginning of feeding. In this way, an ethanol concentration close to the start-up concentration in the dispersion was ensured. The lignin precipitated continuously in the area of the feed pipe inlet because of the ethanol mass fraction drop while mixing with the (start-up) dispersion in the reactor. The distillate volume was measured by means of a level probe in the distillate tank. The distillate tank had to be drained during the experiment. The spent liquor feed was stopped when the tank reached its maximum level or the foam reached the vapor outlet. Half of the dispersion was transferred to another tank, cooled down and filtered. The

remaining dispersion was further evaporated until the dispersion temperature passed the boiling temperature of water at the corresponding pressure (around 45 °C), assuming an ethanol content of < 1 % wt. in the dispersion. Afterwards, the stirred dispersion was heated up to 70 °C followed by slowly cooling down to 50 °C within 16 hours to increase the lignin particle size by agglomeration of the softened lignin particles overnight. Filtration of the dispersions was performed via a chamber filter.

Figure 24: Process flow chart of the experimental setup for semi-continuous lignin precipitation in a pilot scale reactor (680 l) at Fraunhofer CBP Leuna.

3.6.   Continuous lignin precipitation

In order to develop a process with potential to scale up to industry standards and to improve process control, the experimental setup was updated by adding inline analytical techniques for lignin particle size (FBRM®) and shape (PVM) monitoring and recording the ethanol mass fraction (ATR-FT-MIR) in the aqueous lignin dispersion. Additionally, equipment for lignin dispersion removal was installed in order to operate the precipitation continuously.

After numerous continuous experiments in the setup with heating via the jacket of the reactor vessel, a self-made falling film evaporator was installed in order to prevent boiling foam, which caused lignin scaling in the reactor and limited the heating power input because of boiling over dispersion into the distillation column.

The pilot scale setup was vigorously reconstructed to imitate the lab scale setup with the falling film evaporator, but without the distillation column, additional water (or filtrate) inlet to adjust the dispersion solids content. An overview of the experiments that have been performed is given in the appendix A.2.

3.6.1.   Lab scale experiments

Before running precipitation experiments the infrared probe had to be calibrated for in-process ethanol mass fraction measurement.

The accurate control of the ethanol mass fraction has been found to be very important in order to prevent lignin from excessive softening and reactor fouling. A model for the prediction of the ethanol mass fraction in the aqueous phase of the lignin dispersion from its infrared spectrum has been calibrated. In this way, the ethanol mass fraction could be controlled quite well during the process. The strongest ethanol peak at around 1046 cm^{-1} has been selected and the peak height difference to the basepoint at 1067 cm^{-1} has been used for model calibration. The first set of calibration samples was prepared of pulping liquor with a known ethanol mass fraction (GC-headspace) and water. The spectra were measured at 40 °C because this was the average temperature of lignin dispersion during semi-continuous experiments. Infrared spectra are temperature dependent and the expected lignin dispersion temperature for the continuous experiments was around 40 °C again.

The second set of calibration spectra has been collected during the first continuous experiment. Samples of lignin dispersion were removed from the reactor and the spectra were collected at the same time. The ethanol mass fraction in the dispersion has been determined by GC-headspace measurement.

Figure 25 shows the ethanol mass fraction versus peak height plot and the linear least squares regression fit on the left side and the model performance plot on the right side with a root mean square error of calibration of 0.87 wt. %.
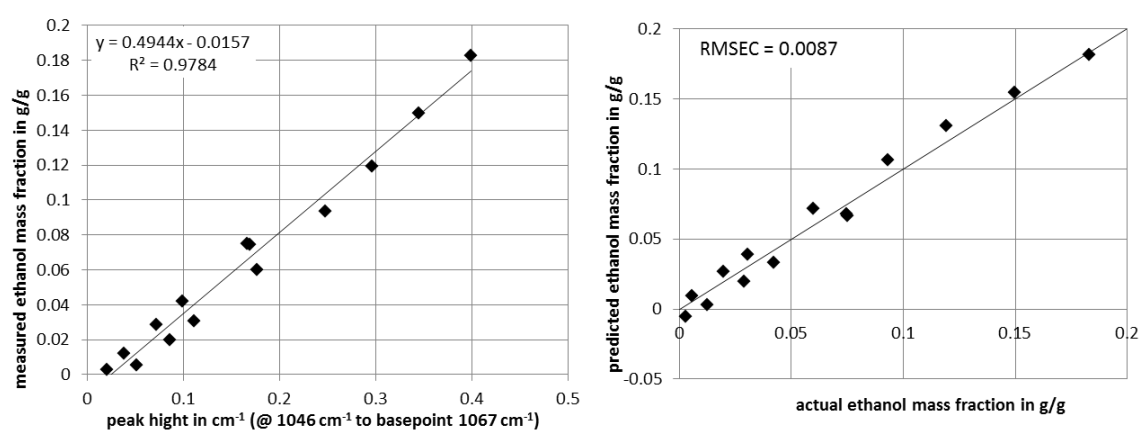
Figure 25: Left: Ethanol mass fraction in calibration samples versus peak height and the linear least squares regression plot with model formula. Right: Actual versus predicted ethanol mass fraction plot for the model on the left side with 0.87 wt. % root mean square error of calibration.

3.6.1.1. Experiments with reactor jacket heating

The continuous precipitation experiments were carried out in the experimental setup shown in Figure 26. The plant mainly consists of 4 different colored sub-units that are each characterized by the process stream they contain. The pulping liquor tank (2 l) and pump (brown), the 2 liter reactor (light brown), the dispersion removal pump and 1l tank (dark brown) and the distillate (rectification column, condenser and 1l tank) and vacuum system (blue).

At the beginning, the empty reactor was sealed gas-tight and the pressure was regulated to the desired amount by a vacuum pump and control valve. About 1 kg of ultrapure water was sucked into the reactor to wet all probes. Subsequently, pulping liquor was added to the stirred water by the feed pump to form the start-up dispersion with an ethanol content of around 8 wt. %. Afterwards, a constant heating power was supplied via the water of the heating-thermostat (Lauda Proline RP845) that was regulating to a temperature around 10 K above the lignin dispersion temperature. Higher water heating temperatures could rarely be adjusted because the risk of boiling over foam. The stirred start-up dispersion was heated to boiling temperature and the distillation column was equilibrated while the reflux valve was completely closed. Cooling power was supplied by a second thermostat (Lauda Proline RP845) for achieving low temperatures for ethanol condensation at low pressures. Distillation column equilibration was achieved when both, steam and dispersion, temperatures were constant. The pulping liquor feed pump was started with around 3 to 4 g/min and was adjusted during the process to obtain ethanol contents around 7.5 wt. % in dispersion, measured by the infrared probe (Mettler Toledo, ReactIR45m) and calculated by the model described above. At nearly the same time the reflux valve was opened to withdraw distillate and the dispersion pump was started to remove dispersion from the reactor in order to maintain constant dispersion level. The lignin precipitated continuously in the area of the feed pipe inlet because of the ethanol mass fraction drop during mixing with the dispersion in the reactor. During the process the reflux valve was adjusted such that the vapor temperature remained below the value, where the ethanol content of the distillate was above 80 wt. % to retain most of the water in the dispersion. Distillate and dispersion masses were recorded by balances to monitor the process mass balance at any time. The chord length distribution of lignin particles in the dispersion was monitored by a FBRM® probe (Mettler Toledo, G400). Lignin particle shape and agglomeration were observed via an inline microscope (Mettler Toledo, V19). The experiment was stopped, when the pulping liquor tank was emptied or a problem occurred. The pulping liquor feed pump, heating-thermostat and pressure control were stopped first to shut down the process. The dispersion in the reactor was then cooled down to around room temperature for lignin solidification. Afterwards, all other devices were stopped and the dispersion was drained from the reactor into a separate bottle. The ethanol mass fraction of the distillate was determined by GC-headspace or density measurement. The ethanol mass fractions were derived from the correlation with the density reported in literature (Khattab et al. 2012).

The continuously removed dispersion and the dispersion drained after the experiment from the reactor were both filtered in a pressure cake filtration setup to determine the average filter cake resistance, as will be described in section 3.7.
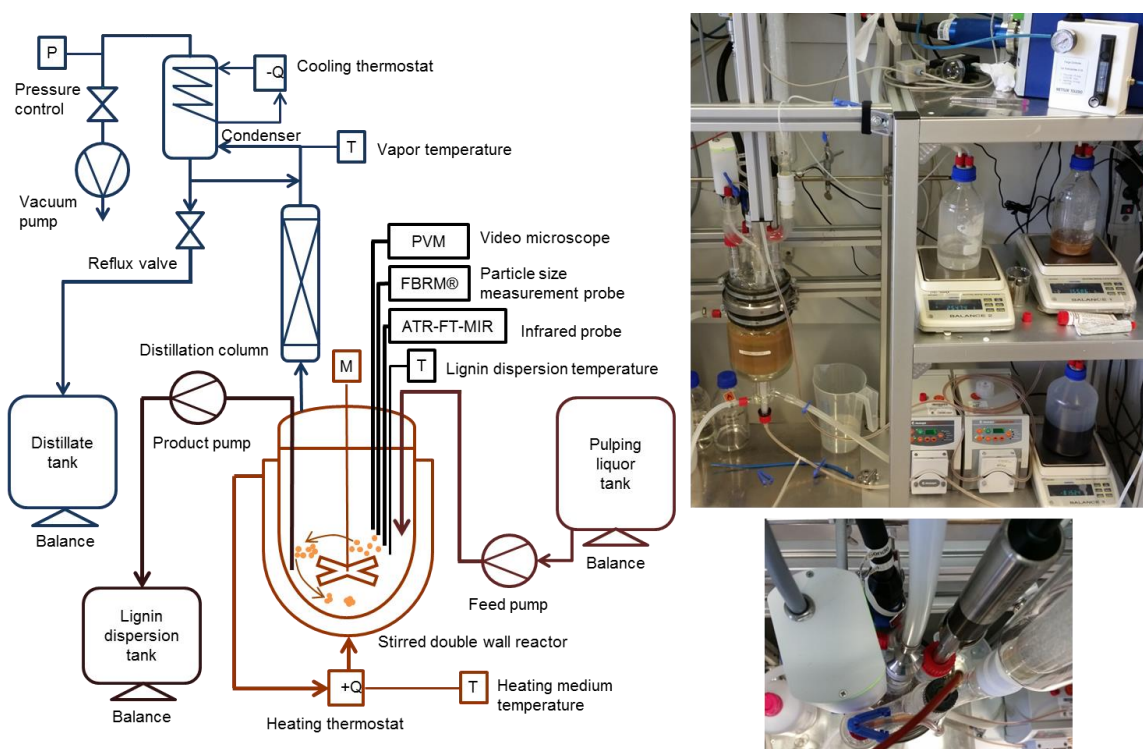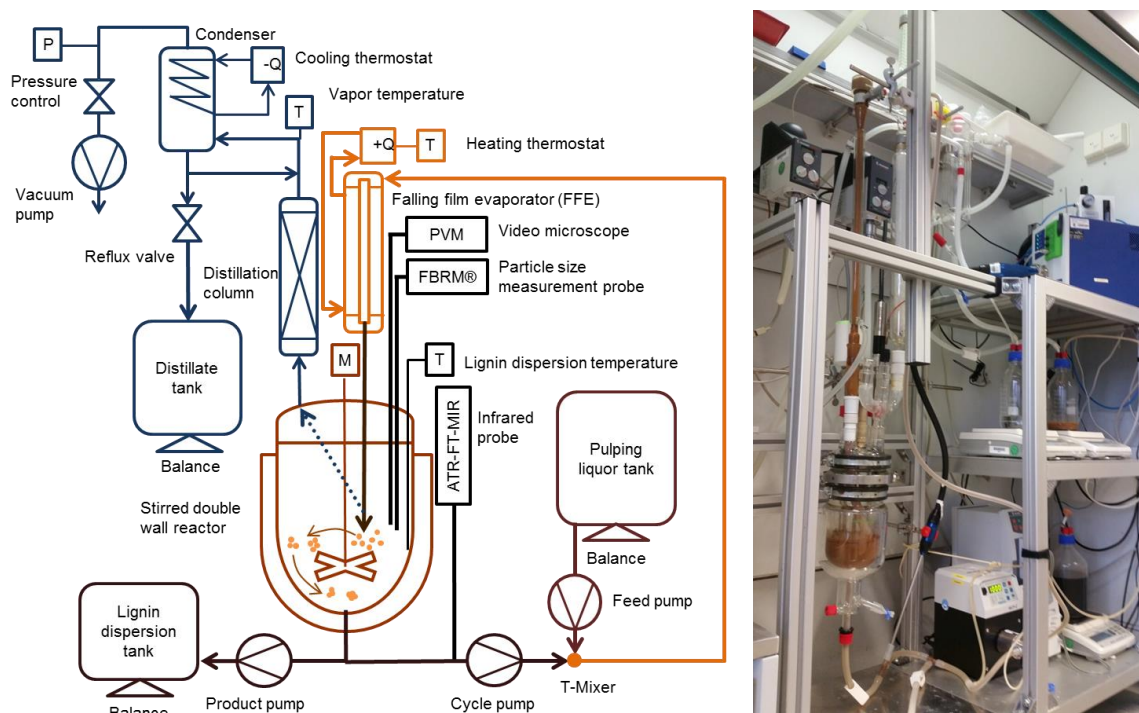
Figure 26: Left: Flowchart of the continuous lignin precipitation process in lab-scale (light brown: 2l reactor, brown: pulping liquor feed pump and 2l tank, dark brown: lignin dispersion removal pump and 1l tank, blue: rectification and vacuum system, black inline measurement devices). Right: Photographs of the experimental setup.

3.6.1.2. Experiments with the falling film evaporator

The continuous precipitation experiments with a falling film evaporator were carried out in the experimental setup shown in Figure 27. The setup distinguished from the previous setup with the reactor jacket heating mainly in an additional lignin dispersion cycle powered by a gear pump in order to supply a constant flow for the falling film evaporator (orange parts in Figure 27). The infrared probe was removed from the reactor lid and installed in the new dispersion cycle to give room for the falling film evaporator. Additionally, as the minimum filling level of the reactor was lowered, because the infrared probe was the shortest probe, the residence time of the lignin dispersion in the reactor could thereby be decreased. Lignin particle agglomeration and changes in particle size distribution were thought to be able to be measured faster and better controlled due to the shortened residence time. The pulping liquor feed position was moved from the reactor to the dispersion cycle in upstream position to the falling film evaporator in order to have the possibility to tune the dilution ratio of fed pulping liquor and thereby the ethanol mass fraction in the dispersion before entering into the evaporator. The falling film evaporator was made of a vertically installed straight Liebig-cooler with a self-made liquid distributor on the top and an extension tube at the bottom to drain the dispersion from the evaporator cycle directly to the dispersion in the reactor, while preventing the dispersion flowing down the reactor lid, causing incrustations. The Liebig-cooler part of the falling film evaporator was heated by water of the heating thermostat. The reactor jacket was empty.

At the beginning of each experiment, the empty reactor was sealed gas-tight and the pressure was regulated to the desired amount (80 or 100 mbara) by a vacuum pump and control valve. About 500 g of ultrapure (type 1) water was sucked into the reactor to wet the two probes in the reactor and to fill the evaporator cycle. The evaporator cycle pump was started with a flow rate between 250 and 500 g/min after the cycle was filled with water. Subsequently, pulping liquor was added into the evaporation cycle by the feed pump to form the start-up dispersion with an ethanol content of around 6 to 7 wt. %. Afterwards, heating power was supplied via the water of the heating-thermostat (Lauda Proline RP845) that was adjusted to temperatures around 10 to 15 K above the lignin dispersion boiling-temperature. The start-up dispersion was heated to boiling temperature and the distillation column was equilibrated while the reflux valve was completely closed. Cooling power was supplied by a second thermostat (Lauda Proline RP845) for achieving low temperatures for ethanol condensation at low pressures. Distillation column equilibration was achieved when both, steam and dispersion, temperatures were constant. The pulping liquor feed pump was started with around 3.5 to 4.5 g/min and was adjusted during the process to obtain ethanol contents around 6.5 wt. % in dispersion, measured by the infrared probe (Mettler Toledo, ReactIR45m) and calculated by the model described earlier in this section. At nearly the same time the reflux valve was opened to withdraw distillate, the dispersion pump was started to remove dispersion from the reactor in order to maintain a constant dispersion level. The lignin precipitated continuously at the T-mixer in the evaporator cycle because of the ethanol mass fraction drop during mixing with the dispersion in the cycle. The mass fraction of fed pulping liquor flow to the dispersion flow after the mixer was in the range of 1.8 to 0.7 wt. %, increasing the ethanol content of the dispersion before entering the evaporator 0.9 to 0.35 wt. %. During the process the reflux valve was adjusted such that the vapor temperature remained below the value where the ethanol content of the distillate was above 80 wt. % to retain most water in the dispersion. Pulping liquor, distillate and dispersion masses were recorded by balances to monitor the process mass balance at any time. The chord length distribution of lignin particles in the dispersion was monitored by a FBRM® probe (Mettler Toledo, G400). Lignin particle shape and agglomeration were observed via an inline microscope (Mettler Toledo, V19). The experiment was stopped, when the pulping liquor tank was emptied or a problem occurred. The pulping liquor feed pump, heating-thermostat and pressure control were stopped first to shut down the process. The dispersion in the reactor was then cooled down to around room temperature for lignin solidification. Afterwards, all other devices were stopped and the dispersion was drained from the reactor into a separate bottle. The ethanol mass fraction of the distillate was determined by density measurement (Khattab et al. 2012).

Again, the continuously removed dispersion and the dispersion drained after the experiment from the reactor were both filtrated in a pressure cake filtration setup to determine the average filter cake resistance, as will be described in section 3.7.

Figure 27: Left: Flowchart of the continuous lignin precipitation process with falling film evaporator (orange colored parts + brown cycle pump) in lab-scale. Right: Photograph of the experimental setup.

3.6.2.   Pilot scale experiments

Continuous pilot scale precipitation experiments with a falling film evaporator were carried out in the experimental setup shown in Figure 28. The pilot plant was upgraded on the basis of the results from the semi-continuous precipitation. Therefore, a falling film evaporator with an accompanying dispersion cycle has been added to the plant. A rectification column was not installed, meaning that the ethanol/water vapor from the evaporator had to be directly condensed without ethanol enrichment. An additional water feed was installed because without it, it would have been possible to evaporate more water than was fed with the pulping liquor, as no distillation column returned water to the system. Consequently, without the water-feed, the lignin dispersion could reach a too high solid-to-liquid content ratio, decreasing the mobility of the dispersion outlet stream. However, the reduction of the water feed to a lowest possible amount was a major goal in the experiments. Furthermore, an infrared probe has been attached to the dispersion cycle in order to improve process control in terms of the ethanol content in the dispersion. Unfortunately, the infrared probe could not be used in all the performed experiments because of some technical problems. During the first experimental campaign the IR probe was out of order and therefore dispersion samples were quickly analyzed with an offline infrared spectrometer to determine the ethanol content half-hourly. At the end of a pilot plant run, the samples were analyzed via headspace-GC for a more exact ethanol mass fraction measurement. Two pulping liquor feed positions, in the dispersion cycle and in the reactor, were installed to investigate their influence on the process. The dispersion removal valve was mounted in a way to allow continuously adjusting the reactor level and withdrawing lignin dispersion into the dispersion tank.

Two experimental campaigns (about one week duration each) have been carried out in the freshly reconstructed pilot plant. During the **first campaign**, experiments with a)

pure water, b) ethanol/water mixture (synthetic pulping liquor without lignin) and c) real pulping liquor K138 were conducted.

In the **second campaign**, experiments with K139 pulping liquor were performed to further improve the process conditions. The water-feed was aimed to be further decreased and the pulping liquor feed and degree of agglomeration increased.

Suitable process conditions (feeds, heating, pressures, etc.) for the prevention of lignin fouling, etc. have been preliminary calculated for all experiments by a **mathematical model**, which describes mass and energy balances and phase transitions in the pilot plant. The model is based on previous investigations and will be described in detail in **section 4.**

The procedure of the second experiment with K138 pulping liquor within the **first campaign** is reported in the following section.

The reactor was filled with around 275 liter lignin dispersion originating from the experiment of the day before. The dispersion was used as start-up dispersion and contained 2.6 wt. % dry substance (lignin and sugars) and 5.3 wt. % ethanol in the aqueous phase. At first, the pressure over the dispersion was regulated to 120 mbara, the evaporator cycle pump was started with a flow rate of 3500 kg/h and the heating steam was turned on to heat-up the system to evaporation conditions, while the distillate was completely refluxed. Cooling power was supplied by the cooling water system to the plate heat exchanger to condense the ethanol/water vapor. The heating steam temperature (~ 51 °C) was adjusted to about 7 K above the lignin dispersion boiling-temperature (~ 44 °C). After reaching stationary evaporation conditions (constant temperatures of heating steam, dispersion, vapor and distillate), the continuous process was initiated. The pulping liquor feed pump was started with ~50 kg/h to obtain ethanol contents between 6-7 wt. % in the dispersion. The desalinated water mass flow was regulated to 45 kg/h to compensate the removal of water by the distillate. The heating steam mass flow was regulated to 33 kg/h, which is equal to ~ 25 kW heating power. The automatic dispersion valve control was started to maintain a constant dispersion level in the reactor. The lignin precipitated continuously at the feeding position in the reactor because of the ethanol mass fraction drop during mixing with the dispersion. Samples of lignin dispersion and distillate were taken half-hourly for analysis. The chord length distribution of lignin particles in the dispersion was monitored offline by a FBRM® probe (Mettler Toledo, G400). Lignin particle shape and agglomeration were observed offline with a microscope probe (Mettler Toledo, V19). The ethanol content of the dispersion was analyzed by an offline infrared spectrometer (Bruker, ALPHA FT-IR-ATR spectrometer) and calculated via a calibration model. The dry substance content of the lignin dispersion was measured gravimetrically (Sartorius, Infrared Moisture Analyzer). The ethanol mass fraction of the distillate was determined by density measurement.

The experiment was stopped, when the pulping liquor tank was emptied. The pulping liquor and water feed, heating steam inlet, dispersion and distillate outflow and pressure control were stopped to shut down the process.

The dispersion was left in the reactor as start-up dispersion for a next experiment. A dispersion sample was taken from the reactor for a filterability measurement at the MPI Magdeburg (as described in section 3.7). The ethanol mass fractions of the distillate

and lignin dispersion samples were determined more accurately by headspace-GC after the experiment.

The procedures of the experiments with K139 pulping liquor within the **second campaign** were similar to that experiment of the first campaign described before. Differing points will be mentioned in the following. The IR probe worked properly this time and was calibrated for ethanol before. So the ethanol content was measured every 30 seconds and the process could be tuned better. However, no FBRM and V19 probe were available for particle size and agglomeration monitoring. So the particle size was estimated from the color and the sedimentation behavior of the dispersion.

In order to find the lowest possible water feed rate, the water feed was stepwise reduced to zero throughout the experiments. The ethanol content and agglomeration behavior was assessed after each water reduction in order to prevent uncontrolled softening of lignin. Subsequently, the pulping liquor feed rate and heating steam flow were increased by 10 % (from 50 to 55 kg/h PL) to test out the operational limits of the plant. Dispersion and distillate samples have been taken regularly throughout the experiment and were analyzed by GC-headspace and FBRM® afterwards.
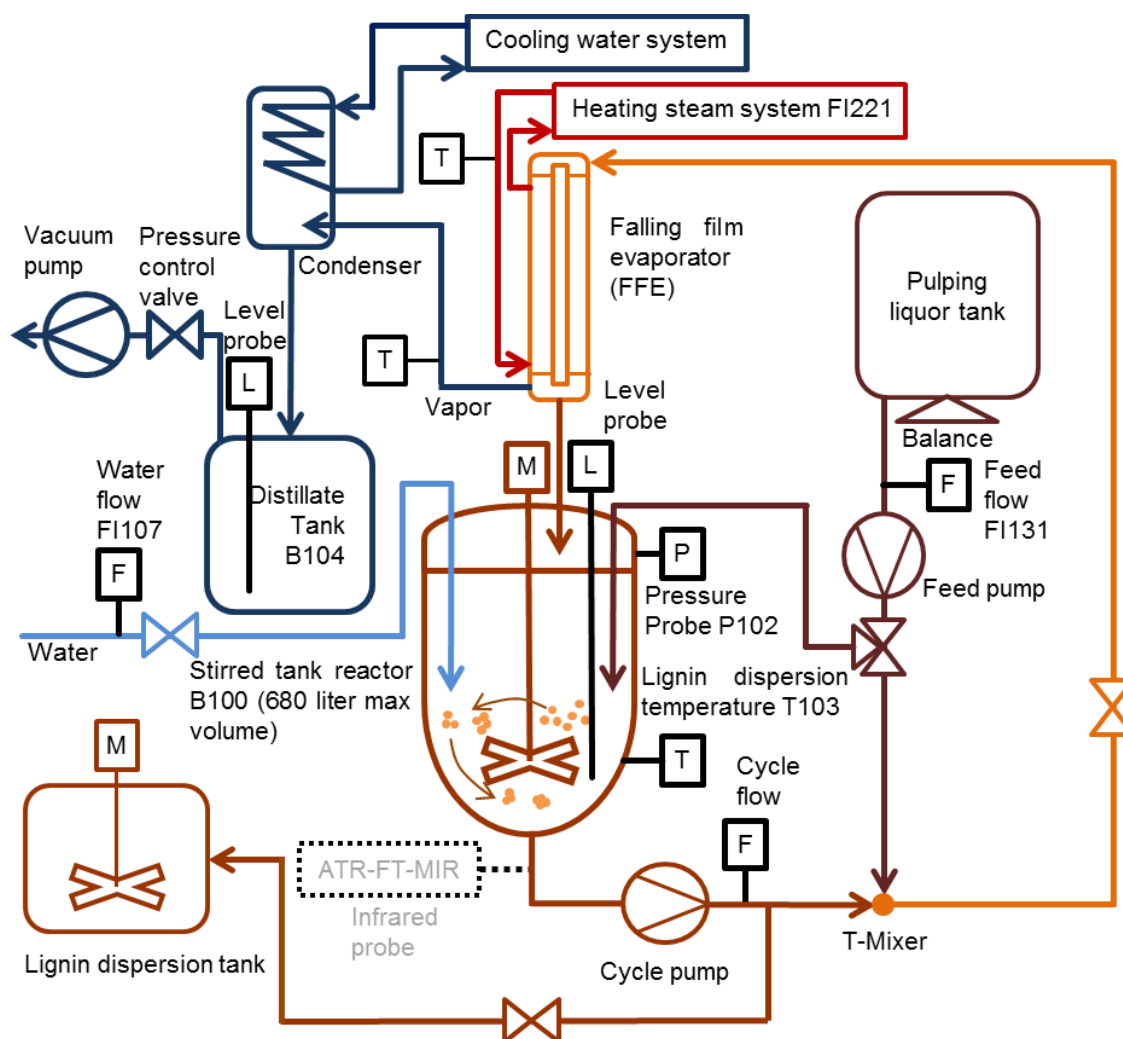
Figure 28: Simplified flowchart of the pilot scale setup for continuous lignin precipitation with a falling film evaporator.

Figure 29 shows a 3D model and photographs of relevant reactors in the lignocellulose biorefinery at the Fraunhofer CBP to give the reader a better impression of the pilot plant.
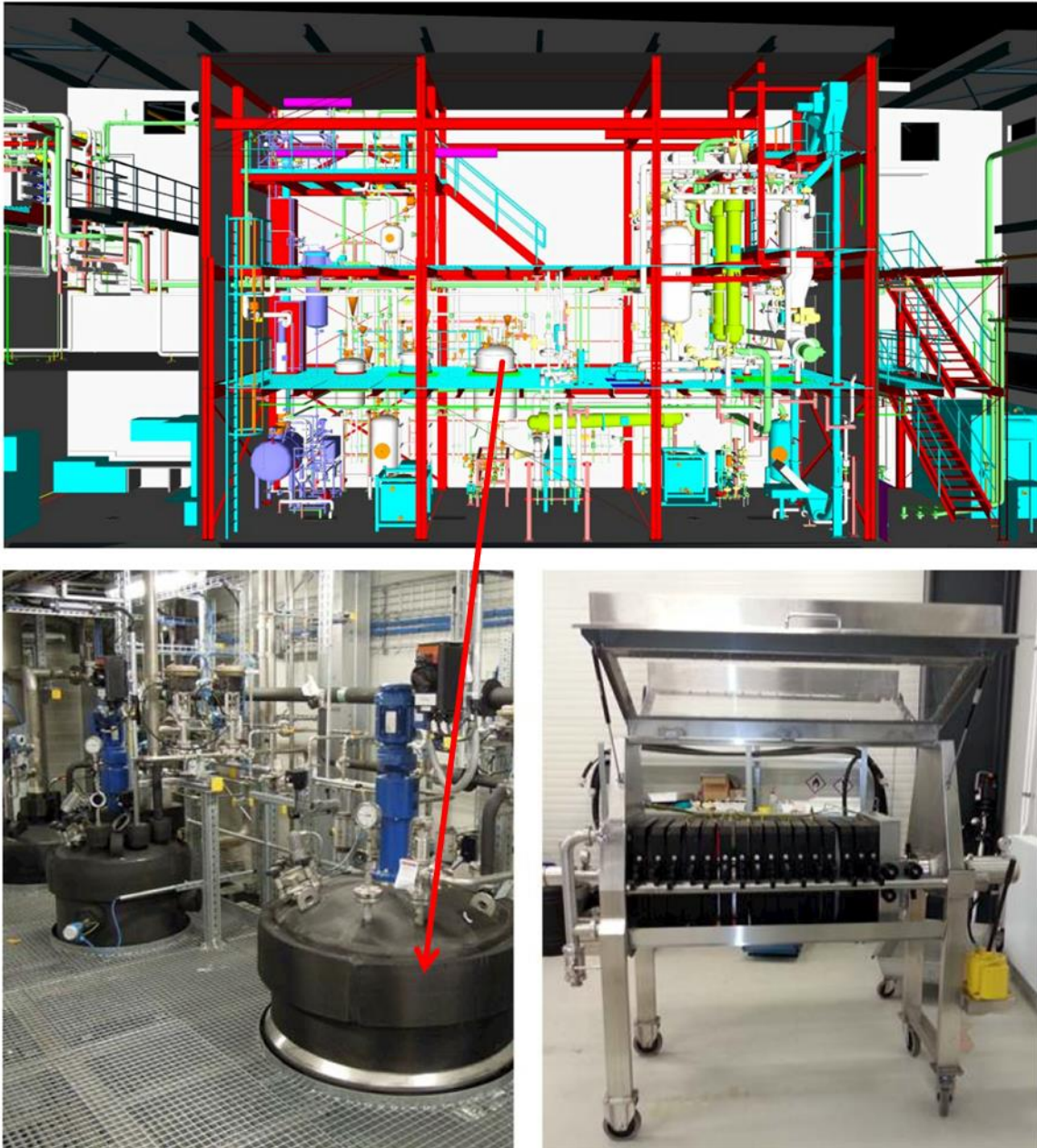
Figure 29: Top: 3D-model of the pulping, lignin precipitation and solvent recovery facilities in the lignocellulose biorefinery pilot plant at Fraunhofer CBP in Leuna. Bottom left: Photograph of the reactors for lignin separation (red arrow shows position of one reactor in the 3D model). Bottom right: Photograph of the chamber filter press for lignin filtration. Pictures have been adapted from the final report of the "Lignocellulose-Bioraffinerie" project (Michels et al. 2014).

3.7.   Filterability measurement procedure

Cake filtration experiments were carried out to determine the average filter cake resistance as a measure for the filterability of the produced lignin dispersions, similar as reported in literature ((Öhman 2006, Dingwell et al. 2011).
The experiments were carried out in a self-constructed pressure filter shown in Figure 30. At first, about 1 liter of lignin dispersion was filled into the transparent cylinder of the filter, while the filtrate and pressure valves were closed. Afterward, the filling valve was closed and the pressure was adjusted between 0.1 and 1 bar above atmospheric pressure. Then the filtrate and pressure valves were opened and the filtration started. The filtrate was collected in the beaker on the balance below the filter. The filtrate mass was recorded over filtration time. After complete filtration, the pressure valve was closed and the filter cake was removed in one piece to measure its height with a caliper. Density and dynamic viscosity of the filtrate were measured by an oscillating U-tube density meter (Mettler Toledo, DM40) and a falling sphere viscometer, respectively.
The average filter cake resistance was calculated applying the modified CARMAN equation, as described in literature (VDI 2010, Beckmann 2013).
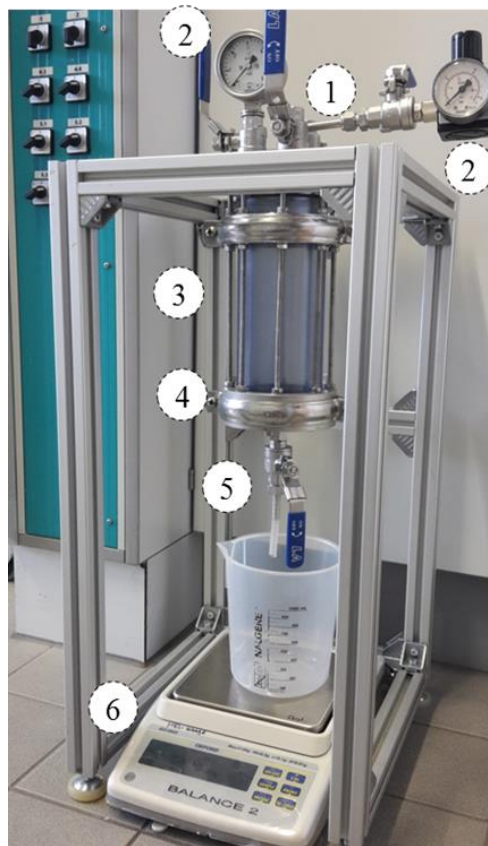
Figure 30: Photograph of the experimental setup for cake filtration experiments to determine the average filter cake resistance of lignin dispersion. The filter consisted mainly of 1: filling valve, 2: pressure regulation valve and gauge, 3: transparent dispersion cylinder, 4: 90 mm round filter holder with Whatman™ 589/2 filter paper, 5: filtrate valve and 6: filtrate balance with beaker.

4. Quantitative description of the lignin separation process

The continuous lignin precipitation process investigated in this thesis is rather complex and affected by many parameters (pressure, mass fractions and temperatures) which partly depend on each other. When one parameter is changed the resulting changes of the other parameters are not easy to predict. Especially during the operation of the pilot plant unforeseen conditions can cause problems, including safety risks. Therefore, a mathematical model of the pilot plant was formulated that should help evaluating the most important process parameters (compositions and temperatures in all parts of the plant) as function of the process time starting from different given initial conditions.

In this section, the developed mathematical model of the lignin precipitation process performed in pilot scale is described. The model was in this work mainly used to find suitable process conditions (feed mass flows, heat inputs, pressures, starting conditions) for the start-up of the upgraded pilot plant at Fraunhofer CBP. The basic mathematical modelling and the implementation in the Matlab™ Software have been performed within the Diploma thesis of Anja Kusian (Kusian 2014) which contains further details. The adaption of this model to the pilot scale process has been performed by the author. The source codes of the Matlab™ functions can be found in the appendix (A.3) to provide more detailed information.

4.1.   Structure of the model describing the pilot plant

The model was devoted to describe main features of the pilot plant in order to predict suitable operation conditions before starting up the plant for the first time after reconstruction (see 3.6.2). The model captures only the main apparatuses, which are necessary to describe the phenomena in the pilot plant. A schematic illustration of the model plant is shown in Figure 31.

The first apparatus A_1 is the **mixer**, where the pulping liquor feed stream **F**, the water feed stream **W** and the dispersion cycle stream **C** are mixed. The content of this mixer is approximately 500g water (initially) or lignin dispersion (during process). The liquor-dispersion mixture leaves the mixer for irrigation of the falling film evaporator (FFE). Lignin precipitates in the mixer as a result of the decreased ethanol mass fraction after dilution of the pulping liquor with the lignin dispersion of the dispersion cycle **C**. The amount of lignin precipitating can be calculated by a sub-model, describing the lignin solubility in aqueous solution in dependence of temperature and ethanol mass fraction.

The **falling film evaporator (FFE)** is described in the model as a cascade of several FFEs (A_2 to A_6). The FFE was divided into 5 parts (equilibrium stages, each containing 700g) in the model. This number is just an estimate of the unknown number of equilibrium stages in the real FFE. In every FFE the same amount of energy is added for liquid-vapor phase transition. The overall heating energy is defined as a constant

value by the user. In every apparatus, the vapor-liquid and solid-liquid equilibria are reached. The vapor phase from the last FFE A_6 leaves the model as gaseous distillate stream. The liquid and solid phases flow from A_6 into the mixed tank reactor A_7.

A_7 is a **mixed tank reactor** with a content between 200 and 600 kg (defined by the specific initial conditions), that acts as a buffer tank for lignin dispersion. No gas phase is present. The mass level of the tank is kept constant and the dispersion stream from A_6 is divided into the cycle stream to A_1 and the dispersion product stream D. The mass content can be defined by the user to a constant value, so that the mean residence of dispersion in the system can be adjusted.
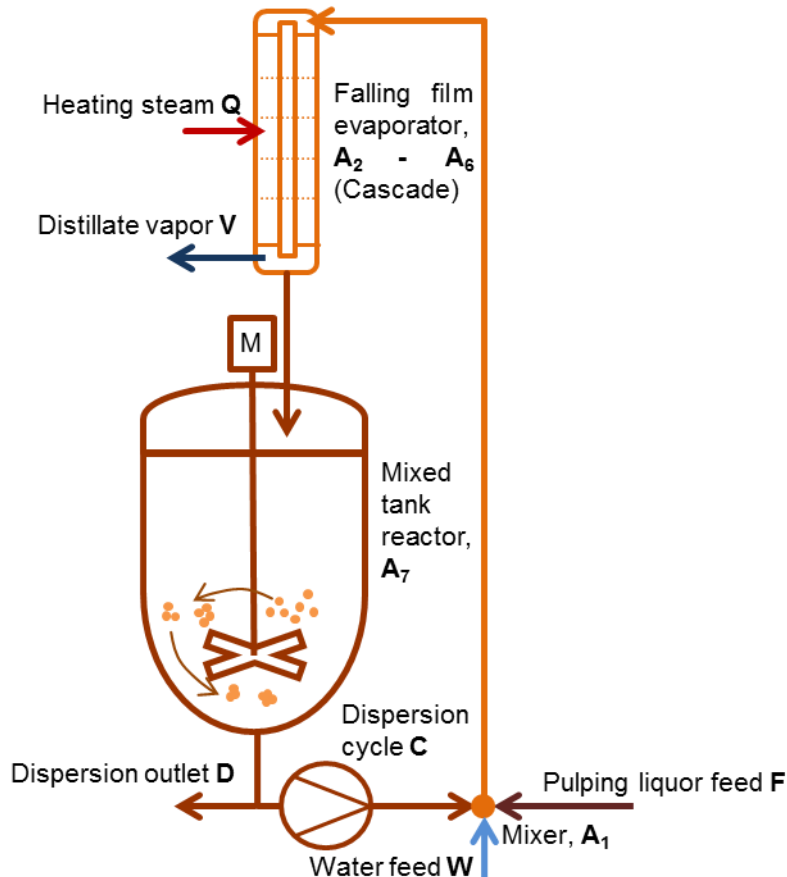
Figure 31: Schematic flowsheet of the pilot plant for lignin precipitation as the basis for the mathematical model of the plant developed.

The dimensions of the apparatuses and process streams are listed in Table 10. Typical ranges for the initial conditions ("water" or "lignin dispersion" means that the apparatus is filled at time zero with water or lignin dispersion) and process conditions (typical mass and energy flows) of each apparatus and process stream are also summarized in this table. The initial temperatures in all apparatuses are equal and can be preset in a reasonable range (20-60 °C). Additional information regarding the apparatuses and streams are also given in Table 10.

Table 10: Table of the single apparatuses and streams "in" and "out" of the plant with their dimensions and typical initial and process conditions. Additional information is listed as "Other properties".

Apparatuses and streams	Dimensions and typcial initial and process conditions	Other properties
A_1 Mixer	500 g (ml) water or lignin dispersion	T-pipe fitting
A_2-A_6 Falling film evaporator cascade	5*700g = 3500 g (or ml) water or lignin dispersion (partitioned in 5 parts for improved VLE calculation)	3.5 m² multi pipe, ca. 1mm film thickness
A_7 Stirred tank reactor	200-600 kg (or l) water or lignin dispersion	isolated and stirred tank reactor with maximum 680 l volume
F pulping liquor feed	50-200 kg/h (≈l/h)	average composition: 47, 3 and 3 wt. % of ethanol, lignin and sugars, respectively
W water feed	0-100 kg/h (≈l/h)	deionized water
C Dispersion cycle	2000- 3500 kg/h (or2- 3.5 m³/h) lignin dispersion	cycle for evaporator irrigiation
V vapor oulet	25-200 kg/h	compositions dependent from mass and energy balances and phase equilibria
D dispersion outlet	25-200 kg/h (≈l/h)	
Q heat input	20-90 kW (≈ 35-115 kg/h 4bar heating steam)	heating steam at 4 bar and 2133 J/g specififc heat of condensation

The task of the model was to calculate the compositions (mass fractions of all component) and temperatures in all apparatuses for every process time.

Starting point of the model is the overall steady state mass balance formulated as follows:

$$F \ (pulping \ liquor \ Feed) + W \ (Water \ feed) = D \ (lignin \ Dispersion \ outlet + V \ (distillate \ Vapor \ outlet)) \tag{7}$$

In Table 11 is given an overview of the different apparatuses considered in the model. The streams "in" and "out" of each apparatus, the phases considered in the streams, the considered components in each phase and the eventually occurring phase transitions of each component are described in this table.

For example, inlets to the mixer A1 are the streams F (pulping liquor), W (water) and C (dispersion cycle). The united streams contain liquid and solid phases but no gaseous phase. In the liquid phase the components 1-4 (ethanol, water, lignin and sugar) are present. In the solid phase only lignin (component 3) is present. The only phase transition that can occur is the precipitation (L→S) of lignin from the liquid phase (L) to the solid phase (S). The dispersion flow out of the mixer is called A1, which is flowing into the first evaporator-part A2 (together with a heat flux Q).

Table 11: Overview of the apparatuses modelled: the streams "in" and "out" of each apparatus, the considered phases (G: gaseous, L: liquid, S: solid) in each apparatus, the components (1: ethanol, 2: water, 3: lignin, 4: sugar) considered in each phase and possible component specific phase transitions.

Apparatus j j=1..7	in	Phases G, L, S	Components 1..4	Phase transitions	out
1	F + W + C	L	1		A1
			2		
			3	L→S	
			4		
		S	3		
2..6	A1 + Q	G	1		V
			2		
		L	1	L→G	A6
			2	L→G	
			3	L→S	
			4		
		S	3		
7	A6	L	1		C + D
			2		
			3		
			4		
		S	3		

Figure 32 illustrates in more detail schematically the mass and energy flows "in" and "out" of a certain apparatus A_j. The single-phase mass streams consist of the combined streams entering or leaving the apparatus (as listed in Table 11). Each phase stream "in" and "out" of an apparatus contains different components. The components that are present in every occurring phase stream are also listed in Table 11.

The phase transitions of a compound i in an apparatus A_j from liquid to gas (L→G) or liquid to solid (L→S) is described as mass flow $\dot{m}_{L \to G,i,A_j}$ or $\dot{m}_{L \to S,i,A_j}$, respectively. For the L→G phase transition a specific amount of enthalpy $h_{L \to G,i,A_j}$ is required and for L→S no enthalpy is released because lignin is amorphous and no other compound will transit to the solid phase.

Figure 32: Schematic illustration of the generalized apparatus j (A_j) with mass and energy flows to and from A_j and mass and energy flows between the three phases including phase transitions. The indices "in" and "out" are equivalent to A_{j-1} and A_j, respectively.

The specific mass balances of each single apparatus can be easily extracted from Table 11. The apparatus specific balances can be derived by specifying the subscripts in the following generalized formula:

$$\frac{dm_{x,i,A_j}}{dt} = \dot{m}_{x,i,A_{j-1},in} - \dot{m}_{x,i,A_j,out} + \sum_{i}^{N} \dot{m}_{x \to y,i,A_j} \tag{8}$$

As an example for the mass balance of lignin in the solid phase in mixer A1 results equation 9. (Equation 9 with slightly different indices can be also found in the line 619 of the Matlab® code given in Appendix A.3):

$$\frac{dm_{S,3,A_1}}{dt} = \dot{m}_{S,3,F} + \dot{m}_{S,3,W} + \dot{m}_{S,3,C} - \dot{m}_{S,3,A_2} + \sum_{i}^{N} \dot{m}_{L \to S,3,A_1} \tag{9}$$

In a similar way the energy balance for each apparatus can be derived from the following generalized formula:

$$\frac{dH_{A_j}}{dt} = \frac{d(m_{A_j} c_{p,A_j} T_{A_j})}{dt} = \dot{H}_{A_{j-1}} - \dot{H}_{A_j} + \sum_{i}^{N} \dot{m}_{x \to y,i,A_j} h_{x \to y,i,A_j}$$
$$= \dot{m}_{A_{j-1}} \cdot c_{p,A_{j-1}} \cdot T_{A_{j-1}} + (Q_{A_{j,(j=2..6)}})$$
$$= \dot{m}_{A_j} \cdot c_{p,A_j} \cdot T_{A_j} (+\dot{m}_{x \to y,i,A_j} \cdot h_{x \to y,i,A_j}) \tag{10}$$

The mass streams "in" $\dot{m}_{A_{j-1}}$ and "out" $\dot{m}_{A_j}$ of an apparatus are also the sum of the mass streams of phases in $\dot{m}_{x,in}$ and out $\dot{m}_{x,out}$ according to Figure 32.

The average specific heat capacity of the phases in a stream $c_{p,in}$ is calculated by weighing the specific heat capacity of each component $c_{p,x,i,in}$ with its mass fraction $w_{x,i,in}$ in the stream. All phases in a stream flowing "in" or "out" of an apparatus are assumed to have the same temperatures T_{in} or T_{out}, respectively. Heat flows Q_{A_j} are added to each evaporator A$_{2..6}$.

The phase transition mass stream $\dot{m}_{x \rightarrow y,i,A_j}$ and the specific phase transition enthalpy $h_{x \rightarrow y,i,A_j}$ form the phase transition energy flow term.

The energy balance of each apparatus can be used now together with the mass balances to calculate the temperature in each apparatus (and the amount of ethanol and water that evaporate in A$_{2-6}$). For example, the energy balance of A$_2$ can be found in the lines 707-714 of the mentioned Matlab$^®$ code given in A.3.

Mass fractions of substances in their corresponding phase are often used in the sub-models and for process illustrations. For example, $w_{L,1,A_j}$ describes the mass fraction of ethanol (i=1) in the liquid phase (x=L) in the apparatus j (j=1..7) and can be expressed as follows:

$$w_{L,1,A_j} = \frac{m_{L,1,A_j}}{\sum_{i=1..4} m_{L,i,A_j}} \tag{11}$$

Whereas, the lignin mass fraction (i=3) in the lignin dispersion (liquid + solid phase) in any apparatus A$_j$ has to be described differently because two phases are involved:

$$w_{L+S,3,A_j} = \frac{m_{S,3,A_j}}{\sum_{i=1..4} m_{L,i,A_j} + m_{S,3,A_j}} \tag{12}$$

4.2. Phase equilibria sub-models

Only evaporation (L→G) and precipitation (L→S) are considered as phase transitions taking place in the process. Dissolution, condensation and lignin glass transition (softening) processes are at this stage not taken into account.

Lignin precipitation (L→S)

Experimentally determined solubility data of lignin in ethanol/water mixtures at different temperatures have been fitted with the *cftool* of Matlab™. The solubility function obtained can be expressed as follows:

$$
\begin{aligned}
w_{L,3}^* = f\left(w_{L,1}, T_L\right) \\
= -0.0003498 + 0.04442 \cdot w_{L,1} + 3.654e - 05 \cdot T_L \\
+ (-0.3131) \cdot w_{L,1}^2 + (-0.001733) \cdot w_{L,1} \cdot T_L \\
+ (-1.558e - 07) \cdot T_L^2 + (0.6933) \cdot w_{L,1}^3 + 0.009525 \\
\cdot w_{L,1}^2 \cdot T_L + 6.225e - 06 \cdot w_{L,1} \cdot T_L^2
\end{aligned} \tag{13}
$$

In equation (13) $w_{L,3}^*$ is the expression for the saturation mass fraction of lignin in the liquid phase, $w_{L,1}$ stands for the mass fraction of ethanol in the liquid phase and T_L is the temperature of the liquid phase.

Figure 33 shows a plot of the fitted solubility function that fits reasonably well to the experimental points (red circles). However, the solubility model should only be applied in the ranges of ethanol contents and temperatures that have been experimentally covered (0-40 wt. % ethanol and 10-70 °C).
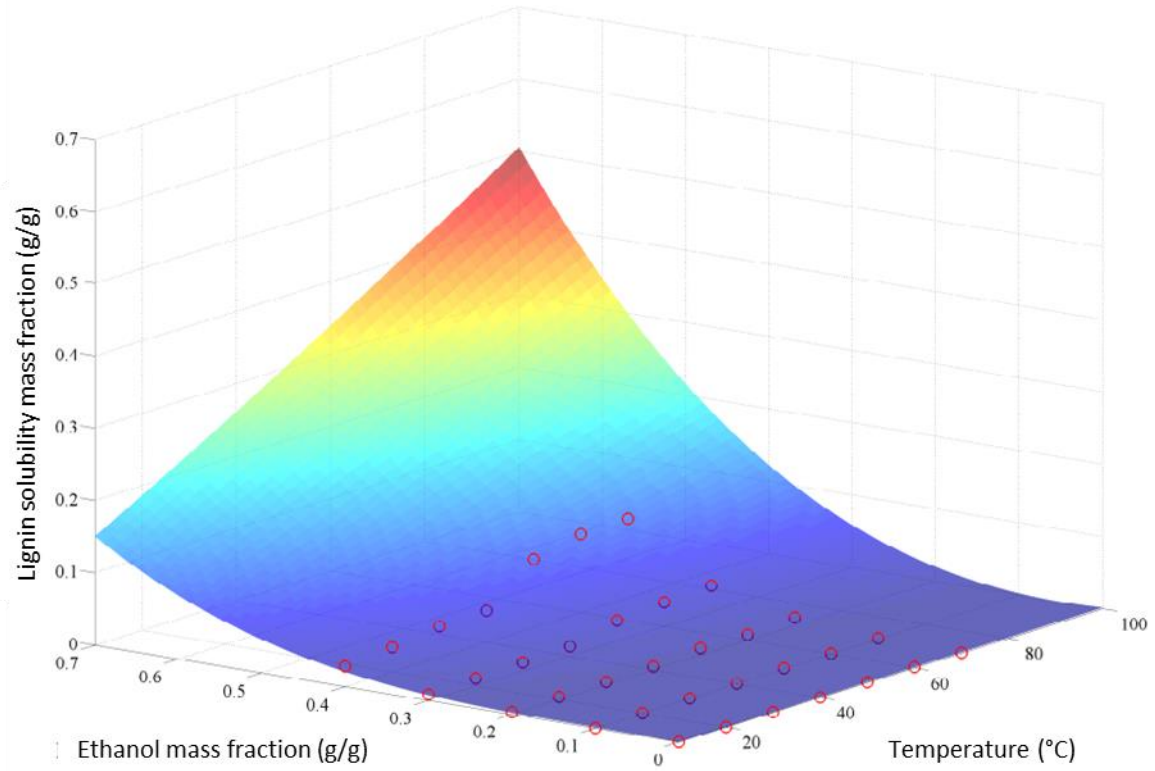
Figure 33: Surface plot of the fitted solubility function $w_{L,3}^* = f(w_{L,1}, T_L)$. The red circles indicate the experimental solubility data. The plot was adapted from the thesis of Kusian (Kusian 2014).

The supersaturation of lignin is calculated in each apparatus A_j as the difference between the lignin mass fraction in the liquid phase $w_{L,3,A_j}$ and the saturation mass fraction of lignin $w_{L,3,A_j}^*$ for the corresponding ethanol mass fraction $w_{L,1}$ and temperature in the liquid phase T_L calculated from Equation (13). The phase transition mass flow $\dot{m}_{L \rightarrow S,3,A_j}$ is calculated from the supersaturation and the mass flow of liquid phase $\dot{m}_{L,A_j}$ using Equation (14).

$$\dot{m}_{L \rightarrow S,3,A_j} = (w_{L,3,A_j} - w_{L,3,A_j}^*) \cdot \dot{m}_{L,A_j} \tag{14}$$

As an example, the calculation of the mass flow of precipitating lignin in the mixer A1 can be found in the mentioned code within the lines 591-603 (Appendix A.3).

It should be mentioned that for simplicity the specific phase transition enthalpy for lignin precipitation $h_{L \rightarrow S,3}$ was assumed to be zero.

The vapor-liquid equilibria between ethanol and water are calculated within another sub-model. Thereby the ethanol mass fraction in the vapor phase is calculated in dependence of the ethanol mass fraction in the liquid phase and the pressure. Ideal gas behavior was assumed because of the relatively low pressures (around 100 mbar absolute). Influences of dissolved solids in the liquid phase on the vapor pressure were neglected. The mass fraction of ethanol in the gas phase is calculated from the ethanol mass fraction in the liquid phase, the overall pressure, the pure ethanol vapor pressure and the activity coefficient of ethanol in the liquid phase. The pure ethanol vapor pressure is calculated by the *Antoine* equation and the activity coefficient is calculated by the *van Laar* equation (e.g. see A.3, lines 636-642 and (Gmehling 1981). The coefficients for both equations have been extracted from literature (Schlünder and Thurner 1995) and are listed in the appendix (A.3, lines 58-64).

The phase transition mass flow (e.g. $\dot{m}_{L \to G, i, A_j}$ for i=1, 2) was calculated from the energy supplied to the apparatus Q_{A_j} and the average specific phase transition enthalpy $h_{L \to G, i}$ of the calculated vapor phase composition.

4.3.   Solution concept and implementation in Matlab®

The mass and energy balance equations (8-10) introduced above form a system of ordinary differential equations (ODEs). The specific equations form a matrix of 1+52 columns (reduced from 91 because not every substance is considered in each phase as shown in Table 11) that is solved numerically using the "ode15s" solver of Matlab® (Shampine and Reichelt 1997). The solution matrix contains the mass of each considered component in each phase + apparatus and their temperature in a row with an adjustable time resolution between the rows. Mass fractions and mass flows can be subsequently calculated then from the matrix by using the preset feed and cycle streams (F, W and C).

4.4.   Application of the model

The model was applied to identify suitable process parameters for the continuous precipitation experiments in the pilot plant. The predicted data of the model are plotted together with the experimental data in the results and discussion chapter 5.5.2.

Below a selection of some design data of the pilot plant have been evaluated with the model. The results are also presented as a plausibility test for the model. In order to evaluate if the model provides logical results a set of parameters that are in the range of the design data characteristic for the pilot plant have been tested. The initial conditions used for this model evaluation are listed in Table 12.

Table 12: Initial conditions that were used for the model evaluation.

Apparatuses and streams	Initial conditions
A_1 Mixer	500 g water at 40°C
A_2-A_6 Falling film evaporator cascade	each 700g (or ml) water at 40 °C
A_7 Stirred tank reactor	200 kg (or l) water at 40 °C
F pulping liquor feed	200 kg/h (≈ l/h), (47.2 wt. % ethanol, 2.3 wt. % lignin, 2.3 wt.% sugars)
W water feed	50 kg/h (≈ l/h)
C Dispersion cycle	3500 kg/h (3.5 m³/h) water
V vapor oulet	0
D dispersion outlet	0
Q heat input	77 kW
Pressure	120 mbar absolute

The process behavior was calculated for 15 hours. Hereby, the streams F, W, C, Q, the pressure and the overall masses in the apparatuses stay constant during the process. The mass fractions of components i and phases x as well as the temperatures in each apparatus j change in the course of the process. Material constants and the other conditions can be found in the lines 10-80 in the program code in appendix A.3.

Figure 34 illustrates predicted changes of the composition of the lignin dispersion in the mixer **A1**. The mass fractions of ethanol, lignin and sugars increase over several hours from zero (pure water) because of feeding pulping liquor and converge each to their steady-state mass fractions. The ethanol mass fraction converged after around 2 hours to about 10.5 wt. % in the liquid phase of the dispersion. The dispersed lignin and dissolved sugar fractions reached for the setup considered 5-6 wt. % after about 12 hours. The reason for the very different approximation times is the large difference between the partial mass flows of ethanol and lignin (and sugar). The mass fraction of dissolved sugar in the liquid phase of the dispersion is higher than that of the dispersed lignin because the dispersed lignin fraction is defined as relative to the complete dispersion mass (liquid + solid phase) and the dissolved sugar fraction is defined as relative to only the liquid phase of the dispersion. The mass fraction of dissolved lignin increases only at the beginning with the increasing ethanol mass fraction and subsequently stays at very low levels corresponding to the low lignin solubility.
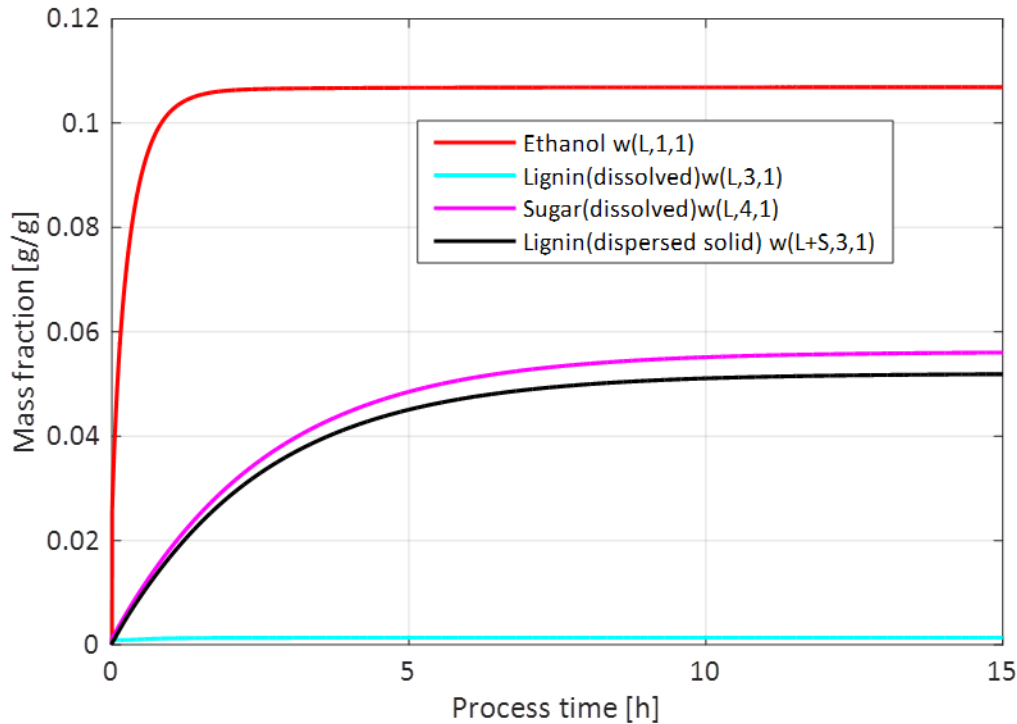
Figure 34: Composition of the dispersion in the mixer A1 plotted over the process time.
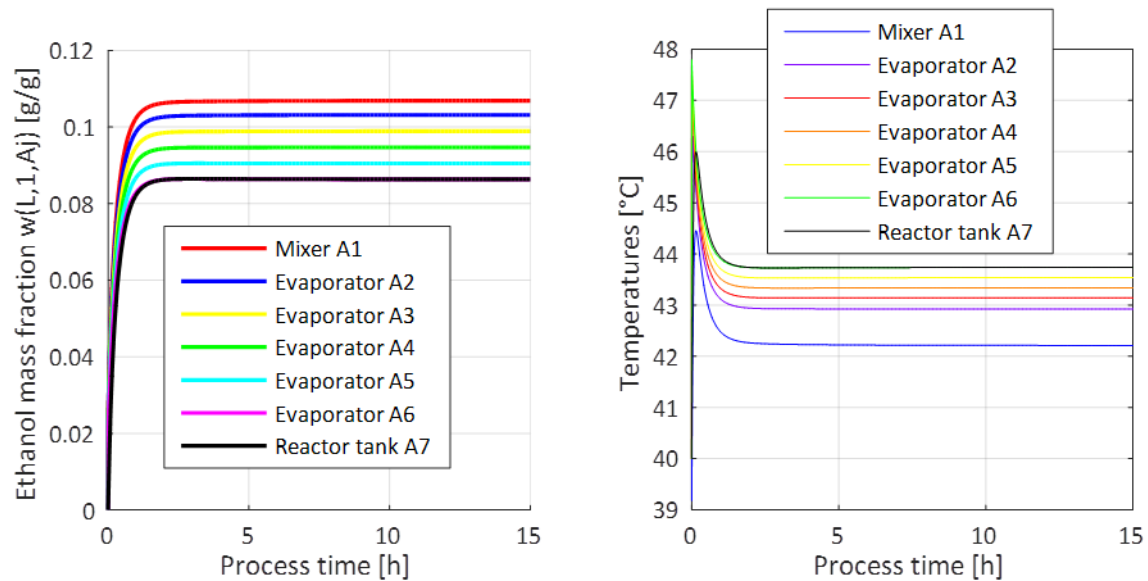
Figure 35: Left: Mass fraction of ethanol in the liquid phase of the lignin dispersion in all apparatuses A1-A7 plotted over the process time. Right: Temperatures in all apparatuses A1-A7 plotted over the process time.

The ethanol mass fraction in the liquid phase of the lignin dispersion is plotted in Figure 35 (left) for all apparatuses. Generally, the ethanol fractions in all apparatuses increase from zero (pure water) because of the feed of pulping liquor in the mixer A1 and approximate their steady-state level as already shown for the mixer A1 in Figure 34. The steady-state ethanol mass fractions decrease starting from the mixer A1 over the evaporator-parts A2-6 because ethanol is evaporated in every evaporator. The mass fraction in the last evaporator A6 and the stirred tank (A7) are equal because the

dispersion flows directly from A6 to A7 without further changes. In fact A7 acts only as a "storage" tank.

Figure 35 (right) shows the temperatures in all apparatuses A1-A7 over the process time. The temperatures depend on the vapor-liquid equilibrium of ethanol and water at the process pressure. Therefore, the temperatures increase at the very beginning (because the ethanol mass fractions are lower and the boiling temperature higher) before they approximate their steady-state value with increasing ethanol mass fractions in all the seven apparatuses.

The composition of the product dispersion D over the process time is shown in Figure 36. The mass fractions behave similar to that in the mixer A1 (Figure 34) but the ethanol mass fraction is lower and the lignin and sugar mass fractions accordingly higher because of the evaporated ethanol and water.
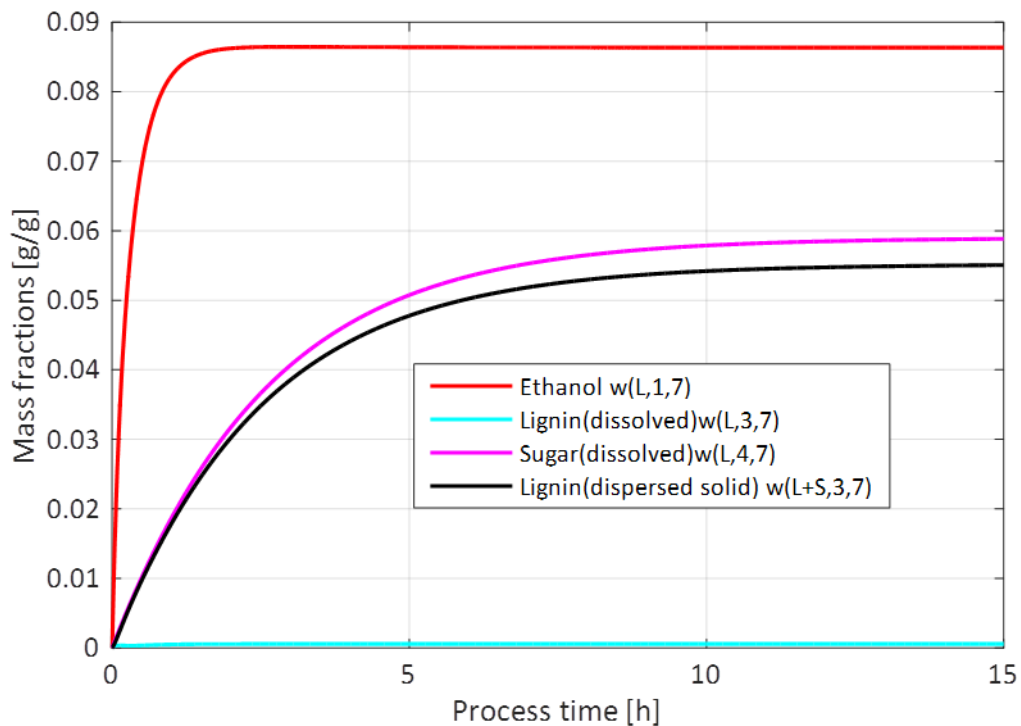
Figure 36: Composition of the dispersion D leaving the stirred tank reactor A7.

Finally, Figure 37 shows the mass flows of gaseous vapor V (leaving the last evaporator A6) and dispersion D (leaving A7) that are strongly dependent from the vapor-liquid equilibrium of ethanol and water. Thus, both converge to their steady-state values like the ethanol mass fractions in the apparatuses. Correspondingly, the ethanol mass fraction of the vapor behaves equivalent. As required, the sum of V and D equals the sum of F and W (both 250 kg/h or 69.4 g/s) and that fulfills equation (7).
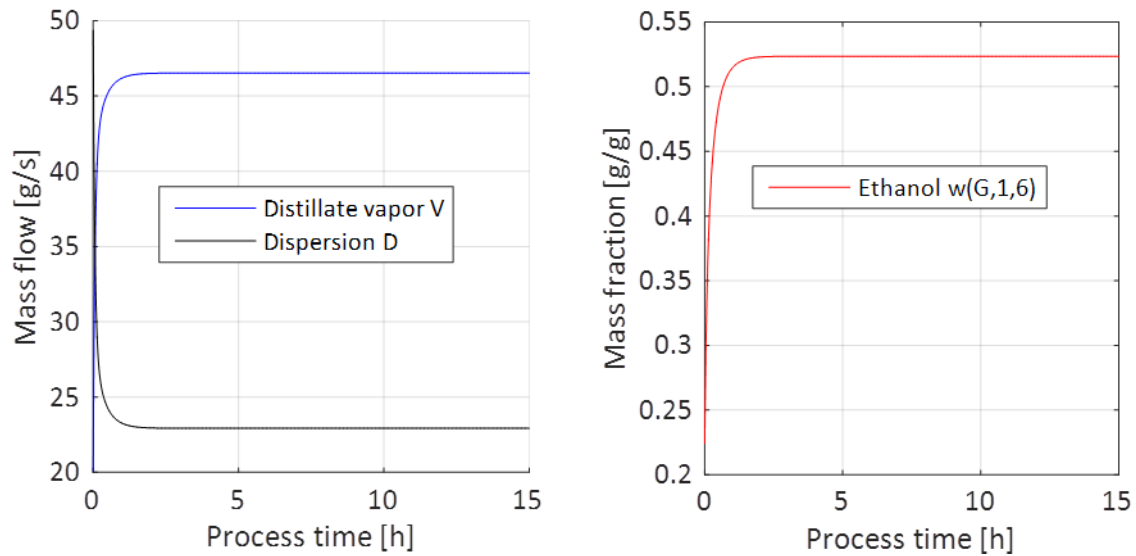
Figure 37: Left: Mass flows of vapor V (leaving the last evaporator A6) and dispersion D (leaving A7). Right: Mass fraction of ethanol in the vapor V.

To summarize the value of the described simplified mathematical model of the process can be stated, that the shown trends appear generally logically and the model captures essential features of the process. Thus, it appears useful for process design. The applicability of the model will be further evaluated in section 5.5.2 by comparison of model predictions with experimental data.

5. Results and discussion

In this chapter, major results of the experiments described in the previous chapter are presented and discussed. Parts of this chapter have been published already before (Schulze et al. 2014, Schulze et al. 2016, Schulze et al. 2016).

5.1. Physical and chemical properties of pulping liquors and lignins

5.1.1. Pulping liquor composition

The pulping liquors provided by the Fraunhofer CBP were investigated in terms of composition and lignin properties before they were processed in the different precipitation experiments described in this work. Table 13 shows lignin (1.35 – 3.35 wt. %) and ethanol (43.8 – 55 wt. %) contents of the liquors processed in this work.

Table 13: Overview of compositions of investigated pulping liquors. Lignin contents were gravimetrically determined and ethanol contents were measured by headspace-GC (n.a.: not analyzed).

Pulping batch No.	Lignin in pulping liquor (wt. %)	Ethanol in pulping liquor (wt. %)
K1	2.2	47.2
K9	2.6	44.2
K29	2	50.7
K37	1.86	45.23
K39	2.41	43.81
K40	2.04	45.42
K41	2.53	44.9
K42	1.93	44.17
K43	1.72	45.18
K44	2.21	45.33
K45	1.49	44.02
F02	2.8	55
K103	2.3	46.39
K128	3.35	43.35
K138	1.35	47.2
K139	1.35	n.a.

The liquor from spruce wood pulping F02 has higher ethanol content due to pulping with 65 wt. % ethanol in the pulping solvent. Dissolved hemicellulose (sugars) contents had about the same value like lignin. However, they are not displayed in the table. Generally, the lignin contents are quite low and originate from the solid to liquid ratio in

the pulping process. The batch pulping is performed with a dry wood content of about 24 wt. %. The subsequent washing step with almost the same amount of solvent reduces the overall wood in the pulping batch content to about 12 wt. %. It can be estimated that approximately 15 – 25 wt. % of lignin are dissolved from the wood, resulting in 1.8 – 3 wt. % lignin content dissolved in the pulping liquor (spent + wash liquor).

The overall biorefinery efficiency could be substantially improved by increasing the wood content in the pulping process to reach higher lignin contents in the liquor. Continuous countercurrent pulping may be a possibility to maintain higher wood-solvent ratios.

5.1.2.   Lignin composition and molecular structure

Elemental analysis

The results from elemental analysis of some lignins investigated in this work are listed in Table 14. The carbon content ranges from 59.6 to 63.85 wt. % and is 62.2 wt. % in average. Sinapyl alcohol (S) that is a predominant monomer of hardwood lignin has a carbon content of 62.9 wt. % indicating the investigated lignins consist of to a great extent of S-monomers. The sulfur and nitrogen contents are low as usual for particularly pure organosolv lignins. The water content arises from air moisture that was adsorbed by the lignin after drying again.

Table 14: Elemental compositions and (airborne) moisture of investigated lignins.

Pulping batch no.	C (wt. %)	H (wt. %)	N (wt. %)	S (wt. %)	H_2O (wt. %)
K1	59.6	6.44	0.05	0.23	4.1
K6	59.83	6.37	0.22	0.24	5.5
K8	60.86	6.55	0.11	0.21	3.4
K9	60.94	6.54	0.14	0.21	4
K37	62.75	6.29	0.1	0.29	3.8
K39	63.85	6.03	0.09	0.27	3.9
K40	63.71	6.15	0.13	0.24	4.1
K41	65.34	5.92	0.15	0.21	3.4
K42	62.93	6.38	0.11	0.35	3.7
K43	61.81	6.36	0.09	0.29	3.8
K44	63.76	6.26	0.04	0.21	2.7
K45	60.97	6.4	0.02	0.23	5.1

Molar mass distribution

The molecular masses of lignins investigated within this work have been measured by size exclusion chromatography (described in 3.2.3.2) and the results are listed in Table 15. The weight-average molar masses range between 1949 (K41) and 5868 (K45) g/mole, whereby K45 lignin was derived from a mild pulping batch resulting in relatively large lignin molecules. Overall, the molar masses are in a typical range for organosolv lignins (Baumberger et al. 2007). The polydispersity, which is a measure for the broadness of molar mass distributions and is 1 if all molecules have the same mass, ranges between 2.2 and 5.2.

Table 15: Molar weights of the investigated lignins determined by HPSEC.

Pulping batch No.	Number avg. molecular mass of lignin (M_n) (g/mol)	Weight avg. molecular mass of lignin (M_w) (g/mol)	Polydispersity M_w/M_n (-)
K1	1056	3949	3.738
K6	1197	4069	3.4
K8	842.3	2737	3.249
K9	1108	4903	4.426
K29	1017	5327	5.236
K37	1101	3041	2.762
K39	961.9	2212	2.3
K40	977.6	2494	2.551
K41	884.3	1949	2.204
K42	1085	3298	3.04
K43	1183	3778	3.194
K44	944.9	2329	2.465
K45	1162	5868	5.052
F02	823	2146	2.608
K103	1045	2816	2.693
K128	1046	3014	2.882
K138	819.2	2160	2.636
K139	n.a.	n.a.	n.a.

Figure 38 shows the correlation between weight-average molar mass and polydispersity, indicating an increase in polydispersity with increasing molar mass. This correlation implicates that lignin molecule masses become more uniform with increasing depolymerization during the pulping process.
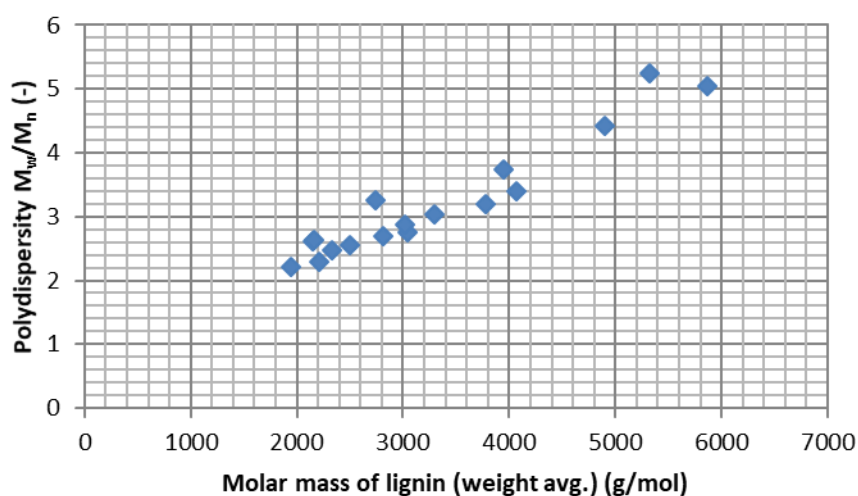
Figure 38: Polydispersity in dependence of molar mass of lignin samples investigated.

Klason lignin content

The acid insoluble lignin content (aka. Klason lignin) of K8 lignin was determined by hydrolysis of a lignin sample in diluted sulfuric acid according to standard procedure provided by NREL (National Renewable Energy Laboratory) (Sluiter et al. 2008). The Klason lignin content is used to estimate the residual carbohydrates attached to the lignin, which could influence factors such as solubility. The Klason lignin content of K8 lignin was quantified to 89.6 wt. %.

Molecular structure analysis

K8 lignin was analyzed using 2D HSQC NMR analysis of the lignin dissolved in DMSO-d6. The acquired spectra and corresponding molecular structures are displayed in Figure 39 and Figure 40. The molecular structures were assigned to the spectral regions as described in the literature (Mainka et al. 2015, Constant et al. 2016). Red marked NMR signals from the red marked carbon atoms in the lignin structures have been used for the semi-quantitative analysis of the spectra. Blue marked NMR areas were not analyzed but assigned to visualize that most signals could be assigned to molecular structures. Only minor signals were not assigned to any molecular structure, meaning that lignin K8 could be characterized quite completely.
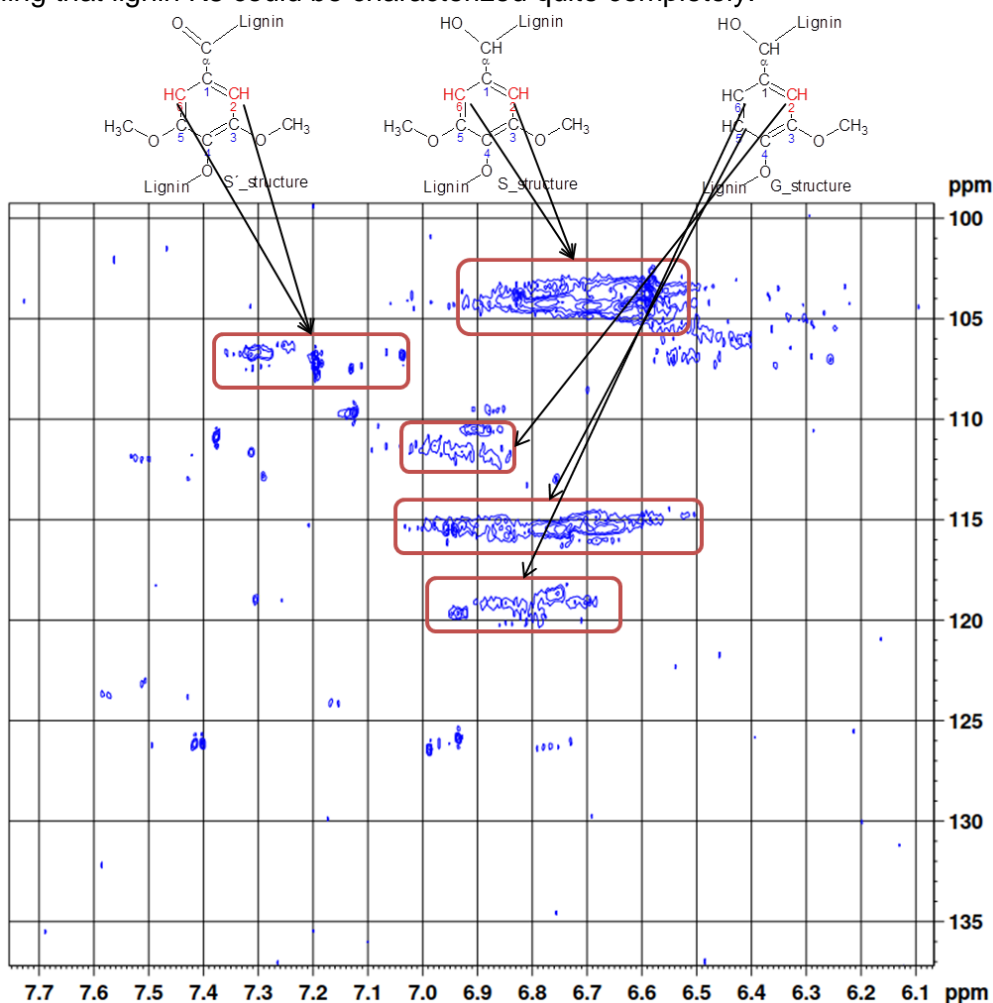
Figure 39: Aromatic region of the 2D HSQC NMR spectrum of lignin K8 and above the main structures corresponding to the marked regions in the spectrum, according to the literature (Mainka et al. 2015, Constant et al. 2016).
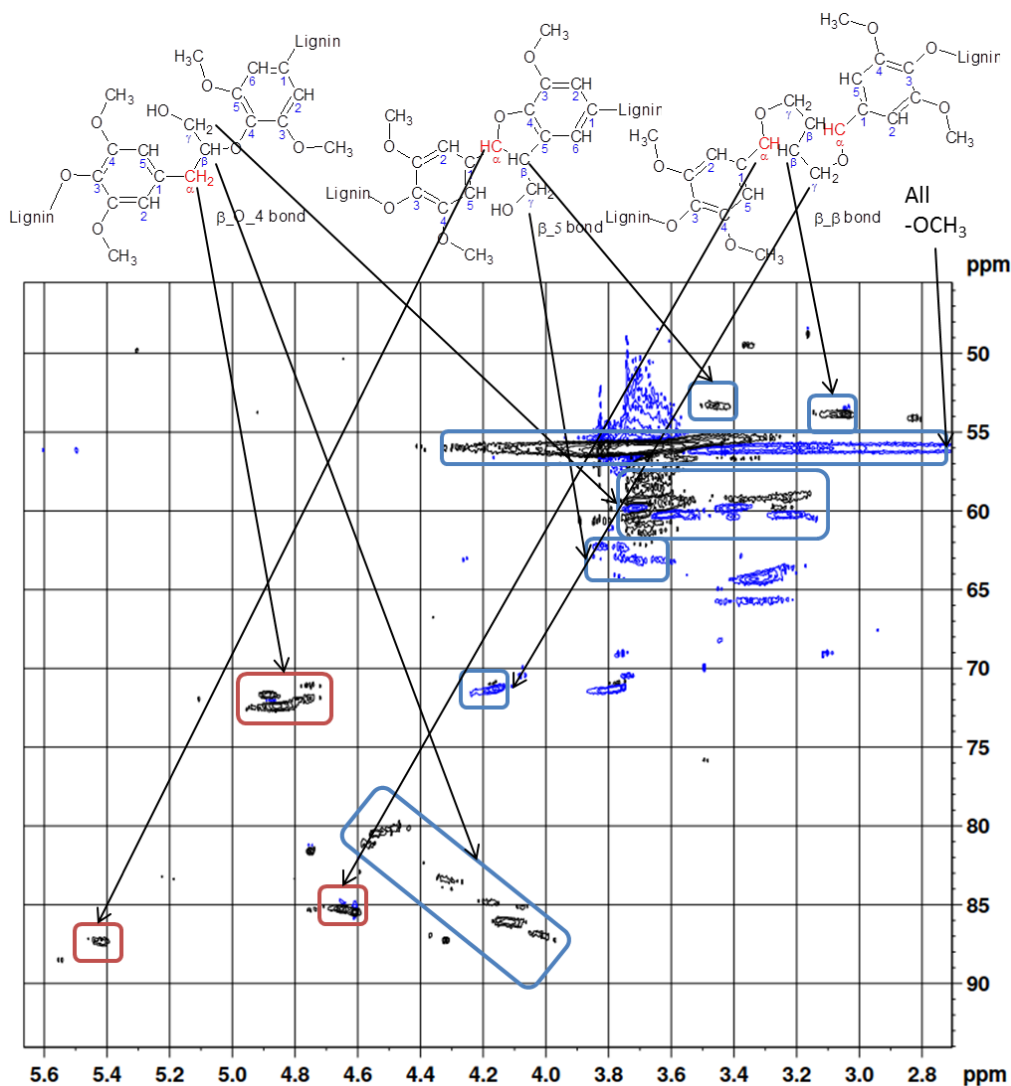
Figure 40: Aliphatic region of the 2D HSQC NMR spectrum of lignin K8 and above the main structures corresponding to the marked regions in the spectrum, according to the literature (Mainka et al. 2015, Constant et al. 2016)

The semi-quantitative composition of the assigned lignin structures were calculated as described in the mentioned literature. The spectral areas of the 2nd ring carbon of the S- and G-structures were summed and defined as 100 % of monomer content. The area of the S-structure had to be halved because the signal of the 6th ring carbon doubles the intensity in the same area. Areas of H structures were not observed in the spectra. The S and G areas were divided by the sum of S and G areas to determine the S and G fractions of the monomer composition. The areas of the α-carbon of every type of bond were divided by the sum of S and G areas to determine the fraction of every bond per lignin monomer. The areas and fractions are summarized in Table 16.

Table 16: Semi-quantitative composition of lignin K8 calculated from the 2D HSQC spectra.

Molecular structure or bond	S(2.6)/2	G(2)	β-O-4	β-5	β-β
Integral	1.07E+10	2.87E+09	5.99E+09	1.00E+09	2.23E+09
Fraction per monomer	0.789	0.211	0.440	0.074	0.164

The calculated composition has been used to design a model molecule with approx. 3000 g/mole (see 3.3.3). This model molecule has been implemented in the COSMO-RS software to calculate liquid-liquid-equilibria in the lignin-water-ethanol system (see 5.2.4).

In comparison to some quantitative NMR studies on hardwood EOS lignin from literature, the K8 lignin shows high amounts of β-O-4 linkages (44 per 100 monomers) and a for hardwood typical S/G/H ratio of 0.79/0.21/0. Constant et al. (see Table 2) found a similar S/G/H ratio of 0.53/0.47/0 for poplar lignin and almost no β-O-4 linkages or other bonds for a poplar EOS lignin (Constant et al. 2016). Other authors (Bauer et al. 2012, Wen et al. 2013) found similar results (44 and 42 β-O-4 bonds per 100 monomers) for EOS lignin from birch and Misanthus giganteus compared to the results of this work. Generally, the K8 lignin has a relatively high amount of ether-linkages (all quantified bonds contain an ether-group) of almost 68 per 100 monomers in sum that may result from carefully mild pulping conditions.

5.2.   Lignin phase behavior

Lignin is not one distinct substance but a mixture of chemically similar molecules in a certain range of molar masses. Therefore, lignin is a pseudo-substance and the phase diagram with ethanol and water is called pseudo-ternary. Further, lignin is considered as an amorphous substance without crystal structure and therefore can be defined as a (subcooled) liquid (glass) from a thermodynamic point of view. When solvated, the glass transition temperature of lignin is substantially lowered and it behaves as liquid phase at room temperature. The (solid-) liquid-liquid equilibria between the lignin-phase and the solvent-phase have been characterized in different experimental approaches and the results are presented in the following sections. The following results have already been published (Schulze et al. 2014).

5.2.1.   Isothermal lignin solubility

Isothermal solubility of K8 lignin in the solvent phase was measured as described in section 3.3.1.1. The solubility data in dependence of temperature and ethanol content in an aqueous solvent are displayed in the contour plot below (Figure 41). From 0 to 10 wt. % ethanol in the solvent, lignin is almost insoluble (<1 wt. %) in the investigated temperature range between 10 and 70 °C. Between 10 and 30 wt. % ethanol in the solvent, the solubility slightly increases to about 1 and 3 wt. % at 10 and 70 °C, respectively. The lignin solubility increases more significant between 30 and 40 wt. % ethanol in the solvent and reaches a maximum of about 11 wt. % at 70 °C.
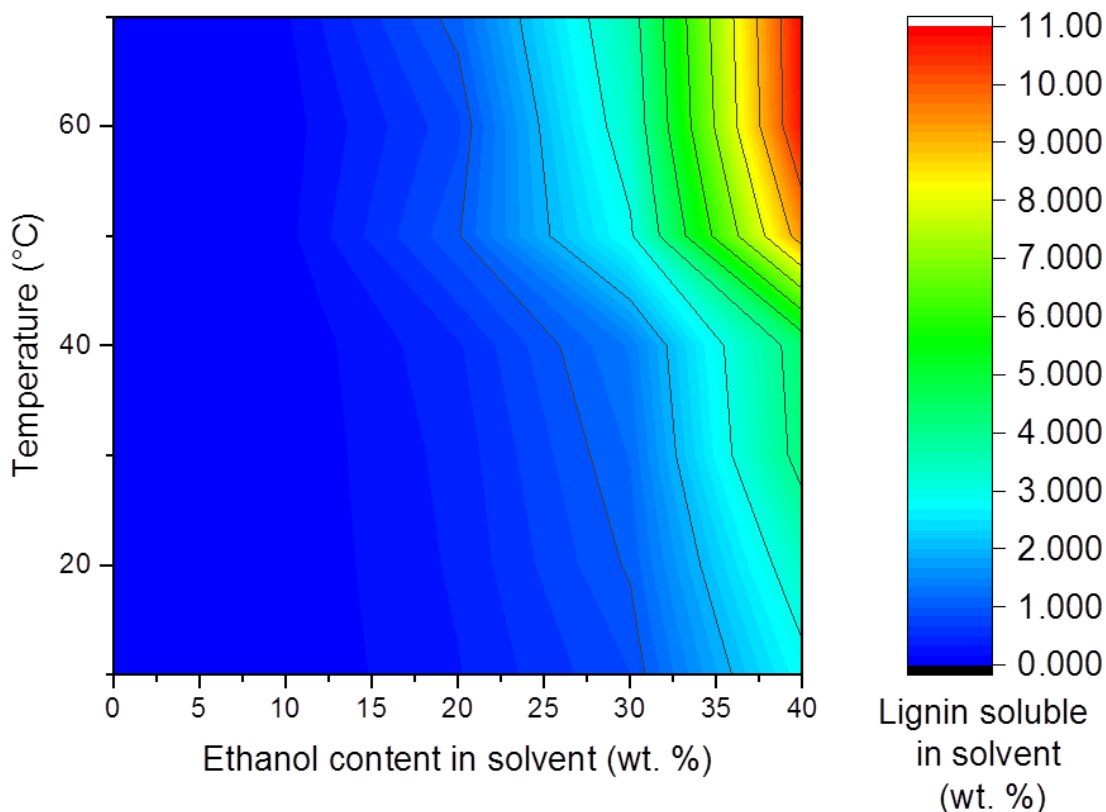
Figure 41: Portions of K8 lignin soluble in different ethanol-water mixtures and temperatures.

As the lignin was never completely dissolved in order to ensure thermodynamic equilibrium between the solvent and lignin phases, it is likely that the lignin was fractionally dissolved in the solvent phase, whereby smaller lignin molecules were enriched in the solvent phase and larger lignin molecules were enriched in the solvated lignin phase. Therefore, it is actually not the solubility of K8 lignin but of an uncharacterized fraction of K8 lignin. However, being aware of this uncertainty, the term solubility is used in this section.

From this solubility data, the operation window for the lignin precipitation process was concluded. To achieve maximum lignin yields during precipitation, the ethanol content has to be decreased below 10 wt. % at any temperature between 10 and 70 °C because the lignin is practically insoluble at this conditions and will precipitate almost completely from the pulping liquor. The second but not less important criterion for the process operation window is the avoidance of precipitation of a sticky solvated lignin phase that could cause incrustations. Figure 42 shows a photograph of such sticky lignin phase in presence of a solvent phase with 40 wt. % of ethanol in water at room temperature. Within the solubility measurements it was recognized that K8 lignin behaves like a glassy solid in presence of solvents with ethanol contents < 10 wt. % and temperatures < 50 °C.

From these observations it can be concluded that the precipitation process should operate at < 10 wt. % ethanol in the solvent phase and at temperatures below 50 °C in order to fulfill the process-goals of high lignin yield and low incrustations.

Figure 42: The photograph shows a glass vial that was turned upside-down a few seconds before taking the photo. It contains a sticky solvated lignin-rich phase that slowly flows down and a black liquid solvent-rich phase beneath that already rinsed down the vial.

5.2.2.   Pseudo-ternary phase diagram of lignin, water and ethanol

The (solid-) liquid-liquid equilibria between lignin-phase and solvent-phase at room temperature (23 °C) have been measured as described in section 3.3.1.2 and the results are displayed in the ternary plot below (Figure 43).
The grey colored symbols show the compositions of the mixtures created in the reactor and the black symbols connected to them show the compositions of the two phases that formed after phase separation at 23 °C. The compositions of the phases have been measured via infrared spectrometry and calibration, as described in section 3.3.1.2. Some compositions lie outside the calibration range and have therefore an undefined accuracy.
The red curves in Figure 43 were fitted to the black symbols in order to illustrate the shape of the miscibility gaps of the system. The system shows two miscibility gaps around the investigated compositions in which two liquid phase, a lignin (-rich) and a solvent (-rich) phase, separate from each other whereby the lignin-rich phase appears solid after vitrification at low ethanol contents.
The gap between lignin and water has already been reported earlier for another organic solvent (Le et al. 2016). The solvent-rich phase of this miscibility gap was already investigated in other isothermal solubility measurements within this work described before in 5.2.1, where obviously lower lignin solubilities ($\approx$ 3 wt. % lower) have been measured at the similar temperature of 20 °C and ethanol contents between 30 and 40 wt. %. The differences between both measurement techniques may be due to the different equilibrations times (> 2 vs. 48 hours) and the different analytical methods for the measurement of lignin content (calibrated infrared spectrometry vs. gravimetry). However, the results of both measurement techniques show similar trends and the very similar results for lower ethanol contents that are most relevant for the precipitation process.
The miscibility gap between lignin and ethanol has not been reported in literature yet but a decrease of solubility beyond ca. 80 wt. % ethanol in water has been previously

reported (Ni and Hu 1995) and gives already an indication for decreased solubility in the pure solvent.

The highest lignin solubility was measured between 60 and 90 wt. % ethanol in the solvent with a maximum around 80 wt. % ethanol. In this region between both miscibility gaps every composition will form one (liquid) phase at 23 °C (and likely also at higher temperatures). Of course the viscosity of the liquid phase will increase with increasing lignin content and above a certain lignin content the phase will vitrify to the glassy state at 23 °C. The vitrification of lignin in presence of different solvent compositions was also measured by TM-DSC (see 3.3.5) and the results will be presented in section 5.2.5.
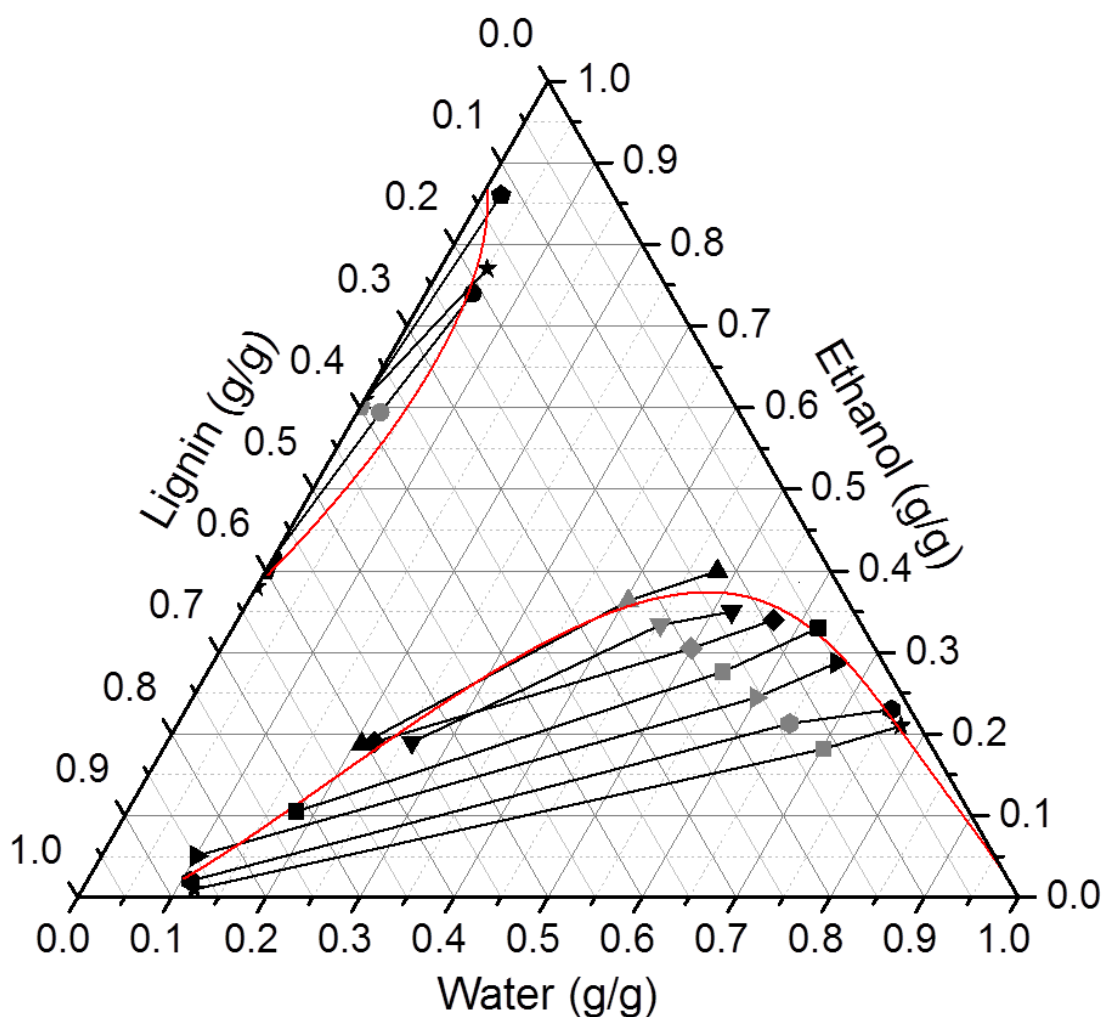
Figure 43: Pseudo-ternary phase diagram of lignin, water and ethanol at 23 °C. The grey data points represent the overall-compositions adjusted in the reactor, which decomposed into two phases connected via the conodes. The compositions of the two phases, lignin (-rich) and solvent (-rich) phase, were measured inline via an infrared spectrometer probe.

This isothermal phase diagram is one slice of the polythermal phase diagram that will be presented in the next section (23 °C correspond to the orange-yellow colored phase borders in Figure 44).

5.2.3.   Polythermal solubility

Some mixing and demixing temperatures have been measured polythermally by heating and cooling a mixture of lignin, ethanol and water of known composition at a defined temperature gradient (mostly 0.1 K/min) while detecting the appearance or disappearance of a second phase by measuring transmissivity, laser reflection and/or infrared spectrometric measurements.

5.2.3.1.   Temperature-resolved pseudo-ternary phase diagram of lignin, water and ethanol

The temperature-resolved ternary plot of lignin-water-ethanol phase equilibria (Figure 44) has been generated from results of the polythermally and isothermally measured solubilities. Additionally, solid-liquid equilibria data of the binary system water-ethanol have been derived from literature (Pickering 1893). The measured data points are displayed as black dots in the ternary plot. Each black dot is situated in an area with an underlying color. Each color indicates the minimum mixing temperature that is necessary to allow the unification of the respective lignin-ethanol-water composition in one liquid phase. The measurements have been performed between 0 and 80 °C. The temperature scale of Figure 44 results from this temperature range, being aware that the solid-liquid equilibria of ethanol-water mixtures are at lower temperatures.

The smooth temperature levels between the measured points have been generated by the smoothing function (total points increase factor = 1000, smoothing parameter = 0.01) within the *OriginLab* software. Each color represents an isothermal level in the diagram, showing regions of compositions that are miscible at and above that temperature. For regions with less measurement points, the smooth-fitted isothermal levels have a more illustrative character because there are not enough data points for a reasonable smooth fitting.

The black field around the composition 0.35 lignin, 0.15 water and 0.5 ethanol indicating miscibility below 0 °C has been measured at three different compositions within this area. However, there are no data points shown because the solution was not cooled until demixing occurred (below 0 °C), and no demixing temperature could be measured and displayed in this plot.

Despite the uncertainties and potential errors in the temperature-resolved pseudo-ternary phase diagram, it is the first time that such type of diagram is reported for lignin, to the best of the author's knowledge. However, similar phase diagrams (see 2.4) have been reported for other polymer-solvent systems (Gruber 1980).
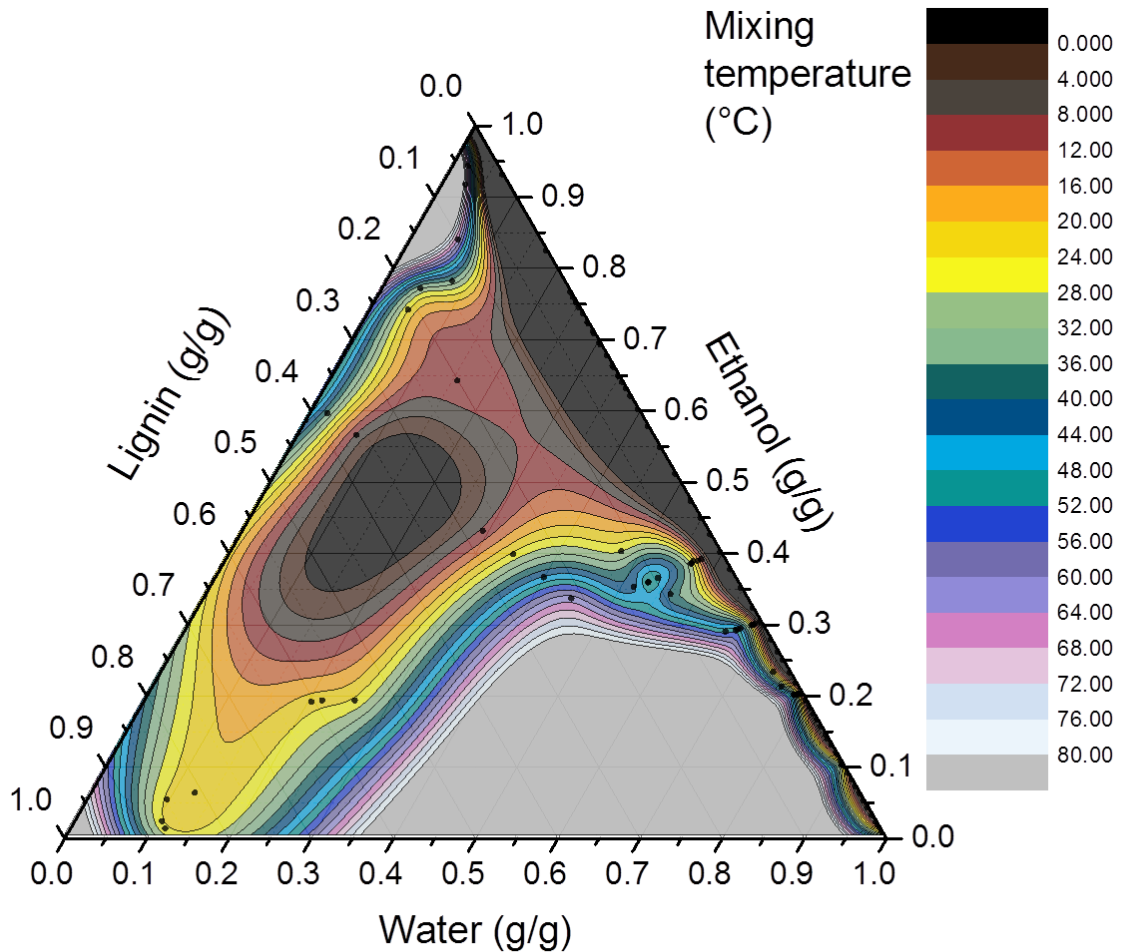
Figure 44: Temperature resolved pseudo-ternary phase diagram of the lignin-water-ethanol system. The smoothed diagram is based on the data points shown as black dots. Each color represents an isothermal level in the diagram, showing regions of compositions that are miscible above that temperature.

The diagram can be used as a basis for the optimization and design of new (separation-) processes and products regarding lignin. For example, a solution containing 60 wt. % of lignin at room temperature could be used as coating agent or resin-type solution for fiber-re-enforced compound materials (Mühe 2017). Or, an 80 wt. % ethanol in water solution could be applied as a CIP (cleaning in place) solvent to dissolve lignin incrustations that may form in future industrial plants. The spent CIP liquor could be fed to the lignin precipitation process to further recover lignin and solvent. Also, the formation of a sponge-like porous lignin material could be possible when triggering spinodal demixing by rapidly adding a specific amount of water to a lignin solution near the critical demixing point around 0.2/0.35/0.45 lignin/ethanol/water (see section 2.4).

5.2.3.2. Lignin-pulping liquor system

The (super-) solubility of pulping liquor dry substance, consisting mainly of sugars and lignin, in pulping liquor and pulping liquor distillate has been determined as described in section 3.3.2 in order to elucidate the maximum amount of lignin dissolvable in the

pulping liquor in dependence of the temperature and in presence of equal amounts of hemicellulose sugars.

As undissolved lignin remained stuck on the magnetic stirrer of the 1.5 ml vial and could not be detected as turbidity, the dissolution temperature could only be determined for some sample compositions (red data points and fitted saturation line in Figure 45). The nucleation temperatures were determined for all investigated sample compositions and are displayed as blue data points and fitted supersaturation line in Figure 45.
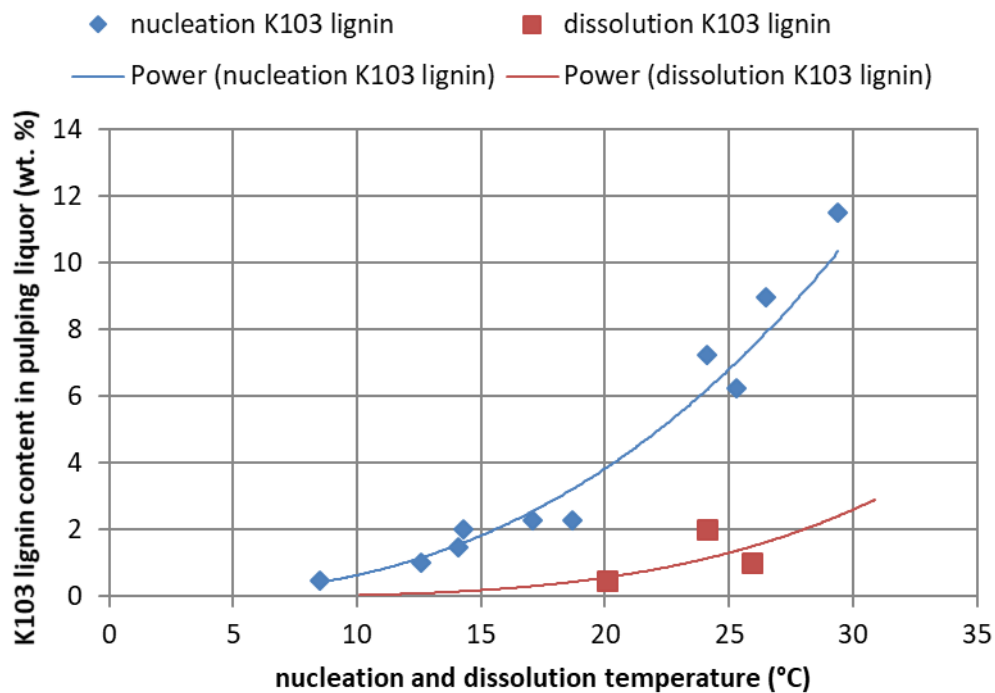
Figure 45: Polythermally measured nucleation and dissolution temperatures of different mass fractions of K103 lignin in its pulping liquor.

The supersaturation line shows significant temperature dependence. The fitted saturation line is rather speculative and will not be discussed further. The metastable zone shows a width of about 10 K between 0 and 2 wt. % lignin. The dissolution temperature at the typical lignin content of pulping liquors (1.5 to 2 wt. %) was determined at values around room temperature, indicating that pulping liquor stored at room temperature is saturated with lignin. This finding corresponds to the presence of lignin incrustations inside the pulping liquor storage vessels. Obviously, the pulping liquor was slightly supersaturated when it was filled into the storage vessel followed by lignin separating from the liquor. Another possibility is that the supersaturation of lignin occurred as result of condensation reactions between smaller and better soluble lignin molecules to bigger and less soluble lignin molecules over time.

Furthermore, the results show that pulping liquors with substantially higher lignin and/or dry substance contents could be processed at slightly elevated temperatures without uncontrolled lignin separation. From this point of view, the pulping process could be distinctly intensified, e.g., increasing the wood-to-liquor ratio in order to decrease the solvent recycling stream and thereby generally enhancing the process economics. Another possibility to reduce the energy demand for solvent recycling is by pre-

concentrating the pulping liquor by membrane filtration or partial solvent evaporation before the precipitation process (see 2.2.2).

A so far untapped concept would be the separation of lignin through precipitation by cooling, which could significantly reduce the energy demand and additionally neglect any antisolvent addition.

5.2.4. COSMO-RS calculations of liquid-liquid equilibria of model lignins in ethanol/water

As phase equilibria measurements of the lignin-water-ethanol system are experimentally challenging, a theoretical method for the estimation of such phase equilibria has been evaluated with experimental data of this work. The phase behaviors of three different sized model lignin molecules in ethanol and water have been calculated with COSMO-RS as described in section 3.3.3.

Figure 46 shows the results of the calculated liquid-liquid-equilibria (LLE) of the three model lignins in comparison to the experimentally derived equilibrium data. The experimental and calculated data show the same miscibility gap between lignin and water in noticeably mutual agreement to each other. However, the experimental (exp.) data show a smaller gap in comparison to the calc. data. Furthermore, the second miscibility gap between lignin and ethanol was not predicted by the COSMO-RS calculations.

The elucidation of the reasons for the deviations between the calculated and the experimental data is out of the scope of this work. However, it should be pointed out that the lignin models used in the COSMO-RS calculations were strongly simplified in comparison to the complex composition of the experimentally investigated lignin. Unlike the simplified lignin molecules used in the calculations, lignin produced in the pulping process contains smaller lignin molecules (dimers or monomers) that can act as co-solvents for larger lignin molecules. This can explain why the solubility of the processed lignin molecule-ensemble is better than of the calculated (calc.) data, which doesn´t consider any interactions between lignin molecules in the solution.

Additionally, the model molecules may have too many OH-groups (about 2 per monomer unit) in comparison to the real lignin (about 0.6 to 0.8 OH-groups per monomer unit) according to literature (Wen et al. 2013, Constant et al. 2016). However, the time-consuming calculations have been already performed when the overestimation of OH-groups was recognized.

Besides the deviations between calculated and experimental data, it is remarkable, how small the deviations are, when considering the simplicity of the lignin model molecules. This case study shows that phase equilibria calculations of a strongly simplified model system can give reasonable results for a complex natural substance system and may be conducted prior to experimental studies in order to reduce the experimental effort.
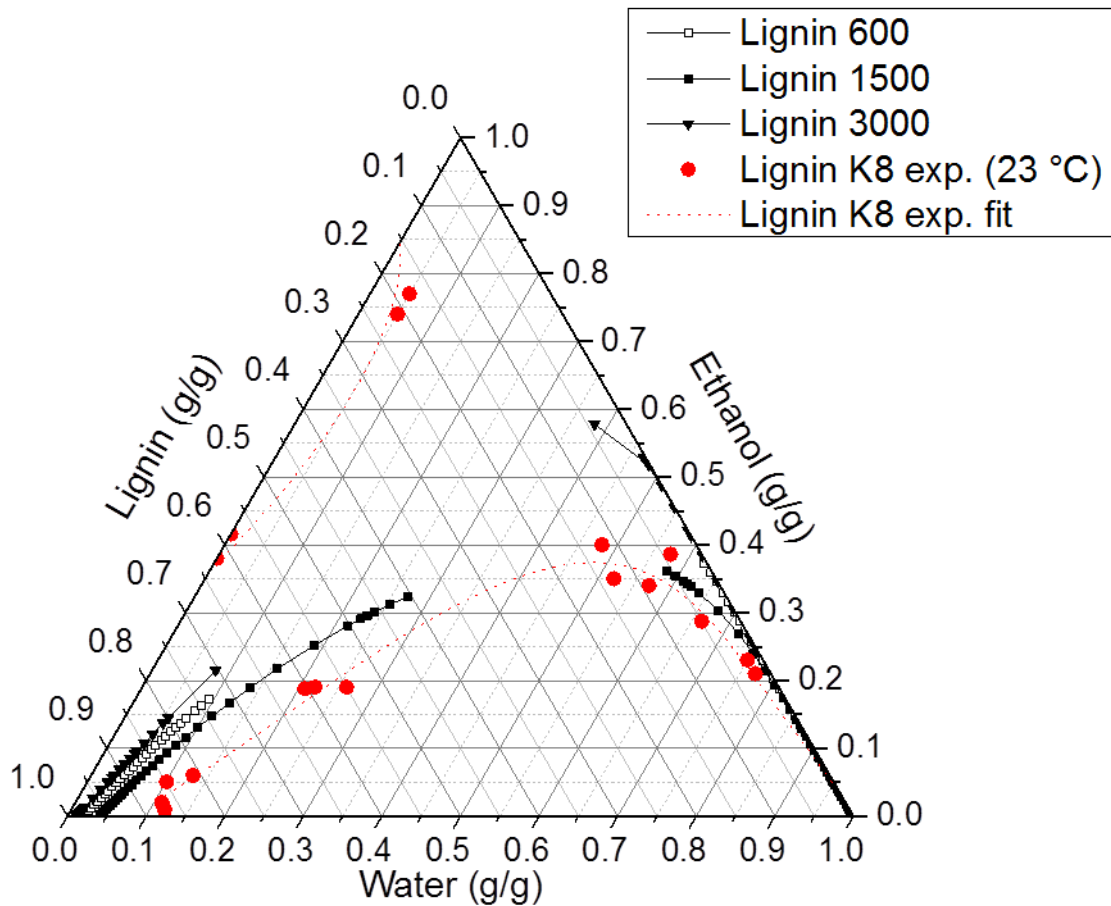
Figure 46: Calculated and experimental LLE (liquid-liquid equilibria) of lignin, water and ethanol at 23 °C. LLE have been calculated for model lignin molecules with a molar mass of about 600, 1500 and 3000 g/mole.

5.2.5.   Glass transition, softening and deliquescence temperatures of lignins

5.2.5.1.   Softening and agglomeration

In order to determine suitable operation conditions for the continuous precipitation process with simultaneous lignin particle agglomeration, the softening and agglomeration behaviors of different lignins were investigated as described in section 3.3.4.

Figure 47 shows typical results of agglomeration temperature measurement. The left micrograph shows dispersed lignin particles at 30 °C that appear gray-colored because they reflect the front light of the camera device and the back light is completely absorbed. At 47 °C the particles appear black because the back light is not absorbed any more by the dispersed particles and the background appears now bright. The particles obviously started to agglomerate. At 80 °C most of the particles deliquesced (melted) and appear as droplets. The amount of visible lignin is clearly lower because it sticks to the stirrer and the glass and is not dispersed any more.

The laser transmissivity through the dispersion shows the onset of an increase at 47 °C that clearly corresponds to lignin agglomeration (black arrow in Figure 47). Therefore the onset of an transmissivity-increase was defined as agglomeration temperature.
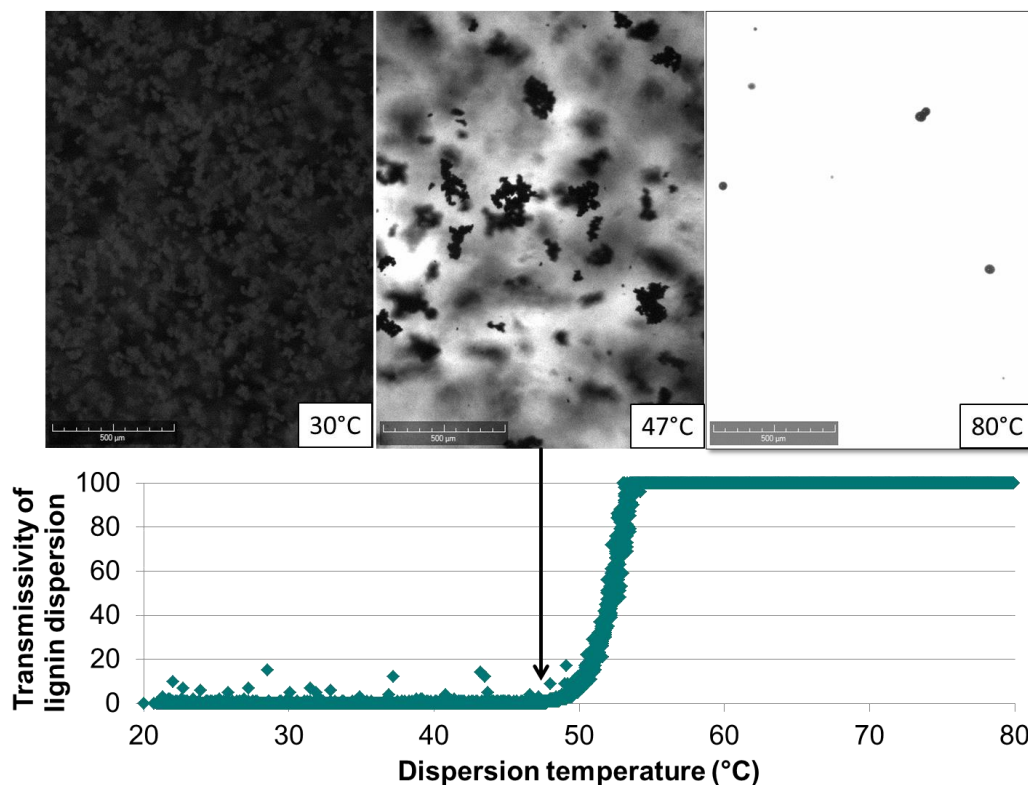
Figure 47: Top: Micrographs of dispersed lignin particles that start to agglomerate at about 47 °C while heated (scale is equal to 500 µm). Bottom: Diagram of the corresponding laser transmissivity through the lignin dispersion. The onset of the increase of transmissivity (here 47 °C) was defined as agglomeration temperature of the distinct lignin at a specified ethanol concentration in the liquid phase.

For most lignins, a linear dependency of the agglomeration temperature from the ethanol mass fraction in the dispersion was found (see Figure 48). The slopes range between -1.4 and -3.1 (°C/wt. % ethanol), showing significant differences of the influence of ethanol on the different lignins. Lignins with larger slopes were softened by ethanol more than those with lower slopes, assuming that agglomeration occurs as result of lignin softening and formation of bridges between single lignin particles by coalescence or sintering. The physical and chemical properties of lignin corresponding to the slope, which were not investigated in detail within this work, should be investigated in future works.

The intersections of the linear regression functions with the y-axes at 0 wt. % ethanol (the softening temperature in pure water) range from 65 to 121 °C, whereas the most lie between 65 and 94 °C. The decrease of the glass transition temperature of lignin by water has already been reported in literature (Hatakeyama and Hatakeyama 1982). The results in this work show that different lignins become softened by water to a different extent. Clear correlations between the softening temperatures in water and other lignin properties were not found within this work. However, plots of different thermal lignin properties against each other are presented in the Appendix A.1 for interested readers. Continuing on, K45 lignin was found to have a significantly higher softening temperature in water and has by far the highest molar mass of the investigated lignins. It is well known in polymer science that glass transition and softening temperatures of polymers increase with increasing molar mass of the polymer and swellability is decreased with increasing polymer molar mass (Gruber

1980). However, it is assumed that the molar mass range of the investigated lignins is too narrow to elucidate correlations to the softening properties.
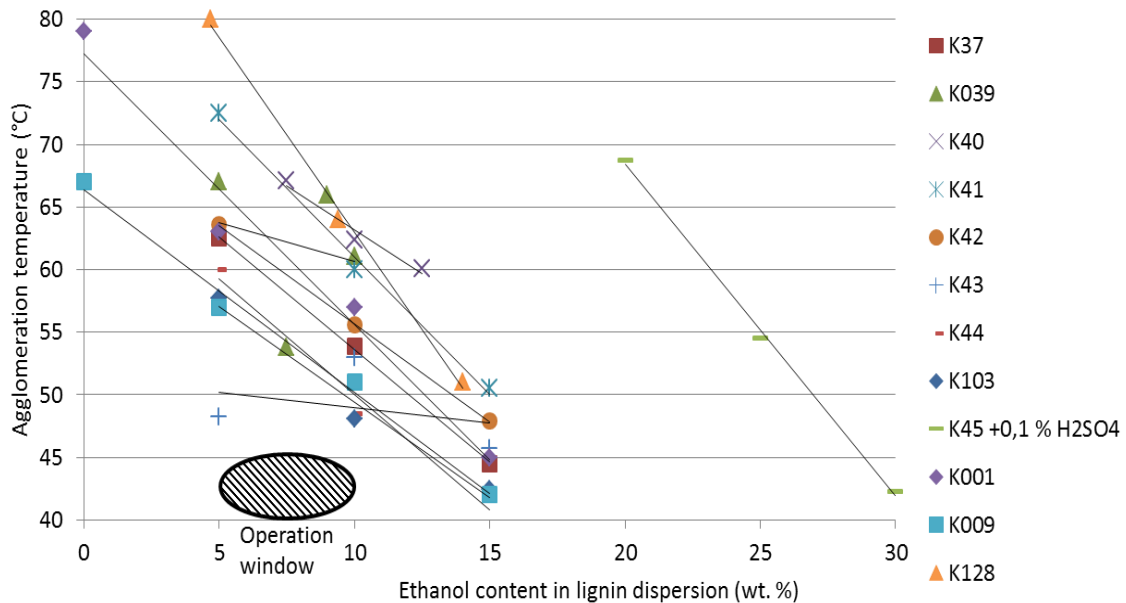
Figure 48: Agglomeration temperatures of various lignin dispersions in dependence of the ethanol content in the dispersions. Agglomeration is assumed to occur because of lignin softening that enables the formation of bridges between particles. Most lignins show a linear dependence of the agglomeration temperature from the ethanol content.

The operation window (40-45 °C and 5-10 wt. % ethanol) for continuous lignin precipitation experiments from organosolv pulping liquors was derived from the results of these agglomeration behavior measurements (marked in Figure 48), in order to prevent uncontrolled lignin softening and fouling during the process. Despite the fact that the operation conditions were selected below the softening conditions determined, agglomeration occurred in the continuous lignin precipitation experiments. This phenomenon is discussed more in detail in section 3.6 where the proposed explanation is that the softening of lignin particles is caused by warmer heating surfaces or locations with higher ethanol contents (foaming).

In addition to softening, agglomeration requires that lignin particles form aggregates at first, so that the particles are in contact with one another. The aggregation of particles in dispersions is strongly influenced by the Zeta-Potential, a measure for the electrostatic charging of the particles (see 2.4). It should be noted that the Zeta-Potential is strongly influenced by the pH value and ion strength of the liquid phase. At a Zeta-Potential around zero, aggregates form easily and agglomeration can be observed immediately at the lignin softening temperature. If the Zeta-Potential of a dispersion is around + or – 30 mV, lignin particles do not aggregate and therefore also do not agglomerate by forming lignin bridges when approaching the softening temperature. In this case, agglomeration would not be observed even if the particles are softened already. For this reason, sulfuric acid had to be added to the K45 lignin dispersions in order to decrease the Zeta-Potential and allow particle agglomeration to identify the K45 lignin softening temperatures (see pulping conditions in Table 5).

5.2.5.2.   Glass transitions

Glass transition temperatures of dry and solvated lignins have been determined as described in section 3.3.5 in order to verify that lignin softening occurs at temperatures above glass transition temperature as well as to determine the impact of solvent swelling or solvation on the glass transition temperature.

The glass transition was detected as a step-like increase of specific heat capacity in a certain temperature range. According to DIN EN ISO 11357-2, the midpoint is defined as the intersecting point of a horizontal line at the half step height with the measurement curve. The step height is defined as the vertical distance between the two intersecting points of the midpoint tangent and the baselines before and after the glass transition. The midpoint tangent is determined iteratively. Additionally to the glass transition temperature midpoint, the increase in c_p and the broadness of the transition have been determined from the c_p vs. temperature curve as illustrated in Figure 49.
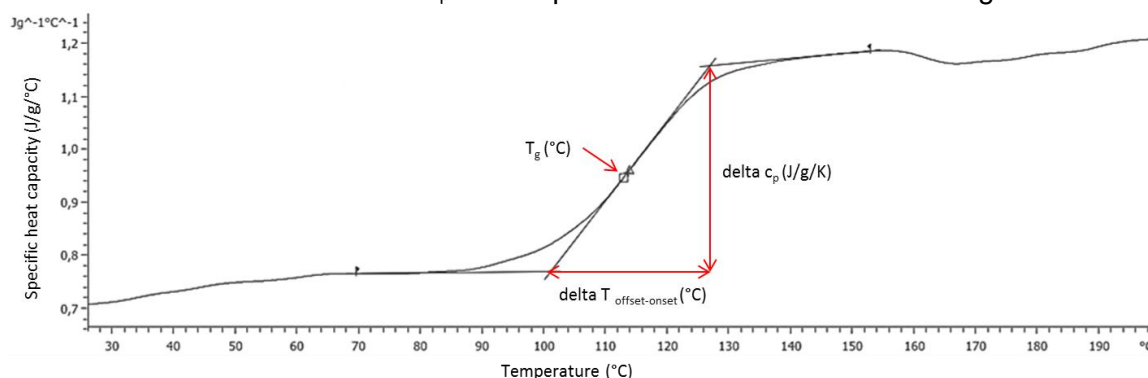
Figure 49: Specific heat capacity c_p vs. temperature plot of dry K42 lignin in a perforated crucible. The step-like increase in c_p indicates the glass transition.

The glass transition temperatures, the difference in specific heat capacity (delta c_p) and the broadness of the glass transition step (delta T $_{offset-onset}$) of dry lignins are listed in Table 17. The glass temperatures of the investigated dry lignins are situated in the range of 105.4 and 135.5 °C and within the temperature range of lignins previously reported in literature (Goring 1962, Blechschmidt et al. 1986). Delta c_p values have been found between 0.21 and 0.5 J/g/K and are therefore typical values for a glass transition of polymers (Ni and Hammer 2012). The broadness of the investigated glass transitions was determined with values between 14 and 34.2 °C.

Counter-intuitively, lignins with higher molar masses (e.g. K45, K29 and K9) were not clearly found to have higher glass transition temperatures, indicating that the glass transition temperature may be more strongly influenced by other lignin properties, e.g., functional groups (e.g., methoxyl and acetyl) that form intra and intermolecular hydrogen bonds (Hatakeyama and Hatakeyama 2005). However, functional groups of lignins were not analyzed, as it is out of the scope of this work. Additionally, the molar mass range of the studied lignins may be too small to find an increase of glass temperature with molar mass, as has been reported in literature (Blanchard et al. 1974).

Table 17: Glass transition temperatures, the difference in specific heat capacity (delta c_p) and the broadness of the glass transition step (delta T offset-onset) of dry lignins. The lignins were heated in an perforated aluminum crucible to allow water evaporation and the glass transition was derived from the specific heat capacity curve.

Lignin batch no.	Glass temp. in perforated Alu crucible via c_p (°C)	Delta c_p (J/g/K)	Delta T offset-onset (°C)
K1	120.5	0.401	14
K8	113.5	0.382	19
K9	131.1	0.28	15
K29	114.7	0.499	19
K37	123.6	0.45	24.1
K39	131.4	0.45	39
K40	126	0.376	28.1
K41	129.4	0.377	26.5
K42	114.07	0.387	25.8
K43	114	0.372	21.5
K44	111.5	0.47	25.4
K45	135.5	0.366	10.1
K103	105.4	0.32	34.2
K128	107.3	0.213	20.2
K138	113.2	0.472	24.3

An unexpected correlation between the glass transition broadness and the broadness of molar mass distribution has been found and is shown in Figure 50. The glass transition broadness decreases with increasing broadness (polydispersity) of the lignin molar mass distribution. In literature, no correlation between polydispersity and glass transition has been reported yet (Li et al. 2016).
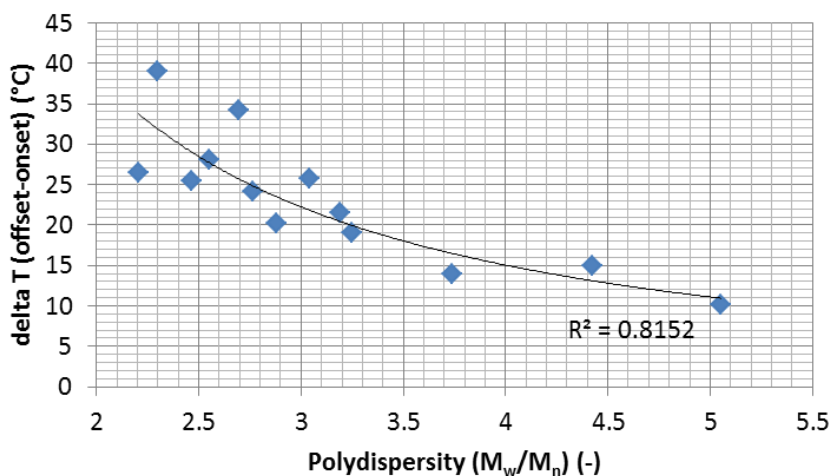
Figure 50: Glass transition broadness and polydispersity show a correlation to each other that may be counter-intuitive. The glass transition broadness decreases with increasing broadness (polydispersity) of the lignin molar mass distribution.

Glass transition of solvated lignin

Lignin (K8) samples of about 20 mg have been dispersed in 20 mg of solvent in 100 µl stainless steel mid-pressure crucibles that have been gas-tightly closed. The ethanol content in the aqueous solvent was step-wise increased from 0 to 100 wt. %. The prepared samples have been stored for solid-liquid-liquid phase equilibration (solvation and dissolution of the lignin) for at least 12 hours at room temperature or at 45 °C. The samples were cooled at 10-15 K/min to the respective starting temperature in the DSC before starting the temperature-modulated DSC measurement as described in 3.3.5.

Figure 51 shows the measured glass transition temperatures (T_g) of the solvated lignin plotted against the solvent composition. For some solvent compositions (0, 49 and 100 wt. % ethanol) a lower (red squares) and an upper (blue rhombs) glass transition have been observed, whereby the lower glass transition always exhibited the larger difference in specific heat capacity. The T_g of K8 lignin was lowered by 73 K in relation to dry K8 lignin due to the saturation with water. Hatakeyama found a decrease of T_g by around 100 K for water saturated dioxane lignin, which is in good correlation to the findings in this work. The glass transition temperatures linearly decrease with increasing ethanol content in the solvent, which is in good correlation with the theories mentioned in 2.3.2, assuming an increasing solvent content in the lignin with increasing ethanol content in the solvent.

The upper glass temperature at zero ethanol (pure water) is slightly lower than the agglomeration temperatures of some lignins shown in 5.2.5.1. The lower glass temperature in water is correspondingly around 25-45 °C lower than the observed agglomeration temperatures. Assumedly, the lignin is not soft enough to form bridges between particles right at the lower glass temperature and has to become softer at higher temperatures to agglomerate.
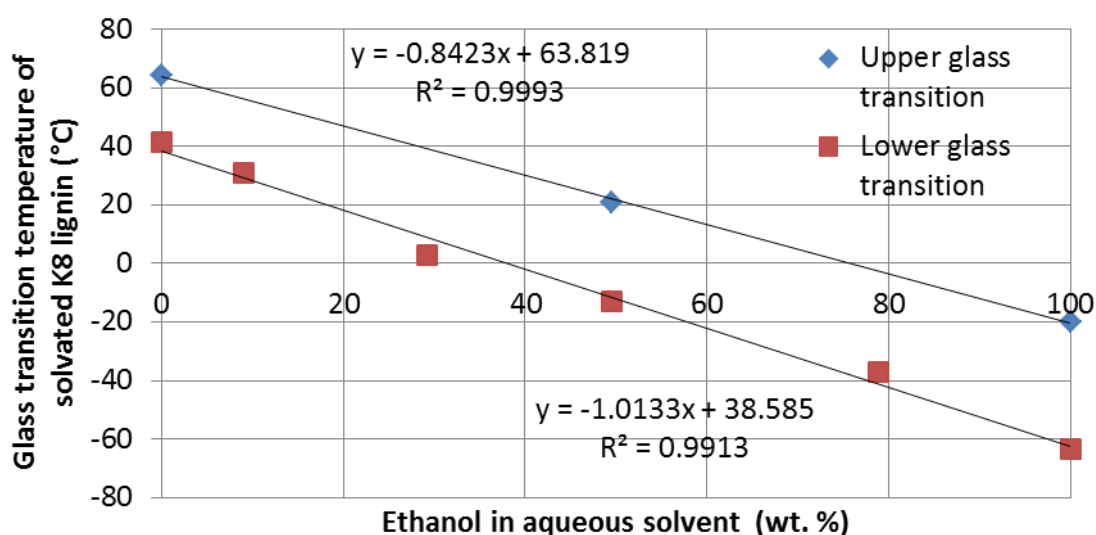
Figure 51: Glass transition temperatures of K8 lignin that was solvated in different ethanol/water solvent mixtures. For some solvent compositions a lower (red) and an upper (blue) glass transitions have been observed. The glass temperatures of the solvated lignin linearly decrease with increasing ethanol content in the solvent.

It should be pointed out here that most investigated lignin-solvent composition (except the 79 wt. % ethanol solvent) are not completely miscible in the investigated

temperature range as was found in the phase equilibria measurements within this work (5.2.2) and therefore the compositions of the lignin phases at glass transitions temperature are unknown. The phase equilibria are temperature-dependent and consequently, the compositions of the phases (lignin and solvent phase) are changing with the temperature and therefore also the glass transition temperature of the solvated lignin changes.

Multiple glass transitions may be an indication for two lignin phases whereby the lower glass transition could originate from a less solvated lignin-rich phase and the upper glass transition could originate from a more solvated solvent-rich phase. Multiple glass transitions have already been observed for other polymer-solvent systems and were found to probably originate from local composition fluctuations in the solvated polymer matrix (Lipson and Milner 2006).

The prediction of the glass temperature of solvated (plasticized) lignin is possible by models mentioned in 2.3.2 if the composition of the solvated lignin phase is known. Unfortunately, the solvent content in the lignin phase at glass temperature is unknown in this work and should be investigated in future works to be able to apply the mentioned models.

5.2.5.3. Deliquescence

Figure 52 shows the optical appearance of a **K1 lignin** sample in an aluminum crucible as micrographs at different temperatures before and after glass transition and the corresponding c_p curve of the glass transition measurement.
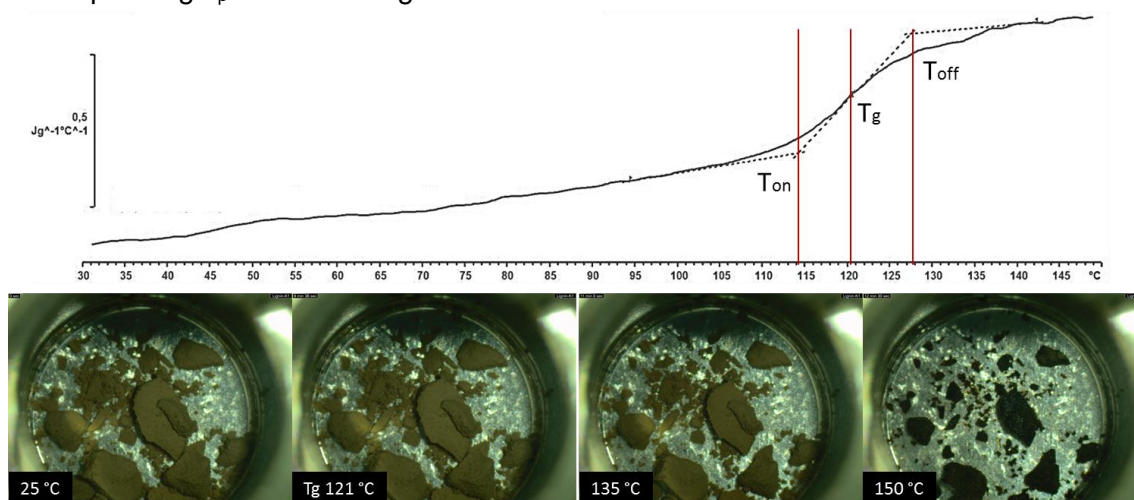
Figure 52: C_p curve with glass transition and corresponding micrographs of a K1 lignin sample (recorded in separate experiments).

The lignin sample did not optically change until the offset temperature of the glass transition at about 128 °C was reached, at which the lignin lumps (aggregates) started shrinking because of the sintering of the primary lignin particles. The primary particles are not visible on the micrographs because the resolution is too low. With increasing temperature the lignin sample melted completely and therefore changed its color to almost black. Smaller lumps of molten lignin are transparent and prove melting occurred without pyrolysis. The color darkens because of the disappearance of very small lignin particles which backscatter light and therefore appear lighter. A macroscopic (massive) peace of lignin thus clearly has a dark brown-red to black color.

The melting of **K8 lignin** was investigated via hot stage microscopy. Smaller and individual particles of lignin were observed via microscope while heated in a glass crucible. The micrographs of the melting process with corresponding temperatures are shown in Figure 53. Melting started at about 130 °C and are therefore at similar temperatures like K1 lignin, as described above. To point out, the lignin did not darken while melting but appeared more brownish-transparent as result of deliquescing to thinner lignin layers.
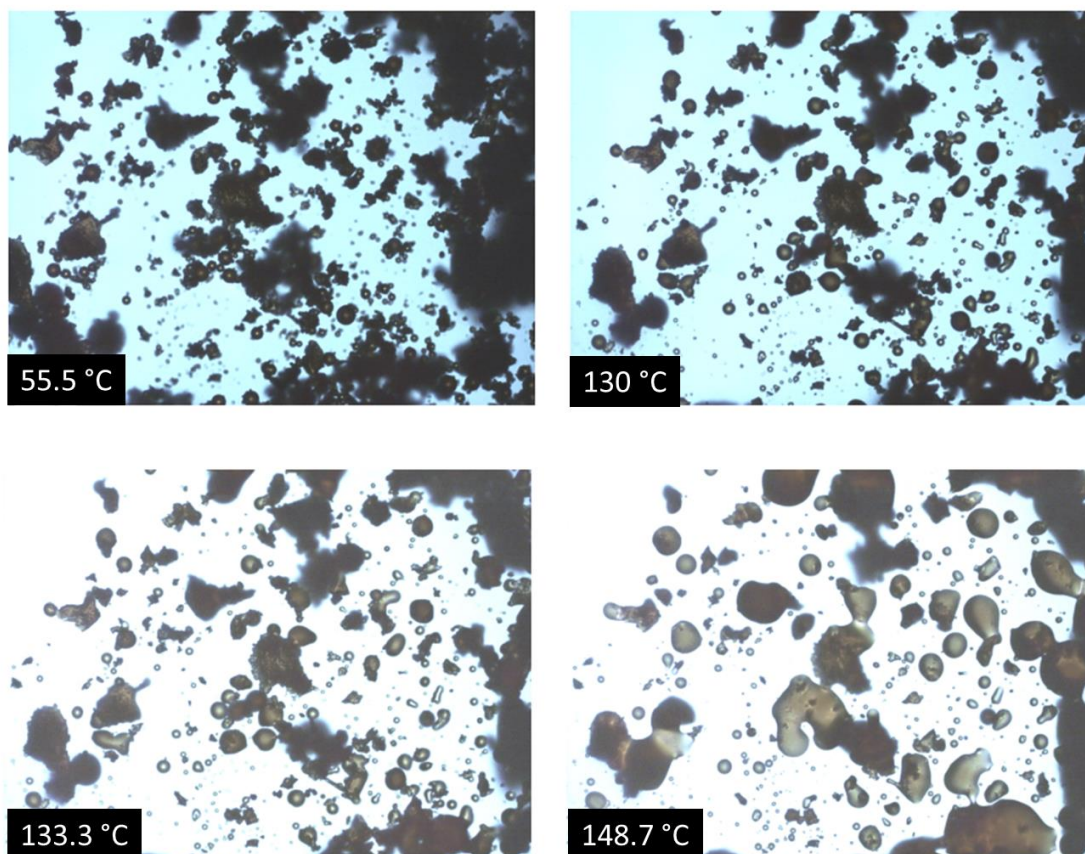
Figure 53: Hot stage micrographs of K8 lignin showing melting at around 130 °C. The background color has shifted from blue to white because the white balance was adjusted during the measurement. The molten lignin looks brownish transparent in thinner layers and dark in thicker layers because of light absorption.

5.3.   Batch lignin precipitation

Parts of this section have already been published within a conference proceedings book (Schulze et al. 2014).
The batch lignin precipitation experiments have been performed as described in section 3.4 at different pressures (50, 100, 200, 400, 1000 mbara). Representative for all batch experiments, the results of the experiment at 1000 mbara is presented and discussed here because all experiments showed similar results. The most important parameters over process time are plotted in Figure 54. The pulping liquor boiling point was reached at about 83 °C and 35 minutes after the heating was started at 0 minutes (blue line). The pulping liquor or dispersion temperature increased during the distillation

process to the boiling temperature of pure water because the ethanol was completely evaporated from the liquor. The distillate mass (green line) increased steadily from the point where the boiling temperature was achieved and reached about 210 g at the end, meaning only one third of the original pulping liquor mass remained as lignin dispersion. The calculated ethanol content in the aqueous phase of the lignin dispersion (orange line) got zero when the dispersion temperature attained 100 °C, the boiling temperature for pure water. The lignin content in the dispersion (red line) increased during the distillation process as consequence of ethanol and water removal. The heating was stopped at the 200th minute and the dispersion was cooled down.
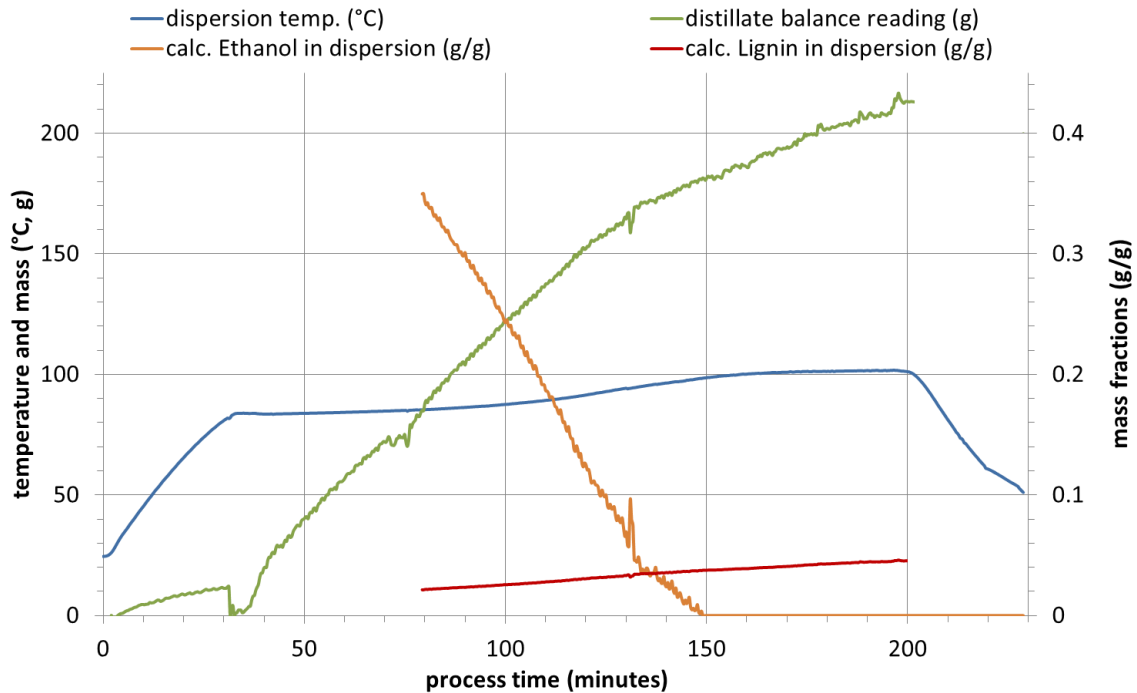
Figure 54: Process trends of the batch lignin precipitation experiment at 1000 mbara.

Figure 55 shows the particle size distribution over process time recorded by the FBRM® probe as a contour plot. Around the 90th minute lignin precipitated at 88 °C, 30 wt. % ethanol and 3.2 wt. % lignin in the liquor. The particle number slowly increased until the 140th minute when the number of particles between 2 and 20 µm chord lengths rapidly increased. It is assumed that lignin incrustations that have formed after precipitation on the FBRM probe window detached at this point and that the cleaner probe window then allowed the detection of more particles. The particle counts abruptly dropped at the 210th minute because of the formation of a lignin lump that united most of the previously dispersed lignin particles in itself (see Figure 56).
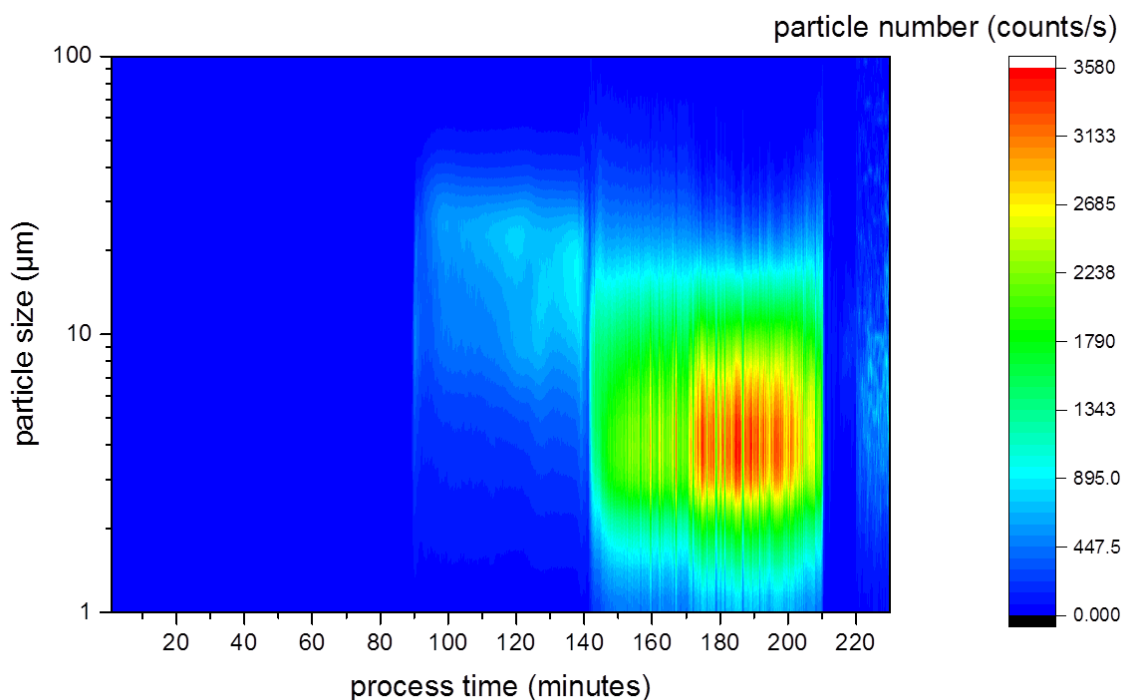
Figure 55: Particle size (chord length) distribution (PSD) of lignin over the process time of the 1000 mbara batch precipitation experiment.

In all batch precipitation experiments performed, the majority of the separated lignin ended up as an incrustation on the reactor internals and walls and as lumps (see photographs in Figure 56). The lignin separated (depending on temperature and ethanol content) as a more or less solvent-swollen viscous liquid phase with adhesive and cohesive properties. This separation can be considered as a liquid-liquid demixing rather than a precipitation (speaking in terms of crystallization) because the ethanol content was slowly decreased and so the supersaturation should have been low.

Figure 56: Lignin incrustations and lumps formed by the soft or liquid lignin during the process.

The lignin precipitation conditions (temperature, ethanol and lignin content) of the different experiments are listed in Table 18. It is clearly apparent that the lignin precipitated earlier at a higher ethanol content throughout the experiments; or the lower the operation pressure (the lower the temperature) was adjusted. As temperature decreased, overall lignin solubility decreased as well.

Table 18: Compositions and temperatures at which lignin started to precipitate from pulping liquors in the experiments with different pressures.

Exp. pressure	Precipitation at:		
(mbara)	Temp. (°C)	Ethanol (wt. %)	Lignin (wt. %)
1000	88	30	3.20
400	63	32	2.60
200	48	36	2.40
100	35	39	2.30
50	22	44	2.20

Figure 57 graphically shows the data of Table 18 with fitted curves in order to predict lignin and ethanol contents at the beginning of precipitation for higher temperatures at increased distillation pressures.
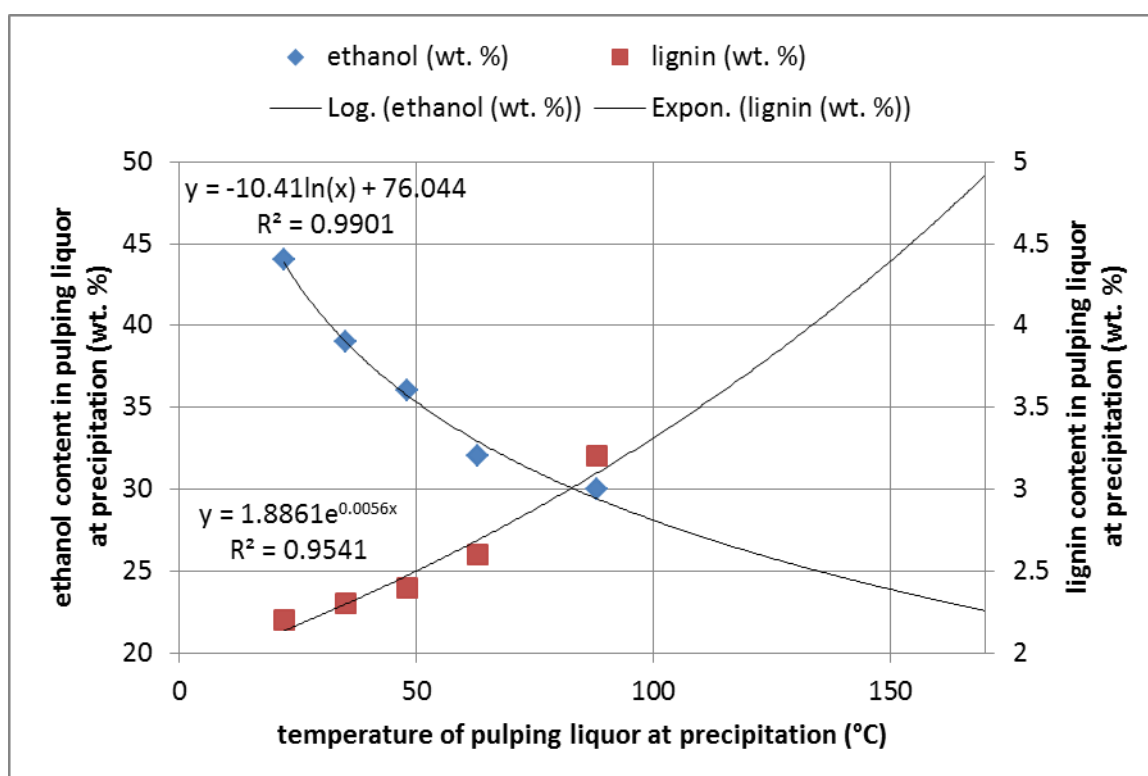
Figure 57: Ethanol and lignin contents of pulping liquors at the corresponding temperature at which lignin started precipitating from the pulping liquor during batch distillation. The fitted curves indicate that at higher precipitation temperatures, which could be achieved at elevated distillation pressures, also the higher lignin contents can be reached before lignin starts to precipitate, while the ethanol concentration could be lower.

Independent of the accuracy of the fitted curves the data show that it is clearly possible to evaporate more ethanol and water from the pulping liquor at elevated temperatures and pressures before lignin precipitates. Such a distillation process could be applied as

a pre-concentration step for the pulping liquor before feeding into the actual lignin precipitation process. In this way, a part of the solvent could be recycled before dilution with the lignin dispersion in continuous lignin precipitation and therefore would decrease the energy demand for ethanol separation. According to the extrapolation of the fitted curves in Figure 57 to 170 °C (pulping temperature) it may be possible to pre-concentrate the liquor to about the twofold lignin content of the original pulping liquor. Consequently, nearly half of the ethanol to be recycled could by evaporated from the liquor without further rectification needed.

The results of the batch precipitation experiments and the isothermal solubility measurements (5.2.1) that both showed the appearance of a sticky lignin phase under certain conditions led to the design of the semi-continuous experimental setup because it was understood that lignin has to be precipitated at relatively low ethanol contents and temperatures in order to yield mainly solid lignin particles, which do not tend to stick on the reactor and form big lumps.

5.4. Semi-continuous lignin precipitation

Parts of these section have already been published in a journal article (Schulze et al. 2016) and have been only slightly changed.

5.4.1. Lab-scale experimental results

Several semi-continuous lignin precipitation experiments were performed in the lab plant. Exemplarily, one representative experiment is presented in this section, as the other obtained results were quite similar.

Trends of the most important process parameters over the process time are shown in Figure 58. After regulating pressure to 100 mbar, about 140 g start-up dispersion (110g water + 30g liquor) with 10 wt. % ethanol content were prepared, followed by heating to boiling temperature (blue line) and thermal equilibration of the rectification column (red line). The K1 pulping liquor feed (violet line) was started and the reflux valve was slightly opened at the 75th minute and the semi-continuous process started at this point. About 240g of pulping liquor (violet line) were fed within 200 minutes (1.2 g/min). The temperatures, and therefore the ethanol contents of dispersion and distillate could be kept nearly constant by simple manual regulation of the pulping liquor feed and reflux valve. The manual regulation lead to slightly nonlinear slopes of the trends of the fed pulping liquor mass and distillate mass (green line). The pulping liquor feed was stopped in the 275th minute because the maximum dispersion level (about 300 g) in the glass vessel was reached. The evaporation was continued without reflux until the temperature of the dispersion reached 46.5 °C, which is slightly higher than the boiling temperature of pure water at 100 mbar (45.5 °C), in order to completely remove ethanol from the dispersion and to yield solid lignin particles for proper filtration.
Formation of foam was problematic during the experiment. Even the addition of an anti-foam agent (silicon oil) did not avoid the foam. Little changes in pressure lead to the move-up of foam into the column and short process interruptions (250th minute).

No incrustations were formed during the semi-continuous process since both ethanol content and temperature in the dispersion were permanently kept in the range, where the precipitated lignin was solid and not adhesive (about 43 °C and 10 wt. % ethanol). The process stream of dispersion could be reduced to 48.5 % of the process stream of spent liquor, if the start-up dispersion is neglected.
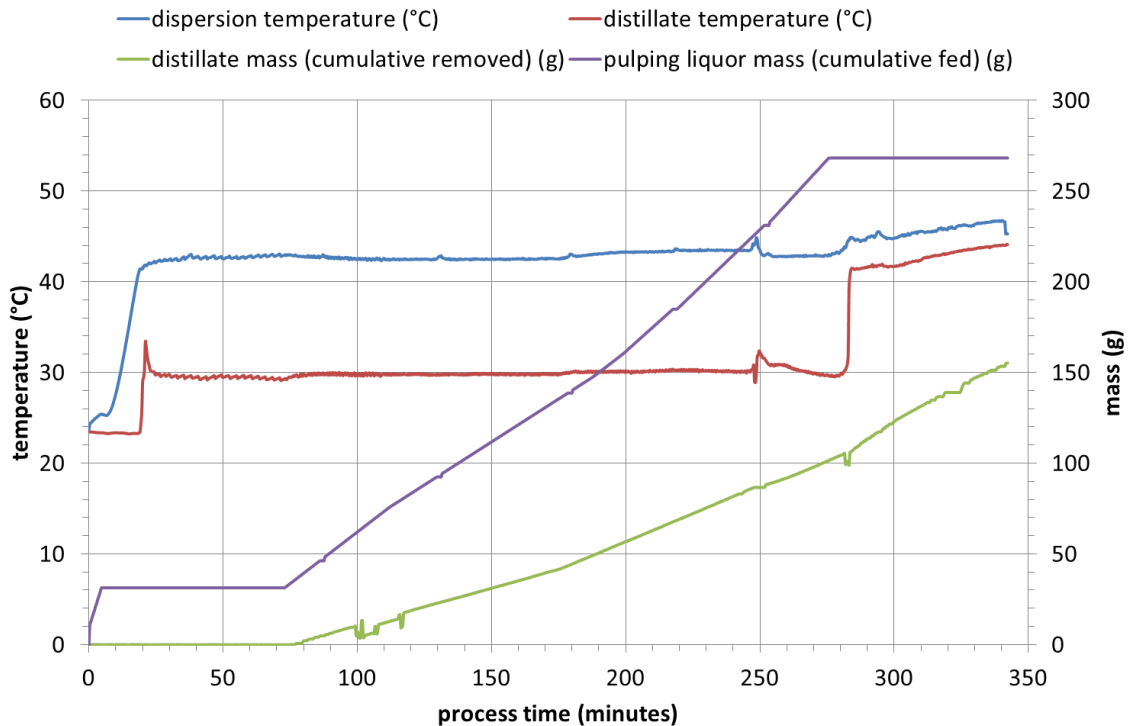
Figure 58: Trends of temperatures and cumulative masses recorded in a semi-continuous lignin precipitation experiment on the lab plant.

The particle size distribution of lignin over process time is shown as a contour plot in Figure 59. During the heating-up and column equilibration phase between the 20th and 75th minute, the lignin particles are already agglomerated and slightly moved the PSD to larger particles. The PSD switched to smaller chord length again right at the start of the pulping liquor feeding because additional small lignin particles entered the population by precipitation. The lignin precipitated from the pulping liquor by dilution with the present lignin dispersion in the vessel. The median particle size of precipitated lignin particles remained almost constant between 10 and 8 µm during the process but the PSD was broadened and flattened throughout the experiment. A potential explanation is that a portion of particles agglomerated to particles with larger chord length and another portion of particles was steadily fed to the population remaining as small primary particles for some time before agglomeration.
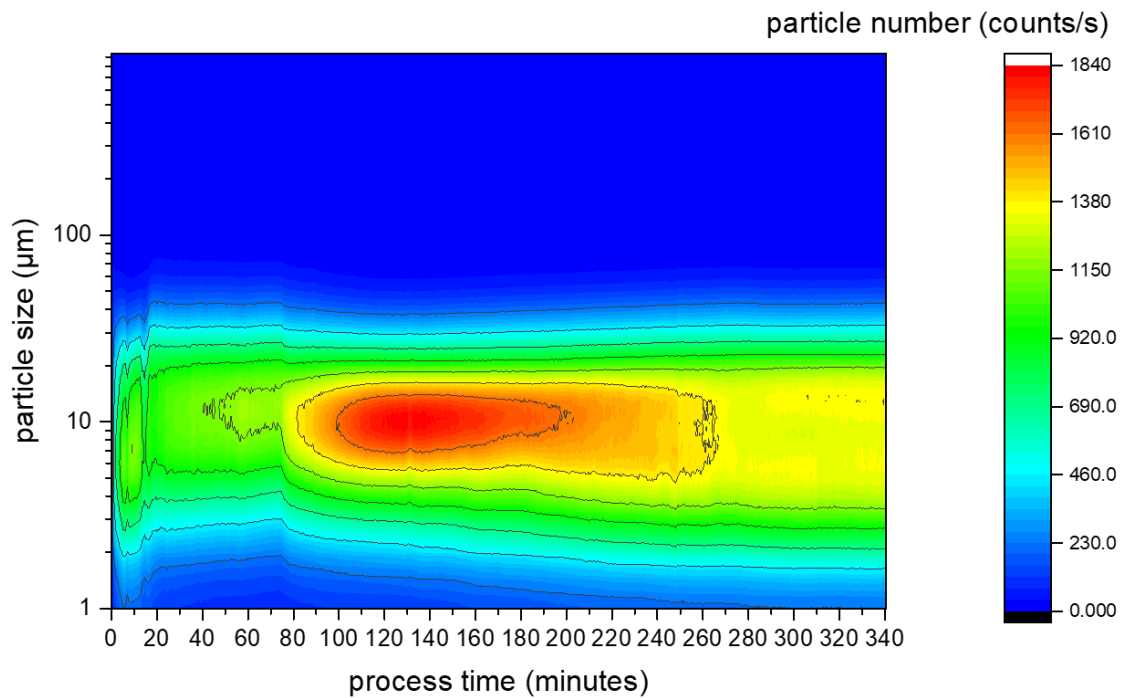
Figure 59: Evolution of the lignin particle size (chord length) distribution in the semi-continuous experiment described above.

Microscopy of the particles showed that these are actually aggregates with around 10 µm diameters, consisting of primary particles with diameters of about 1-3 µm (Figure 60, left).

Figure 60, left shows K1 lignin particles in the dispersion with <1 % wt. ethanol content yielded from semi-continuous precipitation. The dispersion was then stepwise heated to 90 °C and at different temperatures samples of the dispersion were investigated via an offline microscope (Keyence VHX2000). The micrographs and corresponding temperatures are shown in Figure 60.
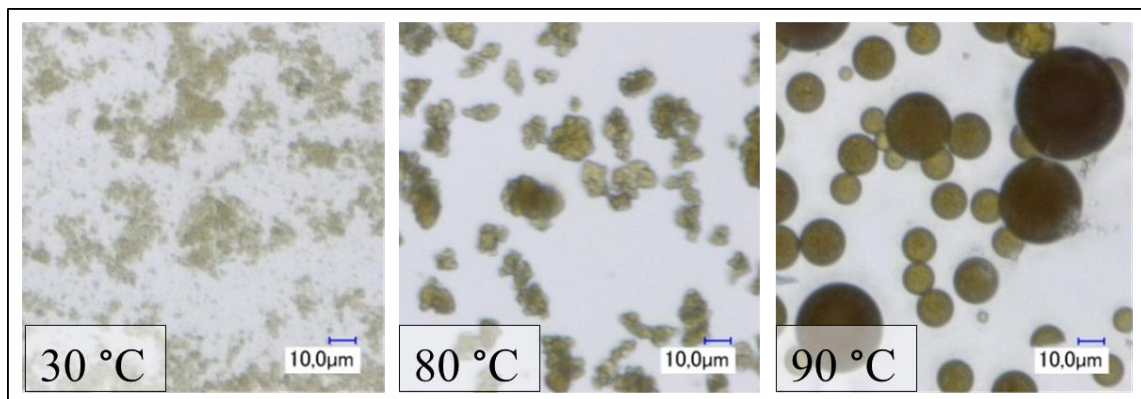
Figure 60: Lignin particle micrographs recorded at different temperatures during a subsequent heat treatment of the lignin dispersion produced in the semi-continuous lignin precipitation experiment in order to enlarge particles by agglomeration (sintering and coalescence).

The aggregated solid lignin particles became soft, agglomerated and finally formed significant bigger droplets by coalescence of molten lignin. The droplets solidified to

spheres after cooling down the dispersion. However, incrustations were formed in the apparatus due to the adhesiveness of soft lignin.

From these results it was understood, that a compromise between particle enlargement and incrustation has to be made in future experiments; that means the optimal ethanol content and temperature combination had to be found in order to minimize incrustations and maximize particle size and filterability at the same time.
A further question arose from this task as it had to be clarified, how large the particles have to become to achieve good filterability. For this reason the filterability measurement device (see section 3.7) was constructed in order to determine the filter cake resistance of the dispersion produced in future continuous lignin precipitation experiments. Additionally, the lignin softening and agglomeration measurement procedures described in section 3.3.4 have been devised in order to find the optimal process conditions for continuous lignin precipitation experiments for a range of different lignins.

5.4.2.   Pilot-scale experimental results

The semi-continuous experiments at the pilot plant have been carried out as described in section 3.5.2. A three day pilot plant campaign was performed; however the results of one exemplary experimental day are presented in this section. The following results are representative for all obtained results.
In Figure 61 the most important process parameter trend of the pilot plant semi-continuous precipitation experiment are plotted over process time. The start-up dispersion was prepared until the 80th minute and the dispersion reached its boiling temperature (red line) at about 110 minutes. The pulping liquor feed (blue line) was started at the same time and the distillate tank level (green line) rose a few minutes later. The pressure ranged around 100 mbara (yellow line) and the dispersion temperature could be adjusted around 41 °C by tuning the pulping liquor feed. The distillate tank had to be emptied three times during the process. The pulping liquor feed had to be interrupted and the pressure increased during distillate emptying. The pulping liquor feed was finally stopped at about 380 minutes. 212 kg pulping liquor (neglecting start-up dispersion) were fed in 230 minutes (time without distillate emptying time) with an average feed rate of 55.3 kg/h.
The evaporation of ethanol was carried on until a dispersion temperature of ca. 44 °C, indicating an ethanol content below 2.5 % wt.
Again, foam was a serious problem during precipitation. Almost no incrustations were formed during this experiment. Only on the hot surface of the heating steam pipe, which was exposed to the foam, some lignin incrustations remained.
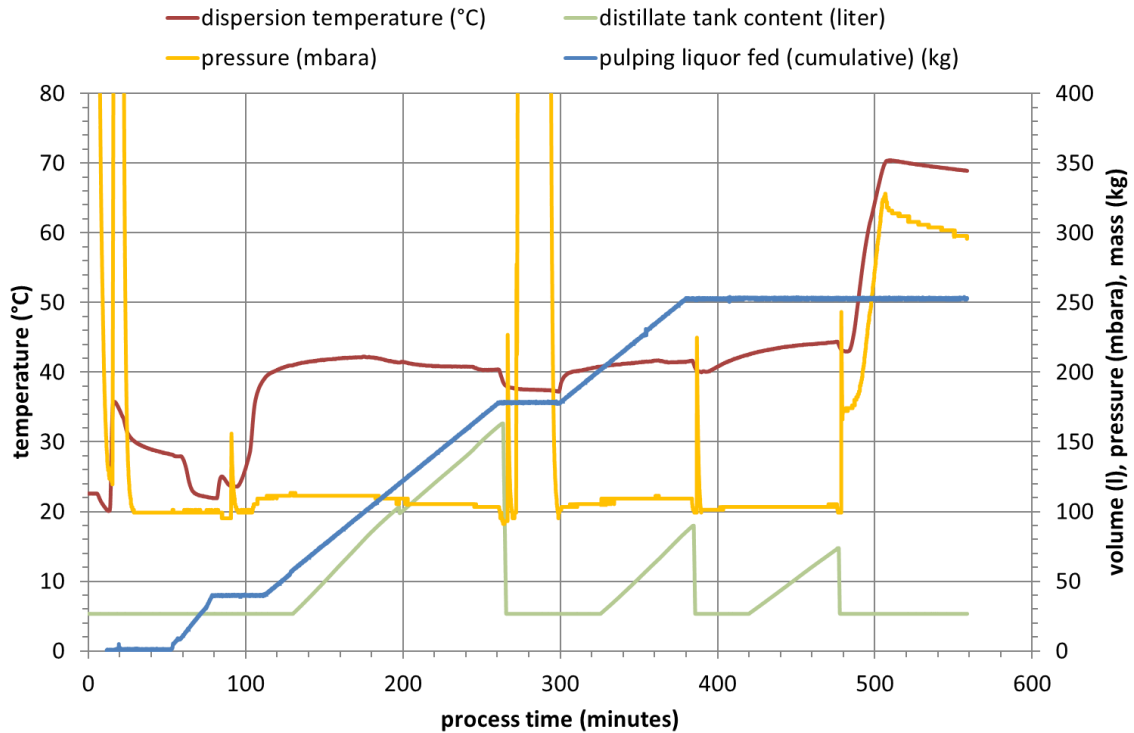
Figure 61: Process data trends of the semi-continuous lignin precipitation experiment in the pilot plant.

Half of the produced dispersion was pumped into another tank for cooling down to room temperature. The other half remained and was heated up to around 70 °C for 12 hours to maintain a sort of "heat-ripening" or sintering of the lignin particles by careful agglomeration (as described for the lab scale experiment in 5.4.1). A micrograph of lignin particles of partial heat ripened dispersion is displayed in Figure 62, left. A small fraction of the lignin formed droplets and the majority of particles melted to agglomerates. Agglomerates distinguish from aggregates in solid bridges between the primary particles, so agglomerates might not break up during filtration and drying. The particles show, that 62 °C were already above the lignin softening temperature but regardless no significant incrustations were formed during the heat ripening process.

The two dispersions were filtered and washed with water in a chamber filter. The heat ripened filter cake (≈60 % wt. solids) appeared much dryer than the non-heat-ripened one (≈30 % wt. solids). The non-heat-ripened filter cake was still somewhat flowable, as visible on the right side of the right photograph in Figure 62. The filter cake resistances were not measured but nevertheless the heat ripened lignin dispersion was filtered much faster than the original dispersion.
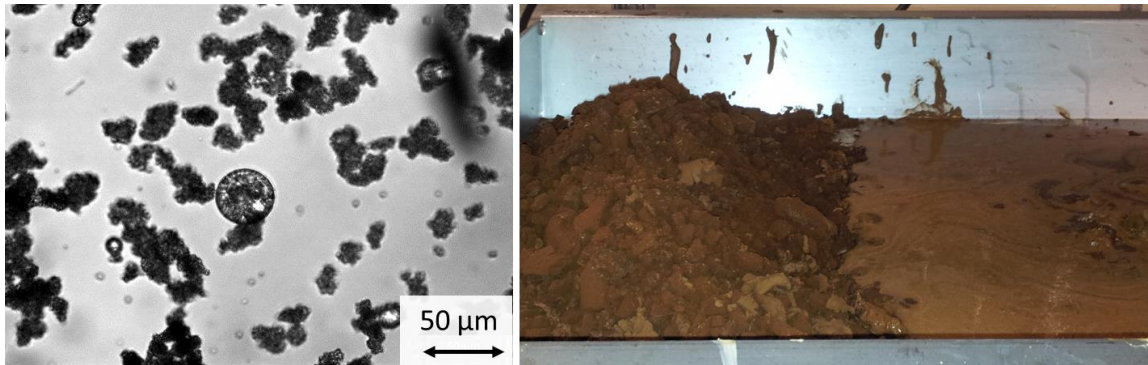
Figure 62: Left picture: Partial agglomerated lignin particles during the heat treatment for lignin sintering at about 62 °C. Right picture: Lignin filter cake that has been heat treated (left side of right picture) and that has not been heat treated (right side of right picture). The sintered lignin filter cake had about 60 wt. % solids content and the untreated only 30 wt. % solids and was still flowable.

The results of the semi-continuous lignin precipitation experiments with a subsequent agglomeration step (heat-ripening or sintering) in lab- and pilot-scale proved that it is possible to precipitate lignin as solid particles and prevent incrustations when the right temperature and ethanol content are adjusted in the process. Additionally, the filterability of the yielded lignin dispersion can be significantly improved by controlled particle agglomeration triggered by careful lignin softening.

It was understood from these experiments that temperature and ethanol content of the dispersion are the most important process parameters to control and that both have to be measured inline. For this reason an inline ATR-FT-MIR probe was calibrated and assembled to the continuously operating plants for fast ethanol content monitoring.

5.5.   Continuous lignin precipitation

The experiments have been carried out in two modifications of a lab plant and in the re-constructed pilot plant at Fraunhofer CBP. 34 experiments were performed in total, thereof 30 in the lab plants and 4 in the pilot plant. Therefore, the presentation of all results in this section would be too extensive. Results of typical experiments are presented in this section, like in the sections before.

5.5.1.   Lab-scale experimental results

The lab plant experiments have been carried out in two modifications of the plant (see 3.6.1). The first lab plant modification was heated via the double-jacket of a stirred reaction vessel. The second optimized modification was equipped with a falling film evaporator that significantly reduced foaming of the boiling lignin dispersion.

5.5.1.1.   Jacket-heating

In total ten different pulping liquors were processed within the 24 experiments in this setup. Eight of these experiments were carried out within the master thesis of Johannes Keitel (Keitel 2016). Representatively, the results of the continuous precipitation of K40 pulping liquor are discussed in Figure 63 and Figure 64.

The most important process parameter trends are plotted over process time in Figure 63. The start-up dispersion was heated up (red line) and the rectification column was equilibrated (green line) at total reflux until the 60th minute. The pressure (blue line) was held constant at 100 mbara. The pulping liquor feed (light blue) was started in the 60th minute and adjusted to about 3.7 g/min during the whole experiment. The distillate flow (orange line) was controlled by the reflux valve, which was in turn manually adjusted in order to keep the vapor temperature (green line) at the head of the distillation column near the azeotropic temperature. The dispersion flow (dark blue line) was also manually controlled in order to keep the dispersion level in the reactor constant. The ethanol content (violet line) was adjusted within the range of 7 to 8 wt. % by tuning the heating jacket temperature (brown line) or the pulping liquor feed. After about 550 minutes the pulping liquor tank was depleted and the experiment was stopped.
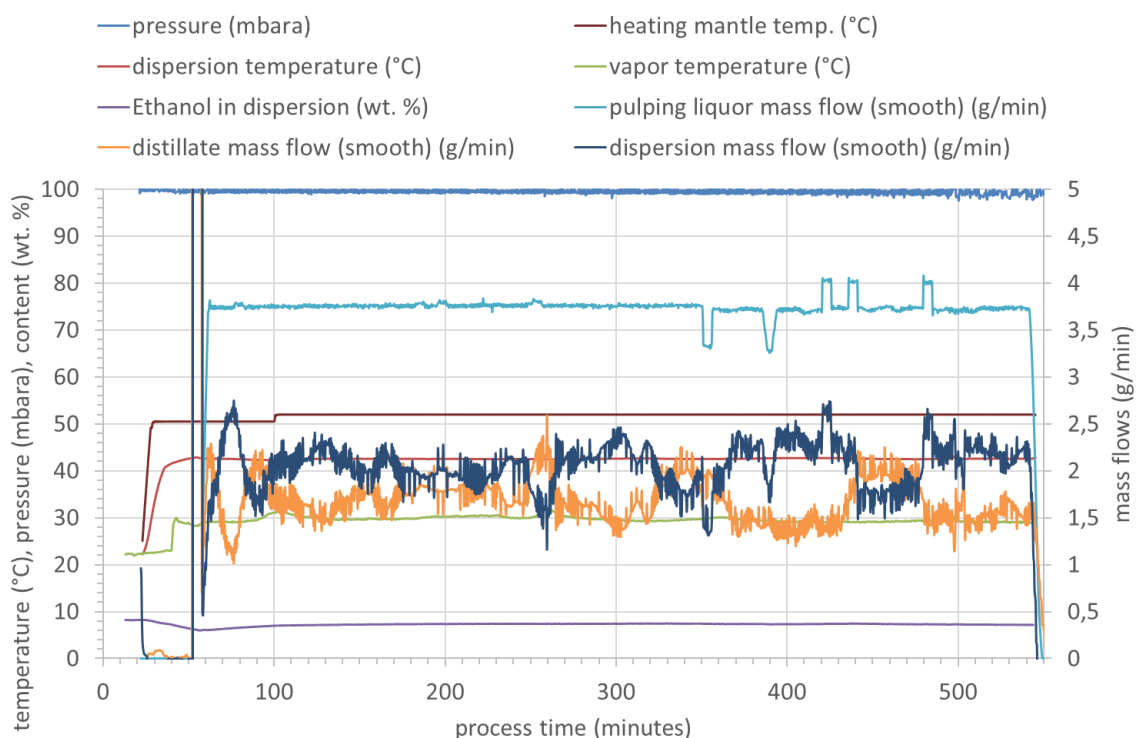
Figure 63: Process trends of continuous K40 pulping liquor precipitation.

Figure 64 shows the particle size distribution (PSD) over the process time as a contour plot and two micrographs of lignin particles recorded with the inline microscope at the beginning and end of the experiment, respectively. During the heating-up phase around the 40th minute the lignin particles of the start-up dispersion agglomerated. The $d_{50,0}$ (median) increased from 8 to 15 µm and the overall particle number decreased in this phase. When the pulping liquor feed was started at 60 minutes, the median decreased again to 10 µm and the particle counts < 10 µm increased because of the addition of freshly precipitated small lignin particles to the population. The trend to smaller particles stopped after 200 minutes and the PSD started to drift to bigger particle sizes until the end of the experiment. Especially particles below 10 µm almost completely disappeared until the end because they were probably incorporated in larger agglomerates. The micrographs support the observations of the FBRM® signal, as they

clearly show larger agglomerates at the end of the experiment when compared to particles at the beginning of the process.
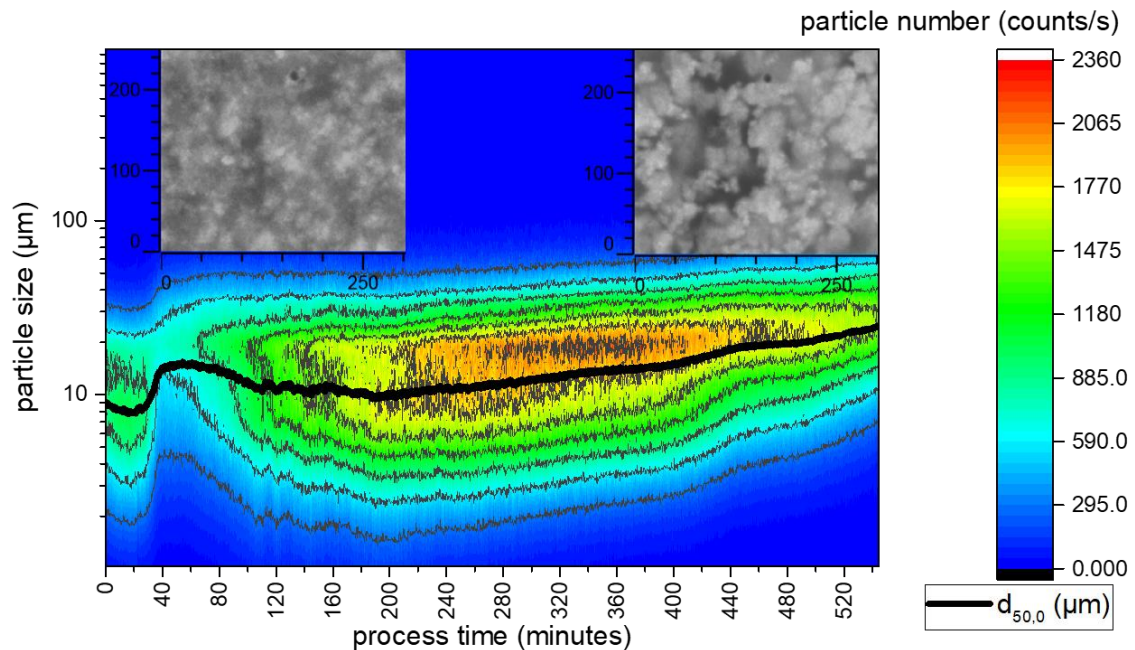
Figure 64: Lignin particle size distribution evolution in the continuous jacket heating precipitation experiment with K40 pulping liquor. The experiments with other pulping liquors showed similar trends.

This trend of particles size distribution during the continuous precipitation process has been observed in the major part of conducted experiments. No experiment reached the steady-state in terms of dispersion composition, and therefore, the start-up to steady period has been observed in every experiment. The mean residence time of the lignin dispersion θ_{disp} in the continuous stirred-tank reactor (CSTR) can be described by equation 10 (m_{disp}: mass of dispersion in the reactor, $\dot{m}_{disp}$: mass flow of dispersion).

$$\theta_{disp} = \frac{m_{disp}}{\dot{m}_{disp}} \approx \frac{1300\ g}{2\frac{g}{min}} = 650\ min \tag{15}$$

Steady-state would have been reached after about 3 to 4 residence times when assuming the behavior as CSTR. Thus, all experiments have been observed during the first quarter of the start-up phase to steady-state. Consequently, the dispersed lignin content of the dispersion and the sugar and acid contents in the aqueous phase of the dispersion increased during the whole experiment. Accordingly, the pH value decreased and the dissolved metal salt (dissolved metal from wood and reactors) concentration increased as result of the reduced water content. Thus, the Zeta potential of lignin particles may get closer to zero by the positively charged ions which correspondingly increases the agglomeration rate. An increasing agglomeration rate throughout the experiment could explain the observations regarding the PSD. The lignin particles were agglomerating right from the beginning but the nucleation rate was higher at the time the feed was started through the time that the PSD decreased at first. After some time the agglomeration rate surpassed the nucleation rate and the PSD

drifted to larger particle sizes. The nucleation rate is assumed to stay practically constant because the feed flow was also almost constant during the experiments.

The conclusion here is that the agglomeration rate would increase until the steady-state composition of the lignin dispersion is reached. Of course, the agglomeration rate will not linearly increase until steady-state is reached because the ion and acid concentrations will not linearly increase, and the Zeta potential and pH value do not linearly change with acid content and ion strength either. However, when getting closer to the steady-state dispersion composition, it would be necessary to adjust the agglomeration rate by tuning the ethanol content or the dispersion temperature in order to prevent uncontrolled agglomeration and formation of lumps.

Table 19 shows mass balances of continuous lignin precipitation experiments with jacket heating. The start-up dispersion mass was around 1300 g for all experiments because it was the minimum filling level of the reactor necessary to properly immerse the analytical probes. The pulping liquor mass fed throughout the experiments ranges from 1046 to 1822 g corresponding to the duration of the respective experiment. The maximum duration of an experiment was given by the mass of pulping liquor in the tank and the feed rate (e.g. K40, K43 and K45). Shorter durations result from problems occurring throughout the experiments forcing a stop (mostly due to plugging of the dispersion outlet tubing by large lignin particles). The masses of distillate and dispersion outputs each correspond to the fed pulping liquor mass. The losses of lignin and ethanol have each been calculated from the partial mass balances. Ethanol losses were quite small for a lab plant and result from air leaking into the system which was pumped out again while taking some ethanol with it.

Table 19: Overview of mass balances of continuous precipitation experiments with jacket heating (data for K37 are missing).

Pulping batch	Input		Output		Losses	
	Start-up disperison (g)	Fed pulping liquor (g)	Distillate (g)	Dispersion (g)	Lignin incrusted (wt.%)	Ethanol via pump (wt.%)
K 39	1362,3	1337,9	542,9	2189,6	-41,76	-2,68
K 40	1333,2	1822,0	827,3	2316,0	-20,60	-3,89
K 41	1311,2	1402,8	596,0	2136,7	-48,31	-2,92
K 42	1292,9	1401,6	619,1	2065,1	-45,13	-1,38
K 43	1303,3	1682,3	771,1	2223,8	-15,59	-1,71
K 44	1302,2	1046,0	479,5	1868,8	-34,96	-1,85
K 45	1277,3	1652,8	758,2	2152,7	-	1,04

Substantial amounts of lignin have been lost in incrustations in most experiments. The incrustations occurred above the dispersion level as a result of the extensive foaming of the lignin dispersion during the evaporation process. The foam bubbles continuously sputtered lignin particles to the probes and reactor wall. The lignin then got softened by the high ethanol content in the gas phase (about 40 wt. % ethanol in vapor) and formed incrustations like shown on the photograph in Figure 65.

From these results, it is clear that vigorous boiling and foaming have to be prevented during the precipitation process in order to prevent lignin incrustations in the gas phase.

Therefore, the experimental setup was equipped with a falling film evaporator (FFE) which avoids bubble boiling. The results of the experiments with FFE are presented in the next section (5.5.1.2).

Figure 65: Lignin incrustations on the FBRM® probe formed by foaming of the boiling lignin dispersion.

No agglomeration or incrustations were observed in the experiment with K45 pulping liquor, as one may have expected from the high softening ethanol contents measured in section 5.2.5. The K45 lignin was not softened during the precipitation process. Therefore, the lignin dispersion of K45 also was practically unfilterable.

The average filter cake resistances of the produced lignin dispersion were measured as described in section 3.7 and the results are displayed in Figure 66. According to literature (VDI 2010, Beckmann 2013) filterability can be rated according to the German school mark system, where $10^{11}\,\mathrm{m^{-2}}$ means very good filterability (mark 1) and $10^{16}\,\mathrm{m^{-2}}$ means insufficient filterability (mark 6). Consequently, all produced lignin dispersions, despite K45, have been good or very good filterable. The K45 lignin dispersion was practically not filterable at all and even the value for the avg. filter cake resistance was hard to measure.
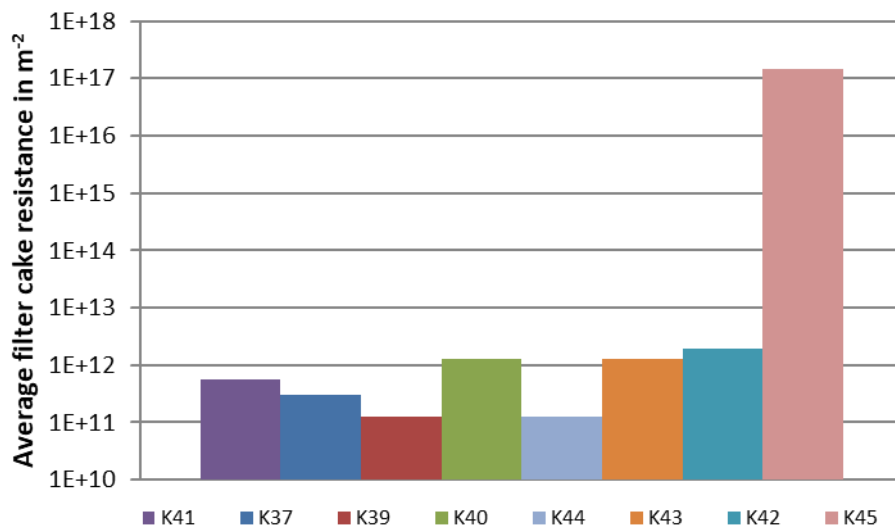
Figure 66: Filter cake resistances determined for the lignin dispersion produced in the continuous precipitation experiments. Scale: $10^{10}\,\mathrm{m^{-2}}$ means excellent filterability and $10^{16}\,\mathrm{m^{-2}}$ means practically unfilterable (VDI 2010, Beckmann 2013) .

The insights of these continuous experiments with jacket or bulk heating state that foaming and vigorous boiling has to be avoided in upcoming experimental setups in order to prevent lignin incrustations in the gas phase. This was done by adding a FFE to the experimental setup. The second insight was that controlled lignin softening and agglomeration is mandatory in order to produce good filterable lignin particles in the

process. If no agglomeration occurs, the lignin dispersion is practically not filterable as could be shown by K45 lignin dispersion.

5.5.1.2.   Falling film evaporator (FFE)

Six continuous precipitation experiments with a FFE were carried out in the lab plant. Two representative experiments with K128 pulping liquor and their results will be presented in this section. The results will show how relatively small changes in the operation conditions (pressure, temperature and ethanol content) influence the lignin particle agglomeration.

The **first experiment** (for trends see Figure 67) was carried out at a pressure of 100 mbara (blue line) and an average ethanol content (violet line) in the lignin dispersion at about 7.5 wt. % corresponding to an average dispersion temperature of 41.3 °C (green line). The pulping liquor feed rate (orange line) was adjusted between 1.8 and 4.3 g/min (6 g/min during start-up phase) and the temperature of the heating medium (dark red line) in the FFE was tuned to 50.8 °C on average. Both the pulping liquor feed and the heating temperature were manually controlled in order to adjust the ethanol content in the lignin dispersion to the desired value. The distillate flow (light blue line) was manually adjusted by tuning the reflux valve in order to keep the vapor temperature at around 30 °C (dark blue line), corresponding to 85 to 90 wt. % ethanol in the distillate. The dispersion flow (light red line) was also manually controlled by the speed of the peristaltic pump to keep a constant dispersion level in the reactor.
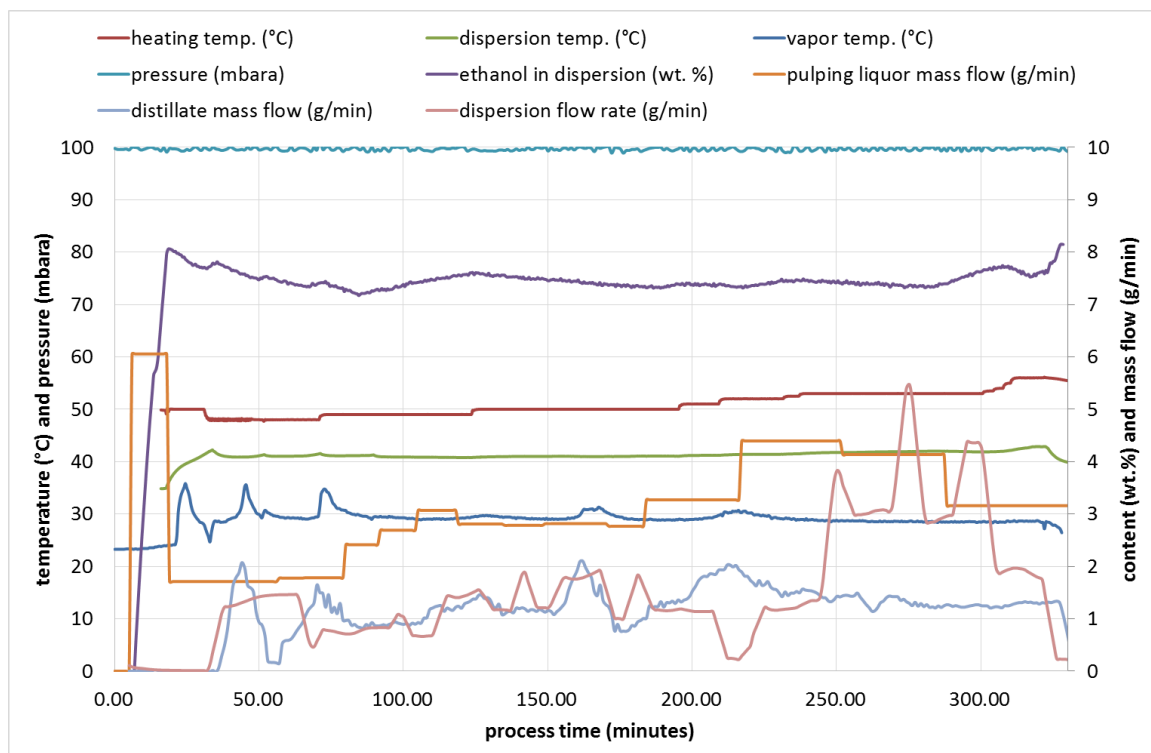
Figure 67: Process data trends of the continuous precipitation of K128 pulping liquor in the falling film evaporator setup at about 100 mbara.

The start-up dispersion was prepared until the 20th minute, where rectification column equilibration was finished after about 30 minutes and then the distillate and dispersion

flows were started in continuous operation. The pulping liquor feed was still in progress since the start-up dispersion was started to be prepared. The process was stopped after 330 minutes because the dispersion tubings were blocked with lignin lumps.

The evolution of the particle size distribution (PSD) over process time is plotted in Figure 68. During the preparation of the start-up dispersion and while the rectification column was equilibrated and the dispersion was heated up until the 30th minute, the PSD did not show signs of agglomeration, when compared to the case in the heat-up and equilibration phase of the experiments with jacket heating (see 5.5.1.1). The reason is that the pulping liquor feed was not stopped during the start and heat-up of this experiment but was in the experiment with jacket heating. Therefore, the agglomeration alone was not visible in this experiment (because nucleation was present all the time). As the nucleation rate was again bigger than the agglomeration rate at the beginning of the experiment, the PSD shifted to smaller particles until agglomeration became more prominent after about 180 minutes. The lignin particles started to strongly agglomerate to a median size of 40 µm until the 300th minute, while not being dispersed by the stirrer any more, but were trapped in the narrow tubings or adhered as incrustations. The FBRM® probe showed the disappearance of the agglomerate fraction sized between 20 to 100 µm and the appearance of a new fraction of small nuclei sized between 1 to 10 µm because the large particles were not flowing any more in front of the probe window. The micrographs of the lignin particles also clearly show the extent of agglomeration and support the information provided by the FBRM® probe.
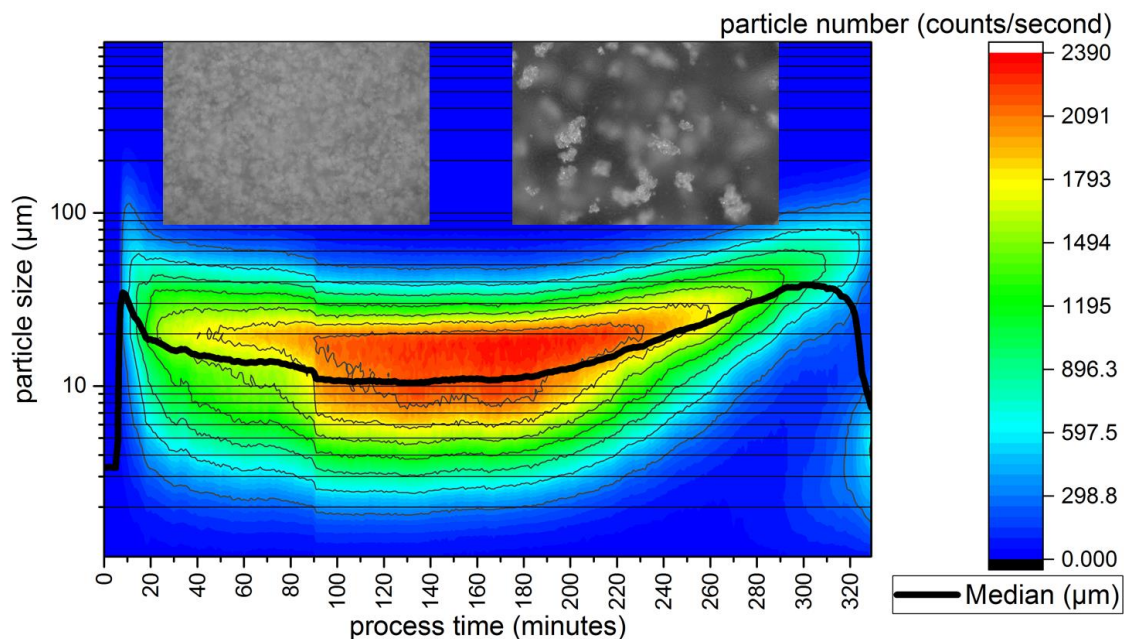
Figure 68: Evolution of the PSD (chord length) of lignin during the continuous precipitation of K128 pulping liquor in the FFE setup at about 100 mbara. Micrographs of lignin particles from the beginning (left) and from the end (right) of the experiment are shown as overlay.

It is strongly assumed that the manual increase of the heating jacket temperature of the FFE triggered the increase of the agglomeration rate from the 180th minute on. Experimental results that are not shown in this work implicate the same assumption because the median particle size increased or decreased when the heating temperature was increased or decreased, respectively. An explanation of this behavior

of the system could be that the lignin particles are softer when they adhere to the warmer surface of the FFE and therefore probably agglomerate faster on the surface of the FFE while being rinsed down to the stirred tank again. The surface temperature of the FFE was assumedly between 42 (dispersion temp.) and 55 °C (maximum heating medium temp.), which is lower than the measured agglomeration temperatures (5.2.5.1) but higher than the expected glass temperature (5.2.5.2).

In this first result, the extent of agglomeration of lignin was too large. The dry lignin yield after filtration was only 59 wt. % of the lignin which was originally fed in with the pulping liquor, corresponding to a lignin loss in incrustation of 41 wt. % (similar to jacket heating exp.).
Because of this obviously undesired result the operation conditions for the next experiment with the same pulping liquor were adjusted to lower temperature and ethanol content.

The **second experiment** (for trends see Figure 69) was carried out at a pressure of 80 mbara (light red line) and an average ethanol content in the lignin dispersion (dark blue line) of about 6.4 wt. % corresponding to an average dispersion temperature of 39.4 °C (green line). The pulping liquor feed rate (blue line) was adjusted around 4 g/min in continuous operation and the temperature of the heating medium in the FFE was tuned to a maximum of 50 °C (dark red line). The heating temperature was under 50 °C during the whole experiment in order to prevent extensive lignin agglomeration. The distillate flow (orange line) was manually adjusted by tuning the reflux valve in order to keep the vapor temperature at around 28 °C (violet line), corresponding to 80 wt. % ethanol in the distillate. The dispersion flow (light blue line) was also manually controlled by the speed of the peristaltic pump to keep a constant dispersion level in the reactor.
The start-up dispersion was prepared until the 20th minute, where rectification column equilibration was finished after about 30 minutes, followed by the distillate and dispersion flows starting in continuous operation. The pulping liquor feed was still in progress since the preparation of the start-up dispersion was started. During the process, the FBRM® probe had to be cleaned between the 75th and 80th minute because it was not properly cleaned before. Between the 260th and 275th minute, the pulping liquor feed T-mixer was plugged and had to be cleaned. The process was stopped after 350 minutes because the pulping liquor tank was exhausted.
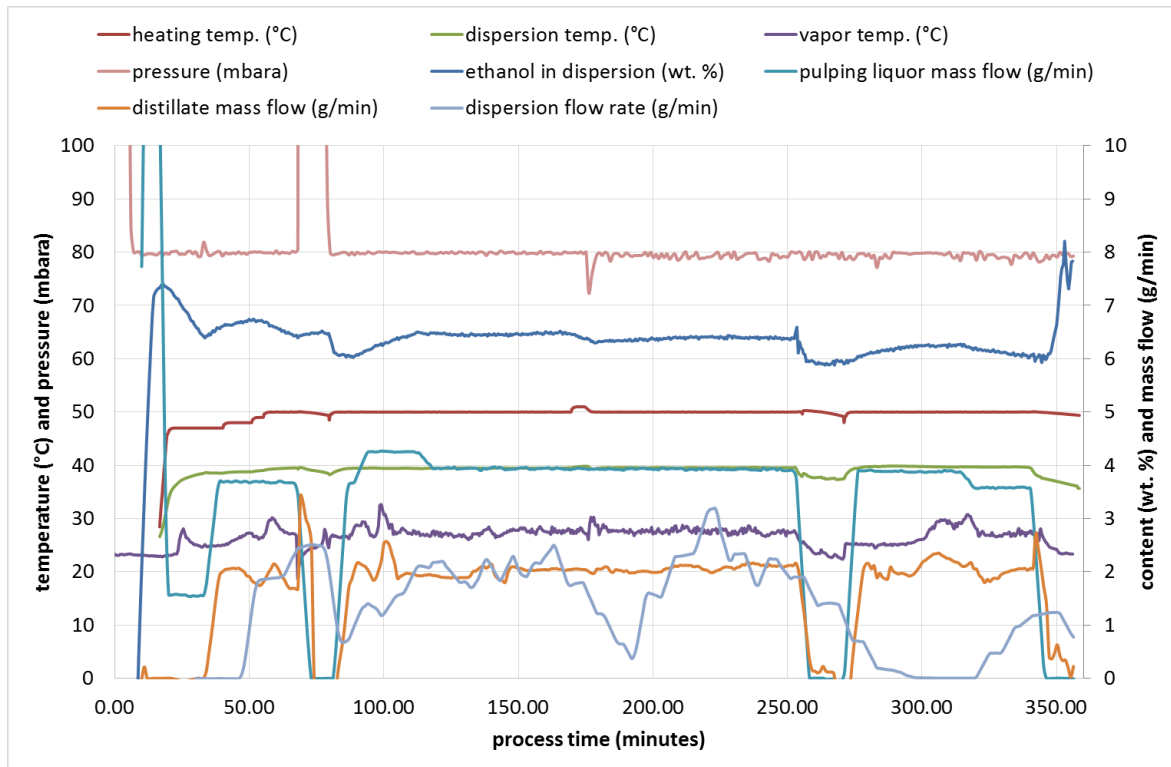
Figure 69: Process data trends of the continuous precipitation of K128 pulping liquor in the falling film evaporator setup at about 80 mbara.

The evolution of the PSD over process time is plotted in Figure 70. During the preparation of the start-up dispersion, and even before heating up the dispersion, a step-like increase in the median particle size was observed which may be due to the remaining particles on the probe window because of insufficient cleaning. The PSD slowly shifted to larger sizes during the start-up phase, which was not typical for these kind of experiments, and may be inaccurate because of the fouled probe window. After the probe was cleaned around the 75th minute, the particles slowly agglomerated until the end of the experiment and reached a median particle size of about 25 µm. The micrographs show almost the same particles in the beginning and end of the process and support the results of the FBRM® probe that showed moderate agglomeration.
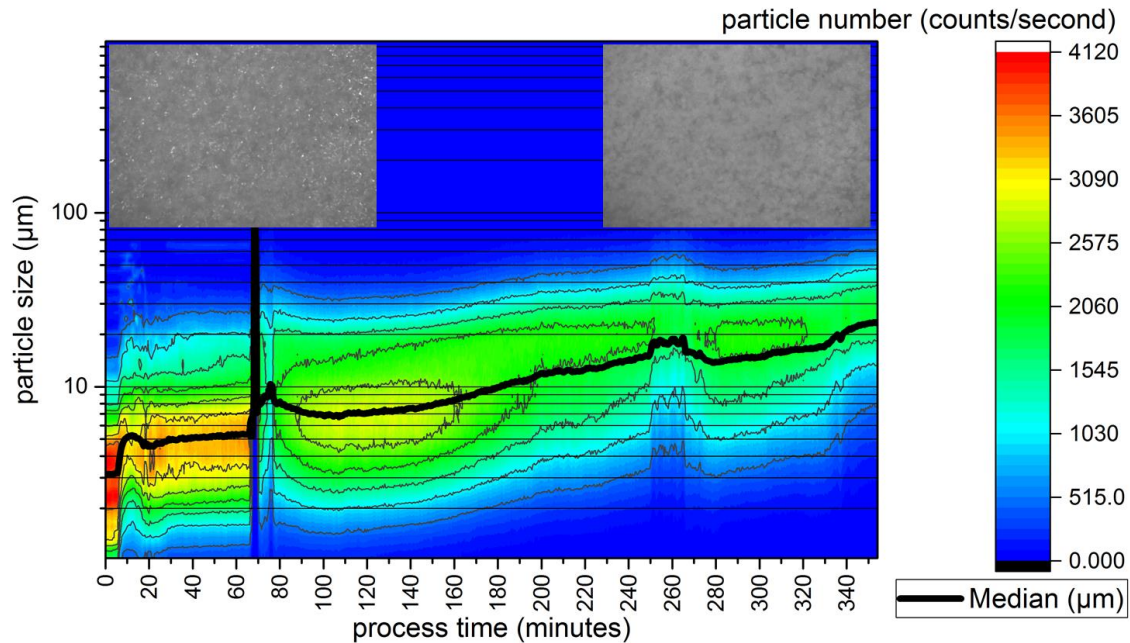
Figure 70: Evolution of the PSD (chord length) of lignin during the continuous precipitation of K128 pulping liquor in the FFE setup at about 80 mbara. Micrographs of lignin particles from the beginning (left) and from the end (right) of the experiment are shown as overlay.

The agglomeration rate in this second experiment could be regulated to a moderate level compared to the first experiment by lowering the pressure, heating temperature (of the FFE) and the ethanol content in dispersion. The dry lignin yield after filtration was 99 wt. % of the lignin that was originally fed in with the pulping liquor, which is a really good result for a lab scale plant.

Table 20 shows a principal mass balance of the continuous lignin precipitation process with 100 wt. % lignin yield, neglecting start-up dispersion and ethanol losses. The compositions of process streams were determined after each experiment, or were calculated from the mass balance. The pseudo-substances are actually each a group of substances with similar behavior within the process. Lignin contains several different lignin fractions but also other water insoluble substances (e.g. sugar oligomers). The sugars fraction contains all types of water soluble carbohydrate fractions and other dissolved solids. The ethanol fraction may also contain volatiles with a lower boiling temperature other than ethanol (e.g. esters). The water fraction also contains water miscible substances with a higher boiling temperature than water (e.g. acetic acid, furfural). The mass balances of the process streams were derived from the mass trends of each process stream during the experiments. The mass balances of single substances and single substances relative to the overall process stream have been calculated from the process stream compositions and the mass balance of process streams.

The mass balance of ethanol clarifies that about 11 wt. % of the ethanol stream still remains in the lignin dispersion or filtrate, respectively. This ethanol has to recycled in a separate downstream process (e.g., rectification of the filtrate) in order to close the solvent cycle as far as possible.

Table 20: Principal mass balance of the continuous lignin precipitation experiments with 100 wt. % lignin yield, neglecting start-up dispersion and ethanol losses. The pseudo-substances are actually a group of substances with similar behavior within the process, as described in the text above.

Process stream	(Pseudo-) Substance	Pulping liquor	Lignin dispersion	Distillate	Sum
Composition of process stream	Lignin (wt. %)	2.0	3.5	0.0	
	Sugars (wt. %)	2.0	3.5	0.0	
	Ethanol (wt. %)	44.8	8.8	92.5	
	Water (wt. %)	51.2	84.2	7.5	
	Sum	100.0	100.0	100.0	
Mass balance of process streams	(wt. %)	100.0	-57.0	-43.0	0.0
Mass balance of single substances	Lignin (wt. %)	100.0	-100.0	0.0	0.0
	Sugars (wt. %)	100.0	-100.0	0.0	0.0
	Ethanol (wt. %)	100.0	-11.2	-88.8	0.0
	Water (wt. %)	100.0	-93.7	-6.3	0.0
Mass balance of single substances relative to overall process stream	Lignin (wt. %)	2	-2.0	0.0	0.0
	Sugars (wt. %)	2	-2.0	0.0	0.0
	Ethanol (wt. %)	44.8	-5.0	-39.8	0.0
	Water (wt. %)	51.2	-48.0	-3.2	0.0
	Sum	100.0	-57.0	-43.0	0.0

Filterability

The average filter cake resistances of the lignin dispersion of both experiments have been determined as described in 3.7. The filtration functions and the calculated average filter cake resistances therefrom are shown in Figure 71. Maybe surprisingly, the filterabilities of both dispersions do not differ too much from each other, as one could expect from the stronger agglomeration of the 100 mbar dispersion. This may be due to the bimodal PSD of the 100 mbar dispersion that forms a less permeable filter cake than the unimodal PSD of the 80 mbar dispersion. Both had a moderate filterability that was satisfactory, but also not as good as the filterabilities of the dispersion derived from the jacket heating experiments.

However, the 80 mbar experiment seems to be a good compromise between filterability and lignin yield because it was the only experiment in this work that resulted in a satisfactory filterable dispersion while the lignin yield was almost 100 wt. % without any incrustations.
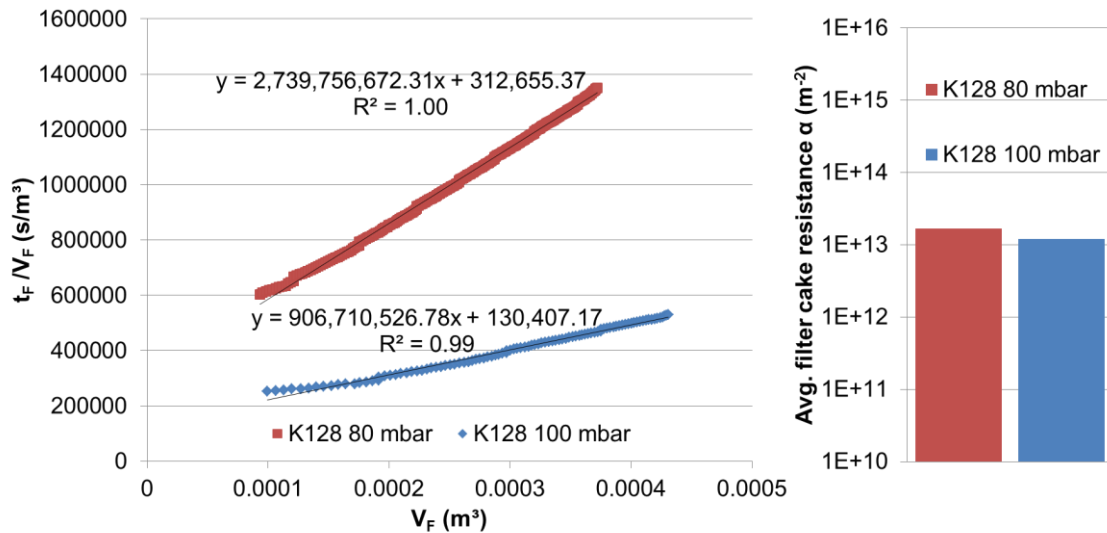
Figure 71: Left plot: Ratio of filtration time and filtrate volume (t/V) as a function of filtrate volume (V) for both lignin dispersions and the formulas of the linear fit (filtration functions) of each plot. Right bar plot: Average filter cake resistances of both dispersions, calculated from the slopes of the filtration functions, showing satisfactory filterability for both cases.

5.5.2.   Pilot scale experimental results

Two experimental campaigns (consisting each of two experimental days) were performed in the pilot plant. The first campaign with K138 pulping liquor was conducted without an inline infrared probe and the infrared spectra of dispersion samples were measured offline for a fast ethanol content measurement. Additionally, the plant was started for the first time after reconstruction and therefore robust operation conditions were not present. In this section, the results of the second experimental day of the first campaign are presented in detail.

The second campaign was performed two months later, when the inline infrared probe was installed and ready to use. In these experiments, the operation parameters have been improved in order to optimize the process. These results will be presented in the second part of this section.

The model described above (section 4) was used to predict suitable process conditions and the predictions are compared with the results of the first campaign.

First campaign:

The most important mass flows of the continuous pilot scale process are presented in Figure 72. The process was started by heating up the system with steam until the boiling temperature of the dispersion was reached at the adjusted pressure of 120 mbara (see Figure 73). The distillate was completely refluxed until the temperatures in the distillate system remained constant. Then, the continuous operation was started at the 72th minute by starting the pulping liquor (green line) and water feed (yellow line), the dispersion (blue line) and distillate removal (red line) and adjusting the heating power by the steam flow (black line). The controller for the pulping liquor, water and steam mass flow worked precisely and the mass flows were constant during the process.

The controller for the dispersion removal was oscillating around a mean value of 13.5 g/s (810 g/min) because of the fluctuations in the dispersion level in the reactor caused by the stirrer. The dispersion flow was not directly measured but calculated from the difference between two other mass flow meters, which are not displayed here. The plotted dispersion flow was averaged over two minutes of process time. The gap of the dispersion flow in the middle of the process corresponds to a downtime of the evaporator cycle pump.

The distillate flow was not directly measured and had to be calculated from the level change of the distillate tank, which starts to measure the level from a certain dead volume on. This dead volume explains the time offset of the distillate flow from the start time of continuous operation. Gaps in the distillate flow trend correspond to draining of the distillate tank when the maximum level was reached. The average distillate flow was calculated to a value of 12.2 g/s (732 g/min).

A mathematical model simulation of the pilot plant process (see chapter 4) has been used to plan the experiments before the implementation of the experiments.

In order to evaluate the model performance, the simulation results were plotted together with the experimental results in Figure 72 (colors of dotted lines correspond to the colors of the experimental data). The pulping liquor and water feed stream trends of experimental and simulated results match perfectly, as both were set to constant values in the experiment and simulation. The distillate mass flows of the simulation (avg. 11.6 g/s) and the experiment (avg. 12.1 g/s) are in sufficient agreement to each other, showing that the simulation model is able to predict vapor-liquid equilibria at these conditions. The simulated dispersion flow lies on average ~2 g/s above the experimentally measured flow. As the mass balance of the simulation is correct and the experimental distillate flow matches with the simulation, the experimental dispersion flow seems to be incorrect. Also, the experimental dispersion flow was strongly oscillating and not directly measured, what contributes to the assumption, that the experimental dispersion flow may contain an error.

The heating steam flows for the simulation had to be set to ~1 g/s higher than the experimental heating steam flow. This difference may correspond to assumptions and simplifications for specific heat capacities and phase transition enthalpies in the simulation. Besides, additional energy was introduced to the experimental process by the stirrer and pumps, which were neglected in the mathematical model.
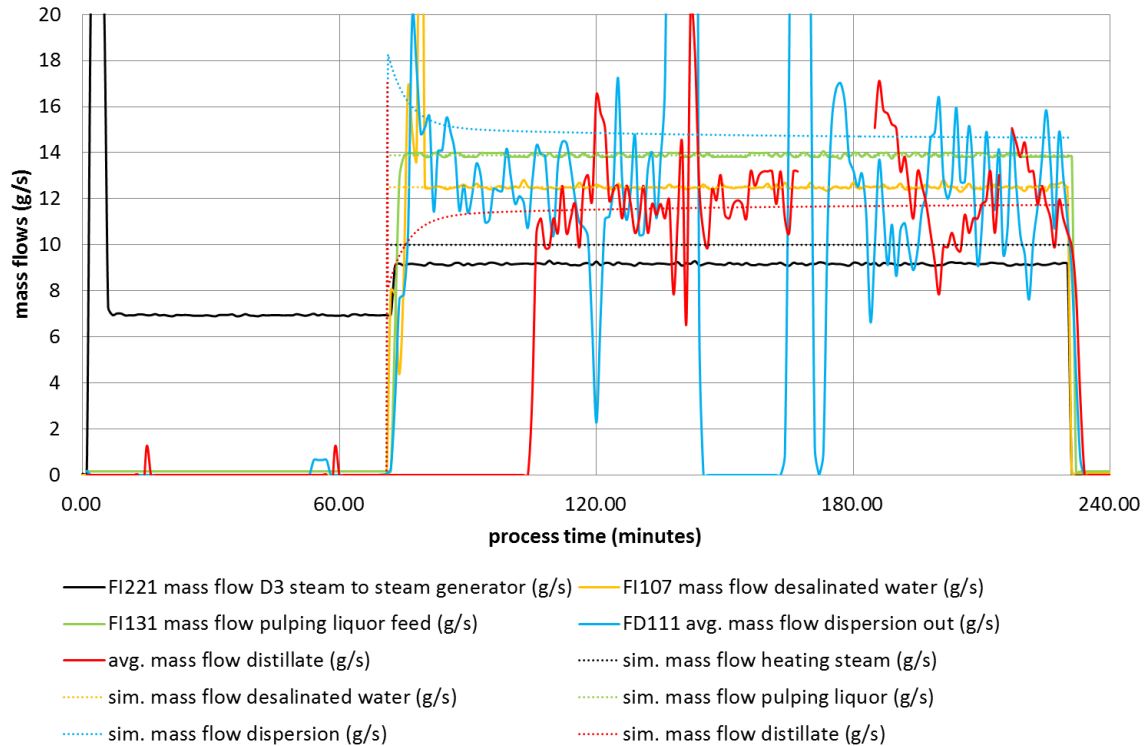
Figure 72: Solid lines: Measured mass flow trends of the most important streams in and out of the continuous precipitation process in pilot scale. Dotted lines: Simulated (see chapter 4) mass flow trends corresponding to the measured mass flows of the precipitation process.

Pressure (black line), temperature (red line) and mass fractions of ethanol (blue bars) and solids (green bars) (solid lignin and dissolved sugars) in the lignin dispersion are plotted together with the corresponding results from the simulation in Figure 73. As the pressure was controlled to a constant value in the experiment and simulation, both trends match well. The measured temperature of the dispersion is in good agreement with the predicted temperature, showing that the model is able to predict the boiling temperature. The ethanol and solids (lignin + sugars) mass fractions of the dispersion could be predicted without significant deviations from the experimentally measured value, verifying the model to correctly calculate vapor-liquid equilibria.

However, the mass fraction of ethanol in the distillate (yellow dots) was overestimated by the model, as the deviation accounts to up to ~5 wt. %. This deviation can be explained by the pulping liquor feed location. In the model, the pulping liquor is fed into the evaporator cycle and in the described experiment, the liquor was fed into the stirred tank. Therefore, the ethanol content in the dispersion of the model was higher than in the experiment, due to the higher dilution ratio in the stirred tank. The higher ethanol content in the liquid phase then results in higher ethanol content in the vapor.
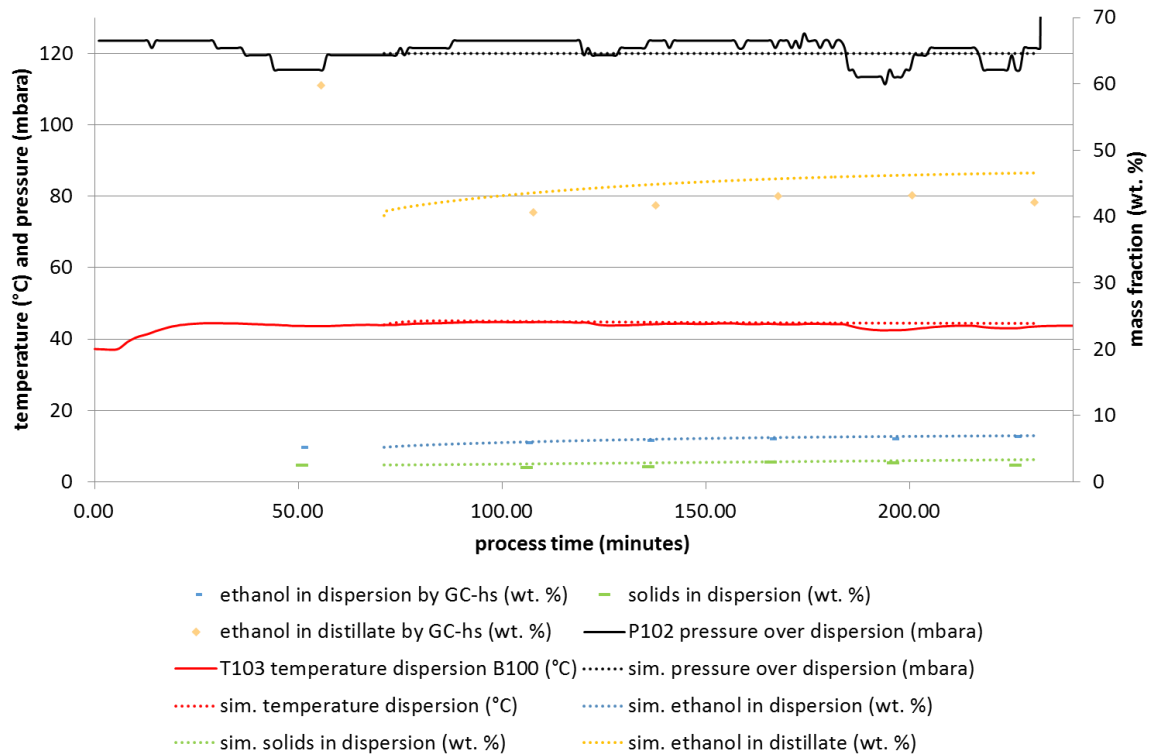
Figure 73: Solid lines and single points: Measured pressure, temperature, ethanol content and solids content of the lignin dispersion and ethanol content of the distillate during the continuous precipitation process in pilot scale. Dotted lines: Simulated data (see chapter 4) corresponding to the measured trends displayed in solid lines and single points.

The particle size (chord length) distribution (PSD) over process time is illustrated in Figure 74 as contour plot. The median particle size ($d_{50,0}$) is plotted as an overlay in the contour plot. The PSD of the initial dispersion ($d_{50,0} \approx 20$ µm) slightly shifted to smaller particles ($d_{50,0} \approx 15$ µm) during the process until it shifted back to larger particles again ($d_{50,0} \approx 18$ µm). Consistent to the PSD, the micrograph recorded at the end of process shows an increased number of fine particles compared to the micrograph captured at the beginning. Generally the PSD changed only slightly during the process.

The observations could be explained as follows: the particles in the initial dispersion had time over night to agglomerate, before newly fine particles were formed in the dispersion by starting the precipitation process, and thus firstly lowered the median particle size until the agglomeration rate increased again, which occurred as a result of the increase in quantity of fine particles as well as lignin softening. The median particle size at the end may show the equilibrium of the population balance of lignin particles. The population balance is mainly influenced by nucleation (precipitation of fed lignin), agglomeration (aggregation and agglomeration of fine particles depending on dispersion density, Zeta potential and lignin softening) and dispersion removal.
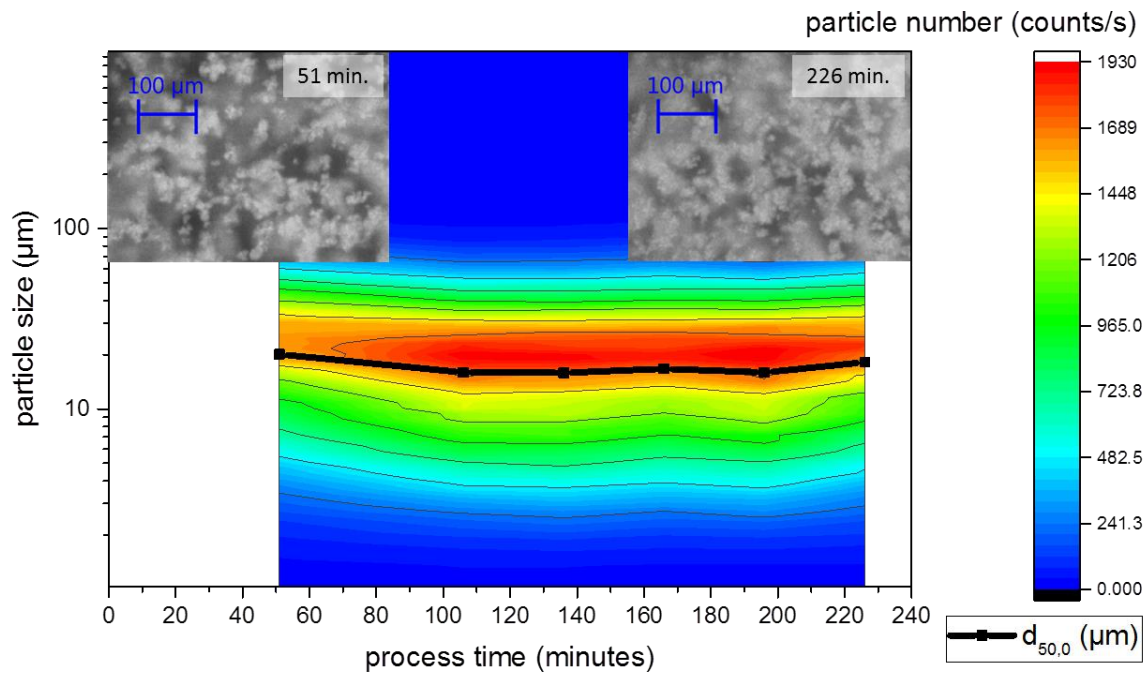
Figure 74: Particle size (chord length) distribution evolution during the continuous precipitation process in pilot scale displayed as contour plot. The median particle size ($d_{50,\,0}$) is plotted as overlay in the contour plot. Particle micrographs from the beginning and end of continuous processing are shown above the plot.

The average filter cake resistance was determined to 6.8×10^{12} m^{-2}, meaning that the produced lignin dispersion was of good filterability on a scale from 10^{10} to 10^{16} m^{-2} for excellent filterability to almost unfilterable, respectively.

The formation of incrustations was not observed, showing that the lignin particles were not too soft to stick on the reactor walls. This observation is consistent with the low agglomeration degree of the lignin particles. Unfortunately, a lignin yield could not be determined correctly because it was calculated to be 114 wt. %, which is impossible. Probably, the originally measured lignin content in the pulping liquor (1.35 wt. %) was incorrect. 8.67 kg dry lignin were separated from 560 kg pulping liquor and that would correspond to an original lignin content of 1.55 wt. % in the pulping liquor if the yield was 100 wt. %.

Despite the relatively high temperature (~45 °C), in comparison to the lab experiments (~41 °C), the lignin was not as soft as one would expect from the experiences from the lab experiments. A possible explanation is the much higher irrigation density of the pilot plant's falling film evaporator (3.5 m³/h and 10 tubes with 37 mm inner diameter, equals ~3 m³/m/h) in comparison to the falling film evaporator in lab scale (250 ml/min and 10 mm inner diameter tube, equals ~0.5 m³/m/h). A higher irrigation density avoids local overheating of the dispersion at the tube surface. It is reasonable to assume that local overheating of dispersion and lignin particles at the tube surface can cause lignin softening and enhances agglomeration. Thus, no incrustations were observed on the lab scale evaporator tube wall.

Second campaign:
Two experiments on two subsequent days have been carried out with K139 pulping liquor derived from pulping at standard conditions (beech wood chips, 170 °C, 50 wt. % ethanol, 0.8 wt. % sulfuric acid, H-factor 1500, 3.2 liquor to wood ratio, 1.35 wt. % lignin in pulping liquor). The results of both experimental days are shown as one in the process parameter trends below. The first experiment ended after 492 minutes and the second experiment was started on the next day with the lignin dispersion of the first day. The start-up procedure of the second day was cut out of the process trends.
The experiments were successfully planned again with help of the mathematical model described in chapter 4 but the predicted trends are not shown in the diagrams this time in order to present the results more clearly.

Figure 75 shows the mass and heat flows of the **two subsequent experiments** (the second experiment starts from around the 500th minute on). The continuous process was started on the first day at around the 170th minute after the start-up dispersion was prepared and the system was heated-up. The pulping liquor flow (violet line), heat flow (black line) and consequently the distillate flow (green line) were initially kept constant. The water feed (red line) were subsequently lowered to zero (around minute 600). Consequently the dispersion flow (blue line) was also markedly lowered to averagely 0.4 g/s (24 g/min). The water flow was lowered in order to reduce the undesired dilution of the dispersion while the dispersion flow was aimed not to decrease to zero because then the operation mode would switch to semi-continuous (fed-batch).
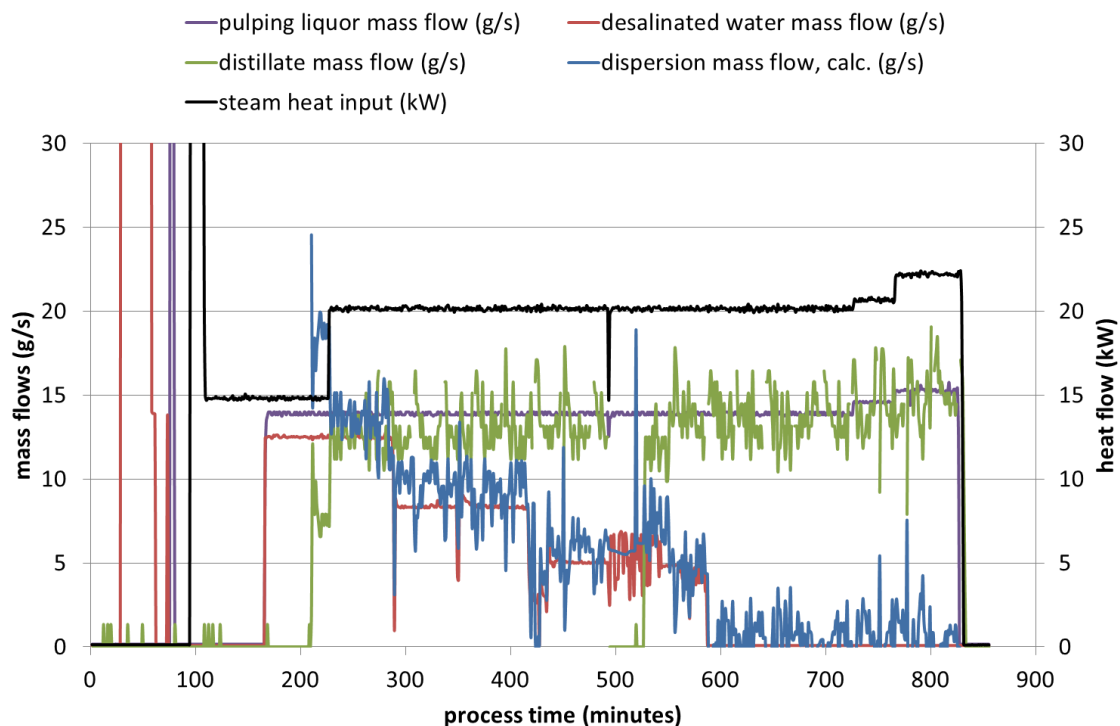
Figure 75: Process parameter trends of important mass and heat flows of two subsequent experiments for continuous precipitation of K139 lignin in pilot scale.

The ethanol content in the lignin dispersion (green line and violet crosses in Figure 76) had to be increased in order to increase the ethanol fraction in the vapor phase and to decrease the water removal by the vapor, as no rectification column was installed to

hold back the water in the dispersion. Otherwise, the dispersion flow would have been decreased to zero or lower, where more distillate mass would have been removed than pulping liquor added to the system (decreasing dispersion level in reactor). The ethanol content therefore increased from 7.3 to 8.6 wt. % during the process, as shown in Figure 76. Consequently, the ethanol content in the distillate also increased (cyan stars) and the dispersion temperature decreased (blue line) during the experiments. The pressure (red line) and the FFE heating temperature (orange line) were kept relatively constant at 120 mbara and 52-53 °C, respectively.
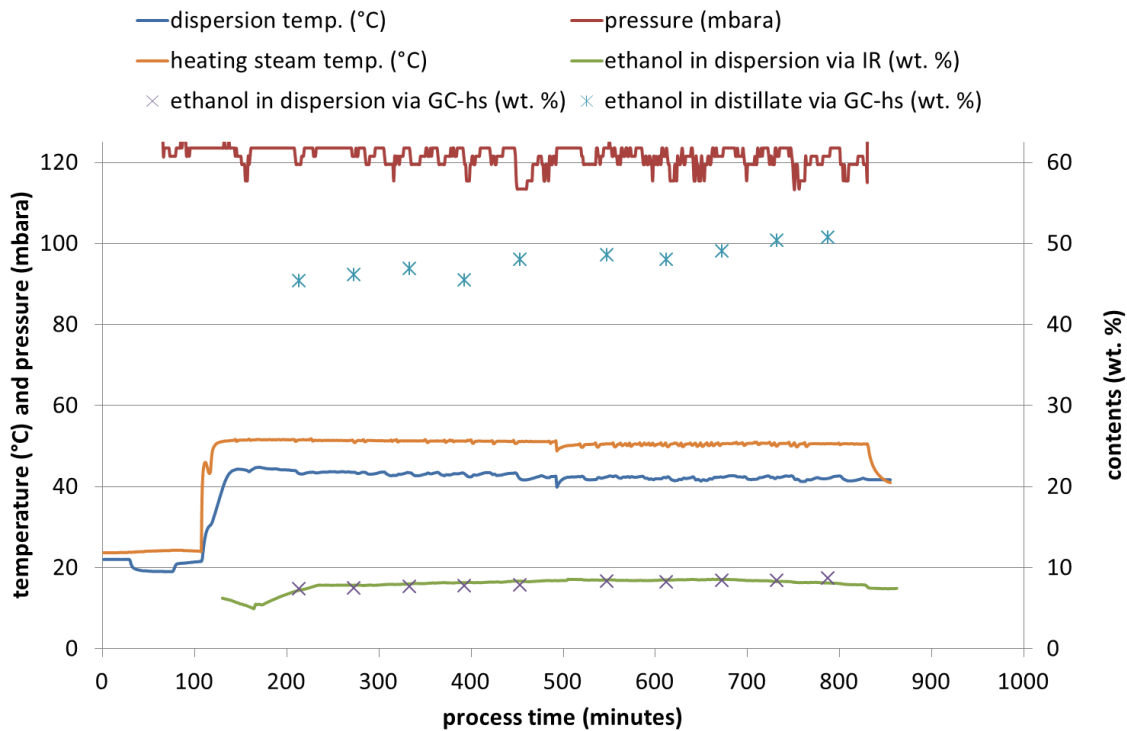
Figure 76: Pressure, temperatures and ethanol contents as a function of process time. Ethanol contents in dispersion were measured twice, by an inline infrared probe and an offline GC-headspace. Ethanol contents in the distillate were only measured with a GC-headspace.

The particle chord length distribution over process time is illustrated as a contour plot in Figure 77. The dispersion samples have been investigated with the FBRM® probe four days after the experiment but normally the particles do not change during storage at room temperature. The contour plot of the PSD shows the typical shape in the first part of the experiment until about 550 minutes. The PSD first shifted to smaller sizes and then to larger sizes from the 300th minute on. Then the dispersion was stirred over night while the temperature dropped from 43 to only 40 °C (not shown here) and the particles agglomerated. This overnight agglomeration time was cut out from the process time and that is the reason for the step-like increase in particle size between 500 and 600 minutes. During the second part of the experiment from 500 minutes to the end, the PSD incurred only minor changes.

The results show that even at 120 mbar, 43 °C dispersion temperature and 8.6 wt. % ethanol in the dispersion, the lignin particles did not agglomerate too much and also no incrustations were formed, while the same parameters probably would have led to incrustations in the lab plant. Consequently, the upscaling from lab to pilot scale influenced also the agglomeration and/or softening behavior of lignin, as already discussed at the end of results of the first campaign.
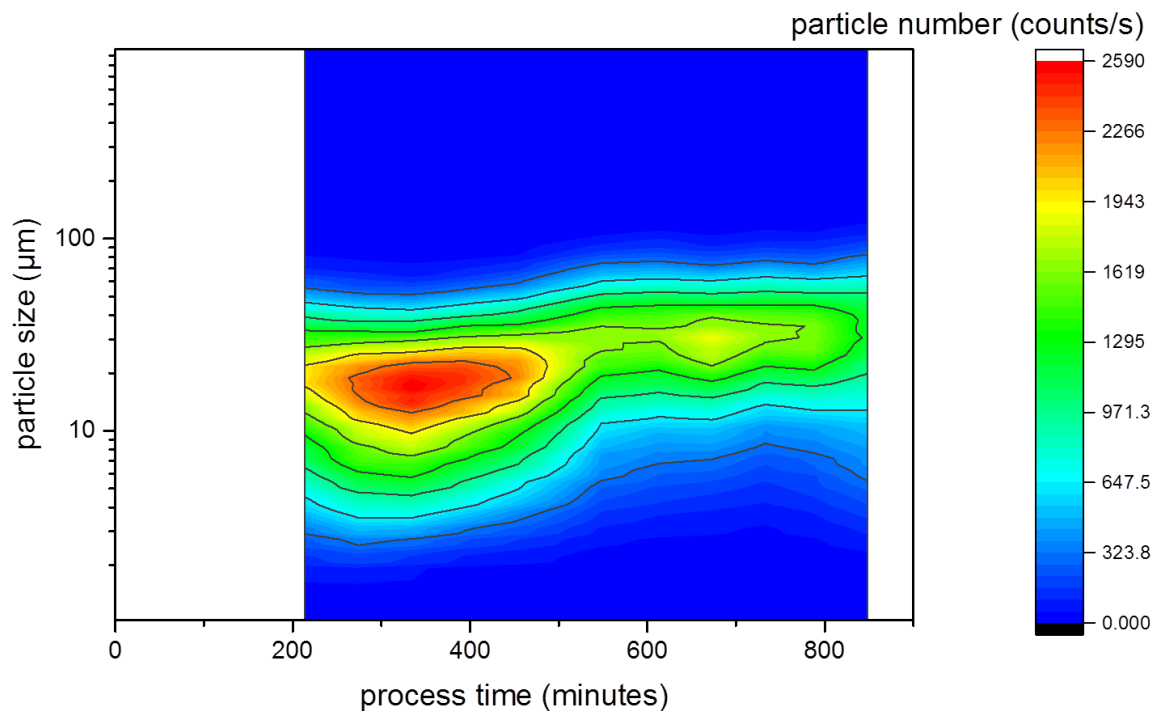
Figure 77: PSD (PCLD) of lignin particles and agglomerates over the process time as contour plot. The decrease of particles < 10 µm between 500 and 600 minutes is a result of agglomeration during the night hours, which were cut out of the time axis at 492 minutes.

The dry lignin yield was determined to be 101.5 wt. %, which is again impossible, yet no incrustations were observed. The yield larger than 100 % may result again from incorrect lignin content measurements of the original pulping liquor.

The average filter cake resistance unfortunately was not measured but the filterability was subjectively judged as good by the pilot plant employees.

In conclusion, the continuous precipitation and agglomeration process investigated in this work was successfully scaled up by a factor of 210 (pulping liquor feed) from lab to pilot scale. The larger scale and different operation conditions of especially the falling film evaporator caused less agglomeration of lignin particles and therefore allowed the process to operate at slightly higher temperatures and ethanol contents, compared to the lab scale process. Because of the higher ethanol content in the dispersion, it was possible to reduce the water feed to zero, which originally had to be added because of the missing rectification column. Incrustations were completely prevented and the lignin yields were near 100 %, while the achieved filterabilities were between good and satisfactory. The specific energy consumption used for lignin precipitation in this experiment was calculated to around 111 kJ/g of lignin, considering only the input of heating steam energy. That is a relatively high value and more energy is consumed in up- and down-stream processing (e.g. pulping, filtration, filtrate distillation, lignin drying). Proposals for decreasing the energy consumption are made in the conclusions (section 6).

5.6. Principles and trajectories of the investigated lignin precipitation processes

The aim of this section is to explain again and summarize the principles of the investigated lignin precipitation processes. Therefore, the process trajectories of the batch process (Figure 78) and the (semi-) continuous process (Figure 79) are plotted in the qualitative pseudo-ternary phase diagrams of the lignin-ethanol-water system. The pseudo-substances lignin, water and ethanol on the edges of the triangular phase diagram represent the various lignin molecules, water together with water soluble substances and ethanol containing other lower boiling substances, respectively.

The **batch precipitation process** starts at the point A (Figure 78) that represents the average composition of pulping liquor. By evaporation of an average ethanol/water composition of 70 wt. % from the pulping liquor the composition of the batch is moving in the direction of point C_B that represents the composition of the lignin dispersion after ethanol was completely evaporated from the liquor. The path from A to C_B is a curve because the ethanol mass fraction of the vapor decreases during the evaporation process. The liquor of composition $C_{B,P}$ separates in the phase diagram into a lignin-rich phase ($E_{B,P}$) and a solvent-rich phase ($D_{B,P}$) when the A-C_B path enters the binodal of the lignin-water miscibility gap. The lignin-rich phase is now in its liquid state and sticks to surfaces. During the slow course of evaporation (lasting for hours), more lignin-rich and solvent-rich phase with binodal-compositions separates until all ethanol is evaporated and the final lignin-rich phase composition E_B and the solvent-rich phase composition D_B are reached. E_B is now situated beyond the vitrification line, meaning that the lignin-rich phase solidified into its glassy state and solid incrustations are formed. The ratio of the distances C_B-D_B and D_B-E_B quantifies the lignin dispersion density (mass fraction of dispersed lignin in the aqueous phase ≈ 11-12 wt. %). Despite of the disadvantage of forming incrustations the batch process results in relatively dense lignin dispersion and a distillate with relatively high ethanol content. Both are advantageous in downstream processing requires and with respect to energy consumption.

Consequently, the process could be improved by decreasing the evaporation time to reach C_B from A so that the lignin-rich phase directly separates in its glassy state. Therefore the ethanol evaporation should approximately be performed within a second what could maybe facilitated by a falling film evaporator (FFE) at low pressure. The FFE would be fed with pulping liquor and the pressure and surface temperature would have to be tuned carefully to yield solid lignin particles. This kind of process variant could eventually be developed in future investigations.
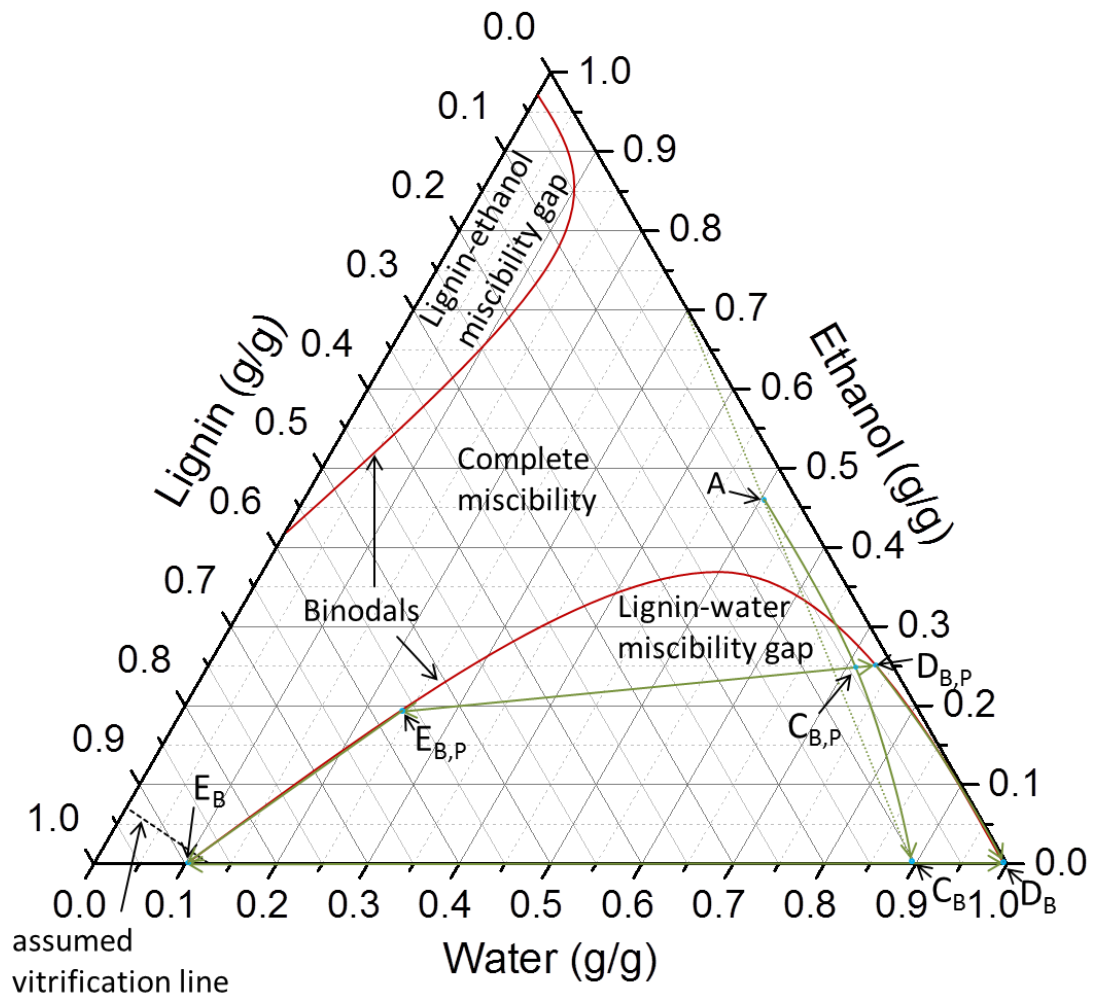
Figure 78: Illustration of the batch precipitation process trajectories in the qualitative pseudo-ternary phase diagram at typical process conditions (≈40 °C, corresponding to 100-200 mbara distillation pressure).

The **(semi-) continuous precipitation process** starts again at the pulping liquor composition in point A in Figure 79. The pulping liquor is quickly mixed (≤ 1s) with the aqueous phase of the lignin dispersion (point B) by feeding the pulping liquor into the stirred tank or evaporator cycle, depending on the experimental setup used. The mixture of pulping liquor (A) and aqueous phase (B) has the composition of point C. C is situated in the lignin-water miscibility gap and thus the mixture separates into a lignin-rich phase E and a lignin-poor phase D. The point E is located in the area of glassy solidified lignin (see vitrification line at 40 °C) and therefore it does not stick to surfaces and causes no incrustations. The ethanol content of the lignin-poor aqueous phase D is decreased to composition B by evaporation and thus the dispersion has to come in contact with a heat-exchanger surface (in the falling film evaporator) that may have e.g. 50 °C. So lignin particles are also transported along the heat-exchanger surface, get heated to 50 °C and pass from the glassy to the liquid state as illustrated by the second vitrification line at 50 °C. The soft lignin particles coalesce with each other and form solid agglomerates when washed away from the heat-exchanger surface. They are solidified again in the dispersion bulk at 40 °C.
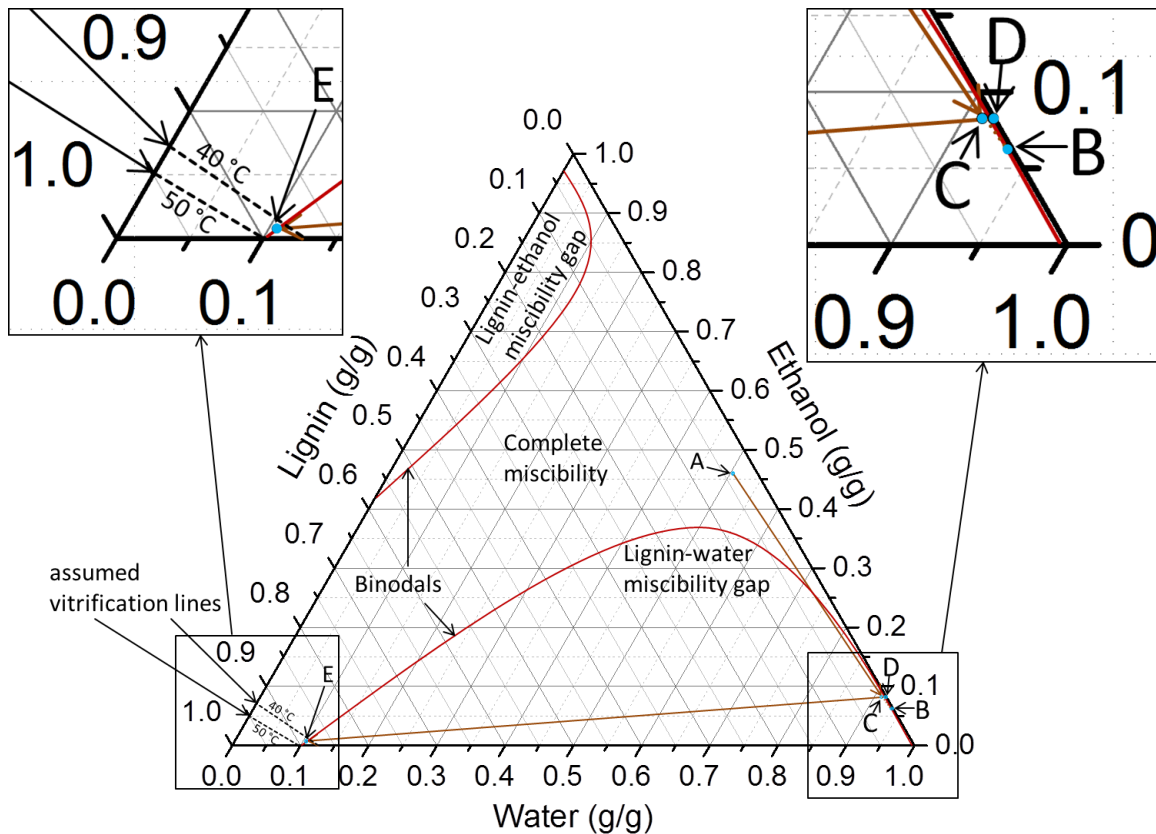
Figure 79: Illustration of the (semi-) continuous precipitation trajectories in a qualitative pseudo-ternary phase diagram at typical process conditions (40-45 °C and 80-120 mbara).

Consequently, the lignin particles formation is much better controlled in the (semi-) continuous than in the batch process. In this way incrustations are prevented and agglomeration can be controlled by the heat-exchanger temperature. However, rectification is needed to get sufficiently high ethanol contents in the distillate and to keep enough water inside the lignin dispersion. Thus, the energy demand is relatively high in comparison to the batch process because the ethanol is evaporated from a more diluted aqueous mixture.

Despite of this drawback mentioned, this (semi-) continuous process described is superior to state-of-the-art precipitation processes (see 2.2.2) because no additional dilution stream is required, incrustations are prevented and the filterability is actively controlled by particle agglomeration.

6. Summary, Conclusions and Outlook

The overall objective of this work, which consisted in the development of a pilot scale process for continuous lignin precipitation from ethanol organosolv pulping liquors on the basis of solvent evaporation, has been achieved. Furthermore, the process has been patented (Schulze et al. 2014). In the following, the main progresses are summarized.

The **fundamentals for the process design** have been mainly obtained in lignin solubility and softening studies, as well as batch evaporation-precipitation experiments with ethanol organosolv pulping liquors. These experiments revealed the mechanisms causing undesired lignin incrustation and provided main data to define the process conditions at which lignin particles are slightly softened and undergo controlled agglomeration (sintering) without the formation of incrustations in the reactor.
First solubility measurements of lignin in ethanol/water mixtures confirmed the practical insolubility in solvents with less than ca. 10 wt. % ethanol. Therefore, lignin yields close to 100 % can be easily attained in separation processes by decreasing the ethanol content. Further, the solubility measurements revealed that not only lignin dissolves in the solvent but also lignin gets solvated (swollen) by the solvent. This finding led to extended solubility measurements that disclosed a large miscibility gap between solvated lignin and water and in addition a small miscibility gap between solvated lignin and ethanol in the (pseudo-) ternary system. This liquid-liquid phase equilibria have been measured with a newly developed procedure using inline infrared spectroscopy in combination with a partial least squares (PLS) regression model of lignin-ethanol-water mixtures.
Surprisingly, an apparently complete miscibility between 80 wt. % ethanol (20 wt. % water) solvent and lignin at room temperature was found. Solutions with up to 60 wt. % lignin and 40 wt.% solvent (32 wt. % ethanol and 8 wt. % water) were prepared that could be applied, for example, as casting resin precursor or as resin for the manufacturing of fiber-reinforced composite materials.

The observation of **sticky liquid lignin-rich phases** in solubility and batch evaporation-precipitation experiments clearly provided the insight that lignin incrustations, which have been reported by the colleagues from Fraunhofer CBP to be a practical problem, were formed by this sticky lignin phase. On that basis, softening and agglomeration of particulate lignin in aqueous dispersions with different ethanol contents has been studied to determine the conditions (temperatures and ethanol contents) where lignins tend to agglomerate and to form incrustations. Noteworthy is that the **agglomeration temperatures** of solvated lignins have been found to be markedly above their glass transition temperatures, which have been measured by TM-DSC.

With the knowledge of temperatures and ethanol content required to understand the separation of a solid (nearly glassy) lignin phase, as a key result of this thesis, a **semi-continuous (fed-batch) process** was designed. An important principle of this process is the fast drop of the ethanol concentration by dilution of the pulping liquor with an

aqueous lignin dispersion of desired temperature and ethanol content. The precipitating lignin particles immediately solidify and thus prevent incrustations. This precipitation step is very similar to established dilution-precipitation processes but the simultaneous evaporation of ethanol from the dispersion (to keep the ethanol content within the desired level) is a significant improvement because no additional aqueous stream is necessary for dilution. Consequently, only about half of fed pulping liquor mass is produced as dispersion and thus the effort in downstream processing is decreased. The process could be rationalized by drawing to process trajectories in the lignin-ethanol-water phase diagram (see section 5.6), clarifying the mechanisms of phase separation and lignin particle formation.

The semi-continuous process was first successfully tested in lab-scale before it was implemented in the pilot plant at Fraunhofer CBP.

A next development step was the controlled thermal treatment of the lignin dispersion after the semi-continuous precipitation was finished in order to soften the lignin particles as much as needed to **trigger agglomeration or sintering**, respectively, while avoiding incrustations. The lignin particles in dispersion contain 10-15 wt. % of water and are close to their glass temperature (vitrification line) during the precipitation process (see also 5.6). The filterability of lignin dispersions could be significantly improved by the sintering step.

Subsequently, a **continuous lab process** variant was developed based on the knowledge acquired from studying semi-continuous processing. The continuous lab plant was equipped with inline particle analytics and ethanol content monitoring for optimized process control. Particle agglomeration occurred after a certain process time although the temperature and ethanol content in the dispersion were below the lignin softening values determined before. It was assumed that the lignin particles got softened on the warm heating jacket or in the foam with higher ethanol vapor content that was generated by bubble boiling. Additionally, the boiling foam caused lignin incrustations above the dispersion level.

For those reasons the continuous lab plant was upgraded with a **falling film evaporator** (FFE) in order to prevent foaming of the lignin dispersion. With this final experimental setup, incrustation could be completely prevented. Lignin yields close to 100 % have been achieved and good filterable dispersions were produced by controlled agglomeration of lignin particles. The agglomeration could be controlled by the heating-medium temperature of falling film evaporator, whereby the optimal temperature was found to be in the region between the glass transition and agglomeration temperatures. Consequently, the glass temperature of solvated lignin will be considered as lower temperature border for controlled agglomeration in the future.

This final process setup could be **scaled-up from lab to pilot plant** but without a rectification column and therefore with an additional (undesired) water feed. Nevertheless, the addition of water to the process could be decreased to zero during the experimental campaign when operating at appropriate high ethanol contents in the lignin dispersion. To keep up continuous operation the ethanol content in the distillate has to be higher than in the pulping liquor. Respectively, more pulping liquor has to be added than distillate is removed. As in the lab plant, lignin yields close to 100 % (no incrustations) and good filterabilities could be achieved in the pilot plant.

A **mathematical model,** covering the major mass and energy balances and phase equilibria of the continuous process, was established and applied to predict suitable process parameter before performing first experiments in the pilot plant.

With the successful operation of the precipitation process in the upgraded pilot plant, most objectives of this work (no incrustations, high lignin yield, good filterability, no addition of aqueous streams for dilution, feasible for pilot plant implementation at Fraunhofer CBP) could be fulfilled.

The process design developed is an up-scalable process concept (industrial scale) and thus its **specific energy consumption** is an issue that should be considered in future investigation in order to enable an economic operation at larger scales. The process is based on ethanol evaporation from a dilute lignin dispersion with ethanol contents between 5 and 10 wt. %. Therefore, the energy consumption is similar to those of established dilution-precipitation processes mentioned in section 2.2.2, because in these processes the similar specific amount of ethanol has to be separated by distillation or rectification from aqueous mixtures with ethanol contents around 10 wt. %. The specific energy consumption could be probably reduced by orders of magnitudes using higher lignin contents in the pulping liquor. This could be achieved by optimization of the pulping process (e.g. counter-current processing) or by pre-concentration of the pulping liquor before feeding it into the precipitation process. The pre-concentration process should of course consume less specific energy for solvent removal than evaporation (e.g. membrane separation). Further possibilities to increase energy efficiency would be the utilization of heat integration and heat pumps (e.g. vapor compression).

In addition a completely novel process concept of **cooling-precipitation** of lignin and sugars from pulping liquor, as derivable from the solubility studies performed, should have great potential for decreasing the energy consumption. The specific energy consumption of cooling is much lower than of evaporation. The concept of lignin cooling-precipitation could be verified in future works.

Alternatively, an advanced **controlled flash-evaporation** of ethanol from pulping liquor in a falling film evaporator may be a suitable concept to reduce the energy demand and yield particulate lignin without incrustations. This advanced flash-evaporation process concept may also be investigated in future works.

In summary, to develop new separation process concepts or to exploit alternative lignin-solvent-antisolvent system in known processes, the (solid-) liquid-liquid phase behavior of the particular system has to be investigated at first. Subsequently, separation processes can be developed systematically on the basis of this knowledge regarding the phase behavior, as successfully demonstrated in this work.

A. Appendix

A.1. Diagrams of various lignin data
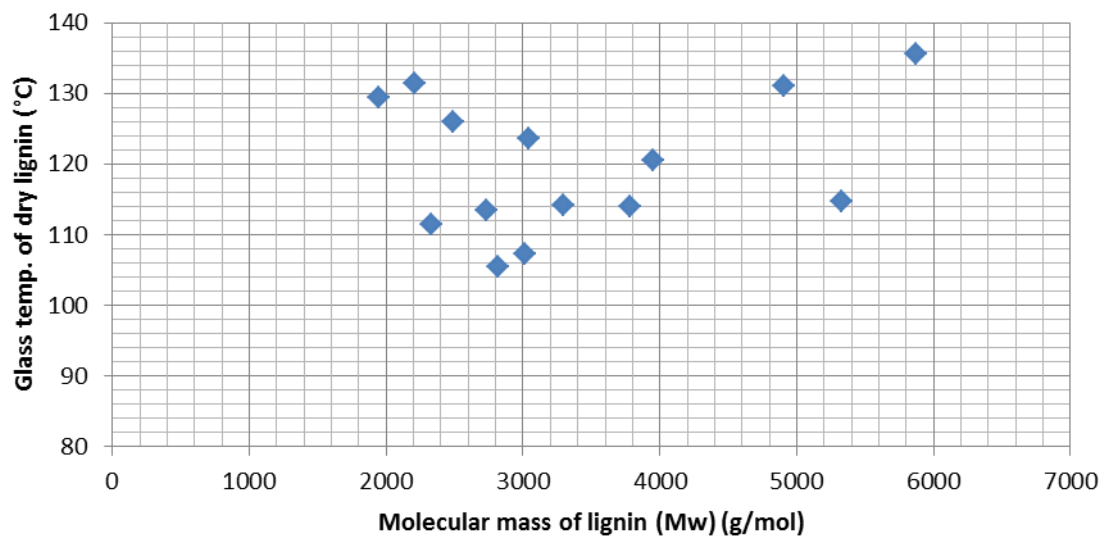
Figure 80: Glass temperatures of lignins plotted against their weight average molar masses.
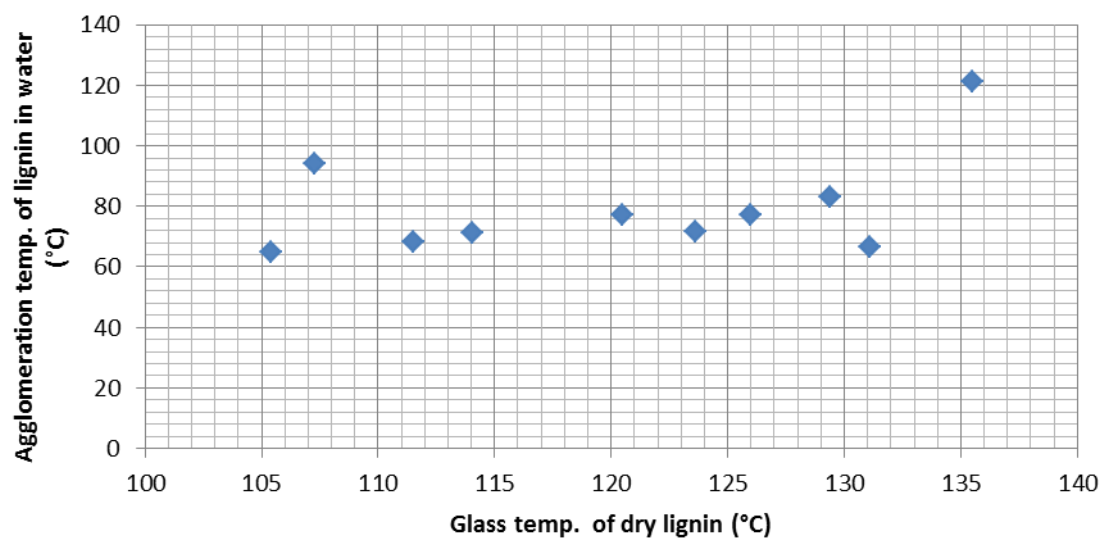
Figure 81: Agglomeration temperatures in water of lignins plotted against their glass temperatures.
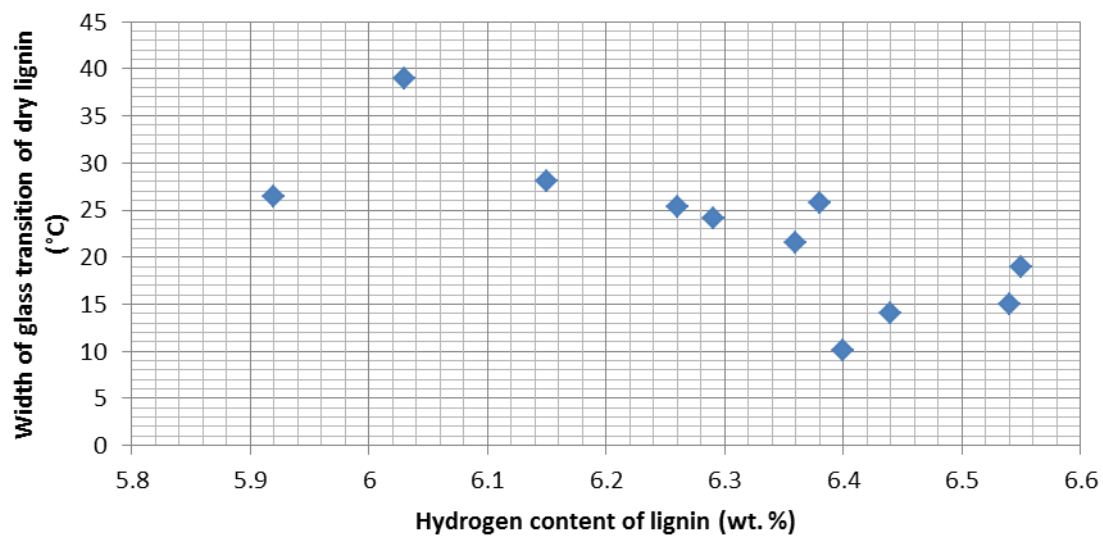
Figure 82: Width of glass transition of dry lignins plotted against their Hydrogen content (from elementary analysis).

A.2.   Overview of lignin precipitation experiments performed

Table 21: Overview of the most lignin precipitation experiments performed in the different experimental setups. Some characteristic process conditions are also shown. The results of the grey marked experiments are presented in detail in section 5. (agglo.: temperature in subsequent agglomeration procedure, end feed: ethanol content after the pulping liquor feed was stopped and during the agglomeration procedure)

Experimental setup (reactor volume)	Pulping liquor batch	Mass of processed pulping liquor (g)	Process pressure (mbara)	Temperature range of lignin dispersion, (°C)	Ethanol content range of lignin dispersion (wt. %)
lab batch (300ml)	K1	≈300	≈1000	82-100	47-0.5
lab batch (300ml)	K1	≈300	≈400	60-76	47-0.5
lab batch (300ml)	K1	≈300	≈200	46-59	47-0.5
lab batch (300ml)	K1	≈300	≈100	34-47	47-0.5
lab batch (300ml)	K1	≈300	≈50	20-38	47-0.5
lab semi-continuous (300ml)	K1	≈120	≈100	42-46 (82 agglo.)	≈10 (0.5 end feed)
lab semi-continuous (300ml)	K1	≈270	≈100	42-47 (90 agglo.)	≈10 (0.5 end feed)
pilot semi-continuous (680l)	K29	≈250kg	≈100	38-44 (70 agglo.)	≈10 (0.5 end feed)
lab continuous (2000ml)	K9	≈1100	≈100	42-43	5-7
lab continuous (2000ml)	K9	≈750	≈240	58-61	12-17
lab continuous (2000ml)	F02	≈860	≈190	53-55	5.5-7.5
lab continuous (2000ml)	F02	≈925	≈130	45-46	7-8.5
lab continuous (2000ml)	K37	≈150	≈200	54-55	5-8
lab continuous (2000ml)	K37	≈1590	≈110	43-44	6-8
lab continuous (2000ml)	K39	≈1600	≈140	46-48	7-8
lab continuous (2000ml)	K39	≈1350	≈100	≈41	7.5-9
lab continuous (2000ml)	K40	≈1800	≈100	41-42	6-7.5
lab continuous (2000ml)	K41	≈1400	≈100	41-42	6-7.5
lab continuous (2000ml)	K42	≈1400	≈100	41-42	6-7.5
lab continuous (2000ml)	K43	≈1700	≈100	41-42	6-7.5
lab continuous (2000ml)	K44	≈1050	≈100	41-42	6-7.5
lab continuous (2000ml)	K45	≈1650	≈100	41-42	6-7.5
lab continuous (2000ml)	K103	≈8000	≈80	38-39	6-8
lab continuous FFE (2000ml)	K45	≈1400	≈100	39-40	8-10
lab continuous FFE (2000ml)	K128	≈1150	≈100	≈41	7-8
lab continuous FFE (2000ml)	K128	≈1130	≈100	41-43	5-6.5
lab continuous FFE (2000ml)	K128	≈1200	≈80	39-40	6-6.5
lab continuous FFE (2000ml)	K103	≈1200	≈100	42-44	6-7.5
pilot continuous FFE (680l)	K138	≈150 kg	≈120	≈44	5-7
pilot continuous FFE (680l)	K138	≈135 kg	≈120	≈44	5-7
pilot continuous FFE (680l)	K139	≈130 kg	≈120	≈44	5-7
pilot continuous FFE (680l)	K139	≈550 kg	≈120	42-44	7.5-8.5

A.3. Matlab™ source codes of the model for the quantitative description of the lignin separation process

Comments (green) are in German language. Names of variables and constants may differ from the model description in chapter 4, but the names from the model description are mostly written in the comments.

Main function:

```matlab
function DGLsys

clear all
close all
clc
%%
%%------------------------------------------------------------------
%Stoffwerte
%Waermekapazitaeten
p.cp_g=[1.7,2.012];                 %Gasphase, Ethanol, Wasser
p.cp_L1=[2.974,4.186,1.417,1.22];   %Fluessigphase, Eth, Wasser, Lignin, Zucker
p.cp_L2=[1.417,1.417];              %Lignin, fluessig, fest

%molare Masse
p.M_1 = 46.07; %Ethanol %g/mol
p.M_2 = 18.02; %Wasser  %g/mol

%Verdampfungsenthalpien bei 40-50 °C
p.hv1=890;    %Ethanol, J/g
p.hv2=2384; %Wasser , J/g
%%
%------------------------------------------------------------------
%Systemdruck
p.p0=120; %mbar
%Verdampfer, Gesamtflaeche 3.5 m^2, 5 Abschnitte
Q=36/3.6*2133; % J/s Gesamtheizleistung
x kg Dampf/h/3600s/h*1000g/kg*2133 joule/g Dampf
%Flaeche fuer einzelnen Abshnitt
p.A=7000; %cm^2
%Waermestromdichte
p.q=Q/5/p.A;  %J/cm^2 s.
% Gesamt Heizleistung ist 5*p.A*p.q
%%
%------------------------------------------------------------------
%festgelegte Stroeme
%Feedstrom gesamt
%feed mit wasser verdünnen und so Zugabe von VE Wasser simulieren!
mtot_F=50/3.6; %g/s entspricht Strom F
mtot_water=45/3.6; %g/s entspricht Strom W
p.mtot_F = mtot_F+mtot_water;
%Zusammensetzung der verdünnten Kochlauge aus der gegebenen Kochlaugenzusammensetzung
berechnen
w_diluteKL_E=0.472*mtot_F/p.mtot_F;
w_diluteKL_L=0.023*mtot_F/p.mtot_F;
w_diluteKL_Z=0.023*mtot_F/p.mtot_F;
w_diluteKL_W=1-w_diluteKL_E-w_diluteKL_L-w_diluteKL_Z;
%Zusammensetzung der KL, Eth, Wasser, geloestes Lignin, Zucker, flüssiges Lignin, festes
Lignin
p.x_F = [w_diluteKL_E, w_diluteKL_W, w_diluteKL_L, w_diluteKL_Z, 0, 0];
%Temperatur der Feedströme F und W
p.T_F = 20; %Â°C
%Gesamtstrom C aus Apparat 7, festgelegt durch Kreislauf-Pumpe
p.mtot_A7=3500/3.6; %g/s, entsprechend 3500 kg/h/3600 s/h*1000 g/kg
p.mges_ref=270000; %g % konstante Füllmenge im Behälter, max ca 500 kg
%%
%------------------------------------------------------------------
%Koeffizienten fuer Antoinegleichung, log10, mbar, Â°C
%         A         B         C
p.Acoeff=[8.23714, 1592.864, 226.184;...   %Ethanol
          8.19625, 1730.63,  233.426];      %Wasser
%Koeffizienten der van Laar Gleichung zur Berechnung der
%Aktivitaetskoeffizienten, C=[C1,C2]
p.C=[1.701,0.9425];
%Siedetemperaturen der reinen Komponenten mittel Antoine Gleichung (Kap. 4.4)
```

```matlab
66   Twasser=p.Acoeff(2,2)/(p.Acoeff(2,1)-log10(p.p0))-p.Acoeff(2,3);
67   Tethanol=p.Acoeff(1,2)/(p.Acoeff(1,1)-log10(p.p0))-p.Acoeff(1,3);
68   p.Tsv1=Twasser; %Startwert fuer function boil
69   %Koeffizienten fuer Lignin Loeslichkeitsfunktion
70   p.pl=[-0.0003498,0.04442,3.654e-05,-0.3131,-0.001733,-1.558e-07,0.6933,0.009525,6.225e-
71   06];
72   % %Erweichungstemperatur für Lignin aus empirischer Gleichung berechnen, Tg = -189*x +
73   71.8;
74   p.Tg=[-189,71.8];
75   % %Zeitkonstanten fuer Phasenuebergang fluessiges Lignin auf NULL gesetzt
76   % und somit DEAKTIVIERT! Lignin ERWEICHUNG wird hier nicht berücksichtigt
77   p.k1=0;
78   p.k2=0;
79   %%
80   %-------------------------------------------------------------------
81   %Einstellungen solver
82   %Zeitvektor
83   dt=10;%sekunden %dt bestimmt nur, mit welchem Intervall Werte in csv Datei ausgegeben
84   werden
85   tspan=[0:dt:9600];  %Sekunden
86   %Anfangsbedingungen !!!!!!! AB!!!!!
87   %Startmassenteile in den Apparaten
88   %Konzentrationen in Startdispersion überall gleich
89   % Startdispersion Massenanteile festlegen
90   w0_L1_etoh=5.3/100;
91   w0_L1_lig=0;
92   w0_L1_Z=1.3/100;
93   w0_L2=0; %kein flüssiges Lignin
94   w0_s=1.3/100;
95   w0_L1_water=1-w0_L1_etoh-w0_L1_lig-w0_L1_Z;
96   %Startmassen in einzelnen Apparaten und Starttemperatur
97   %[Ethanol G, Wasser G, Ethanol L1, Wasser L1, geloestes Lignin L1,
98   % Zucker L1, fluessiges Lignin L2, festes Lignin S, Temperatur]
99   %Mischer, Apparat 1, keine Gasphase
100  m0_A1=[500*w0_L1_etoh,500*w0_L1_water,500*w0_L1_lig,500*w0_L1_Z,500*w0_L2,500*w0_s,44];
101  %g, °C
102  %Verdampfer
103  %Schichtdicke 1mm, 7000cm^2 pro Verdampfer-->700 ml oder gramm Inhalt pro
104  %Verdampferteil
105  %Apparat 2
106  m0_A2=[1.15,2.65,700*w0_L1_etoh,700*w0_L1_water,700*w0_L1_lig,700*w0_L1_Z,700*w0_L2,700*
107  w0_s,44];
108  %Apparat 3
109  m0_A3=[2.1,3,700*w0_L1_etoh,700*w0_L1_water,700*w0_L1_lig,700*w0_L1_Z,700*w0_L2,700*w0_s
110  ,44];
111  %Apparat 4
112  m0_A4=[3,4.5,700*w0_L1_etoh,700*w0_L1_water,700*w0_L1_lig,700*w0_L1_Z,700*w0_L2,700*w0_s
113  ,44];
114  %Apparat 5
115  m0_A5=[4,5.9,700*w0_L1_etoh,700*w0_L1_water,700*w0_L1_lig,700*w0_L1_Z,700*w0_L2,700*w0_s
116  ,44];
117  %Apparat 6
118  m0_A6=[4.9,7.3,700*w0_L1_etoh,700*w0_L1_water,700*w0_L1_lig,700*w0_L1_Z,700*w0_L2,700*w0
119  _s,44];
120  %Behaelter, Apparat 7,
121  m0_A7=[p.mges_ref*w0_L1_etoh,p.mges_ref*w0_L1_water,p.mges_ref*w0_L1_lig,p.mges_ref*w0_L
122  1_Z,p.mges_ref*w0_L2,p.mges_ref*w0_s,44];
123  %zusammengefasster Vektor
124  dm0=[m0_A1,m0_A2,m0_A3,m0_A4,m0_A5,m0_A6,m0_A7];
125  %solver Aufruf
126  %optionen : 'MassSingular','MvPattern','Sparse matrix','MStateDependence'
127  tic
128  options = odeset('Mass',@massenmatrix,'MassSingular','no');
129  [t,dm] = ode15s(@rechteseite, tspan, dm0, options,p);
130  toc
131  %Dateinamen angeben!, wird sonst bei jedem run ueberschrieben
132  csvwrite('validation20170616pilotplant.csv',[t,dm]);
133  %% Ergebnisse plotten
134  %Daten einlesen
135  data=csvread('validation20170616pilotplant.csv');
136  %Spalten der csv in Variablen
137  %Zeit
138  t=data(:,1);
139  %Apparat 1, Massen-Zeit Vektoren aus csv lesen und als Variablen setzen
140  m1_A1=data(:,2);m2_A1=data(:,3);
141  m3_A1=data(:,4);m4_A1=data(:,5);m5_A1=data(:,6);m6_A1=data(:,7);
142  mges_A1=m1_A1+m2_A1+m3_A1+m4_A1+m5_A1+m6_A1;
143  mfl_A1=m1_A1+m2_A1+m3_A1+m4_A1;
```

```matlab
144   %Zusammensetzungen in Phasen
145   x1_A1=m1_A1./mges_A1;
146   x2_A1=m2_A1./mges_A1;
147   x3_A1=m3_A1./mges_A1;
148   x4_A1=m4_A1./mges_A1;
149   %Phasenanteil
150   epsL1_A1=mfl_A1./mges_A1;
151   epsL2_A1=m5_A1./mges_A1;
152   epsS_A1=m6_A1./mges_A1;
153   %%
154   %Apparat 2, Massen-Zeit Vektoren aus csv lesen und als Variablen setzen
155   mg1_A2=data(:,9);mg2_A2=data(:,10);
156   m1_A2=data(:,11);m2_A2=data(:,12);m3_A2=data(:,13);m4_A2=data(:,14);m5_A2=data(:,15);m6_
157   A2=data(:,16);
158   mges_A2=mg1_A2+mg2_A2+m1_A2+m2_A2+m3_A2+m4_A2+m5_A2+m6_A2;
159   mfl_A2=m1_A2+m2_A2+m3_A2+m4_A2;
160   mG_A2=mg1_A2+mg2_A2;
161   %Zusammensetzungen in Phasen
162   xg1_A2=mg1_A2./mges_A2;
163   xg2_A2=mg2_A2./mges_A2;
164   x1_A2=m1_A2./mges_A2;
165   x2_A2=m2_A2./mges_A2;
166   x3_A2=m3_A2./mges_A2;
167   x4_A2=m4_A2./mges_A2;
168   %Phasenanteil
169   epsG_A2=mG_A2./mges_A2;
170   epsL1_A2=mfl_A2./mges_A2;
171   epsL2_A2=m5_A2./mges_A2;
172   epsS_A2=m6_A2./mges_A2;
173   % %%
174   %Apparat 6
175   mg1_A6=data(:,45);mg2_A6=data(:,46);
176   m1_A6=data(:,47);m2_A6=data(:,48);m3_A6=data(:,49);m4_A6=data(:,50);
177   m5_A6=data(:,51);m6_A6=data(:,52);
178   %%
179   %-------------------------------------------------------------------
180   %Apparat 7. um 1 verschoben, da in der ersten Spalte die Zeit steht
181   m1_A7=data(:,54);m2_A7=data(:,55);m3_A7=data(:,56);m4_A7=data(:,57);
182   m5_A7=data(:,58);m6_A7=data(:,59);
183   mges_A7=m1_A7+m2_A7+m3_A7+m4_A7+m6_A7;
184   mfl_A7=m1_A7+m2_A7+m3_A7+m4_A7;
185   %Zusammensetzungen in Phasen
186   x1_A7=m1_A7./mfl_A7; % mges auf mfl verändert
187   x2_A7=m2_A7./mfl_A7;
188   x3_A7=m3_A7./mfl_A7;
189   x4_A7=m4_A7./mfl_A7;
190   %Phasenanteil
191   epsL1_A7=mfl_A7./mges_A7;
192   epsL2_A7=m5_A7./mges_A7;
193   epsS_A7=m6_A7./mges_A7;
194   %%
195   %Temperatur
196   TA1 = data(:,8);TA2 = data(:,17);
197   TA3 = data(:,26);TA4 = data(:,35);
198   TA5 = data(:,44);TA6 = data(:,53);
199   TA7 = data(:,60);
200   %%
201   %Destillatstrom berechnen
202    mtot_A6=p.mtot_F + p.mtot_A7;
203    xgaseth_A6=mg1_A6./(mg1_A6+mg2_A6);
204    xgaswa_A6=mg2_A6./(mg1_A6+mg2_A6);
205    eg_A6=(mg1_A6+mg2_A6)./(mg1_A6+mg2_A6+m1_A6+m2_A6+m3_A6+m4_A6+m5_A6+m6_A6);
206    mG_1_A6 = mtot_A6.*xgaseth_A6.*eg_A6;
207    mG_2_A6 = mtot_A6.*xgaswa_A6.*eg_A6;
208    MD=(mG_1_A6+mG_2_A6); % MD = V in model description
209   %Dispersionsstrom berechnen aus Gesamtmassenbilanz
210   Mdisp=p.mtot_F -MD; %Mdisp = D in model description
211   %%
212   % Mischer A1
213   figure(1);
214   subplot(1,2,1)
215   hold all
216   plot(t,m1_A1,'r','Linewidth',1.5);
217   plot(t,m2_A1,'b','Linewidth',1.5);
218   plot(t,m3_A1,'c','Linewidth',1.5);
219   plot(t,m4_A1,'m','Linewidth',1.5);
220   plot(t,m5_A1,'g','Linewidth',1.5);
221   plot(t,m6_A1,'k','Linewidth',1.5);
```

```
222    plot(t,mges_A1,'g--','Linewidth',1.5);
223    title('Massen im Mischer');
224    ylabel('Masse [g]');
225    hold off
226    grid on
227    legend('Eth','Wasser','geloestes Lignin','Zucker','fluessiges Lignin','festes
228    Lignin','Gesamtmasse');
229    axis([0 t(end) 0 mges_A1(1)]);
230    subplot(1,2,2)
231    hold all
232    %Massenanteile in Bezug auf die Gesamtmasse!
233    plot(t,x1_A1.*epsL1_A1,'r','Linewidth',1.5);
234    plot(t,x2_A1.*epsL1_A1,'b','Linewidth',1.5);
235    plot(t,x3_A1.*epsL1_A1,'c','Linewidth',1.5);
236    plot(t,x4_A1.*epsL1_A1,'m','Linewidth',1.5);
237    plot(t,epsL2_A1,'g','Linewidth',1.5);
238    plot(t,epsS_A1,'k','Linewidth',1.5);
239    title('Massenkonzentrationen im Mischer');
240    xlabel('Zeit [s]');
241    ylabel('Massenkonzentrationen [g/g]');
242    hold off
243    grid on
244    box on
245    legend('Ethanol','Wasser','geloestes Lignin','Zucker','fluessiges Lignin','festes
246    Lignin');
247    axis([0 t(end) 0 1]);
248    %%
249    %Verdampfer, Apparat 2
250    figure(2);
251    subplot(1,2,1)
252    hold all
253    plot(t,mg1_A2,'r--','Linewidth',1.5);
254    plot(t,mg2_A2,'b--','Linewidth',1.5);
255    plot(t,m1_A2,'r','Linewidth',1.5);
256    plot(t,m2_A2,'b','Linewidth',1.5);
257    plot(t,m3_A2,'c','Linewidth',1.5);
258    plot(t,m4_A2,'m','Linewidth',1.5);
259    plot(t,m5_A2,'g','Linewidth',1.5);
260    plot(t,m6_A2,'k','Linewidth',1.5);
261    plot(t,mges_A2,'g--','Linewidth',1.5);
262    hold off
263    title('Massen im Verdampfer');
264    xlabel('Zeit [s]');
265    ylabel('Masse [g]');
266    grid on
267    legend('EthDampf','Wasserdampf','Ethanol','Wasser','geloestes
268    Lignin','Zucker','fluessiges Lignin','festes Lignin','Gesamtmasse');
269    %axis([0 100 0 8]);
270    subplot(1,2,2)
271    hold all
272    %Massenanteile in Bezug auf die Gesamtmasse!
273    plot(t,xg1_A2.*epsG_A2,'r--','Linewidth',1.5);
274    plot(t,xg2_A2.*epsG_A2,'b--','Linewidth',1.5);
275    plot(t,x1_A2.*epsL1_A2,'r','Linewidth',1.5);
276    plot(t,x2_A2.*epsL1_A2,'b','Linewidth',1.5);
277    plot(t,x3_A2.*epsL1_A2,'c','Linewidth',1.5);
278    plot(t,x4_A2.*epsL1_A2,'m','Linewidth',1.5);
279    plot(t,epsL2_A2,'g','Linewidth',1.5);
280    plot(t,epsS_A2,'k','Linewidth',1.5);
281    hold off
282    xlabel('Zeit [s]');
283    ylabel('Massenkonzentrationen [w%]')
284    grid on
285    box on
286    legend('EthDampf','Wasserdampf','Ethanol','Wasser','geloestes
287    Lignin','Zucker','fluessiges Lignin','festes Lignin');
288    title('Massenkonzentrationen im Verdampfer');
289    axis([0 t(end) 0 1]);
290    %%
291    %Behaelter Apparat 7
292    figure(3);
293    subplot(1,2,1)
294    hold all
295    plot(t,m1_A7,'r','Linewidth',1.5);
296    plot(t,m2_A7,'b','Linewidth',1.5);
297    plot(t,m3_A7,'c','Linewidth',1.5);
298    plot(t,m4_A7,'m','Linewidth',1.5);
299    plot(t,m5_A7,'g','Linewidth',1.5);
```

```
300    plot(t,m6_A7,'k','Linewidth',1.5);
301    plot(t,mges_A7,'b--','Linewidth',1.5);
302    title('Massen im Behälter');
303    ylabel('Masse [g]');
304    hold off
305    grid on
306    legend('Ethanol','Wasser',' geloestes Lignin','Zucker','fluessiges Lignin','festes
307    Lignin','Gesamtmasse');
308    axis([0 t(end) 0 mges_A7(end)]);
309    subplot(1,2,2)
310    hold all
311    %Massenanteile in Bezug auf die Gesamtmasse!
312    plot(t,x1_A7.*epsL1_A7,'r','Linewidth',1.5);
313    plot(t,x2_A7.*epsL1_A7,'b','Linewidth',1.5);
314    plot(t,x3_A7.*epsL1_A7,'c','Linewidth',1.5);
315    plot(t,x4_A7.*epsL1_A7,'m','Linewidth',1.5);
316    plot(t,epsL2_A7,'g','Linewidth',1.5);
317    plot(t,epsS_A7,'k','Linewidth',1.5);
318    title('Massenkonzentration im Behälter');
319    xlabel('Zeit [s]');
320    ylabel('Massenkonzentrationen [g/g]');
321    hold off
322    grid on
323    box on
324    legend('Ethanol','Wasser','geloestes Lignin','Zucker','fluessiges Lignin','festes
325    Lignin');
326    axis([0 t(end) 0 1]);
327    %%
328    %--------------------------------------------------------------------
329    %Temperaturen
330    figure(4);
331    hold all
332    plot(t,TA1,'b');
333    plot(t,TA2,'Color',[0.5 0 1]);
334    plot(t,TA3,'r');
335    plot(t,TA4,'Color',[1 0.5 0]);
336    plot(t,TA5,'y');
337    plot(t,TA6,'g');
338    plot(t,TA7,'k')
339    legend('A1','A2','A3','A4','A5','A6','A7');
340    grid on
341    box on
342    title('Temperaturprofile');
343    xlabel('Zeit [s]');
344    ylabel('Temperatur [Â°C]');
345    %axis([0 t(end) TA1(1) max(TA6)]);
346    %%
347    %Destillat und Dispersion
348    figure(5);
349    subplot(1,2,1)
350    hold all
351    plot(t,MD,'b');
352    plot(t,Mdisp,'k');
353    grid on
354    title('Destillat und Dispersion');
355    xlabel('Zeit [s]');
356    ylabel('Masse [g/s]');
357    legend('Destillatstrom','Dispersion');
358    hold off
359    %Ethanolgehalt im Destillat
360    subplot(1,2,2)
361    hold all
362    plot(t,xgaseth_A6,'r');
363    legend('Ethanol');
364    grid on
365    box on
366    title('Ethanolmassenteil Destillat');
367    xlabel('Zeit [s]');
368    ylabel('Massenteil [g/g]');
369    hold off
370    end
371
372    Function for the construction of the time-mass-temperature matrix:
373    function M = massenmatrix(t,dy,p)
374    %Massenmatrix wegen Kopplung Massenbilanzen und Enthalpiebilanz
375    %Enthalpieterm: d(H)=d(cp*m*T)
376    %Waermekapazitaeten
377    %[Gasphase, waessrige Phase L1, fluessiges Lignin und festes Lignin cp gleich]
```

```
378    cp=[p.cp_g, p.cp_L1, p.cp_L2];
379    %Systemvariablen y in Variablen schreiben fuer Berechnung
380    %Eintraege Massen
381    mA1=[dy(1),dy(2),dy(3),dy(4),dy(5),dy(6)];
382    mA2=[dy(8),dy(9),dy(10),dy(11),dy(12),dy(13),dy(14),dy(15)];
383    mA3=[dy(17),dy(18),dy(19),dy(20),dy(21),dy(22),dy(23),dy(24)];
384    mA4=[dy(26),dy(27),dy(28),dy(29),dy(30),dy(31),dy(32),dy(33)];
385    mA5=[dy(35),dy(36),dy(37),dy(38),dy(39),dy(40),dy(41),dy(42)];
386    mA6=[dy(44),dy(45),dy(46),dy(47),dy(48),dy(49),dy(50),dy(51)];
387    mA7=[dy(53),dy(54),dy(55),dy(56),dy(57),dy(58)];
388    %Eintraege Temperatur
389    TA1=dy(7);
390    TA2=dy(16);
391    TA3=dy(25);
392    TA4=dy(34);
393    TA5=dy(43);
394    TA6=dy(52);
395    TA7=dy(59);
396    %Gesamtmatrix 59x59 definieren
397    M=speye(59);
398    %Massenmatrix besetzen
399    M(7,1:6)=cp(3:8).*TA1;
400    M(7,7)=cp(3:8)*mA1';
401    M(16,8:15)=cp.*TA2;
402    M(16,16)=cp*mA2';
403    M(25,17:24)=cp.*TA3;
404    M(25,25)=cp*mA3';
405    M(34,26:33)=cp.*TA4;
406    M(34,34)=cp*mA4';
407    M(43,35:42)=cp.*TA5;
408    M(43,43)=cp*mA5';
409    M(52,44:51)=cp.*TA6;
410    M(52,52)=cp*mA6';
411    M(59,53:58)=cp(3:8).*TA7;
412    M(59,59)=cp(3:8)*mA7';
413    End
```

Function for the calculation of mass and energy balances, streams and phase transitions of each component in each apparatus:

```
417    function BLG = rechteseite(t,dy,p)
418    %%
419    %aktuelle Massen
420    %Mischer, Apparat 1, keine Gasphase
421    mL_1_A1=dy(1);mL_2_A1=dy(2);mL_3_A1=dy(3);mL_4_A1=dy(4);
422    mL2_3_A1=dy(5);ms_A1=dy(6);T_A1=dy(7);
423    %Berechnung der Zusammensetzungen
424    x1_A1=mL_1_A1/(mL_1_A1+mL_2_A1+mL_3_A1+mL_4_A1);
425    x2_A1=mL_2_A1/(mL_1_A1+mL_2_A1+mL_3_A1+mL_4_A1);
426    x3_A1=mL_3_A1/(mL_1_A1+mL_2_A1+mL_3_A1+mL_4_A1);
427    x4_A1=mL_4_A1/(mL_1_A1+mL_2_A1+mL_3_A1+mL_4_A1);
428    %Phasenanteile
429    %epsL1_A1=(mL_1_A1+mL_2_A1+mL_3_A1+mL_4_A1)/(mL_1_A1+mL_2_A1+mL_3_A1+mL_4_A1+mL2_3_A1+ms
430    _A1);
431    epsL2_A1=mL2_3_A1/(mL_1_A1+mL_2_A1+mL_3_A1+mL_4_A1+mL2_3_A1+ms_A1);
432    epsS_A1=ms_A1/(mL_1_A1+mL_2_A1+mL_3_A1+mL_4_A1+mL_3_A1+ms_A1);
433    epsL1_A1=1-epsL2_A1-epsS_A1;
434    %%
435    %-----------------------------------------------------------------------
436    %aktuelle Massen
437    %erster Verdampfer, Apparat 2
438    mg1_A2=dy(8);
439    mg2_A2=dy(9);
440    mL_1_A2=dy(10);
441    mL_2_A2=dy(11);
442    mL_3_A2=dy(12);
443    mL_4_A2=dy(13);
444    mL2_3_A2=dy(14);
445    ms_A2=dy(15);
446    T_A2=dy(16);
447    %Berechnung der Massenzusammensetzungen
448    if mg1_A2 <= 0 || mg2_A2 <= 0
449    xg1_A2=0;
450    xg2_A2=0;
451    eg_A2=0;
452    else
453        xg1_A2=mg1_A2/(mg1_A2+mg2_A2);
454        xg2_A2=mg2_A2/(mg1_A2+mg2_A2);
455        eg_A2=(mg1_A2+mg2_A2)/(mg1_A2+mg2_A2+mL_1_A2+mL_2_A2+mL_3_A2+mL_4_A2+mL2_3_A2+ms_A2);
```

```
456   end
457   x1_A2=mL_1_A2/(mL_1_A2+mL_2_A2+mL_3_A2+mL_4_A2);
458   x2_A2=mL_2_A2/(mL_1_A2+mL_2_A2+mL_3_A2+mL_4_A2);
459   x3_A2=mL_3_A2/(mL_1_A2+mL_2_A2+mL_3_A2+mL_4_A2);
460   x4_A2=mL_4_A2/(mL_1_A2+mL_2_A2+mL_3_A2+mL_4_A2);
461   %Phasenanteile
462   epsL1_A2=(mL_1_A2+mL_2_A2+mL_3_A2+mL_4_A2)/(mg1_A2+mg2_A2+mL_1_A2+mL_2_A2+mL_3_A2+mL_4_A
463   2+mL2_3_A2+ms_A2);
464   epsL2_A2=mL2_3_A2/(mg1_A2+mg2_A2+mL_1_A2+mL_2_A2+mL_3_A2+mL_4_A2+mL2_3_A2+ms_A2);
465   epsS_A2=ms_A2/(mg1_A2+mg2_A2+mL_1_A2+mL_2_A2+mL_3_A2+mL_4_A2+mL2_3_A2+ms_A2);
466   %%
467   %-----------------------------------------------------------------------
468   %2. verdampfer, Apparat 3
469   mg1_A3=dy(17);mg2_A3=dy(18);
470   mL_1_A3=dy(19);mL_2_A3=dy(20);mL_3_A3=dy(21);mL_4_A3=dy(22);
471   mL2_3_A3=dy(23);ms_A3=dy(24);T_A3=dy(25);
472   %Berechnung der Massenzusammensetzungen
473   if mg1_A3 <= 0 || mg2_A3 <= 0
474   xg1_A3=0;
475   xg2_A3=0;
476   eg_A3=0;
477    else
478       xg1_A3=mg1_A3/(mg1_A3+mg2_A3);
479       xg2_A3=mg2_A3/(mg1_A3+mg2_A3);
480       eg_A3=(mg1_A3+mg2_A3)/(mg1_A3+mg2_A3+mL_1_A3+mL_2_A3+mL_3_A3+mL_4_A3+mL2_3_A3+ms_A3);
481   end
482   x1_A3=mL_1_A3/(mL_1_A3+mL_2_A3+mL_3_A3+mL_4_A3);
483   x2_A3=mL_2_A3/(mL_1_A3+mL_2_A3+mL_3_A3+mL_4_A3);
484   x3_A3=mL_3_A3/(mL_1_A3+mL_2_A3+mL_3_A3+mL_4_A3);
485   x4_A3=mL_4_A3/(mL_1_A3+mL_2_A3+mL_3_A3+mL_4_A3);
486   %Phasenanteile
487   epsL1_A3=(mL_1_A3+mL_2_A3+mL_3_A3+mL_4_A3)/(mg1_A3+mg2_A3+mL_1_A3+mL_2_A3+mL_3_A3+mL_4_A
488   3+mL2_3_A3+ms_A3);
489   epsL2_A3=mL2_3_A3/(mg1_A3+mg2_A3+mL_1_A3+mL_2_A3+mL_3_A3+mL_4_A3+mL2_3_A3+ms_A3);
490   epsS_A3=ms_A3/(mg1_A3+mg2_A3+mL_1_A3+mL_2_A3+mL_3_A3+mL_4_A3+mL2_3_A3+ms_A3);
491   %%
492   %-----------------------------------------------------------------------
493   %3. Verdampfer, Apparat 4
494   mg1_A4=dy(26);mg2_A4=dy(27);
495   mL_1_A4=dy(28);mL_2_A4=dy(29);mL_3_A4=dy(30);mL_4_A4=dy(31);
496   ML2_3_A4=dy(32);ms_A4=dy(33);T_A4=dy(34);
497   %Berechnung der Massenzusammensetzungen
498   if mg1_A4 <= 0 || mg2_A4 <= 0
499   xg1_A4=0;
500   xg2_A4=0;
501   eg_A4=0;
502    else
503       xg1_A4=mg1_A4/(mg1_A4+mg2_A4);
504       xg2_A4=mg2_A4/(mg1_A4+mg2_A4);
505       eg_A4=(mg1_A4+mg2_A4)/(mg1_A4+mg2_A4+mL_1_A4+mL_2_A4+mL_3_A4+mL_4_A4+ML2_3_A4+ms_A4);
506   end
507   x1_A4=mL_1_A4/(mL_1_A4+mL_2_A4+mL_3_A4+mL_4_A4);
508   x2_A4=mL_2_A4/(mL_1_A4+mL_2_A4+mL_3_A4+mL_4_A4);
509   x3_A4=mL_3_A4/(mL_1_A4+mL_2_A4+mL_3_A4+mL_4_A4);
510   x4_A4=mL_4_A4/(mL_1_A4+mL_2_A4+mL_3_A4+mL_4_A4);
511   %Phasenanteile
512   epsL1_A4=(mL_1_A4+mL_2_A4+mL_3_A4+mL_4_A4)/(mg1_A4+mg2_A4+mL_1_A4+mL_2_A4+mL_3_A4+mL_4_A
513   4+ML2_3_A4+ms_A4);
514   epsL2_A4=ML2_3_A4/(mg1_A4+mg2_A4+mL_1_A4+mL_2_A4+mL_3_A4+mL_4_A4+ML2_3_A4+ms_A4);
515   epsS_A4=ms_A4/(mg1_A4+mg2_A4+mL_1_A4+mL_2_A4+mL_3_A4+mL_4_A4+ML2_3_A4+ms_A4);
516   %%
517   %-----------------------------------------------------------------------
518   %4. Verdampfer, Apparat 5
519   mg1_A5=dy(35);mg2_A5=dy(36);
520   mL_1_A5=dy(37);mL_2_A5=dy(38);mL_3_A5=dy(39);mL_4_A5=dy(40);
521   ML2_3_A5=dy(41);ms_A5=dy(42);T_A5=dy(43);
522   %Berechnung der Massenzusammensetzungen
523   if mg1_A5 <= 0 || mg2_A5 <= 0
524   xg1_A5=0;
525   xg2_A5=0;
526   eg_A5=0;
527    else
528       xg1_A5=mg1_A5/(mg1_A5+mg2_A5);
529       xg2_A5=mg2_A5/(mg1_A5+mg2_A5);
530       eg_A5=(mg1_A5+mg2_A5)/(mg1_A5+mg2_A5+mL_1_A5+mL_2_A5+mL_3_A5+mL_4_A5+ML2_3_A5+ms_A5);
531   end
532   x1_A5=mL_1_A5/(mL_1_A5+mL_2_A5+mL_3_A5+mL_4_A5);
533   x2_A5=mL_2_A5/(mL_1_A5+mL_2_A5+mL_3_A5+mL_4_A5);
```

```
534  x3_A5=mL_3_A5/(mL_1_A5+mL_2_A5+mL_3_A5+mL_4_A5);
535  x4_A5=mL_4_A5/(mL_1_A5+mL_2_A5+mL_3_A5+mL_4_A5);
536  %Phasenanteile
537  epsL1_A5=(mL_1_A5+mL_2_A5+mL_3_A5+mL_4_A5)/(mg1_A5+mg2_A5+mL_1_A5+mL_2_A5+mL_3_A5+mL_4_A
538  5+ML2_3_A5+ms_A5);
539  epsL2_A5=ML2_3_A5/(mg1_A5+mg2_A5+mL_1_A5+mL_2_A5+mL_3_A5+mL_4_A5+ML2_3_A5+ms_A5);
540  epsS_A5=ms_A5/(mg1_A5+mg2_A5+mL_1_A5+mL_2_A5+mL_3_A5+mL_4_A5+ML2_3_A5+ms_A5);
541  %%
542  %-----------------------------------------------------------------------
543  %Apparat 6
544  mg1_A6=dy(44);mg2_A6=dy(45);
545  mL_1_A6=dy(46);mL_2_A6=dy(47);mL_3_A6=dy(48);mL_4_A6=dy(49);
546  mL2_3_A6=dy(50);ms_A6=dy(51);T_A6=dy(52);
547  %Berechnung der Massenzusammensetzungen
548  if mg1_A6 <= 0 || mg2_A6 <= 0
549  xg1_A6=0;
550  xg2_A6=0;
551  eg_A6=0;
552   else
553      xg1_A6=mg1_A6/(mg1_A6+mg2_A6);
554      xg2_A6=mg2_A6/(mg1_A6+mg2_A6);
555      eg_A6=(mg1_A6+mg2_A6)/(mg1_A6+mg2_A6+mL_1_A6+mL_2_A6+mL_3_A6+mL_4_A6+mL2_3_A6+ms_A6);
556  end
557  x1_A6=mL_1_A6/(mL_1_A6+mL_2_A6+mL_3_A6+mL_4_A6);
558  x2_A6=mL_2_A6/(mL_1_A6+mL_2_A6+mL_3_A6+mL_4_A6);
559  x3_A6=mL_3_A6/(mL_1_A6+mL_2_A6+mL_3_A6+mL_4_A6);
560  x4_A6=mL_4_A6/(mL_1_A6+mL_2_A6+mL_3_A6+mL_4_A6);
561  epsL1_A6=(mL_1_A6+mL_2_A6+mL_3_A6+mL_4_A6)/(mg1_A6+mg2_A6+mL_1_A6+mL_2_A6+mL_3_A6+mL_4_A
562  6+mL2_3_A6+ms_A6);
563  epsL2_A6=mL2_3_A6/(mg1_A6+mg2_A6+mL_1_A6+mL_2_A6+mL_3_A6+mL_4_A6+mL2_3_A6+ms_A6);
564  epsS_A6=ms_A6/(mg1_A6+mg2_A6+mL_1_A6+mL_2_A6+mL_3_A6+mL_4_A6+mL2_3_A6+ms_A6);
565  %%
566  %-----------------------------------------------------------------------
567  %Behaelter, Apparat 7
568  mL_1_A7=dy(53);mL_2_A7=dy(54);mL_3_A7=dy(55);mL_4_A7=dy(56);
569  mL2_3_A7=dy(57);ms_A7=dy(58);T_A7=dy(59);
570  %Berechnung der Massenzusammensetzungen
571  x1_A7=mL_1_A7/(mL_1_A7+mL_2_A7+mL_3_A7+mL_4_A7);
572  x2_A7=mL_2_A7/(mL_1_A7+mL_2_A7+mL_3_A7+mL_4_A7);
573  x3_A7=mL_3_A7/(mL_1_A7+mL_2_A7+mL_3_A7+mL_4_A7);
574  x4_A7=mL_4_A7/(mL_1_A7+mL_2_A7+mL_3_A7+mL_4_A7);
575  %Phasenanteile
576  epsL1_A7=(mL_1_A7+mL_2_A7+mL_3_A7+mL_4_A7)/(mL_1_A7+mL_2_A7+mL_3_A7+mL_4_A7+mL2_3_A7+ms_
577  A7);
578  epsL2_A7=mL2_3_A7/(mL_1_A7+mL_2_A7+mL_3_A7+mL_4_A7+mL2_3_A7+ms_A7);
579  epsS_A7=ms_A7/(mL_1_A7+mL_2_A7+mL_3_A7+mL_4_A7+mL2_3_A7+ms_A7);
580  %%
581  %Berechnung Stroeme und Bilanzgleichungen
582  %%
583  %Berechnung der Ausgangsstroeme aus Zustaenden im Apparat A1
584  mtot_A1 = p.mtot_F + p.mtot_A7; %Gesamtausgangsstrom F+W+C
585  mL1_1_A1 = mtot_A1*x1_A1*epsL1_A1;
586  mL1_2_A1 = mtot_A1*x2_A1*epsL1_A1;
587  mL1_3_A1 = mtot_A1*x3_A1*epsL1_A1;
588  mL1_4_A1 = mtot_A1*x4_A1*epsL1_A1;
589  mL2_3_A1 = mtot_A1*epsL2_A1;
590  mS_3_A1 = mtot_A1*epsS_A1;
591  %Loeslichkeit A1
592  xLoes_A1 = p.pl(1)+ p.pl(2)*x1_A1 + p.pl(3)*T_A1 + p.pl(4)*x1_A1^2 + p.pl(5)*x1_A1*T_A1
593  + p.pl(6)*T_A1^2 + ...
594             p.pl(7)*x1_A1^3 + p.pl(8)*x1_A1^2*T_A1 + p.pl(9)*x1_A1*T_A1^2;
595  %Uebersaettigung
596  S_A1=(x3_A1*epsL1_A1-xLoes_A1);
597  %Berechnung Strom gefaelltes Lignin
598  if S_A1>0
599     mL1S_A1=(p.mtot_F + p.mtot_A7)*S_A1;
600  else
601      mL1S_A1=0;
602  end
603
604  %Glasgrenztemperatur A1 (Gl. 82)
605  Tglas1 = p.Tg(1)*x1_A1 + p.Tg(2);
606  if T_A1>=Tglas1 && ms_A1>=0
607      ML2_3_A1=ms_A1*p.k1+mL1S_A1*p.k2;
608  else
609      ML2_3_A1=0;
610  end
611  %Bilanzen A1
```

```matlab
Mout=p.mtot_A7; %Gesamtstrom aus Behaelter

ML1_1_A1 = Mout*x1_A7*epsL1_A7 + p.mtot_F*p.x_F(1) - mL1_1_A1 ;
ML1_2_A1 = Mout*x2_A7*epsL1_A7 + p.mtot_F*p.x_F(2) - mL1_2_A1 ;
ML1_3_A1 = Mout*x3_A7*epsL1_A7 + p.mtot_F*p.x_F(3) - mL1_3_A1  - mL1S_A1;
ML1_4_A1 = Mout*x4_A7*epsL1_A7 + p.mtot_F*p.x_F(4) - mL1_4_A1 ;
%ML2_3_A1 = Mout*epsL2_A7 + p.mtot_F*p.x_F(5) - mL2_3_A1 + m_SL2_3_A1;
MS_3_A1 =  Mout*epsS_A7 + p.mtot_F*p.x_F(6) - mS_3_A1 + mL1S_A1;
TA1 = -(mL1_1_A1*p.cp_L1(1) + mL1_2_A1*p.cp_L1(2) + mL1_3_A1*p.cp_L1(3) +
mL1_4_A1*p.cp_L1(4) + mL2_3_A1*p.cp_L2(1) + mS_3_A1*p.cp_L2(2))*T_A1 ...
      + (p.mtot_F*p.x_F(1:4)*p.cp_L1(1:4)')*p.T_F ...
      + (Mout*x1_A7*epsL1_A7*p.cp_L1(1) + Mout*x2_A7*epsL1_A7*p.cp_L1(2) +
Mout*x3_A7*epsL1_A7*p.cp_L1(3) + Mout*x4_A7*epsL1_A7*p.cp_L1(4)...
      + Mout*epsL2_A7*p.cp_L2(1) + Mout*epsS_A7*p.cp_L2(2))*T_A7 ;
%%
%-------------------------------------------------------------------------
%1. Verdampfer, Apparat A2
%Umrechnung Massenbruch in Molenbruch
if x1_A2 <= 0
    xmol1_A2=0;
else
    xmol1_A2 = 1/(1+p.M_1/p.M_2*(1-x1_A2)/x1_A2);
end
%Aktivitaetskoeffizienten
gamma1_A2=exp(p.C(1)./(1+p.C(1)/p.C(2).*xmol1_A2./(1-xmol1_A2)).^2); %(Gl. 75)
gamma2_A2=exp(p.C(2)./(1+p.C(2)/p.C(1).*(1-xmol1_A2)./xmol1_A2).^2); %(Gl. 76)
%Siedetemperatur berechnen
if xmol1_A2 <=0
    Ts_A2=p.Tsv1;
else
    Ts_A2=fzero(@boil,p.Tsv1,[],xmol1_A2,p.p0,gamma1_A2,gamma2_A2,p.Acoeff);
end
%Dampfdruck Ethanol
psat1_A2=10.^(p.Acoeff(1,1)-p.Acoeff(1,2)./(p.Acoeff(1,3)+Ts_A2));
%Verteilungskoeffizient
K1_A2 = (gamma1_A2*psat1_A2)/p.p0;
%Bedingung an der Phasengrenze
ymol1_A2=K1_A2*xmol1_A2;
%Loeslichkeitsfunktion
xLoes_A2 = p.pl(1) + p.pl(2)*x1_A2 + p.pl(3)*T_A2 + p.pl(4)*x1_A2^2 + p.pl(5)*x1_A2*T_A2
+ p.pl(6)*T_A2^2 + ...
          p.pl(7)*x1_A2^3 + p.pl(8)*x1_A2^2*T_A2 + p.pl(9)*x1_A2*T_A2^2;
%Uebersaettigung
S_A2=x3_A2*epsL1_A2-xLoes_A2;
if S_A2>0
   m_L1S_3_A2=(mtot_A1)*S_A2;
 else
     m_L1S_3_A2=0;
end
%Glasuebergangstemperatur
 Tglas2 = p.Tg(1)*x1_A2 + p.Tg(2);
if T_A2>=Tglas2 && ms_A2>=0
    ML2_3_A2=ms_A2*p.k1+m_L1S_3_A2*p.k2;
 else
    ML2_3_A2=0;
end
%Berechnung der Ausgangsstroeme aus Zustaenden
mtot_A2=mtot_A1;
mG_1_A2 = mtot_A2*xg1_A2*eg_A2;
mG_2_A2 = mtot_A2*xg2_A2*eg_A2;
mL1_1_A2 = mtot_A2*x1_A2*epsL1_A2;
mL1_2_A2 = mtot_A2*x2_A2*epsL1_A2;
mL1_3_A2 = mtot_A2*x3_A2*epsL1_A2;
mL1_4_A2 = mtot_A2*x4_A2*epsL1_A2;
mL2_3_A2 = mtot_A2*epsL2_A2;
mS_3_A2 = mtot_A2*epsS_A2;
%Waerme eintretende Stroeme
Ql_A2=(mL1_1_A1*p.cp_L1(1) + mL1_2_A1*p.cp_L1(2) + mL1_3_A1*p.cp_L1(3) +
mL1_4_A1*p.cp_L1(4))*(Ts_A2-T_A1);
Qs_A2=(mL2_3_A1*p.cp_L2(1) + mS_3_A1*p.cp_L2(2))*(Ts_A2-T_A1);
%gegebener Waermestrom
Qin = p.A*p.q;
%Enthalpie des Dampfstromes
hgas_A2=p.hv1/(1+p.M_2/p.M_1*(1-ymol1_A2)/ymol1_A2) + p.hv2*(1 - 1/(1+ p.M_2/p.M_1*(1-
ymol1_A2)/ymol1_A2));
if T_A2<=Ts_A2
   mgas_A2=0;
   mL1G_1_A2=0;
```

```
690        mL1G_2_A2=0;
691        Qv_A2=0;
692    else
693        Qv_A2=Qin-Ql_A2-Qs_A2; %restlicher Waermestrom bei Erreichen der Siedetemperatur
694        mgas_A2=Qv_A2/hgas_A2; %Gesamtgasstrom
695        mL1G_1_A2=mgas_A2/(1+p.M_2/p.M_1*(1-ymol1_A2)/ymol1_A2); %Dampfstrom Ethanol
696        mL1G_2_A2=mgas_A2-mL1G_1_A2;
697    end
698    %Bilanzen A2
699    Mg1_A2 =                - mG_1_A2  + mL1G_1_A2;
700    Mg2_A2 =                - mG_2_A2  + mL1G_2_A2;
701    ML1_1_A2 = mL1_1_A1 - mL1_1_A2 - mL1G_1_A2;
702    ML1_2_A2 = mL1_2_A1 - mL1_2_A2 - mL1G_2_A2;
703    ML1_3_A2 = mL1_3_A1 - mL1_3_A2            - m_L1S_3_A2;
704    ML1_4_A2 = mL1_4_A1 - mL1_4_A2 ;
705    %ML2_3_A2 = mL2_3_A1 - mL2_3_A2           + m_SL2_3_A2;
706    Ms_3_A2 =  mS_3_A1 - mS_3_A2           + m_L1S_3_A2;
707    TA2 = -(mG_1_A2*p.cp_g(1) + mG_2_A2*p.cp_g(2) ...
708        + mL1_1_A2*p.cp_L1(1)+ mL1_2_A2*p.cp_L1(2) + mL1_3_A2*p.cp_L1(3) +
709    mL1_4_A2*p.cp_L1(4)...
710        + mL2_3_A2*p.cp_L2(1) + mS_3_A2*p.cp_L2(2))*T_A2...
711        + (mL1_1_A1*p.cp_L1(1) + mL1_2_A1*p.cp_L1(2) + mL1_3_A1*p.cp_L1(3) +
712    mL1_4_A1*p.cp_L1(4))*T_A1...
713        + (mL2_3_A1*p.cp_L2(1) + mS_3_A1*p.cp_L2(2))*T_A1...
714        + Qin -mL1G_1_A2*p.hv1 - mL1G_2_A2*p.hv2;
715    %%
716    %2. Verdampfer, Apparat A3
717    %Berechnung der Stroeme aus Zustaenden
718    mtot_A3=mtot_A1;
719    mG_1_A3 = mtot_A3*xg1_A3*eg_A3;
720    mG_2_A3 = mtot_A3*xg2_A3*eg_A3;
721    mL1_1_A3 = mtot_A3*x1_A3*epsL1_A3;
722    mL1_2_A3 = mtot_A3*x2_A3*epsL1_A3;
723    mL1_3_A3 = mtot_A3*x3_A3*epsL1_A3;
724    mL1_4_A3 = mtot_A3*x4_A3*epsL1_A3;
725    mL2_3_A3 = mtot_A3*epsL2_A3;
726    mS_3_A3 = mtot_A3*epsS_A3;
727    %Loeslichkeit A3
728    xLoes_A3 = p.pl(1) + p.pl(2)*x1_A3 + p.pl(3)*T_A3 + p.pl(4)*x1_A3^2 + p.pl(5)*x1_A3*T_A3
729    + p.pl(6)*T_A3^2 + ...
730            p.pl(7)*x1_A3^3 + p.pl(8)*x1_A3^2*T_A3 + p.pl(9)*x1_A3*T_A3^2;
731    %Uebersaettigung
732    S_A3=x3_A3*epsL1_A3-xLoes_A3;
733    if S_A3>0
734        m_L1S_3_A3=(mtot_A2)*S_A3;
735    else
736        m_L1S_3_A3=0;
737    end
738    %Glasuebergangstemperatur
739    Tglas3 = p.Tg(1)*x1_A3 + p.Tg(2);
740    if T_A3<Tglas3 || ms_A3<=0
741    ML2_3_A3=0;
742    else
743        ML2_3_A3=ms_A3*p.k1+m_L1S_3_A3*p.k2;
744    end
745    %Umrechnung Massenbruch in Molenbruch
746    if x1_A3 <= 0
747        xmol1_A3=0;
748    else
749        xmol1_A3 = 1/(1+p.M_1/p.M_2*(1-x1_A3)/x1_A3);
750    end
751    %Aktivitaetskoeffizienten
752    gamma1_A3=exp(p.C(1)./(1+p.C(1)/p.C(2).*xmol1_A3./(1-xmol1_A3)).^2);
753    gamma2_A3=exp(p.C(2)./(1+p.C(2)/p.C(1).*(1-xmol1_A3)./xmol1_A3).^2);
754    %Siedetemperatur
755    if xmol1_A3 <=0
756        Ts_A3=p.Tsv1;
757    else
758        Ts_A3=fzero(@boil,p.Tsv1,[],xmol1_A3,p.p0,gamma1_A3,gamma2_A3,p.Acoeff) ;
759    end
760    %Dampfdruck Ethanol
761    psat1_A3=10.^(p.Acoeff(1,1)-p.Acoeff(1,2)./(p.Acoeff(1,3)+Ts_A3));
762    %Verteilungskoeffizient
763    K1_A3 = (gamma1_A3*psat1_A3)/p.p0;
764    %Bedingung an der Phasengrenze
765    ymol1_A3=K1_A3*xmol1_A3;
766    %Waerme eintretende Stroeme
```

```
767  Ql_A3=(mL1_1_A2*p.cp_L1(1)+mL1_2_A2*p.cp_L1(2)+mL1_3_A2*p.cp_L1(3)+mL1_4_A2*p.cp_L1(4))*
768  (Ts_A3-T_A2);
769  Qs_A3=(mL2_3_A2*p.cp_L2(1)+mS_3_A2*p.cp_L2(2))*(Ts_A3-T_A2);
770  %Enthalpie des Dampfstromes
771  hgas_A3=p.hv1/(1+p.M_2/p.M_1*(1-ymol1_A3)/ymol1_A3) + p.hv2*(1 - 1/(1+ p.M_2/p.M_1*(1-
772  ymol1_A3)/ymol1_A3));
773  if T_A3<=Ts_A3
774      mgas_A3=0;
775      mL1G_1_A3=0;
776      mL1G_2_A3=0;
777      Qv_A3=0;
778  else
779      Qv_A3=Qin-Ql_A3-Qs_A3;
780      mgas_A3=Qv_A3/hgas_A3;
781      mL1G_1_A3=mgas_A3/(1+p.M_2/p.M_1*(1-ymol1_A3)/ymol1_A3);
782      mL1G_2_A3=mgas_A3-mL1G_1_A3;
783  end
784  %Bilanzen Apparat A3
785  Mg1_A3 = mG_1_A2 - mG_1_A3       + mL1G_1_A3;
786  Mg2_A3 = mG_2_A2 - mG_2_A3       + mL1G_2_A3;
787  ML1_1_A3 = mL1_1_A2 - mL1_1_A3 - mL1G_1_A3;
788  ML1_2_A3 = mL1_2_A2 - mL1_2_A3 - mL1G_2_A3;
789  ML1_3_A3 = mL1_3_A2 - mL1_3_A3       - m_L1S_3_A3;
790  ML1_4_A3 = mL1_4_A2 - mL1_4_A3;
791  %ML2_3_A3 = mL2_3_A2 - mL2_3_A3      + m_SL2_3_A3;
792  Ms_3_A3 = mS_3_A2 - mS_3_A3        + m_L1S_3_A3;
793  TA3 = -(mG_1_A3 *p.cp_g(1) + mG_2_A3*p.cp_g(2) + mL1_1_A3*p.cp_L1(1)...
794          + mL1_2_A3*p.cp_L1(2) + mL1_3_A3*p.cp_L1(3) + mL1_4_A3*p.cp_L1(4)...
795          + mL2_3_A3*p.cp_L2(1) + mS_3_A3*p.cp_L2(2))*T_A3 ...
796          + (mG_1_A2*p.cp_g(1) + mG_2_A2*p.cp_g(2))*T_A2...
797          + (mL1_1_A2*p.cp_L1(1) + mL1_2_A2*p.cp_L1(2)...
798          + mL1_3_A2*p.cp_L1(3)  + mL1_4_A2*p.cp_L1(4))*T_A2...
799          + (mL2_3_A2*p.cp_L2(1)  +  mS_3_A2*p.cp_L2(2))*T_A2 ...
800          + Qin -mL1G_1_A3*p.hv1 - mL1G_2_A3*p.hv2;
801  %%
802  %3. Verdampfer, Apparat A4
803  %Berechnung der Stroeme aus Zustaenden
804  mtot_A4=mtot_A1;
805  mG_1_A4 = mtot_A4*xg1_A4*eg_A4;
806  mG_2_A4 = mtot_A4*xg2_A4*eg_A4;
807  mL1_1_A4 = mtot_A4*x1_A4*epsL1_A4;
808  mL1_2_A4 = mtot_A4*x2_A4*epsL1_A4;
809  mL1_3_A4 = mtot_A4*x3_A4*epsL1_A4;
810  mL1_4_A4 = mtot_A4*x4_A4*epsL1_A4;
811  mL2_3_A4 = mtot_A4*epsL2_A4;
812  mS_3_A4 = mtot_A4*epsS_A4;
813  %Loeslichkeitsfunktion
814  xLoes_A4 = p.pl(1) + p.pl(2)*x1_A4 + p.pl(3)*T_A4 + p.pl(4)*x1_A4^2 + p.pl(5)*x1_A4*T_A4
815  + p.pl(6)*T_A4^2 + ...
816              p.pl(7)*x1_A4^3 + p.pl(8)*x1_A4^2*T_A4 + p.pl(9)*x1_A4*T_A4^2;
817  %Uebersaettigung
818  S_A4=x3_A4*epsL1_A4-xLoes_A4;
819  if S_A4>0
820      m_L1S_3_A4=(mtot_A3)*S_A4;
821   else
822          m_L1S_3_A4=0;
823  end
824  %Glasuebergangstemperatur
825  Tglas4 = p.Tg(1)*x1_A4 + p.Tg(2);
826  if T_A4>=Tglas4 && ms_A4>=0
827      ML2_3_A4=ms_A4*p.k1+m_L1S_3_A4*p.k2;
828  else
829      ML2_3_A4=0;
830  end
831  %Umrechnung Massenbruch in Molenbruch
832  if x1_A4 <= 0
833      xmol1_A4=0;
834  else
835      xmol1_A4 = 1/(1+p.M_1/p.M_2*(1-x1_A4)/x1_A4);
836  end
837  %Aktivitaetskoeffizienten
838  gamma1_A4=exp(p.C(1)./(1+p.C(1)/p.C(2).*xmol1_A4./(1-xmol1_A4)).^2);
839  gamma2_A4=exp(p.C(2)./(1+p.C(2)/p.C(1).*(1-xmol1_A4)./xmol1_A4).^2);
840  %Berechnung Siedetemperatur
841  if xmol1_A4 <=0
842      Ts_A4=p.Tsv1;
843  else
844      Ts_A4=fzero(@boil,p.Tsv1,[],xmol1_A4,p.p0,gamma1_A4,gamma2_A4,p.Acoeff) ;
```

```
845   end
846   %Dampfdruck Ethanol
847   psat1_A4=10.^(p.Acoeff(1,1)-p.Acoeff(1,2)./(p.Acoeff(1,3)+Ts_A4));
848   %Verteilungskoeffizient
849   K1_A4 = (gamma1_A4*psat1_A4)/p.p0;
850   %Bedingung an der Phasengrenze
851   ymol1_A4=K1_A4*xmol1_A4;
852   %Waerme eintretende Stroeme
853   Ql_A4=(mL1_1_A3*p.cp_L1(1)+mL1_2_A3*p.cp_L1(2)+mL1_3_A3*p.cp_L1(3)+mL1_4_A3*p.cp_L1(4))*
854   (Ts_A4-T_A3);
855   Qs_A4=(mL2_3_A3*p.cp_L2(1)+mS_3_A3*p.cp_L2(2))*(Ts_A4-T_A3);
856   %Enthalpie des Dampfstromes
857   hgas_A4=p.hv1/(1+p.M_2/p.M_1*(1-ymol1_A4)/ymol1_A4) + p.hv2*(1 - 1/(1+ p.M_2/p.M_1*(1-
858   ymol1_A4)/ymol1_A4));
859   if T_A4<=Ts_A4
860      mgas_A4=0;
861      mL1G_1_A4=0;
862      mL1G_2_A4=0;
863      Qv_A4=0;
864   else
865       Qv_A4=Qin-Ql_A4-Qs_A4;
866       mgas_A4=Qv_A4/hgas_A4;
867       mL1G_1_A4=mgas_A4/(1+p.M_2/p.M_1*(1-ymol1_A4)/ymol1_A4);
868       mL1G_2_A4=mgas_A4-mL1G_1_A4;
869   end
870   %Bilanzen
871   Mg1_A4 = mG_1_A3 - mG_1_A4      + mL1G_1_A4;
872   Mg2_A4 = mG_2_A3 - mG_2_A4      + mL1G_2_A4;
873   ML1_1_A4 = mL1_1_A3 - mL1_1_A4 - mL1G_1_A4;
874   ML1_2_A4 = mL1_2_A3 - mL1_2_A4 - mL1G_2_A4;
875   ML1_3_A4 = mL1_3_A3 - mL1_3_A4     - m_L1S_3_A4;
876   ML1_4_A4 = mL1_4_A3 - mL1_4_A4;
877   %ML2_3_A4 = mL2_3_A3 - mL2_3_A4     + m_SL2_3_A4;
878   Ms_3_A4 = mS_3_A3 - mS_3_A4      + m_L1S_3_A4;
879   TA4 = -(mG_1_A4*p.cp_g(1) + mG_2_A4*p.cp_g(2) + mL1_1_A4*p.cp_L1(1)...
880        + mL1_2_A4*p.cp_L1(2) + mL1_3_A4*p.cp_L1(3) + mL1_4_A4*p.cp_L1(4)...
881        + mL2_3_A4*p.cp_L2(1) + mS_3_A4*p.cp_L2(2))*T_A4 ...
882        + (mG_1_A3*p.cp_g(1) + mG_2_A3*p.cp_g(2))*T_A3...
883        + (mL1_1_A3*p.cp_L1(1) + mL1_2_A3*p.cp_L1(2)...
884        +  mL1_3_A3*p.cp_L1(3)  + mL1_4_A3*p.cp_L1(4))*T_A3...
885        + (mL2_3_A3*p.cp_L2(1)  +  mS_3_A3*p.cp_L2(2))*T_A3 ...
886        + Qin -mL1G_1_A4*p.hv1 - mL1G_2_A4*p.hv2;
887   %%
888   %4.verdampfer, Apparat 5
889   %Berechnung der Ausgangsstroeme aus Zustaenden
890   mtot_A5=mtot_A1;
891   mG_1_A5 = mtot_A5*xg1_A5*eg_A5;
892   mG_2_A5 = mtot_A5*xg2_A5*eg_A5;
893   mL1_1_A5 = mtot_A5*x1_A5*epsL1_A5;
894   mL1_2_A5 = mtot_A5*x2_A5*epsL1_A5;
895   mL1_3_A5 = mtot_A5*x3_A5*epsL1_A5;
896   mL1_4_A5 = mtot_A5*x4_A5*epsL1_A5;
897   mL2_3_A5 = mtot_A5*epsL2_A5;
898   mS_3_A5 = mtot_A5*epsS_A5;
899   %Loeslichkeit
900   xLoes_A5 = p.pl(1) + p.pl(2)*x1_A5 + p.pl(3)*T_A5 + p.pl(4)*x1_A5^2 + p.pl(5)*x1_A5*T_A5
901   + p.pl(6)*T_A5^2 + ...
902            p.pl(7)*x1_A5^3 + p.pl(8)*x1_A5^2*T_A5 + p.pl(9)*x1_A5*T_A5^2;
903   %Uebersaettigung
904   S_A5=x3_A5*epsL1_A5-xLoes_A5;
905   if S_A5>0
906      m_L1S_3_A5=(mtot_A4)*S_A5;
907    else
908        m_L1S_3_A5=0;
909   end
910   %Glasuebergangstemperatur
911   Tglas5 = p.Tg(1)*x1_A5 + p.Tg(2);
912   if T_A5>=Tglas5 && ms_A5>=0
913      ML2_3_A5=ms_A5*p.k1+m_L1S_3_A5*p.k2;
914   else
915      ML2_3_A5=0;
916   end
917   %Siedetemperatur
918   if x1_A5 <= 0
919      xmol1_A5=0;
920   else
921      xmol1_A5 = 1/(1+p.M_1/p.M_2*(1-x1_A5)/x1_A5);
922   end
```

```
923    %Aktivitaetskoeffizienten
924    gamma1_A5=exp(p.C(1)./(1+p.C(1)/p.C(2).*xmol1_A5./(1-xmol1_A5)).^2);
925    gamma2_A5=exp(p.C(2)./(1+p.C(2)/p.C(1).*(1-xmol1_A5)./xmol1_A5).^2);
926    if xmol1_A5 <=0
927        Ts_A5=p.Tsv1;
928    else
929        Ts_A5=fzero(@boil,p.Tsv1,[],xmol1_A5,p.p0,gamma1_A5,gamma2_A5,p.Acoeff) ;
930    end
931    %Dampfdruck Ethanol
932    psat1_A5=10.^(p.Acoeff(1,1)-p.Acoeff(1,2)./(p.Acoeff(1,3)+Ts_A5));
933    %Verteilungskoeffizient
934    K1_A5 = (gamma1_A5*psat1_A5)/p.p0;
935    %Bedingung an der Phasengrenze
936    ymol1_A5=K1_A5*xmol1_A5;
937    %Waerme eintretende Stroeme
938    Ql_A5=(mL1_1_A4*p.cp_L1(1)+mL1_2_A4*p.cp_L1(2)+mL1_3_A4*p.cp_L1(3)+mL1_4_A4*p.cp_L1(4))*
939    (Ts_A5-T_A4);
940    Qs_A5=(mL2_3_A4*p.cp_L2(1)+mS_3_A4*p.cp_L2(2))*(Ts_A5-T_A4);
941    %Enthalpie des Dampfstromes
942    hgas_A5=p.hv1/(1+p.M_2/p.M_1*(1-ymol1_A5)/ymol1_A5) + p.hv2*(1 - 1/(1+ p.M_2/p.M_1*(1-
943    ymol1_A5)/ymol1_A5));
944    if T_A5<=Ts_A5
945        mgas_A5=0;
946        mL1G_1_A5=0;
947        mL1G_2_A5=0;
948        Qv_A5=0;
949    else
950        Qv_A5=Qin-Ql_A5-Qs_A5;
951        mgas_A5=Qv_A5/hgas_A5;
952        mL1G_1_A5=mgas_A5/(1+p.M_2/p.M_1*(1-ymol1_A5)/ymol1_A5);
953        mL1G_2_A5=mgas_A5-mL1G_1_A5;
954    end
955    Mg1_A5 = mG_1_A4 - mG_1_A5      + mL1G_1_A5;
956    Mg2_A5 = mG_2_A4 - mG_2_A5      + mL1G_2_A5;
957    ML1_1_A5 = mL1_1_A4 - mL1_1_A5 - mL1G_1_A5;
958    ML1_2_A5 = mL1_2_A4 - mL1_2_A5 - mL1G_2_A5;
959    ML1_3_A5 = mL1_3_A4 - mL1_3_A5     - m_L1S_3_A5;
960    ML1_4_A5 = mL1_4_A4 - mL1_4_A5;
961    %ML2_3_A5 = mL2_3_A4 - mL2_3_A5      + m_SL2_3_A5;
962    Ms_3_A5 = mS_3_A4 - mS_3_A5         + m_L1S_3_A5;
963    TA5 = -(mG_1_A5*p.cp_g(1) + mG_2_A5*p.cp_g(2) + mL1_1_A5*p.cp_L1(1)...
964         + mL1_2_A5*p.cp_L1(2) + mL1_3_A5*p.cp_L1(3) + mL1_4_A5*p.cp_L1(4)...
965         + mL2_3_A5*p.cp_L2(1) + mS_3_A5*p.cp_L2(2))*T_A5 ...
966         + (mG_1_A4*p.cp_g(1) + mG_2_A4*p.cp_g(2))*T_A4...
967         + (mL1_1_A4*p.cp_L1(1) + mL1_2_A4*p.cp_L1(2)...
968         +  mL1_3_A4*p.cp_L1(3)  + mL1_4_A4*p.cp_L1(4))*T_A4...
969         + (mL2_3_A4*p.cp_L2(1)  +  mS_3_A4*p.cp_L2(2))*T_A4 ...
970         + Qin -mL1G_1_A5*p.hv1 - mL1G_2_A5*p.hv2;
971    %%
972    %5. Verdampfer, Apparat 6
973    %Berechnung der Stroeme aus Zustaenden
974    mtot_A6=(mtot_A1);
975    mG_1_A6 = mtot_A6*xg1_A6*eg_A6;
976    mG_2_A6 = mtot_A6*xg2_A6*eg_A6;
977    mL1_1_A6 = mtot_A6*x1_A6*epsL1_A6;
978    mL1_2_A6 = mtot_A6*x2_A6*epsL1_A6;
979    mL1_3_A6 = mtot_A6*x3_A6*epsL1_A6;
980    mL1_4_A6 = mtot_A6*x4_A6*epsL1_A6;
981    mL2_3_A6 = mtot_A6*epsL2_A6;
982    mS_3_A6 = mtot_A6*epsS_A6;
983    %Loeslichkeitsfunktion A6
984    xLoes_A6 = p.pl(1) + p.pl(2)*x1_A6 + p.pl(3)*T_A6 + p.pl(4)*x1_A6^2 + p.pl(5)*x1_A6*T_A6
985    + p.pl(6)*T_A6^2 + ...
986                p.pl(7)*x1_A6^3 + p.pl(8)*x1_A6^2*T_A6 + p.pl(9)*x1_A6*T_A6^2;
987    %Uebersaettigung
988    S_A6=x3_A6*epsL1_A6-xLoes_A6;
989    if S_A6>0
990        m_L1S_3_A6=(mtot_A5)*S_A6;
991     else
992        m_L1S_3_A6=0;
993    end
994    %Glasuebergangstemperatur
995    Tglas6 = p.Tg(1)*x1_A6 + p.Tg(2);
996    if T_A6>=Tglas6 && ms_A6>=0
997        ML2_3_A6=ms_A6*p.k1+m_L1S_3_A6*p.k2;
998    else
999        ML2_3_A6=0;
1000   end
```

```
1001    %Siedetemperatur
1002    if x1_A6 <= 0
1003        xmol1_A6=0;
1004    else
1005        xmol1_A6 = 1/(1+p.M_1/p.M_2*(1-x1_A6)/x1_A6);
1006    end
1007    %Aktivitaetskoeffizienten
1008    gamma1_A6=exp(p.C(1)./(1+p.C(1)/p.C(2).*xmol1_A6./(1-xmol1_A6)).^2);
1009    gamma2_A6=exp(p.C(2)./(1+p.C(2)/p.C(1).*(1-xmol1_A6)./xmol1_A6).^2);
1010    if xmol1_A6 <=0
1011        Ts_A6=p.Tsv1;
1012    else
1013        Ts_A6=fzero(@boil,p.Tsv1,[],xmol1_A6,p.p0,gamma1_A6,gamma2_A6,p.Acoeff) ;
1014    end
1015    %Dampfdruck Ethanol
1016    psat1_A6=10.^(p.Acoeff(1,1)-p.Acoeff(1,2)./(p.Acoeff(1,3)+Ts_A6));
1017    %Verteilungskoeffizient
1018    K1_A6 = (gamma1_A6*psat1_A6)/p.p0;
1019    %Bedingung an der Phasengrenze)
1020    ymol1_A6=K1_A6*xmol1_A6;
1021    %Waerme eintretende Stroeme
1022    Ql_A6=(mL1_1_A5*p.cp_L1(1)+mL1_2_A5*p.cp_L1(2)+mL1_3_A5*p.cp_L1(3)+mL1_4_A5*p.cp_L1(4))*
1023    (Ts_A6-T_A5);
1024    Qs_A6=(mL2_3_A5*p.cp_L2(1)+mS_3_A5*p.cp_L2(2))*(Ts_A6-T_A5);
1025    %Enthalpie des Dampfstromes
1026    hgas_A6=p.hv1/(1+p.M_2/p.M_1*(1-ymol1_A6)/ymol1_A6) + p.hv2*(1 - 1/(1+ p.M_2/p.M_1*(1-
1027    ymol1_A6)/ymol1_A6));
1028    if T_A6<=Ts_A6
1029        mgas_A6=0;
1030        mL1G_1_A6=0;
1031        mL1G_2_A6=0;
1032        Qv_A6=0;
1033    else
1034        Qv_A6=Qin-Ql_A6-Qs_A6;
1035        mgas_A6=Qv_A6/hgas_A6;
1036        mL1G_1_A6=mgas_A6/(1+p.M_2/p.M_1*(1-ymol1_A6)/ymol1_A6);
1037        mL1G_2_A6=mgas_A6-mL1G_1_A6;
1038    end
1039
1040    %Bilanzen Apparat A6
1041    Mg1_A6 = mG_1_A5 - mG_1_A6     + mL1G_1_A6;
1042    Mg2_A6 = mG_2_A5 - mG_2_A6     + mL1G_2_A6;
1043    ML1_1_A6 = mL1_1_A5 - mL1_1_A6 - mL1G_1_A6;
1044    ML1_2_A6 = mL1_2_A5 - mL1_2_A6 - mL1G_2_A6;
1045    ML1_3_A6 = mL1_3_A5 - mL1_3_A6     - m_L1S_3_A6;
1046    ML1_4_A6 = mL1_4_A5 - mL1_4_A6;
1047    %mL2_3_A6 = mL2_3_A5 - mL2_3_A6     + m_SL2_3_A6;
1048    Ms_3_A6 = mS_3_A5 - mS_3_A6       + m_L1S_3_A6;
1049    TA6 = -(mG_1_A6*p.cp_g(1) + mG_2_A6*p.cp_g(2) + mL1_1_A6*p.cp_L1(1)...
1050        + mL1_2_A6*p.cp_L1(2) + mL1_3_A6*p.cp_L1(3) + mL1_4_A6*p.cp_L1(4)...
1051        + mL2_3_A6*p.cp_L2(1) + mS_3_A6*p.cp_L2(2))*T_A6 ...
1052        + (mG_1_A5*p.cp_g(1) + mG_2_A5*p.cp_g(2))*T_A5...
1053        + (mL1_1_A5*p.cp_L1(1) + mL1_2_A5*p.cp_L1(2)...
1054        +  mL1_3_A5*p.cp_L1(3)  + mL1_4_A5*p.cp_L1(4))*T_A5...
1055        + (mL2_3_A5*p.cp_L2(1)  +  mS_3_A5*p.cp_L2(2))*T_A5 ...
1056        + Qin -mL1G_1_A6*p.hv1 - mL1G_2_A6*p.hv2;
1057    %%
1058    %Behaelter Apparat 7
1059    %konstanter Massenstrom Mout entspricht C in Beschreibung
1060    %Gasstrom direkt in die Kolonne
1061    %keine Gleichung fuer die Gasphase
1062    %Bilanz fuer Destillatstrom
1063    mL1_2_A8=0;%keine Kolonne, Dampf wird komplett entzogen,
1064    % kein Destillatstrom aus Kolonne A8 in Behälter A7
1065    %berechnung der Ausgangsstroeme aus Behaelter A7
1066    mL1_1_A7 = Mout*x1_A7*epsL1_A7;
1067    mL1_2_A7 = Mout*x2_A7*epsL1_A7;
1068    mL1_3_A7 = Mout*x3_A7*epsL1_A7;
1069    mL1_4_A7 = Mout*x4_A7*epsL1_A7;
1070    mL2_3_A7 = Mout*epsL2_A7;
1071    mS_3_A7  = Mout*epsS_A7;
1072
1073    % % Dispersionsablauf
1074    % Bilanz über alles :Feed=Destillat+Dispersion
1075    mtot_F=p.mtot_F;
1076    if mtot_F-Mg1_A6-Mg2_A6>0;
1077        Mout_2=mtot_F-Mg1_A6-Mg2_A6;
1078    else
```

```
1079         Mout_2=0;
1080     end
1081     % Berechnung der Ausgangsstroeme aus Behaelter A7: KONTI JK
1082     mL1_1_A7_2 = Mout_2*x1_A7*epsL1_A7;
1083     mL1_2_A7_2 = Mout_2*x2_A7*epsL1_A7;
1084     mL1_3_A7_2 = Mout_2*x3_A7*epsL1_A7;
1085     mL1_4_A7_2 = Mout_2*x4_A7*epsL1_A7;
1086     %mL2_3_A7_2 = Mout_2*epsL2_A7;
1087     mS_3_A7_2  = Mout_2*epsS_A7;
1088     %Loeslichkeitsfunktion
1089     xLoes_A7 = p.pl(1) + p.pl(2)*x1_A7 + p.pl(3)*T_A7 + p.pl(4)*x1_A7^2 + p.pl(5)*x1_A7*T_A7
1090     + p.pl(6)*T_A7^2 + ...
1091                 p.pl(7)*x1_A7^3 + p.pl(8)*x1_A7^2*T_A7 + p.pl(9)*x1_A7*T_A7^2;
1092     %Uebersaettigung
1093     S_A7=(x3_A7*epsL1_A7-xLoes_A7);
1094     if S_A7>0
1095         mL1S_3_A7=(mtot_A5)*S_A7;
1096      else
1097          mL1S_3_A7=0;
1098     end
1099     %Glasuebergangstemperatur
1100     Tglas7 = p.Tg(1)*x1_A7 + p.Tg(2);
1101     if T_A7>=Tglas7 && ms_A7>=0
1102         ML2_3_A7=ms_A7*p.k1+mL1S_3_A7*p.k2;   %ms_A7*p.k1+mL1S_3_A7*p.k2
1103     else
1104         ML2_3_A7=0;
1105     end
1106     %Bilanzen Behaelter A7 : Anpassung 120720017 Peter
1107     ML1_1_A7 = -mL1_1_A7 -mL1_1_A7_2 + mL1_1_A6 ;
1108     ML1_2_A7 = -mL1_2_A7 -mL1_2_A7_2 + mL1_2_A6 + mL1_2_A8;
1109     ML1_3_A7 = -mL1_3_A7 -mL1_3_A7_2 + mL1_3_A6 - mL1S_3_A7;
1110     ML1_4_A7 = -mL1_4_A7 -mL1_4_A7_2 + mL1_4_A6;
1111     %ML2_3_A7 = -mL2_3_A7 -mL2_3_A7_2 + mL2_3_A6 + m_SL2_3_A7;
1112     Ms_3_A7  = - mS_3_A7 - mS_3_A7_2 + mS_3_A6 + mL1S_3_A7 ;
1113     TA7   = -((mL1_1_A7+mL1_1_A7_2)*p.cp_L1(1) + (mL1_2_A7+mL1_2_A7_2)*p.cp_L1(2)...
1114             + (mL1_3_A7+mL1_3_A7_2)*p.cp_L1(3) + (mL1_4_A7+mL1_4_A7_2)*p.cp_L1(4)...
1115             + mL2_3_A7*p.cp_L2(1) + (mS_3_A7+mS_3_A7_2)*p.cp_L2(2))*T_A7 ...
1116             +
1117     (mL1_1_A6*p.cp_L1(1)+mL1_2_A6*p.cp_L1(2)+mL1_3_A6*p.cp_L1(3)+mL1_4_A6*p.cp_L1(4))*T_A6...
1118             + (mL2_3_A6*p.cp_L2(1)+mS_3_A6*p.cp_L2(2))*T_A6 ...
1119             + mL1_2_A8*p.cp_L1(2)*T_A6 ;
1120     %%
1121     %Uebergabe aller Stroeme an solver
1122     BLG =  [ML1_1_A1;ML1_2_A1;ML1_3_A1;ML1_4_A1;ML2_3_A1;MS_3_A1;TA1...
1123            ;Mg1_A2;Mg2_A2;ML1_1_A2;ML1_2_A2;ML1_3_A2;ML1_4_A2;ML2_3_A2;Ms_3_A2;TA2...
1124            ;Mg1_A3;Mg2_A3;ML1_1_A3;ML1_2_A3;ML1_3_A3;ML1_4_A3;ML2_3_A3;Ms_3_A3;TA3...
1125            ;Mg1_A4;Mg2_A4;ML1_1_A4;ML1_2_A4;ML1_3_A4;ML1_4_A4;ML2_3_A4;Ms_3_A4;TA4...
1126            ;Mg1_A5;Mg2_A5;ML1_1_A5;ML1_2_A5;ML1_3_A5;ML1_4_A5;ML2_3_A5;Ms_3_A5;TA5...
1127            ;Mg1_A6;Mg2_A6;ML1_1_A6;ML1_2_A6;ML1_3_A6;ML1_4_A6;ML2_3_A6;Ms_3_A6;TA6...
1128            ;ML1_1_A7;ML1_2_A7;ML1_3_A7;ML1_4_A7;ML2_3_A7;Ms_3_A7;TA7];
1129     End
1130
1131     Function for the calculation of vapor-liquid equilibria of ethanol and water:
1132     function f=boil(T,x,p,g1,g2,coeff)
1133     %Funktion  zur Siedetemperaturberechnung
1134     %Dampfdruecke fuer Ethanol und Wasser
1135     psat=10.^(coeff(:,1)-coeff(:,2)./(coeff(:,3)+T));
1136     %Gesamtdruck fuer Ethanol-Wasser-Gemisch
1137     f=g1*x*psat(1)+g2*(1-x)*psat(2)-p;
1138     end
```

B. References

Acton, Q. A. (2013). Acyclic Acids—Advances in Research and Application: 2013 Edition. Atlanta, ScholaryEditions.

Alriols, M. G., A. García, R. Llano-ponte and J. Labidi (2010). "Combined organosolv and ultrafiltration lignocellulosic biorefinery process." Chemical Engineering Journal 157(1): 113-120.

Ayyachamy, M., F. E. Cliffe, J. M. Coyne, J. Collier and M. G. Tuohy (2013). "Lignin: untapped biopolymers in biomass conversion technologies." Biomass Conversion and Biorefinery 3(3): 255-269.

Banerjee, T., R. K. Sahoo, S. S. Rath, R. Kumar and A. Khanna (2007). "Multicomponent Liquid−Liquid Equilibria Prediction for Aromatic Extraction Systems Using COSMO-RS." Industrial & Engineering Chemistry Research 46(4): 1292-1304.

Bauer, S., H. Sorek, V. D. Mitchell, A. B. Ibanez and D. E. Wemmer (2012). "Characterization of Miscanthus giganteus lignin isolated by ethanol organosolv process under reflux condition." J Agric Food Chem 60(33): 8203-8212.

Baumberger, S., A. Abaecherli, M. Fasching, G. Gellerstedt, R. Gosselink, B. Hortling, J. Li, B. Saake and E. de Jong (2007). "Molar mass determination of lignins by size-exclusion chromatography: towards standardisation of the method." Holzforschung 61(4).

Becke, A. D. (1988). "Density-functional exchange-energy approximation with correct asymptotic behavior." Physical Review A 38(6): 3098-3100.

Beckmann, W. (2013). Crystallization: Basic Concepts and Industrial Applications. Weinheim, Wiley.

Beisl, S., A. Miltner and A. Friedl (2017). "Lignin from Micro- to Nanosize: Production Methods." International Journal of Molecular Sciences 18(6): 1244.

Berlin, A., M. Y. Balakshin, R. Ma, V. M. Gutman and D. Ortiz (2013). "Organosolv process." US 20130210100 A1

Berlin, A., C. Muñoz, N. Gilkes, S. M. Alamouti, P. Chung, K.-Y. Kang, V. Maximenko, J. Baeza, J. Freer, R. Mendonça and J. Saddler (2007). "An Evaluation of British Columbian Beetle-Killed Hybrid Spruce for Bioethanol Production." Applied Biochemistry and Biotecnology: 267-280.

Blanchard, L.-P., J. Hesse and S. L. Malhotra (1974). "Effect of Molecular Weight on Glass Transition by Differential Scanning Calorimetry." Canadian Journal of Chemistry 52(18): 3170-3175.

Blechschmidt, J., P. Engert and M. Stephan (1986). "The glass transition of wood from the viewpoint of mechanical pulping." Wood Science and Technology 20(3): 263-272.

Botello, J. I., M. A. Gilarranz, F. RodrÍGuez and M. Oliet (1999). "Recovery of Solvent and By-Products from Organosolv Black Liquor." Separation Science and Technology **34**(12): 2431-2445.

Bundesregierung (2010). Nationale Forschungsstrategie BioÖkonomie 2030- Unser Weg zu einer bio-basierten Wirtschaft. Berlin, Bundesministerium für Bildung und Forschung.

Cazacu, G., M. Capraru and V. I. Popa (2013). Advances Concerning Lignin Utilization in New Materials. Advanced Structured Materials. S. Thomas. Berlin-Heidelberg, Springer. **18:** 255-312.

Constant, S., H. L. J. Wienk, A. E. Frissen, P. d. Peinder, R. Boelens, D. S. van Es, R. J. H. Grisel, B. M. Weckhuysen, W. J. J. Huijgen, R. J. A. Gosselink and P. C. A. Bruijnincx (2016). "New insights into the structure and composition of technical lignins: a comparative characterisation study." Green Chem. **18**(9): 2651-2665.

Cybulska, I., G. Brudecki, K. Rosentrater, J. L. Julson and H. Lei (2012). "Comparative study of organosolv lignin extracted from prairie cordgrass, switchgrass and corn stover." Bioresour Technol **118**: 30-36.

Dahl, G. F. (1884). "Process of manufacturing cellulose from wood." US 296935 A

Diebold, V. B., W. F. Cowan and J. K. Walsh (1978). "Solvent pulping process." US 4100016 A

Dingwell, K., M. Sedin and H. Theliander (2011). "Filtration of Lignin from a Lignocellulose-Based Ethanol Pilot Plant." Environmental Engineering Science **28**(11): 775-779.

DOE (2017). Website: Integrated biorefineries. https://energy.gov/eere/bioenergy/integrated-biorefineries, U.S. Department of Energy.

Engelhardt, H. (1979). High Performance Liquid Chromatography. Berlin Heidelberg New York, Springer-Verlag.

Fackler, K., T. Ters, O. Ertl and K. Messner (2012). "Method for lignin recovery." WO2011AT00357

Fernando, E. F., E. M. Vallejos and M. C. Area (2010). "Lignin Recovery from Spent Liquors from Ethanol-Water Fractionation of Sugar Cane Bagasse." Cellulose Chemistry and Technology **44**(9): 311-318.

FNR (2009). Aktionsplan der Bundesregierung zur stofflichen Nutzung nachwachsender Rohstoffe, BMELV.

FNR (2012). Roadmap Bioraffinerien im Rahmen der Aktionspläne der Bundesregierung zur stofflichen und energetischen Nutzung nachwachsender Rohstoffe. B. BMELV, BMU, BMWi. Gülzow, BRD.

Garcia, A., M. G. Alriols and J. Labidi (2012). "Evaluation of the effect of ultrasound on organosolv black liquor from olive tree pruning residues." Bioresour Technol **108**: 155-161.

Gidh, A. V., S. R. Decker, T. B. Vinzant, M. E. Himmel and C. Williford (2006). "Determination of lignin by size exclusion chromatography using multi angle laser light scattering." J Chromatogr A **1114**(1): 102-110.

Gmehling, J. (1981). Grundlagen der Stofftrennung: Modellierung von Phasengleichgewichten als Grundlage von Stofftrennprozessen. Berlin–Ost, Akademie–Verlag.

Goring, D. A. I. (1962). "The physical chemistry of lignin." Pure and Applied Chemistry **5**(1-2).

Griffith, P. R. and J. A. de Haseth (2007). Fourier Transform Infrared Spectrometry (Second Edition). Hoboken, WILEY-INTERSCIENCE.

Gruber, E. (1980). Polymerchemie. Darmstadt, Steinkopff.

Hallberg, C., D. O'connor, M. Rushton, E. K. Pye, G. Gjennestad, A. Berlin and J. R. MacLachlan (2013). "Modular system for organosolv fractionation of lignocellulosic feedstock." US8528463 B2

Hatakeyama, H. and T. Hatakeyama (2009). Lignin Structure, Properties, and Applications. Advances in Natural Polymers- Composites and Nanocomposites. S. Thomas, P. M. Visakh and A. P. Mathew. Berlin-Heidelberg, Springer. **232:** 1-63.

Hatakeyama, T. and H. Hatakeyama (1982). "Temperature dependence of X-ray diffractograms of amorphous lignins and polystyrenes." Polymer **23**(3): 475-477.

Hatakeyama, T. and H. Hatakeyama (2005). Thermal Properties of Green Polymers and Biocomposites. Dordrecht, Kluwer Academic.

Hideno, A., A. Kawashima, M. Fukuoka, T. Endo, K. Honda and M. Morita (2012). "Effect of alcohol-based organosolv treatment combined with short-time ball milling on the enzymatic hydrolysis of Japanese cypress (Chamaecyparis obtusa)." Wood Science and Technology **47**(2): 381-393.

Holladay, J. E., J. F. White, J. J. Bozell and D. Johnson (2007). Top Value Added Chemicals from Biomass Volume II: Results of Screening for Potential Candidates from Biorefinery Lignin, Pacific Northwest National Laboratory (PNNL) and National Renewable Energy Laboratory (NREL).

Hu, T. Q. (2002). Chemical modification, properties, and usage of lignin. New York, Kluwer Academic.

Huijgen, W. J. J., J. H. Reith and H. den Uil (2010). "Pretreatment and Fractionation of Wheat Straw by an Acetone-Based Organosolv Process." Industrial & Engineering Chemistry Research **49**(20): 10132-10140.

Iakovlev, M., H. Sixta and A. van Heiningen (2011). "SO2-Ethanol-Water (SEW) Pulping: II. Kinetics for Spruce, Beech, and Wheat Straw." Journal of Wood Chemistry and Technology **31**(3): 250-266.

Junker, E. (1941). "Zur Kenntnis der kolloidchemischen Eigenschaften des Humus." Kolloid-Zeitschrift **95**(2).

Kamm, B., P. R. Gruber and M. Kamm (2005). Biorefineries – Industrial Processes and Products. Ullmann´s Encyclopedia of Industrial Chemistry. Weinheim, Wiley-Blackwell.

Keitel, J. (2016). Kontinuierliche Fällung von Lignin aus Organosolv-Kochlaugen Master thesis, Otto-von-Guericke Universität Magdeburg.

Khattab, I. S., F. Bandarkar, M. A. A. Fakhree and A. Jouyban (2012). "Density, viscosity, and surface tension of water+ethanol mixtures from 293 to 323K." Korean Journal of Chemical Engineering **29**(6): 812-817.

Kishimoto, A. and H. Fujita (1958). "Diffusion-controlled stress relaxation in polymers. III. Stress relaxation in a swelling polymer." Journal of Polymer Science **28**(118): 569-585.

Klamt, A. (1995). "Conductor-like Screening Model for Real Solvents: A New Approach to the Quantitative Calculation of Solvation Phenomena." The Journal of Physical Chemistry **99**(7): 2224-2235.

Klamt, A. and G. Schüürmann (1993). "COSMO: a new approach to dielectric screening in solvents with explicit expressions for the screening energy and its gradient." J. Chem. Soc., Perkin Trans. **2**.

Klason, P. (1893). "On the composition and pulping of spruce wood (in Swed.)." *Teknisk Tidskr. Afd. Kemi Metall* **23**: 33-39.

Kleinert, T. (1971). "Organosolv pulping and recovery process." US3585104 (A)

Kleinert, T. and K. v. Tayenthal (1931). "Über neuere Versuche zur Trennung von Cellulose und Inkrusten verschiedener Hölzer." Angewandte Chemie **44**(39): 788-791.

Köhnke, J., C. Fürst, C. Unterweger, H. Rennhofer, H. Lichtenegger, J. Keckes, G. Emsenhuber, A. Mahendran, F. Liebner and W. Gindl-Altmutter (2016). "Carbon Microparticles from Organosolv Lignin as Filler for Conducting Poly(Lactic Acid)." Polymers **8**(6): 205.

Kühnel, I., B. Saake and R. Lehnen (2017). "Comparison of different cyclic organic carbonates in the oxyalkylation of various types of lignin." Reactive and Functional Polymers **120**: 83-91.

Kusian, A. (2014). Simulation der Fällung von Organosolv-Lignin Diploma thesis, Otto-von-Guericke Univerity Magdeburg.

Laity, P. R., P. M. Glover and J. N. Hay (2002). "Composition and phase changes observed by magnetic resonance imaging during non-solvent induced coagulation of cellulose." Polymer **43**(22): 5827-5837.

Laure, S., M. Leschinsky, M. Frohling, F. Schultmann and G. Unkelbach (2014). "Assessment of an Organosolv Lignocellulose Biorefinery Concept Based on a Material Flow Analysis of a Pilot Plant." Cellulose Chemistry and Technology **48**(9-10): 793-798.

Le, H. Q., A. Zaitseva, J. P. Pokki, M. Stahl, V. Alopaeus and H. Sixta (2016). "Solubility of Organosolv Lignin in gamma-Valerolactone/Water Binary Mixtures." ChemSusChem **9**(20): 2939-2947.

Li, S.-J., S.-J. Xie, Y.-C. Li, H.-J. Qian and Z.-Y. Lu (2016). "Influence of molecular-weight polydispersity on the glass transition of polymers." Physical Review E **93**(1).

Lignol   (2011).   Demonstration-Scale   Biorefinery.
https://energy.gov/sites/prod/files/2014/03/f14/ibr_demonstration_lignol.pdf,   U.S.
Department of Energy.

Lin, S. Y. and C. W. Dence (1992). Methods in Lignin Chemistry. Berlin-Heidelberg, Springer.

Lipson, J. E. G. and S. T. Milner (2006). "Multiple glass transitions and local composition effects on polymer solvent mixtures." Journal of Polymer Science Part B: Polymer Physics **44**(24): 3528-3545.

Liu, W.-J., H. Jiang and H.-Q. Yu (2015). "Thermochemical conversion of lignin to functional materials: a review and future directions." Green Chemistry **17**(11): 4888-4907.

Loutfi, H., B. Blackwell and V. Uloth (1991). "Lignin Recovery from Kraft Black Liquor - Preliminary Process Design." Tappi Journal **74**(1): 203-210.

Lupoi, J. S., S. Singh, R. Parthasarathi, B. A. Simmons and R. J. Henry (2015). "Recent innovations in analytical methods for the qualitative and quantitative assessment of lignin." Renewable and Sustainable Energy Reviews **49**: 871-906.

Ma, Y., S. Asaadi, L.-S. Johansson, P. Ahvenainen, M. Reza, M. Alekhina, L. Rautkari, A. Michud, L. Hauru, M. Hummel and H. Sixta (2015). "High-Strength Composite Fibers from Cellulose-Lignin Blends Regenerated from Ionic Liquid Solution." ChemSusChem **8**(23): 4030-4039.

Macfarlane, A. L., R. Prestidge, M. M. Farid and J. J. J. Chen (2009). "Dissolved air flotation: A novel approach to recovery of organosolv lignin." Chemical Engineering Journal **148**(1): 15-19.

Mainka, H., L. Hilfert, S. Busse, F. Edelmann, E. Haak and A. S. Herrmann (2015). "Characterization of the major reactions during conversion of lignin to carbon fiber." Journal of Materials Research and Technology **4**(4): 377-391.

Mainka, H., O. Täger, E. Körner, L. Hilfert, S. Busse, F. T. Edelmann and A. S. Herrmann (2015). "Lignin – an alternative precursor for sustainable and cost-effective automotive carbon fiber." Journal of Materials Research and Technology **4**(3): 283-296.

Mansfield, S. D., H. Kim, F. Lu and J. Ralph (2012). "Whole plant cell wall characterization using solution-state 2D NMR." Nat Protoc **7**(9): 1579-1589.

Mcdonough, T. J. (1992). The Chemistry of Organosolv Delignification. 1992 Solvent Pulping Symposium**:** 1-7.

Menon, V. and M. Rao (2012). "Trends in bioconversion of lignocellulose: Biofuels, platform chemicals & biorefinery concept." Progress in Energy and Combustion Science **38**(4): 522-550.

Michels, J., A. Imami, A. Stücker, A. Duwe, A. Susanto, B. Saake, D. Meier, E. Küstermann, E. Fliedner, E. Meier, G. Unkelbach, H. Zorn, I. Kühnel, J. Podschun, J.-O. Strüven, J. Schweinle, K. Becker, L. Ziegler, M. Fröhling, M. Amann, M. Naundorf, M.

Haase, M. Leschinsky, N. Tippkötter, P. Engel, R. Schweppe, R. Lehnen, S. Böringer, S. Laure, S. Riemer, S. Zibek, T. Sieker, U. Pohsner and W. Bäcker (2014). "Lignocellulose-Bioraffinerie" Aufschluss lignocellulosehaltiger Rohstoffe und vollständige stoffliche Nutzung der Komponenten (Phase 2)- Gemeinsamer Abschlussbericht zu den wissenschaftlich-technischen Ergebnissen aller Teilvorhaben. J. Michels.

Michels, J. and K. Wagemann (2010). "The German Lignocellulose Feedstock Biorefinery Project." Biofuels, Bioproducts and Biorefining **4**(3): 263-267.

Morreel, K., O. Dima, H. Kim, F. Lu, C. Niculaes, R. Vanholme, R. Dauwe, G. Goeminne, D. Inze, E. Messens, J. Ralph and W. Boerjan (2010). "Mass spectrometry-based sequencing of lignin oligomers." Plant Physiol **153**(4): 1464-1478.

Mühe, C. (2017). VIELSCHICHTIG Master thesis, Hochschule für Künste Bremen Bremen.

Muurinen, E. (2000). Organosolv pulping- A review and distillation study related to peroxyacid pulping Doctoral thesis, University of Oulu Oulu.

Nandanwar R.A., C. A. R., Ekhe J.D. (2012). "Utilization Of Industrial Waste Lignin In Polymer Systems." InternationalJournal of Knowledge Engineering **3**(1): 165-167.

Ni, Y. and A. Hammer (2012). "Thermische Analyse von Polymeren, Teil 5: DSC und TGA von Elastomeren." Mettler Toledo UserCom35.

Ni, Y. and Q. Hu (1995). "Alcell® lignin solubility in ethanol–water mixtures." Journal of Applied Polymer Science **57**(12): 1441-1446.

Ni, Y. and A. Van Heiningen (1994). Lignin Removal of ALCELL Pulp by Washing with an Ethanol-Water Solution. Pulping Conference, San Diego, TAPPI Proceedings.

Niemi, H., J. Lahti, H. Hatakka, S. Kärki, S. Rovio, M. Kallioinen, M. Mänttäri and M. Louhi-Kultanen (2011). "Fractionation of Organic and Inorganic Compounds from Black Liquor by Combining Membrane Separation and Crystallization." Chemical Engineering & Technology **34**(4): 593-598.

Öhman, F. (2006). Precipitation and separation of lignin from kraft black liquor Doctoral thesis, Chalmers University of Technology Göteborg.

Pan, X., C. Arato, N. Gilkes, D. Gregg, W. Mabee, K. Pye, Z. Xiao, X. Zhang and J. Saddler (2005). "Biorefining of softwoods using ethanol organosolv pulping: preliminary evaluation of process streams for manufacture of fuel-grade ethanol and co-products." Biotechnol Bioeng **90**(4): 473-481.

Papatheofanous, M. G., E. Billa, D. P. Koullas, B. Monties and E. G. Koukios (1995). "Two-stage acid-catalyzed fractionation of lignocellulosic biomass in aqueous ethanol systems at low temperatures." Bioresource Technology **54**(3): 305-310.

Perdew, J. P. (1986). "Density-functional approximation for the correlation energy of the inhomogeneous electron gas." Physical Review B **33**(12): 8822-8824.

Pickering, S. U. (1893). "The hydrate theory of solutions. Some compounds of the alkyl-amines and ammonia with water." J. Chem. Soc., Trans. **63**(0): 141-195.

Pu, Y., N. Jiang and A. J. Ragauskas (2007). "Ionic Liquid as a Green Solvent for Lignin." Journal of Wood Chemistry and Technology **27**(1): 23-33.

Pye, E. (2002). "Integrated processing of biomass and liquid effluents." US 2002/0069987 A1

Pye, E. K. and J. H. Lora (1991). "The Alcell Process - a Proven Alternative to Kraft Pulping." Tappi Journal **74**(3): 113-118.

Retsina, T., V. Pylkkanen, K. Nelson and M. SZCZEPANIK (2014). "Processes and apparatus for lignin separation in biorefineries." WO2014092873A1

Rinaldi, R., R. Jastrzebski, M. T. Clough, J. Ralph, M. Kennema, P. C. A. Bruijnincx and B. M. Weckhuysen (2016). "Wege zur Verwertung von Lignin: Fortschritte in der Biotechnik, der Bioraffination und der Katalyse." Angewandte Chemie **128**(29): 8296-8354.

Russel, W. B., D. A. Saville and W. R. Schowalter (1989). Colloidal Dispersions. New York, Cambridge University PressColloidal Dispersions.

Sannigrahi, P., Y. Pu and A. Ragauskas (2010). "Cellulosic biorefineries—unleashing lignin opportunities." Current Opinion in Environmental Sustainability **2**(5-6): 383-393.

Schlünder, E.-U. and F. Thurner (1995). Destillation, Absorption, Extraktion. Braunschweig/Wiesbaden, Vieweg+Teubner Verlag.

Schuerch, C. (1952). "The solvent properties of liquids and their relation to solubilty, swelling, isolation and fractionation of lignin." Am. Chem. Soc. **74**(20): 5061–5067.

Schulze, P., H. Lorenz and A. Seidel-Morgenstern (2014). Precipitation of lignin from ethanol organosolv black liquor. ISIC 2014 - International Symposium on Industrial Crystallization Book of Abstracts, Toulouse.

Schulze, P., H. Lorenz, A. Seidel-Morgenstern, M. Leschinsky and G. Unkelbach (2014). "Method for precipitating lignin from organosolv pulping liquors." WO2016062676A1

Schulze, P., A. Seidel-Morgenstern and H. Lorenz (2016). Continuous separation of lignin from ethanol-water pulping liquors. EWLP 2016 - 14th European Workshop on Lignocellulosics and Pulp: Proceedings for Poster Presentations.

Schulze, P., A. Seidel-Morgenstern, H. Lorenz, M. Leschinsky and G. Unkelbach (2016). "Advanced process for precipitation of lignin from ethanol organosolv spent liquors." Bioresour Technol **199**: 128-134.

Schwiderski, M. and A. Kruse (2015). "Aluminiumchlorid-katalysierter Organosolv-Aufschluss von Buchenholz." Chemie Ingenieur Technik **87**(7): 922-930.

Shampine, L. F. and M. W. Reichelt (1997). "The MATLAB ODE Suite." SIAM Journal on Scientific Computing **18**: 1–22.

Sluiter, A., B. Hames, R. Ruiz, C. Scarlata, J. Sluiter and D. Templeton (2008). Determination of Sugars, Byproducts, and Degradation Products in Liquid Fraction Process Samples. Laboratory Analytical Procedure NREL/TP-510-42623. Golden (USA), National Renewable Energy Laboratory.

Smith, B. (2013). Best Practice for Inline Particle Size Characterization, Mettler-Toledo AutoChem.

Streffer, F. (2014). "Lignocellulose to Biogas and other Products." JSM Biotechnol Bioeng **2**(1): 1023.

Tayenthal, K. and T. Kleinert (1932). "Process of decomposing vegetable fibrous matter for the purpose of the simultaneous recovery both of the cellulose and of the incrusting ingredients." US1856567 (A)

Teipel, U. (2002). "Influence of Droplet Size on the Rheological Behavior of Emulsions." Chemical Engineering Technology **25**: 609-615.

Thring, R. W., E. Chornet and R. P. Overend (1990). "Recovery of a solvolytic lignin: Effects of spent liquor/acid volume ratio, acid concentration and temperature." Biomass **23**(4): 289-305.

Thring, R. W., M. N. Vanderlaan and S. L. Griffin (1996). "Fractionation Of Alcell® Lignin By Sequential Solvent Extraction." Journal of Wood Chemistry and Technology **16**(2): 139-154.

Tjeerdsma, B. F., F. H. A. Zomers, E. C. Wilkinson and R. Sierra-Alvarez (1994). "Modelling Organosolv Pulping of Hemp." Holzforschung **48**(5): 415-422.

Tomas, J. (2006). Mechanics of Particle Adhesion. Internional Congress of Chemical and Process Engineering. Praque.

Tomas, J. (2017). Vorlesung Partikeltechnologie. Magdeburg, Lehrstuhl für Mechanische Verfahrenstechnik, Otto-von-Guericke Universität http://www.mvt.ovgu.de/Lehre/Vorlesung+GPVT.html.

van de Witte, P., P. J. Dijkstra, J. W. A. van den Berg and J. Feijen (1996). "Phase separation processes in polymer solutions in relation to membrane formation." Journal of Membrane Science **117**(1-2): 1-31.

van Tuel, M. M. A., W. J. J. Huijgen and H. M. van Veen (2016). "Separation of lignin and sugars from biomass pre-treatment liquors." WO2016131828 A1

VDI (2010). Richtlinie 2762 Blatt 2: Filtrierbarkeit von Suspensionen - Bestimmung des Filterkuchenwiderstands.

Vebber, G. C., P. Pranke and C. N. Pereira (2014). "Calculating hansen solubility parameters of polymers with genetic algorithms." Journal of Applied Polymer Science **131**(1): n/a-n/a.

Viell, J., A. Harwardt, J. Seiler and W. Marquardt (2013). "Is biomass fractionation by Organosolv-like processes economically viable? A conceptual design study." Bioresour Technol **150**: 89-97.

Vishtal, A. G. and A. Kraslawski (2011). "Challenges in industrial applications of technical lignins." BioResources **6**(3): 3547-3568.

Vroom, K. E. (1957). "The"H"factor: A means of expressing cooking times and temperature as a single variable." Pulp and Paper Magazine of Canada **58**(3): 228-231.

Wang, G. and H. Chen (2013). "Fractionation of alkali-extracted lignin from steam-exploded stalk by gradient acid precipitation." <u>Separation and Purification Technology</u> **105**: 98-105.

Weinwurm, F., A. Drljo, T. L. S. Silva and A. Friedl (2014). "Principles of Ethanol Organosolv Lignin Precipitation: Process Simulation and Energy Demand." <u>Pres 2014, 17th Conference on Process Integration, Modelling and Optimisation for Energy Saving and Pollution Reduction, Pts 1-3</u> **39**: 583-588.

Weinwurm, F., A. Drljo, W. Waldmüller, B. Fiala, J. Niedermayer and A. Friedl (2016). "Lignin concentration and fractionation from ethanol organosolv liquors by ultra- and nanofiltration." <u>Journal of Cleaner Production</u> **136**: 62-71.

Wen, J.-L., B.-L. Xue, S.-L. Sun and R.-C. Sun (2013). "Quantitative structural characterization and thermal properties of birch lignins after auto-catalyzed organosolv pretreatment and enzymatic hydrolysis." <u>Journal of Chemical Technology & Biotechnology</u> **88**(9): 1663-1671.

White, R. P. and J. E. G. Lipson (2016). "Polymer Free Volume and Its Connection to the Glass Transition." <u>Macromolecules</u> **49**(11): 3987-4007.

Wienk, I. M., R. M. Boom, M. A. M. Beerlage, A. M. W. Bulte, C. A. Smolders and H. Strathmann (1996). "Recent advances in the formation of phase inversion membranes made from amorphous or semi-crystalline polymers." <u>Journal of Membrane Science</u> **113**(2): 361-371.

Wildschut, J., A. T. Smit, J. H. Reith and W. J. Huijgen (2013). "Ethanol-based organosolv fractionation of wheat straw for the production of lignin and enzymatically digestible cellulose." <u>Bioresour Technol</u> **135**: 58-66.

Williams, M. L., R. F. Landel and J. D. Ferry (1955). "The Temperature Dependence of Relaxation Mechanisms in Amorphous Polymers and Other Glass-forming Liquids." <u>Journal of the American Chemical Society</u> **77**(14): 3701-3707.

Xu, Y., K. Li and M. Zhang (2007). "Lignin precipitation on the pulp fibers in the ethanol-based organosolv pulping." <u>Colloids and Surfaces A: Physicochemical and Engineering Aspects</u> **301**(1-3): 255-263.

Zakzeski, J., P. C. Bruijnincx, A. L. Jongerius and B. M. Weckhuysen (2010). "The catalytic valorization of lignin for the production of renewable chemicals." <u>Chem Rev</u> **110**(6): 3552-3599.

Zdravkov, A. N. (2004). <u>Interfacial phenomena during drop coaleszence in polymeric systems</u> Doctoral thesis, Technische Universität Eindhoven

Zhang, K., Z. Pei and D. Wang (2016). "Organic solvent pretreatment of lignocellulosic biomass for biofuels and biochemicals: A review." <u>Bioresour Technol</u> **199**: 21-33.

Zhang, X., M. Tu and M. G. Paice (2011). "Routes to Potential Bioproducts from Lignocellulosic Biomass Lignin and Hemicelluloses." <u>BioEnergy Research</u> **4**(4): 246-257.

Zlokarnik, M. (1999). <u>Rührtechnik</u>. Berlin, Springer.

C. List of figures

D. List of tables

E. Nomenclature

Symbol	Name
A	Ampere
a	year
g	gram
h	hour
kg	kilogram (1 kg = 1000 g)
mbara	millibar absolute (e.g. 1013 mbara = atmospheric pressure)
mbarg	millibar relative to atmospheric pressure (gauge) (e.g. 0 mbarg =atm. pressure)
min	minute
p	pico
w	mass fraction
wt.%	weight percent or mass percent
γ	activity coefficient
ε	dielectric constant
χ	molar fraction

Abbreviations

Index	Name
[DBNH][OAc]	1,5-diazabicyclo[4.3.0]non-5-enium acetate
ATR	Attenuated total reflection
BR	Biorefinery
CIP	Cleaning in place
COSMO-RS	Conductor like screening model for real solvents
CSTR	Continuous stirred tank reactor
DCTS	Dynamics of Complex Technical Systems
DFT	Density functional theory
DLVO theory	Derjaguin, Landau, Verwey, Overbeek theory
DMSO	Dimethylsulfoxide
DSC	Differential scanning calorimetry
EOS	Ethanol Organosolv
FBRM®	Focused beam reflectance measurement
FFE	Falling film evaporator
Fh CBP	Fraunhofer Center for Chemical-Biotechnological Processes
FID	Flame ionization detector
FT-IR	Fourier-transform- infrared
GC	Gas chromatography
HPLC	High performance liquid chomatography
HPSEC	High Performance size exclusion chromatography
HSQC	Heteronuclear single quantum coherence
IR	Infrared
IRE	Internal reflection element
KL	Kraft lignin
LC	Lignocellulose
LLE	Liquid-liquid-eqilibrium
LSF	Lignosulfonate

LWE	Lignin-water-ethanol (system, mixture or solution)
MALLS	Multi angle laser light scattering
MCT	Mercury Cadmium Telluride (infrared detector)
MD	Molecular dynamics
MIR	Mid-field infrared
MM	Molecular mass
MMD	Molecular mass distribution
MPI	Max Planck Institute
MS	Mass Spectroscopy
MSD	Molecular simulation and design
MWL	Milled wood lignin
NMR	Nuclear magnetic resonance
NREL	National renewable energy laboratory (U.S.)
o.d.w.	Oven dry wood
OS	Organosolv
OSL	Organosolv lignin
PCF	Physical and Chemical Foundations
PCLD	Particle chord length distribution
PL	Pulping liquor
PLS	Partial least squares
PSD	Particle size distribution
PVM	Process video microscope
R^2	Coefficient of correlation
RBI	Relative backscatter index
RMSEC	Root mean square error of calibration
RMSECV	Root mean square error of cross-validation
RMSEP	Root mean square error of prediction
SEC	Size exclusion chromatography
TMA	Thermo-mechanic analysis
TM-DSC	Temperature-modulated differential scanning calorimetry
TMS	Tetramethylsilan
UV	Ultraviolet
XRD	X-ray diffraction

F. List of publications

Journal articles:

Schulze, P., Seidel-Morgenstern, A., Lorenz, H., Leschinsky, M., & Unkelbach, G. (2016). Advanced process for precipitation of lignin from ethanol organosolv spent liquors. Bioresource Technology, 199, 128-134. doi:10.1016/j.biortech.2015.09.040.

(In preparation: 2018, "Phase equilibria in the lignin-ethanol-water system")

(In preparation: 2018, "Continuous lignin precipitation and agglomeration")

Patent:

Schulze, P., H. Lorenz, A. Seidel-Morgenstern, M. Leschinsky and G. Unkelbach (2014). Method for precipitating lignin from organosolv pulping liquors. Max-Planck-Gesellschaft and Fraunhofer-Gesellschaft. Germany. WO2016062676A1.

Conference contributions:

Proceddings
Horosanskaia, E., Schulze, P., Seidel-Morgenstern, A., Lorenz, H.: Crystallization-based isolation of a target compound from complex multicomponent mixtures originating from plant processing. Proceedings 20th Int. Symposium on Industrial Crystallization (ISIC 20), Dublin (Ireland), pp. 34–35

Schulze, P., Seidel-Morgenstern, A., & Lorenz, H. (2016). Continuous separation of lignin from ethanol-water pulping liquors. In EWLP 2016 - 14th European Workshop on Lignocellulosics and Pulp: Proceedings for Poster Presentations (pp. 161-165).

Schulze, P., Seidel-Morgenstern, A., & Lorenz, H. (2016). Continuous Separation of Lignin Particles from Ethanol-Water Pulping Liquors. In BIWIC 2016, 23rd International Workshop on Industrial Crystallization (pp. 276-276). Göttingen: Cuvillier.

Schulze, P., Seidel-Morgenstern, A., & Lorenz, H. (2015). Advanced process for continuous lignin precipitation from ethanol organosolv spent liquor. In ECCE10+ECAB3+EPIC5 Chemical Engineering and Biochemical Engineering for a new sustainable process industry in Europe (pp. 1023-1023).

Schulze, P., Seidel-Morgenstern, A., & Lorenz, H. (2014). Process monitoring of lignin precipitation. In Tagungsband – 10. Kolloquium Prozessanalytik, Gerlingen, 25.–26. November 2014 (pp. 22-22).

Schulze, P., Lorenz, H., & Seidel-Morgenstern, A. (2014). Precipitation of lignin from ethanol organosolv black liquor. In ISIC 2014 - International Symposium on Industrial Crystallization Book of Abstracts (pp. 397-399).

Talks

Schulze, P., Seidel-Morgenstern, A., & Lorenz, H. (2016). Continuous precipitation of lignin from organosolv spent liquors. Talk presented at Jahrestreffen der ProcessNet-Fachgruppe Kristallisation. Frankfurt am Main, Germany. 2016-03-10 - 2016-03-11.

Schulze, P., Seidel-Morgenstern, A., & Lorenz, H. (2016). Separation of Lignin from Organosolv Spent Liquor- from Phase Behavior to Continuous Processing. Talk presented at 2016 AIChE Annual Meeting. San Francisco, USA. 2016-11-13 - 2016-11-18.

Schulze, P., Lorenz, H., & Seidel-Morgenstern, A. (2016). Continuous precipitation and sintering of lignin particles from ethanol water pulping liquors. Talk presented at Kristallisations-Symposium 2016: A better Route to optimized Crystallization Processes and Product Quality. Frankfurt am Main, Germany. 2016-09-27 - 2016-09-27.

Schulze, P., Lorenz, H., & Seidel-Morgenstern, A. (2015). Untersuchungen zur Fällung von Lignin aus Ethanol-Organosolv Kochlaugen. Talk presented at Jahrestreffen der Fachgruppen Kristallisation, Partikelmesstechnik, Zerkleinern & Klassieren, mit Fachgemeinschaftstag Formulierung. Magdeburg, Germany. 2015-03-18 - 2015-03-20.

Posters

Schulze, P., Seidel-Morgenstern, A., & Lorenz, H. (2017). Fällung und Agglomeration von Lignin aus Ethanol/Wasser-Holzaufschluss-Lösungen. Poster presented at 8. Symposium Produktgestaltung in der Partikeltechnologie, Karlsruhe, Germany.

Schulze, P., Seidel-Morgenstern, A., & Lorenz, H. (2016). Continuous separation of lignin from ethanol-water pulping liquors. Poster presented at EWLP 2016 - 14th European Workshop on Lignocellulosics and Pulp, Autrans, France.

Schulze, P., Seidel-Morgenstern, A., & Lorenz, H. (2016). Continuous Separation of Lignin Particles from Ethanol-Water Pulping Liquors. Poster presented at BIWIC 2016 - 23rd International Workshop on Industrial Crystallization, Magdeburg, Germany.

Schulze, P., Seidel-Morgenstern, A., & Lorenz, H. (2015). Advanced process for continuous lignin precipitation from ethanol organosolv spent liquor. Poster presented at ECAB3 - 3rd European Congress of Applied Biotechnology, Nice, France.

Schulze, P., Seidel-Morgenstern, A., & Lorenz, H. (2014). Process monitoring of lignin precipitation. Poster presented at 10. Kolloquium Prozessanalytik, Gerlingen, Germany.

Schulze, P., Lorenz, H., & Seidel-Morgenstern, A. (2014). Solubility measurement of lignin and its separation from ethanol organosolv spent liquor. Poster presented at Lignin 2014 - biosynthesis and utilization, Umeå, Sweden.

Schulze, P., Lorenz, H., & Seidel-Morgenstern, A. (2014). Precipitation of lignin from ethanol organosolv black liquor. Poster presented at ISIC 2014 - International Symposium on Industrial Crystallization, Toulouse, France.

G. Cirriculum vitae

Personal Details

Name .... Peter Schulze
City, Date of birth Schönebeck (Elbe), 28.02.1986
Address .... Am Burgwall 1, 39249 Pömmelte

Education and work experience

2003-2005 .... Abitur at Dr. Carl Hermann Gymnasium in Schönebeck/Elbe

2005-2010 .... Studies of Chemical Engineering: Molecular and Structural Product Design (Dipl.-Ing.) at Otto-von-Guericke University Magdeburg

2010-2013 .... Project engineer at Sodawerk Staßfurt GmbH & Co.KG (large scale industry, calcinated sodium carbonate manufacturer)

Since 2013 .... Doctoral student and research assistant at Max Planck Institute for Dynamics of Complex Technical Systems in Magdeburg

_____

Location, Date, Signature